

**Contract No. FO4703-91-C-0112  
RTI Report No. RTI/5180/77-43F  
September 10, 1996**

# **Modeling Unlikely Space-Booster Failures in Risk Calculations**

**Final Report**

**Prepared for**

**Department of the Air Force  
45th Space Wing (AFSPC)  
Safety Office - 45 SW/SE  
Patrick AFB, FL 32925**

**and**

**Department of the Air Force  
30th Space Wing (AFSPC)  
Safety Office - 30 SW/SE  
Vandenberg AFB, CA 93437**

19961025 122

Distribution authorized to US Government agencies and their contractors to protect administrative/operational use data, 10 September 96. Other requests for this document shall be referred to the 30th Space Wing (AFSPC) Safety Office (30 SW/SE), Vandenberg AFB, CA 93437, or 45th Space Wing (AFSPC) Safety Office (45 SW/SE), Patrick AFB, FL 32925.

**DTIC QUALITY INSPECTED 2**



30360-TR-96-12

Contract No. FO4703-91-C-0112  
Task No. 10/95-77, Subtask 2.0

RTI Report No. RTI/5180/77-43F  
September 10, 1996

## **Modeling Unlikely Space-Booster Failures in Risk Calculations**

Final Report

Prepared by

James A. Ward, Jr.  
Robert M. Montgomery

of

Research Triangle Institute  
Center for Aerospace Technology  
Launch Systems Safety Department

Prepared for

Department of the Air Force  
45th Space Wing (AFSPC)  
Safety Office - 45 SW/SE  
Patrick AFB, FL 32925

and

Department of the Air Force  
30th Space Wing (AFSPC)  
Safety Office - 30 SW/SE  
Vandenberg AFB, CA 93437

Distribution authorized to US Government agencies and their contractors to protect administrative/operational use data, 10 September 96. Other requests for this document shall be referred to the 30th Space Wing (AFSPC) Safety Office (30 SW/SE), Vandenberg AFB, CA 93437, or 45th Space Wing (AFSPC) Safety Office (45 SW/SE), Patrick AFB, FL 32925.

# REPORT DOCUMENTATION PAGE

Form Approved  
OMB No. 0704-0188

Public reporting burden for this collection of information is estimated to average 1 hour per response, including the time for reviewing instructions, searching existing data sources, gathering and maintaining the data needed, and completing and reviewing the collection of information. Send comments regarding this burden estimate or any other aspect of this collection of information, including suggestions for reducing this burden, to Washington Headquarters Services, Directorate for Information Operations and Reports, 1215 Jefferson Davis Highway, Suite 1204, Arlington, VA 22202-4302, and to the Office of Management and Budget, Paperwork Reduction Project (0704-0188), Washington, DC 20503.

1. AGENCY USE ONLY (Leave blank)	2. REPORT DATE September 10, 1996	3. REPORT TYPE AND DATES COVERED Final
----------------------------------	--------------------------------------	---

4. TITLE AND SUBTITLE Modeling Unlikely Space-Booster Failures in Risk Calculations	5. FUNDING NUMBERS C: FO4703-91-C-0112 TA: 10/95-77
--	---

6. AUTHOR(S) James A. Ward, Jr. Robert M. Montgomery	
--	--

7. PERFORMING ORGANIZATION NAME(S) AND ADDRESS(ES) Research Triangle Institute * 3000 N. Atlantic Avenue Cocoa Beach, FL 32931	8. PERFORMING ORGANIZATION REPORT NUMBER RTI/5180/77-43F
---	---

9. SPONSORING/MONITORING AGENCY NAME(S) AND ADDRESS(ES) Department of the Air Force (AFSPC) 30th Space Wing Vandenberg AFB, CA 93437 Mr. Martin Kinna (30 SW/SEY)	10. SPONSORING/MONITORING AGENCY REPORT NUMBER 30510-TR-96-12
---	--

11. SUPPLEMENTARY NOTES  
\* Subcontractor  
\*\* Prime Contractor

12a. DISTRIBUTION/AVAILABILITY STATEMENT Distribution authorized to US Government agencies and their contractors to protect administrative/operational use data, 10 September 96. Other requests for this document shall be referred to the 30th Space Wing (AFSPC) Safety Office (30 SW/SE), Vandenberg AFB, CA 93437, or 45th Space Wing (AFSPC) Safety Office (45 SW/SE), Patrick AFB, FL 32925.	12b. DISTRIBUTION CODE 
--	----------------------------

13. ABSTRACT (Maximum 200 words)  
Missile and space-vehicle performance histories contain many examples of failures that cause, or have the potential to cause, significant vehicle deviations from the intended flight line. In RTI's risk-analysis program, DAMP, such failures are referred to as Mode-5 failure responses. Although Mode-5 failure responses are much less likely to occur than those that result in impacts near the flight line, risk-analysis studies are incomplete without them. This report shows how impacts from Mode-5 failures are modeled in program DAMP. The impact density function used for this purpose contains two shaping constants that control the rate at which the density function drops in value as the angular deviation from the flight line and the impact range increase. Certain Mode-5 malfunctions are simulated, and the two shaping constants then chosen by trial and error so that impacts from the simulated malfunctions and the theoretical density function are in close agreement. An appendix to the report contains a listing and brief narrative failure history of the Atlas, Delta, and Titan missile and space-vehicle launches from the Eastern and Western Ranges from the beginning of each program through August 1996. Each entry gives the vehicle configuration, whether the flight was a success, the flight phase in which any anomalous behavior occurred, and a classification of vehicle behavior in accordance with defined failure-response modes.

14. SUBJECT TERMS launch risk, unlikely failure modeling, booster failure probabilities	15. NUMBER OF PAGES 180
	16. PRICE CODE

17. SECURITY CLASSIFICATION OF REPORT Unclassified	18. SECURITY CLASSIFICATION OF THIS PAGE Unclassified	19. SECURITY CLASSIFICATION OF ABSTRACT Unclassified	20. LIMITATION OF ABSTRACT SAR
---	--	---	-----------------------------------

## Abstract

Missile and space-vehicle performance histories contain many examples of failures that cause, or have the potential to cause, significant vehicle deviations from the intended flight line. In RTI's risk-analysis program, DAMP, such failures are referred to as Mode-5 failure responses. Although Mode-5 failure responses are much less likely to occur than those that result in impacts near the flight line, risk-analysis studies are incomplete without them. This report shows how impacts from Mode-5 failures are modeled in program DAMP. The impact density function used for this purpose contains two shaping constants that control the rate at which the density function drops in value as the angular deviation from the flight line and the impact range increase. Certain Mode-5 malfunctions are simulated, and the two shaping constants then chosen by trial and error so that impacts from the simulated malfunctions and the theoretical density function are in close agreement.

An appendix to the report contains a listing and brief narrative failure history of the Atlas, Delta, and Titan missile and space-vehicle launches from the Eastern and Western Ranges from the beginning of each program through August 1996. Each entry gives the vehicle configuration, whether the flight was a success, the flight phase in which any anomalous behavior occurred, and a classification of vehicle behavior in accordance with defined failure-response modes. Various filtering or data weighting techniques are described. The empirical data are then filtered to estimate (1) failure probabilities for Atlas, Delta, and Titan, and (2) percentages of future failures that will result in Mode-5 (and other Mode) responses.

## Table of Contents

1. Introduction.....	1
2. Examples Showing Need for Mode 5 .....	3
3. Understanding the Mode-5 Failure Response.....	7
3.1 Effects of Mode-5 Shaping Constants.....	9
3.2 Effects of Shaping Constant on DAMP Results.....	9
4. Methodology for Assessing Failure Probabilities.....	13
4.1 The Parts-Analysis Approach.....	13
4.2 The Empirical Approach.....	15
5. Computation of Failure Probabilities.....	16
5.1 Overall Failure Probability.....	16
5.2 Relative and Absolute Probabilities for Response Modes.....	24
5.3 Relative Probability of Tumble for Response-Modes 3 and 4.....	30
6. Shaping Constants Through Simulation.....	31
6.1 Malfunction Turn Simulations.....	31
6.1.1 Random-Attitude Failures.....	31
6.1.2 Slow-Turn Failures.....	32
6.1.3 Factors Affecting Malfunction-Turn Results .....	33
6.1.4 Malfunction-Turn Results for Atlas IIAS.....	35
6.2 Shaping Constants for Atlas IIAS.....	37
6.2.1 Optimum Mode-5 Shaping Constants.....	37
6.2.2 Launch-Area Mode-5 Risks.....	49
6.2.3 Effects of Mode-5 Constants on Ship-Hit Contours .....	51
6.2.4 Range Distributions of Theoretical and Simulated Impacts.....	58
6.3 Shaping Constants for Delta-GEM.....	60
6.3.1 Optimum Mode-5 Shaping Constants.....	61
6.3.2 Launch-Area Mode-5 Risks.....	64
6.4 Shaping Constants for Titan IV.....	65
6.5 Shaping Constants for LLV1.....	69
6.6 Shaping Constants for Other Launch Vehicles.....	72
7. Potential Future Investigations.....	73
8. Summary.....	74

Appendix A. Failure Response Modes in Program DAMP .....	79
Appendix B. Shaping-Constant Effects on Mode-5 Impact Distributions.....	81
Appendix C. Filter Characteristics .....	90
Appendix D. Launch and Performance Histories .....	96
D.1 Basic Data .....	96
D.1.1 Data Sources .....	96
D.1.2 Assignment of Failure-Response Modes.....	98
D.1.3 Assignment of Flight Phase.....	98
D.1.4 Representative Configurations .....	100
D.2 Atlas Launch and Performance History .....	101
D.2.1 Atlas Launch History.....	103
D.2.2 Atlas Failure Narratives .....	115
D.3 Delta Launch and Performance History .....	133
D.3.1 Delta Launch History.....	136
D.3.2 Delta Failure Narratives.....	142
D.4 Titan Launch and Performance History .....	146
D.4.1 Titan Launch History.....	149
D.4.2 Titan Failure Narratives .....	157
D.5 Thor Launch and Performance History (Not Including Delta) .....	164
D.5.1 Thor and Thor-Boosted Launch History.....	164
D.5.2 Thor and Thor-Boosted Failure Narratives .....	167
References.....	171

## Table of Figures

Figure 1. Joust Impact Trace Showing a Mode-5 Failure Response.....	6
Figure 2. Atlas IIAS Risk Contours for Inner-Ear Injury with $A = 3.0$ .....	11
Figure 3. Atlas IIAS Risk Contours for Inner-Ear Injury with $A = 3.5$ .....	12
Figure 4. Filter Factor Results for Representative Configurations of Atlas.....	23
Figure 5. Combined Random-Attitude and Slow-Turn Results.....	36
Figure 6. Atlas IIAS Breakup Percentages for Random-Attitude Turns.....	37
Figure 7. Atlas IIAS Impacts with No Breakup .....	39
Figure 8. Atlas IIAS Impacts with Breakup.....	40
Figure 9. Atlas IIAS Simulation Results with $B = 1,000$ .....	42
Figure 10. Atlas IIAS Simulation Results with $B = 50,000$ .....	44
Figure 11. Atlas IIAS Simulation Results with $B = 100,000$ .....	45
Figure 12. Atlas IIAS Simulation Results with $B = 500,000$ .....	46
Figure 13. Atlas IIAS Simulation Results with $B = 5,000,000$ .....	47
Figure 14. Effects of Breakup $q$ -alpha on $A$ for Atlas IIAS .....	49
Figure 15. Mode-5 Density-Function Values at Three Miles .....	51
Figure 16. Atlas IIAS Mode-5 Ship-Hit Contours with $A = 3.00$ .....	53
Figure 17. Atlas IIAS All-Mode Ship-Hit Contours with $A = 3.00$ .....	54
Figure 18. Atlas IIAS Mode-5 Ship-Hit Contours with $A = 3.45$ .....	55
Figure 19. Atlas IIAS All-Mode Ship-Hit Contours with $A = 3.45$ .....	56
Figure 20. Atlas IIAS Mode-5 Ship-Hit Contours with $A = 6.30$ .....	57
Figure 21. Atlas IIAS All-Mode Ship-Hit Contours with $A = 6.30$ .....	58
Figure 22. Impact-Range Distributions.....	59
Figure 23. Delta-GEM Breakup Percentages.....	61
Figure 24. Delta-GEM Simulation Results with $B = 1,000$ .....	62
Figure 25. Delta-GEM Simulation Results with Best-Fit Shaping Constants .....	63
Figure 26. Titan IV Breakup Percentages .....	65
Figure 27. Titan Simulation Results with $B = 1,000$ .....	66
Figure 28. Titan Simulation Results with Best-Fit Shaping Constants.....	67
Figure 29. LLV1 Breakup Percentages.....	69
Figure 30. LLV1 Simulation Results with $B = 1,000$ .....	70

Figure 31. LLV1 Simulation Results with Best-Fit Shaping Constants .....	71
Figure 32. f-Ratios for Ranges from 1 to 25 Miles .....	86
Figure 33. Percentage of Impacts Between Flight Line and Any Radial .....	87
Figure 34. Percentage of Impacts in 5-Degree Sectors.....	88
Figure 35. Exponential Weights for Fading-Memory Filters.....	93
Figure 36. Recursive Filter Factor for Last Data Point.....	94
Figure 37. Atlas Launch Summary.....	102
Figure 38. Delta Launch Summary.....	135
Figure 39. Titan Launch Summary.....	148
Figure 40. Thor Launch Summary .....	164

#### Table of Tables

Table 1. Effects of Mode-5 Shaping Constant A on Atlas IIA Risks.....	10
Table 2. Predicted Failure Probabilities for Representative Configurations.....	17
Table 3. Predicted Failure Probabilities for All Configurations.....	18
Table 4. Comparison of Weighting Percentages .....	19
Table 5. Filter Factor Influence on Weighting Percentages.....	21
Table 6. Failure Probabilities for Atlas, Delta, and Titan.....	24
Table 7. Number of Atlas Failures - All Configurations (532 Flights).....	25
Table 8. Number of Delta Failures - All Configurations (232 Flights).....	25
Table 9. Number of Titan Failures - All Configurations (337 Flights).....	25
Table 10. Number of Eastern-Range Thor Failures (85 Flights) .....	25
Table 11. Number of Failures for All Vehicles (1186 Flights).....	26
Table 12. Date of Most Recent Failure .....	26
Table 13. Percentage Weighting for Sample of 1186 Launches .....	27
Table 14. Response-Mode Occurrence Percentages.....	27
Table 15. Recommended Response-Mode Percentages for Flight Phases 0 - 2.....	28
Table 16. Recommended Response-Mode Percentages for Flight Phases 0 - 1.....	29
Table 17. Absolute Failure Probabilities for Response Modes 1 - 5 .....	29
Table 18. Percent of Response Modes 3 and 4 That Tumble.....	30

Table 19. Sample Impact Distribution for Atlas IIAS with No Breakup .....	41
Table 20. Shaping Constants for Atlas IIAS.....	48
Table 21. Shaping Constants and Related Risks for Atlas IIAS.....	50
Table 22. Best-Fit Conditions for Atlas IIAS.....	52
Table 23. Shaping Constants and Related Risks for Delta-GEM .....	64
Table 24. Shaping Constants for Titan IV .....	68
Table 25. Shaping Constants for LLV1.....	72
Table 26. Summary of A Values for B = 1,000.....	72
Table 27. Failure Probabilities for Atlas, Delta, and Titan.....	75
Table 28. Recommended Response-Mode Percentages for Flight Phases 0 -2.....	75
Table 29. Recommended Response-Mode Percentages for Flight Phases 0 - 1.....	75
Table 30. Absolute Failure Probabilities for Response Modes 1 - 5 .....	76
Table 31. Summary of A Values for B = 1,000.....	77
Table 32. Summary of Optimum Mode-5 Shaping Constants.....	77
Table 33. Effect on f-Ratio of Varying Mode-5 Constant A (B = 1000) - Part 1 .....	82
Table 34. Effect on f-Ratio of Varying Mode-5 Constant A (B = 1000) - Part 2 .....	83
Table 35. Effect on f-Ratio of Varying Mode-5 Constant B (A = 3) - Part 1 .....	84
Table 36. Effect on f-Ratio of Varying Mode-5 Constant B (A = 3) - Part 2.....	85
Table 37. Filter Application for Failure Probability.....	95
Table 38. Flight-Phase Definitions.....	99
Table 39. Flight Phases by Launch Vehicle .....	99
Table 40. Summary of Atlas Vehicle Configurations .....	101
Table 41. Atlas Launch History .....	103
Table 42. Summary of Delta Vehicle Configurations .....	133
Table 43. Delta Launch History.....	136
Table 44. Summary of Titan Vehicle Configurations .....	147
Table 45. Titan Launch History .....	149
Table 46. Thor Launch History.....	165

## 1. Introduction

The debris from most launch vehicles that fail catastrophically tend to impact close to the intended flight line. Typical failures that produce such results are premature thrust termination, stage ignition failure, tank rupture or explosion, or rapid out-of-control tumble. Less likely malfunctions may cause a vehicle to execute a sustained turn away from the flight line. Examples are control failures that cause the rocket engine to lock in a fixed position near null, or failures leading to erroneous orientation of the guidance platform. Such failures should not be ignored, since they may produce nearly all or a significant part of the risks to population centers that are more than a mile or so uprange or many miles away from the flight line. Consequently, RTI has been tasked to estimate the probabilities of occurrence of these less-likely failures, and to determine optimum values for the shaping constants of the associated impact-density function.

RTI has developed a prototype risk-analysis program (1) to analyze the level of risk in the launch area when ballistic missiles and space vehicles are launched, and (2) to provide guidelines for launch operations and launch-area risk management. This program, "facility DAMAge and Personnel injury" (DAMP), uses information about the launch vehicle, its trajectory and failure responses, and facilities and populations in the launch area to estimate hit probabilities and casualty expectations. When a missile or space vehicle malfunctions, people and facilities may be subjected to significant risks from falling inert debris, or from overpressures and secondary debris produced by a stage, component, or large propellant chunk that explodes on impact. Although fire, toxic materials, and radiation may also subject personnel to significant danger, these hazards are not addressed in program DAMP. Hazards are greatest in the launch area and along the intended flight line, but lesser hazards exist throughout the area inside the impact limit lines. Small hazards exist even outside these lines if the flight termination system fails or other unlikely events occur.

In computing launch-area risks, DAMP makes no attempt to model vehicle failures per se. A list of possible failures for any vehicle would be extensive, and variations in failures from vehicle to vehicle would complicate the modeling process. Instead, DAMP models failure *responses*. Regardless of the exact nature of the failures that can occur, there are only six possible response modes that affect risks on the ground, five for failure responses, and one to model the behavior of a normal vehicle. The six modes are described in Appendix A. It can be seen from the descriptions that impacts resulting from failure-response Modes 1, 2, and 3 occur at most a mile or two from the launch point, while those from Mode 4 can only occur near the flight line, even though the vehicle may tumble before breakup or destruct. Although the hazards outside the launch area and away from the flight line may be small, vehicle flight tests through the years have demonstrated that finite hazards do exist in these areas. Such hazards are due almost entirely to Mode-5 failure responses, even though the probability of a Mode-5 failure may be only a small part of the total failure probability. The Mode-5 failure-response, theoretical though it is, was developed to reflect the facts that: (1) unlikely vehicle failures

can cause impacts uprange or well away from the intended flight line, and (2) some vehicle failures cannot logically be classified as Response Modes 1, 2, 3, or 4.

In keeping with the above, the Mode-5 impact-density function was developed with the characteristics listed below. The function, which fills the void left by Modes 1 through 4, is sufficiently robust to include all possible impacts, yet seemingly comports with observed test results.

- (1) Impacts can occur in any direction from the launch point and at any range within the vehicle's energy capabilities.
- (2) At any given impact range from the launch point, the likelihood of impact decreases as the angular deviation from the flight line increases, becoming least likely in the uprange direction. For any fixed angular deviation from the flight line, the likelihood of impact decreases as the impact range increases.
- (3) At fixed impact ranges near the launch point, the impact density function changes gradually as the impact direction swings 180° from downrange to uprange. As the impact range increases, the decrease in the density function becomes progressively more and more rapid with change in impact direction. In other words, the greater the impact range, the more rapidly the density function changes with angular deviation from the flight line.

As modeled in DAMP, the effects of destruct action on the Mode-5 density function are accounted for in the launch area by supplementing impacts inside the impact limit lines with those that would occur outside the impact limit lines if no destruct action were taken.

The Mode-5 failure-response methodology was fully developed in an earlier RTI report<sup>(1)</sup>. As pointed out there, the shape of the impact density function can be controlled somewhat through the selection of shaping constants that appear in the defining equation. Intuition suggests that the constants should be vehicle dependent, since (1) ruggedly built missiles would, after a malfunction, be more likely to impact well away from the flight line than would a fragile space vehicle that tends to break up before deviating significantly; and (2) certain vehicles, after a malfunction, tend to stabilize and continue thrusting at large angles of attack, while other vehicles that experience similar malfunctions tend to tumble. Hit probabilities computed by program DAMP for targets located more than two miles or so uprange from the pad or more than a few miles from the flight line, are due almost entirely to the Mode-5 impact-density function. Thus, the assumed probability of occurrence of a Mode-5 response as well as the selected Mode-5 constants are of considerable importance.

The tasking for this study is set forth as Task No. 10/95-77, Paragraph 2.0, of Contract FO4703-91-C-0112. The primary purpose of the tasking is: "Perform a study to determine the best values for Mode-5 failure probability and the Mode-5 density-function shaping constant  $\Lambda$ ." Although not explicitly included in the statement of work, the study also develops absolute failure probabilities for Atlas, Delta, and Titan, and

relative probabilities of occurrence for all failure-response modes for these vehicles, LLV1, and other new launch systems.

Although it may be reasonable to establish the relative probability of occurrence of a Mode-5 failure response by empirical means, the number of Mode-5 failures is too small to have any hope of establishing accurate values for the shaping constants from this sample alone. Inadequate descriptions of vehicle behavior in the available historical records and uncertainty in impact location following a malfunction add to the difficulty of classifying failure responses. In view of the limited data available for vehicles that have experienced Mode-5 failures, the values chosen for the Mode-5 constants must depend on simulations of vehicle behavior following failure.

## 2. Examples Showing Need for Mode 5

The need for a Mode-5 response or some similar response mode (or a multiplicity of other response modes) can be seen from the following vehicle performance descriptions extracted from Appendix D:

- (1) Atlas 8E, 24 Jan 61. Missile stability was lost at about 161 seconds, some 30 seconds after BECO, probably due to failure of the servo-amplifier power supply. The sustainer engine shut down at 248 seconds, and the vernier engines about 10 seconds later. Impact occurred 1316 miles downrange and 215 miles crossrange.
- (2) Titan M-4, 6 Oct 61. A one-bit error in the W velocity accumulation caused impact 86 miles short and 14 miles right of target.
- (3) Atlas 145D (Mariner R-1), 22 July 62. Booster stage and flight appeared normal until after booster staging at guidance enable at about 157 seconds. Operation of guidance rate beacon was intermittent. Due to this and faulty guidance equations, erroneous guidance commands were given based on invalid rate data. Vehicle deviations became evident at 172 seconds and continued throughout flight with a maximum yaw deviation of 60° and pitch deviation of 28° occurring at 270 seconds. The vehicle deviated grossly from the planned trajectory in azimuth and velocity, and executed abnormal maneuvers in pitch and yaw. The missile was destroyed by the RSO at 293.5 seconds, some 12 seconds after SECO.
- (4) Atlas SLV-3 (GTA-9), 17 May 66. Vehicle became unstable when B2 pitch control was lost at 121 seconds. Loss of pitch control resulted in a pitch-down maneuver much greater than 90°. Guidance control was lost at 132 seconds. After BECO, the vehicle stabilized in an abnormal attitude. Although the vehicle did not follow the planned trajectory, SECO (at 280 seconds), VECO (at 298 seconds), and Agena separation occurred normally from programmer commands.
- (5) Atlas 95F (ABRES/AFSC), 3 May 68. Immediately after liftoff the telemetered roll and yaw rates indicated that the missile was erratic. During the first 10 seconds of flight the missile yawed hard to the left. It then began a hard yaw to the right,

crossed over the flight line and continued toward the right destruct line. Shortly thereafter the missile apparently pitched up violently and the IIP began moving back toward the beach. The missile was destructed at about 45 seconds when the altitude was about 14,000 feet and the downrange distance about 9 miles. Major pieces impacted less than a mile offshore, indicating uprange movement of the impact point during the last part of thrusting flight.

- (6) Delta Intelsat III, 18 Sep 68. Due to loss of rate gyro, undamped pitch oscillations began at 20 seconds. A series of violent maneuvers followed at 59 seconds. During the 13-second period while these maneuvers continued, the vehicle pitched down some 270°, then up 210°, and then made a large yaw to the left. At 72 seconds the vehicle regained control and flew stably in a down and leftward direction until 100 seconds. At this time, with the main engine against the pitch and yaw stops, the destabilizing aerodynamic forces became so large that quasi-control could no longer be maintained. The first stage broke up at 103 seconds. The second stage was destroyed by the RSO at 110.6 seconds. Major pieces impacted about 12 miles downrange and 2 miles left of the flight line.
- (7) Delta Pioneer E, 27 Aug 69. First-stage hydraulics system failed a few seconds before first-stage burnout (MECO). The vehicle pitched down, yawed left, rolled counterclockwise driving all gyros off limits, and then tumbled. Second-stage separation and ignition occurred while the vehicle was out of control. After about 20 seconds, the second stage regained control in a yaw-right, pitch-up attitude. It flew stably in this attitude for about 240 seconds until destroyed by the safety officer at T+484 seconds.
- (8) Atlas 68E, 8 Dec 80. Flight appeared normal until 102.7 seconds when the lube oil pressure on the B2 booster engine suddenly dropped. At 120.1 seconds, the engine shut down, followed 385 msec later by guidance shutdown of the B1 engine. The asymmetric thrust during shutdown caused yaw and roll rates that the flight control system could not correct. As a result, attitude control was lost and the thrusting sustainer pivoted the missile to a retrofire attitude before the vehicle could be stabilized. After the booster package was jettisoned, the missile was stabilized and decelerating in the retrofire mode by 148 seconds. The sustainer continued thrusting in this attitude until 282.9 seconds when reentry heating apparently caused sustainer shutdown and vehicle breakup.

It is obvious from the response-mode definitions in Appendix A that none of the described vehicle failures can be considered as a Mode 1, 2, or 3 response, or a Mode-4 on-trajectory failure.\* Except possibly for (2), it also seems apparent that none can be modeled as either a rapid tumble or a slow turn.

---

\* Although prompt destruct action during any of the described flights might have resulted in a Mode-4 classification, the safety officer typically needs several seconds to evaluate data after a malfunction. Quick action is contrary to safety philosophy if impact limit lines are not threatened and the destruct system is not at risk, since additional flight time enhances the user's opportunity to pinpoint the nature of the problem.

A good illustration of a Mode-5 failure response occurred during launch of Prospector (Joust) on the Eastern Range in June 1991. The Joust consists of a single-stage Castor IV-A solid-propellant rocket motor and a payload module. The "vehicle made a radical pitch-up maneuver due to aft-skirt structural failure at approximately T+14 Seconds." <sup>21</sup> The vacuum instantaneous impact trace from the RSO console is shown in Figure 1. If the safety officer had taken destruct action during the time interval from 18 to 25 seconds, impact would have been well away from the flight line.

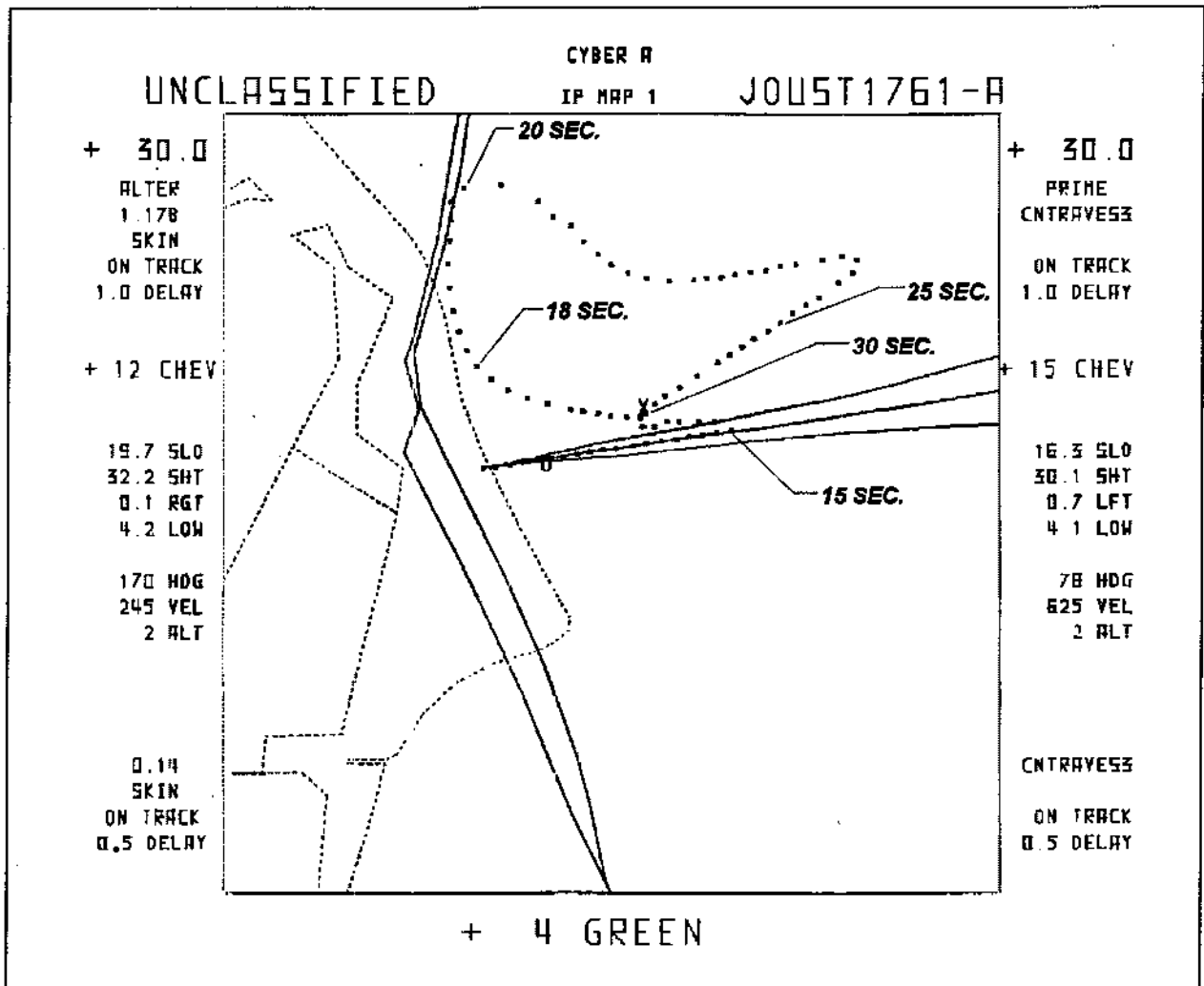


Figure 1. Joust Impact Trace Showing a Mode-5 Failure Response

As still another example of a Mode-5 failure response, a guided Red Tigris sounding rocket was launched from Pad 20 at Cape Canaveral on 20 Aug 91. Within a second or two after clearing the launcher, the rocket made a near 90° right turn, and flew stably in this direction until destroyed by the safety officer at 23.3 seconds. Pieces impacted some two or three miles from the launch pad. This failure might have been classified as a Mode-2 response if destruct action had been taken shortly after launch.

### 3. Understanding the Mode-5 Failure Response

Unlike failure response Modes 3 and 4, response Mode 5 (and also Mode 2) is not a direct function of time from launch. For Modes 3 and 4, the mean point of impact (MPI) for each debris class is fixed, once the failure time is established. At each instant there is only one possible location for the MPI for each debris class. On the other hand, the Mode-5 impact-density function for each debris class consists of a primary part and a secondary superimposed part. The primary impact-density function accounts for impact variability due to the erratic flight of the vehicle. It is used to determine the probability that the mean piece in a debris class resulting from vehicle breakup falls in a given area (say on a building or open field). The secondary density function accounts for debris dispersion due to vehicle breakup and to aerodynamic effects during free fall. It is used to determine the probability that fragments from the class actually hit a building or field. In other words, the primary impact-density function is used to compute the probability that the secondary function is centered in some specified area; the secondary function, which describes the distribution of class pieces about the mean point, is then used to compute the probability that one or more class pieces impacts on the specified population center or area.

The primary part of the Mode-5 impact density function, which was presented as Eq. (9.5) in Ref. [1], is reproduced here as Eq. (1):

$$f(R, \phi) = \frac{Ce^{A\phi} + \frac{D}{R}}{2(T_B - T_P) \left[ \frac{C}{A}(e^{A\pi} - 1) + \frac{D\pi}{R} \right] RR} \quad (1)$$

where  $R$  is the range from the launch point in miles,  $\phi^*$  is the angle in radians between the uprange direction and a line from the pad through the impact point,  $\dot{R}$  is the impact-range rate in miles per second.  $A$  and  $C$  are dimensionless shaping constants, and shaping-constant  $D$  is in miles. For a Mode-5 response, there is by definition an earliest time of occurrence  $T_p$  (pitch-over time) and a latest time of occurrence  $T_b$  (burnout, orbital injection, or some other specified termination time). The specific time in this span at which a Mode-5 response manifests itself is of no consequence, although the duration of the span must be considered in assigning a probability of occurrence for a Mode-5 response.

Given that a Mode-5 response has occurred, the probability that the center of the secondary function lies in some region or on some building (population center) is determined by integrating the primary impact-density function for the class over the region or building. The primary function depends on range ( $R$ ) and direction ( $\phi$ ) from the launch point to the population center, but not directly on time from launch. The primary function does,

---

\* As an aid to understanding, the supplement of  $\phi$ , designated as  $\theta$ , is used in plots and tables in this report.

however, involve the quantity  $\dot{R}$  which is expressed explicitly as a function of R and only implicitly as a function of time. Values of R from the nominal trajectory are differenced to compute  $\dot{R}$ .

The secondary Mode-5 impact-density function is circular normal in form and expressed by the equation

$$f(d) = \frac{1}{2\pi\sigma_c^2} e^{-\frac{1}{2}\left(\frac{d}{\sigma_c}\right)^2} \quad (2)$$

where d is the distance from the impact point of the mean piece to the center of the target, and  $\sigma_c$  is the standard deviation (dispersion) for the debris class. The fact that the center of the secondary impact-density function (or secondary MPI for a debris class) lies on some population center does not necessarily mean that pieces in the class hit the center. The probability that one or more pieces actually hits the pop center is determined by integrating the secondary impact-density function over the center and combining results for all pieces in the class. The dispersions for the secondary function are computed by root-sum-squaring individual dispersions\* arising from the effects of winds, vehicle-breakup velocities, and drag uncertainties for the class. They are computed from the nominal trajectory, and can be explicitly expressed as a function of impact range. Since the pop center can also be hit if the MPI of the secondary density function lies outside the pop center, all possible mutually-exclusive locations of the secondary function that can result in impact on the pop center must be considered. For each mutually-exclusive location, the probability that one or more class pieces impacts on the pop center is calculated, and the results combined to obtain the total hit probability for the class.

The Mode-5 primary impact-density function is modeled so it is independent of how the impact point arrives at a particular location. For example, there are myriad paths that a vehicle can travel to impact at a location two miles crossrange left from the launch pad. Figure 1 shows one such way for a Joust vehicle that failed at 15 seconds, but four seconds later had moved the impact point uprange and crossrange to a position two miles crossrange left from the launch point. Another way to place the impact point two miles crossrange left is for the vehicle to fly in the wrong direction (north instead of east) from liftoff.

Although numerous failure mechanisms and vehicle behaviors can lead to a Mode-5 response and impact in a particular area, the exact mechanism and behavior are irrelevant. All such possibilities are assumed to be accounted for by Eq. (1). Four specific failures that produce Mode-5 responses are easily described: (1) a re-orientation of the guidance platform, (2) insertion of an erroneous spatial target into the guidance system, (3) locking of the engine nozzle in a fixed position near null thus producing a near-constant angular

---

\* These dispersions are a subset of the Mode-4 impact dispersions.

acceleration of the vehicle body and a slow turn of the velocity vector, (4) erroneous accumulation of velocity bits by the guidance system. Many other Mode-5 responses are so convoluted that they defy description or categorization.

### 3.1 Effects of Mode-5 Shaping Constants

The primary part of the Mode-5 impact-density function was presented previously as Eq. (1). As originally formulated, the function contained three shaping constants. If both numerator and denominator of the equation are divided by the constant C, and B is substituted for D/C, one unnecessary constant disappears so that the function may be expressed as follows:

$$f(R, \phi) = \frac{e^{A\phi} + B/R}{2(T_b - T_p) \left[ \frac{1}{A} (e^{A\pi} - 1) + \frac{B\pi}{R} \right] RR} \quad (3)$$

The values chosen for the shaping constants A and B that appear in Eq. (3) influence, but do not change, the basic nature of the Mode-5 impact-density function. For many years values of A = 2.5 and B = 1000 were used in the Eastern Range ship-hit computations, although in more recent risk studies the value of A has been increased to 3.0. This increase resulted from the observation that, in recent years, vehicles that experience Mode-5 failure responses seem less likely than earlier developmental vehicles to deviate significantly from the intended flight line. To see how A and B affect the distribution of Mode-5 impacts, and to further understanding of the function, the results of choosing various values of A and B are provided in Appendix B.

### 3.2 Effects of Shaping Constant on DAMP Results

As pointed out in the Introduction, two important types of constant parameters required by DAMP for risk estimations must be determined. They are: (1) probability of a Mode-5 failure response, and (2) values of the Mode-5 shaping constants A and B, currently set at 3.0 and 1000, respectively. As will be demonstrated later, DAMP results are far more sensitive to changes in A than in B.

The following cases illustrate the effects that constant A has on calculated risks.

#### Case 1: Baseline Risks for Atlas IIA

In the baseline risk analysis for Atlas IIA<sup>(3)</sup>, the probability of a Mode-5 failure response was estimated at 12.5% of the total failure probability during the first 120 seconds of flight. Even so, risks resulting from Mode-5 responses accounted for about 90% of the total risks for people inside the impact limit lines (ILL). Table 1 indicates the range of risks inside the ILLs for day launches from Pad A using various estimates of the shaping constant A and a value of B = 1000.

Table 1. Effects of Mode-5 Shaping Constant A on Atlas IIA Risks

B = 1,000 Constant A	Percent of Mode-5 IPs Uprange	Casualty Expectancy ( $\times 10^6$ ) inside ILLs	
		Mode 5	Total for all Modes
2.5	28.6	246	259.9
3.0	20.7	136	149.4
3.5	14.6	58.9	72.7
4.0	10.0	30.5	44.3

The results in the third column are directly proportional to the probability that a Mode-5 failure occurs. For the Atlas IIA analysis, a value of  $1/200 = 0.005$  was assumed.

### Case 2: Risk Contours for Atlas IIAS

Definitions of *Flight Hazard Area* and *Flight Caution Area* may be based on the risk contours for inner-ear injury. Constant A can have a significant effect on the location of the  $10^{-6}$  contour, as illustrated in Figure 2 and Figure 3 for the Atlas IIAS. For these figures, the Mode-5 absolute probability of occurrence was 0.005, constant A was 3.0 and 3.5, and constant B was 1000.

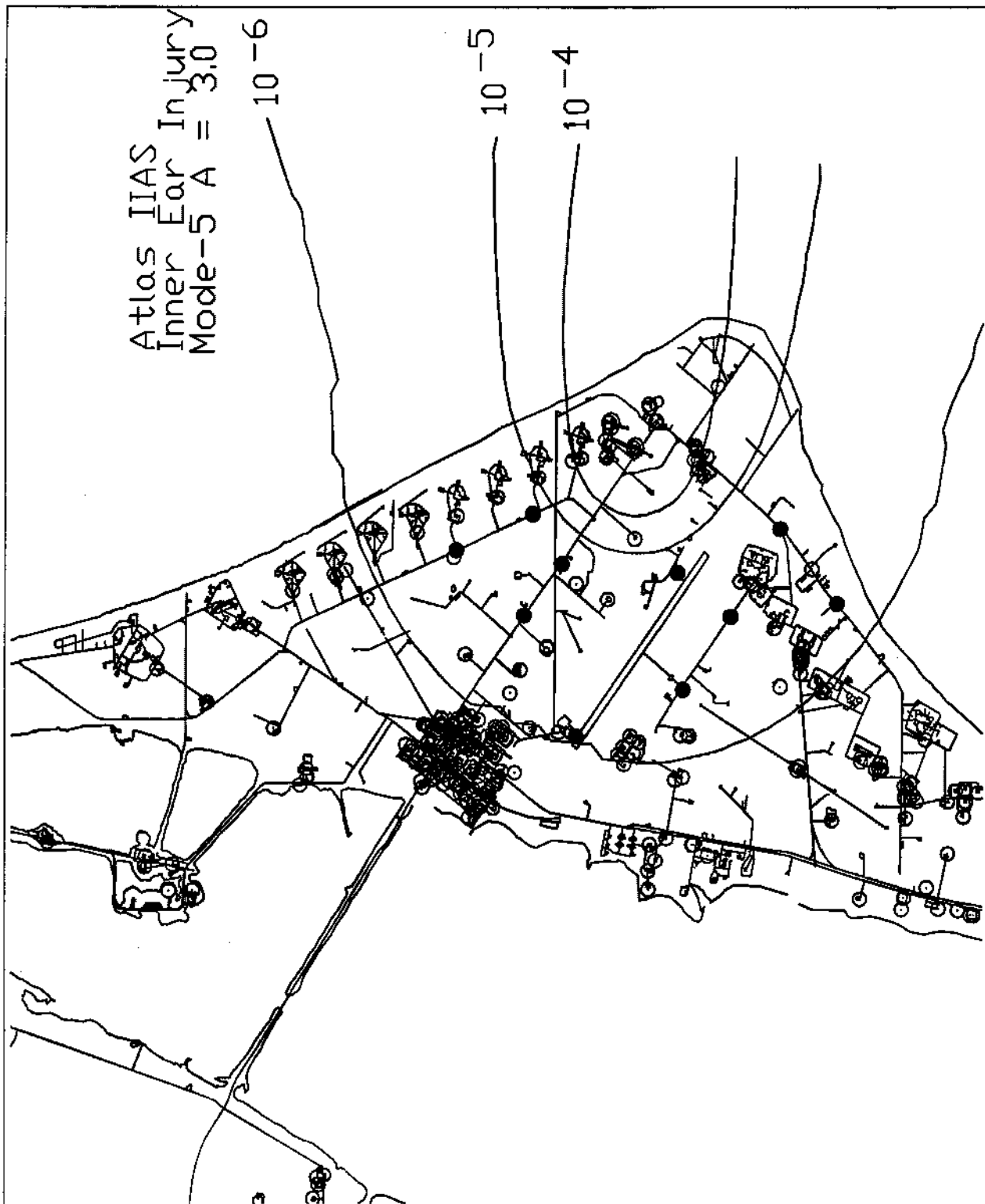


Figure 2. Atlas IIAS Risk Contours for Inner-Ear Injury with A = 3.0

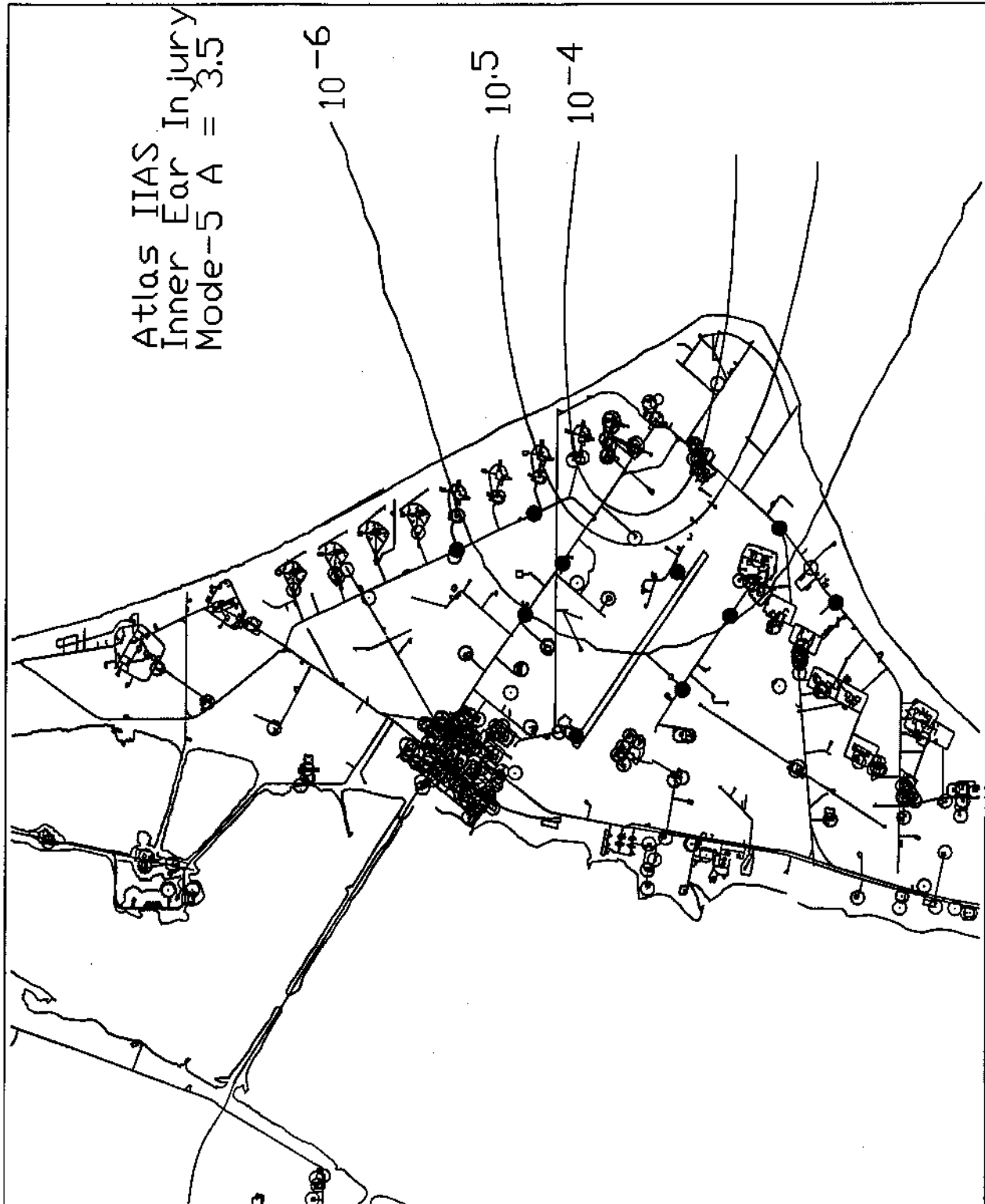


Figure 3. Atlas IIAS Risk Contours for Inner-Ear Injury with A = 3.5

## 4. Methodology for Assessing Failure Probabilities

A primary purpose of this study is to develop estimates of the relative probabilities of occurrence of a Mode-5 failure response for Atlas, Delta, Titan, and as a by-product, for other launch vehicles as well. Natural fallouts of this effort are the relative probabilities of occurrence of other failure-response modes used in program DAMP as well as overall vehicle failure probabilities. There are at least two approaches commonly used in estimating launch-vehicle failure probabilities: (1) a so-called parts-analysis or engineering approach, involving an engineering assessment of the reliability of various parts and components comprising each missile subsystem, and the effects of a part, component or subsystem failure; and (2) an empirical statistical approach based on actual launch results. There are serious problems with both approaches.

### 4.1 The Parts-Analysis Approach

A description of this approach, its difficulties and shortcomings, are discussed in some detail in a draft report by Booz•Allen & Hamilton, Inc.<sup>(4)</sup> prepared in 1992 for the Air Force Space Command. Since we cannot improve on the ideas and words expressed by Booz•Allen, we quote the following from that report:

"The engineering approach for calculation of launch vehicle success rates is based on measurement/estimation of piece-part reliabilities and their combination into reliability block models of the launch system. These block models ... include consideration of the criticality of individual components, the presence (or absence) of redundant capabilities, the likelihood that one component failure might cause a failure in another component, as well as other needed data. By combining the individual piece-part reliabilities in this model, the engineering approach produces an overall reliability estimate for the launch system.

"The engineering approach has several significant limitations that tend to reduce confidence in its results. First, the approach assumes that the interrelationships among and between sub-systems are understood sufficiently to enable development of a reliability block diagram. This assumption is highly questionable in complex systems, such as space launch vehicles, whose operational histories include many anecdotes regarding unexpected relationships between 'independent' sub-systems.

"The second drawback of the engineering approach is that it assesses the reliability of the system in a perfectly assembled condition. As a result, it assesses reliability without regard to manufacturing, processing, or operations variations and errors."

Effects typically overlooked or ignored include:

- a. Improper installation of components
- b. Erroneous computer programs

- c. Insertion of improper computer programs
- d. Support-personnel fatigue

A third limitation of the parts-analysis approach discussed in Ref. [4] deals with the subjectivity and invalid assumptions often used to estimate piece/component reliabilities. Here Booz•Allen quotes from a report<sup>[5]</sup> by the Office of Technology Assessment, and we do likewise:

"The design reliability of proposed vehicles is generally estimated using:

Data from laboratory tests of vehicle systems (e.g., engines and avionics) and components that have already been built;

Engineer's judgments about the reliability achievable in systems and components that have not been built;

Analyses of whether a failure in one system or component would cause other systems and components, or the vehicle to fail; and

Assumptions (often tacit) that:

the laboratory conditions under which systems were tested precisely duplicate the conditions under which the systems will operate,

the conditions under which the system will operate are those under which they were designed to operate,

the engineer's judgments about reliability are correct, and

the failure analyses considered all circumstances and details that influence reliability.

Such engineering estimates of design reliability are incomplete and subjective...".

Effects influencing reliability that the analyst may fail to consider include:

- a. Lightning strikes
- b. Aging effects, particularly for solid propellants
- c. Corrosion
- d. Insufficient heat or cold insulation for critical components
- e. Icing
- f. Erroneous antennae patterns or instrumentation

Booz•Allen concludes as follows:

"Finally, due to its nature, the engineering approach can not account for undetected design flaws. (If these flaws were detected, and could be modeled,

they would be corrected.) However, experience has shown that design flaws do cause failures in operational launch systems, and will likely do so in the future."

The major objection to the parts-analysis approach, hinted at above but not actually expressed, is that all such approaches involve either explicitly or implicitly a so-called K-factor. The K-factor is included in the reliability calculations in an attempt to compensate for the fact that the environment in which a part or system is tested is not the same as the flight environment. Since the K-factor is surely not the same for all components and systems, multiple values must be assumed and the entire process becomes highly subjective.

In view of the objections and limitations just presented, in this report the parts-analysis approach is not considered in assessing vehicle reliability or in estimating the relative probabilities of occurrence of the various failure-response modes.

#### **4.2 The Empirical Approach**

A seemingly more objective way to evaluate vehicle reliability (or conversely, vehicle failure probabilities) is by examining the actual performance of flight-tested vehicles. In support of this approach, the following is quoted from the Office of Technology Assessment<sup>[5]</sup> report previously referenced:

"The only completely objective method of estimating a vehicle's probability of failure is by statistical analysis of number of failures observed in identical vehicles under conditions representative of those under which future launches will be attempted."

Although we agree with the Office of Technology Assessment statement, the obvious difficulty with this approach is that no such sample of identical vehicles exists or is ever likely to exist.

In their report<sup>[6]</sup> previously referenced, Booz • Allen makes the same point in different words by stating that "the empirical approach has one significant drawback in that it can not project the effects of changes in the launch systems". The effects of such changes can only be assessed objectively by further flight testing.

The difficulty in projecting success rates (or failure rates) from past tests to future tests is clearly recognized. Nevertheless, RTI has relied exclusively on this method to estimate the relative probabilities of occurrence for the various failure-response modes. Even so, total objectivity cannot be claimed since, as will be seen later, the answers depend to a large extent on how the performance data are filtered, and how big a risk one wants to take that the true failure probability is underestimated.

## 5. Computation of Failure Probabilities

The test results for Atlas, Delta, and Titan in the tables of Appendix D have been used for three primary purposes:

- (1) To predict or estimate the overall probability that each vehicle will fail during the various phases of flight (see Table 39, Appendix D, for flight-phase definitions).
- (2) To establish the relative and overall probabilities for Response Modes 1 through 5.
- (3) To establish the relative frequency of tumble for Response Modes 3 and 4.

### 5.1 Overall Failure Probability

To predict failure probabilities for Atlas, Delta, and Titan, the test results in Appendix D for representative configurations (i.e., "1" in last column) have been filtered using three different weighting techniques described in Appendix C:

- (1) Equal weighting
- (2) Index-count weighting
- (3) Exponential weighting

In computing filtered or weighted failure probabilities, a test is assigned a score of one to indicate the occurrence of a failure or some anomalous behavior, and a score of zero if no failure occurred. Admittedly, there may be disagreements about the classification of a few flights, since the launch agency may consider as successful or partially successful some flights that are shown as failures in Appendix D. To avoid such disagreements, it is better to think of some non-normal events, particularly those occurring late in flight, as anomalies rather than failures. The flight phases, as shown in column 2 of Table 2 and defined in Appendix D.1.3, are inclusive; e.g., flight phase "0 - 3" includes phases 0, 1, 1.5, 2, 2.5, and 3. An 'NA' in the response-mode column in the tables of Appendix D indicates that some failure or anomalous behavior has had an effect on the final orbit or impact point without producing additional risks to people on the ground or necessarily failing the mission. In the failure-probability calculations of Table 2 and Table 3, an 'NA' has been considered as a success for all flight phases except "0 - 5", irrespective of the phase in which the failure or anomalous behavior took place. Only in flight phase "0 - 5" is an 'NA' response considered a failure. The filtered results for representative configurations (defined in Appendix D.1.4) are given in Table 2 for six flight phases. For flights with multiple entries in the Response-Mode and Flight-Phase columns (e.g., see Appendix D.2.1, No. 257), the first listed value was used in the filtering process.

Table 2. Predicted Failure Probabilities for Representative Configurations

Vehicle	Flight Phase	Filter Technique					Sample Failures /Total
		Equal Weight	Index Count	Expon. F = 0.99	Expon. F = 0.98	Expon. F = 0.97	
Atlas	0	0	0	0	0	0	0/7
	0 - 1	0.0256	0.0253	0.0245	0.0219	0.0186	4/156
	0 - 2	0.0449	0.0385	0.0387	0.0313	0.0243	7/156
	0 - 3	0.0769	0.0715	0.0714	0.0643	0.0568	12/156
	0 - 4	0.0833	0.0811	0.0801	0.0740	0.0663	13/156
	0 - 5 *	0.1090	0.1100	0.1078	0.1019	0.0929	17/156
Delta	0	0	0	0	0	0	0/125
	0 - 1	0.0160	0.0126	0.0134	0.0104	0.0075	2/125
	0 - 2	0.0160	0.0126	0.0134	0.0104	0.0075	2/125
	0 - 3	0.0160	0.0126	0.0134	0.0104	0.0075	2/125
	0 - 4	0.0160	0.0126	0.0134	0.0104	0.0075	2/125
	0 - 5 *	0.0640	0.0447	0.0535	0.0469	0.0442	8/125
Titan	0	0.0306	0.0210	0.0225	0.0292	0.0352	3/98
	0 - 1	0.0234	0.0305	0.0314	0.0403	0.0470	4/171
	0 - 2	0.0409	0.0496	0.0514	0.0642	0.0750	7/171
	0 - 3	0.0526	0.0581	0.0597	0.0689	0.0773	9/171
	0 - 4	0.0526	0.0581	0.0597	0.0689	0.0773	9/171
	0 - 5 *	0.1111	0.1167	0.1188	0.1284	0.1358	19/171

\* Includes response mode 'NA'

It is apparent from the data in Table 2 that estimates of future vehicle reliability depend on the filtering (i.e., weighting) technique applied. Since there are many ways to perform the filtering, all generally producing slightly different results, the choice of method to use in deriving empirical failure probabilities cannot be totally objective. Subjective decisions must also be made about which past configurations to consider as representative of future vehicles, which flight tests to include in the sample, how to weight the individual flights, and, in unusual cases, whether to consider a flight a success or a failure, and to which flight phase to attribute a failure. Except for data weighting (i.e., choice of filter), these decisions were made for Atlas, Delta, and Titan before computing the failure probabilities shown in Table 2.

For Atlas and Delta, it can be seen from Table 2 that the predicted failure probabilities computed with the exponential filter decrease as the value of F decreases. Since a decreasing F means more emphasis on recent data and less emphasis on the old, the launch reliability for these vehicles is apparently improving. The reverse seems to be true for Titan, suggesting either that Titan reliability is not improving or, possibly, that improvements that have been or are being made to the vehicle are not yet fully reflected in the test results. For Atlas and Delta, the computed failure probabilities based on equal weighting are higher than for all other filters, and the predicted failure

probabilities using index-count filtering are larger than those for exponential filtering. For Titan, the results are mixed, further suggesting that Titan reliability has not improved in recent years.

For comparison purposes, the same filtering techniques have been applied to all flight tests shown in the tables of Appendix D, regardless of configuration. The results are presented in Table 3.

Table 3. Predicted Failure Probabilities for All Configurations

Vehicle	Flight Phase	Filter Technique					Sample Failures /Total
		Equal Weight	Index Count	Expon. F = 0.99	Expon. F = 0.98	Expon. F = 0.97	
Atlas	0	0	0	0	0	0	0/7
	0 - 1	0.1053	0.0641	0.0422	0.0273	0.0190	56/532
	0 - 2	0.1711	0.0990	0.0555	0.0311	0.0204	91/532
	0 - 3	0.2086	0.1261	0.0802	0.0559	0.0455	111/532
	0 - 4	0.2143	0.1330	0.0873	0.0627	0.0511	114/532
	0 - 5 *	0.2575	0.1671	0.1150	0.0866	0.0725	137/532
Delta	0	0	0	0	0	0	0/196
	0 - 1	0.0172	0.0164	0.0148	0.0110	0.0077	4/232
	0 - 2	0.0259	0.0232	0.0201	0.0133	0.0085	6/232
	0 - 3	0.0431	0.0279	0.0263	0.0150	0.0089	10/232
	0 - 4	0.0431	0.0279	0.0263	0.0150	0.0089	10/232
	0 - 5 *	0.1078	0.0766	0.0740	0.0536	0.0459	25/232
Titan	0	0.0306	0.0137	0.0187	0.0281	0.0349	3/98
	0 - 1	0.0534	0.0319	0.0351	0.0399	0.0467	18/337
	0 - 2	0.1424	0.0771	0.0719	0.0662	0.0750	48/337
	0 - 3	0.1632	0.0924	0.0830	0.0711	0.0770	55/337
	0 - 4	0.1662	0.0942	0.0840	0.0712	0.0771	56/337
	0 - 5 *	0.1958	0.1369	0.1326	0.1277	0.1346	66/337

\* Includes response mode 'NA'

A comparison of Table 2 and Table 3 shows that in most cases, but not all, exponential filtering produces failure probabilities for the representative configuration samples that are smaller than the corresponding probabilities for the all-configuration samples. The fact that most differences between corresponding samples are relatively small attests to the effectiveness of the exponential filter in down-weighting early launch failures. This is not the case for equal weighting of tests, where the predicted failure probabilities based on all configurations are up to 3.6 times as large.

With respect to the weighting of missile and space-vehicle performance data, RTI favors an exponential filter over either the equal-weight or index-count filters. Weighting percentages for the three filters are given in Table 4 for sample sizes of 4 to 1,000. Except for small samples, the percentages produced by equal weighting place too much emphasis on old data, thus failing to account for the learning process and

hardware improvements that have taken place through the years. For samples approaching 100 or so, it seriously over-weights the old data and under-weights the more recent events. Although equal weighting does not seem suitable for this application, it could be appropriate in other large-sample situations, for example, predicting the failure probability of devices that are all manufactured at the same time by the same process, and tested to the same standards.

Table 4. Comparison of Weighting Percentages

Sample Size	Filter *	Last + Point	Last 5 Points	Last 10 Points	Last 25 Points	Last 50 Points	Last Half
4	Expon.	25.8	-	-	-	-	51.0
	Index	40.0	-	-	-	-	70.0
	Equal	25.0	-	-	-	-	50.0
10	Expon.	10.9	52.5	100.0	-	-	52.5
	Index	18.2	72.7	100.0	-	-	72.5
	Equal	10.0	50.0	100.0	-	-	50.0
20	Expon.	6.0	28.9	55.0	-	-	55.0
	Index	9.5	42.9	73.8	-	-	73.8
	Equal	5.0	25.0	50.0	-	-	50.0
100	Expon.	2.3	11.1	21.1	45.7	73.3	73.3
	Index	2.0	9.7	18.9	43.6	74.8	74.8
	Equal	1.0	5.0	10.0	25.0	50.0	50.0
200	Expon.	2.0	9.8	18.6	40.4	64.7	88.3
	Index	1.0	4.9	9.7	23.4	43.7	74.9
	Equal	0.5	2.5	5.0	12.5	25.0	50.0
500	Expon.	2.0	9.6	18.3	39.7	63.6	99.4
	Index	0.4	2.0	4.0	9.7	19.0	75.0
	Equal	0.2	1.0	2.0	5.0	10.0	50.0
1000	Expon.	2.0	9.6	18.3	39.7	63.6	99.996
	Index	0.1	1.0	2.0	4.9	9.7	75.0
	Equal	0.1	0.5	1.0	2.5	5.0	50.0

\* F = 0.98 for exponential filter

+ "Last" refers to the most recent data point

The index-count filter has serious deficiencies when applied to either small or large samples of missiles and space vehicles. For small samples, too much emphasis is placed on recent data. For a sample of four, 40% of the total weight is given to the last test, and 70% to the last two tests. For a sample of ten, 18.2% of the total weight is given to the last test and 72.7% to the last five tests. The reliability improvement rate implied by these weightings seems too optimistic unless there were serious design flaws in the early configurations that were discovered and corrected. Since many types of failures surely exist that occur only once in 50 or once in 100 or more launches, the tenth launch may be no better than the first for predicting the probability of occurrence of such failures. For large samples, the index-count filter under-weights current data

more and more as the sample size increases. For samples of 200, 500, and 1000, the weighting of the last 50 tests are, in each case, 43.7%, 19.0%, and 9.7% of the total weight. For samples of 100 or more, no matter how large, the index-count filter assigns 25% of the data weight to the oldest half of the data sample - too much in RTI's opinion.

For missiles and space vehicles, the data weightings imposed by the exponential filter ( $F = 0.98$ ) appear reasonable. For small samples less than 20 or so, there is little difference between equal and exponential weightings. For sample sizes near 80, the index-count and exponential filters produce similar results. For sample sizes of 200 and more, the weights assigned to the most recent 5, 10, 25, and 50 tests are essentially constant, showing the fading-memory nature of the exponential filter.

The denominator of the exponential-filter equation [Eq. (18), Appendix C] is a geometric series that asymptotically approaches a limit of  $[1/(1 - F)]$  as  $n$  approaches infinity. For  $F = 0.98$ , that limit is 50. Thus, the last data point, which is always given a weight of one, can never be weighted less than 2% of the total, no matter how large the sample. For samples of 200 and 300, the oldest half of the data receives only 11.7% and 5% of the total weight. For samples of 500 and larger, the oldest half of the data sample is essentially omitted altogether. The exponential filter is clearly a fading-memory filter, as it should be for space-vehicle performance data.

Having decided upon the exponential filter as the best method for weighting missile and space-vehicle performance data, a filter constant  $F$  must be chosen. To see how data weighting varies with filter-factor value, weighting percentages for various samples were computed for representative configurations of Atlas, Delta, and Titan using values of  $F$  from 0.96 to 0.995. The results are shown in Table 5.

Table 5. Filter Factor Influence on Weighting Percentages

Vehicle (sample)	Filter Const	Last Point	Last 10 Points	Last 50 Points	Last Half *	Last 100 Points	Pt. Ratio last: first
Atlas (156)	0.96	4.01	33.6	87.2	96.0	98.5	560
	0.97	3.03	26.5	78.9	91.5	96.1	112
	0.98	2.09	19.1	66.4	82.9	90.6	22.9
	0.99	1.26	12.1	49.9	68.7	80.1	4.7
	0.995	0.92	9.0	40.9	59.7	72.7	2.2
Delta (125)	0.96	4.02	33.5	87.5	92.9	98.9	158
	0.97	3.07	26.9	80.0	87.3	97.4	43.7
	0.98	2.17	19.9	69.1	78.3	94.3	12.2
	0.99	1.40	13.4	55.2	65.6	88.6	3.5
	0.995	1.07	10.5	47.6	58.2	84.7	1.9
Titan (171)	0.96	4.00	33.5	87.1	97.1	98.4	1030
	0.97	3.02	26.4	78.6	93.2	95.8	177
	0.98	2.07	18.9	65.7	85.1	89.6	31.0
	0.99	1.22	11.7	48.1	70.5	77.2	5.5
	0.995	0.87	8.5	38.5	60.8	68.5	2.3

\* Last half + 1 if sample size is odd

Although the choice of a filter constant cannot be completely objective, use of a value less than 0.97 or greater than 0.99 produces undesirable weightings. For  $F = 0.96$ , for example, the most recent test result for Titan is weighted 1030 times that for the oldest test; the last 50 data points receive 87.1% of the total weighting, leaving only 12.9% for the first 121 flights; the last 100 flights receive 98.4% of the total weighting thus, in effect, omitting the oldest 71 flights from the solution.

At the high end of the  $F$  spectrum, a value of 0.995 fails to down-weight the old test results sufficiently. Using Atlas as an example, the most recent data point (1/31/96) is weighted only 2.2 times that of the oldest data point (8/14/64). The oldest half of the data, stretching from 8/14/64 to 3/06/73, receives 40% of the total weight, and the earliest 56 launches, comprising 36% of the data, receive 27% (100 - 73) of the total weight. This is not too different from equal weighting of tests, a procedure that fails to acknowledge the improvements in Atlas reliability that have taken place over a period of 32 years.

In choosing a value of  $F$ , an attempt is made to strike a suitable balance between two contrary objectives:

- (1) to down-weight substantially those failures for which the probability of occurrence has been greatly reduced through redesign and replacement of components, improved test procedures, and the like;

- (2) to down-weight only slightly, or not at all, those failures that are random in nature, that can still occur in replacement components, or that occur only once in 100 or several hundred launches in components that have not yet failed.

No matter what technique is employed, filtering is at best a compromise. The perfect filter would somehow down-weight to some extent or entirely those failures that have been "fixed" or made less likely, without down-weighting those random failures with unknown causes. The filters considered in this study have no such capabilities; they produce a result based solely on the launch sequence, and where in the sequence failures have occurred.

In predicting vehicle failure probabilities from empirical data, large representative samples are essential for a good estimate, and the more reliable the vehicle, the greater the need for a large sample. For example, if some characteristic exists in exactly 1% of a population, the probability is 0.37 that it will not appear in a random sample of 100, and 0.61 that it will not appear if the sample size is 50. If the characteristic exists in 2% of the population, it fails to appear about 36% of the time in a random sample of 50.

For reasons presented above, the data samples for Atlas, Delta, and Titan have been made as large as possible consistent with the notion of representative configurations, as set forth in Ref. [4]. In RTI's judgment, the value of  $F$  that best weights the performance data is 0.98, although a value anywhere in the interval 0.97 to 0.99 cannot be ruled out. For consistency in data weighting, the same values of  $F$  have been used for all vehicle programs. The differences in predicted failure probability that result from these three  $F$ 's are illustrated in Figure 4 for Atlas. The plots show the inverse relationship between filter volatility and the value of  $F$ . For  $F = 0.97$  vis-à-vis larger values, it can be seen that the filtered failure probability jumps higher with each failure and drops at a faster rate with each successful launch that follows.

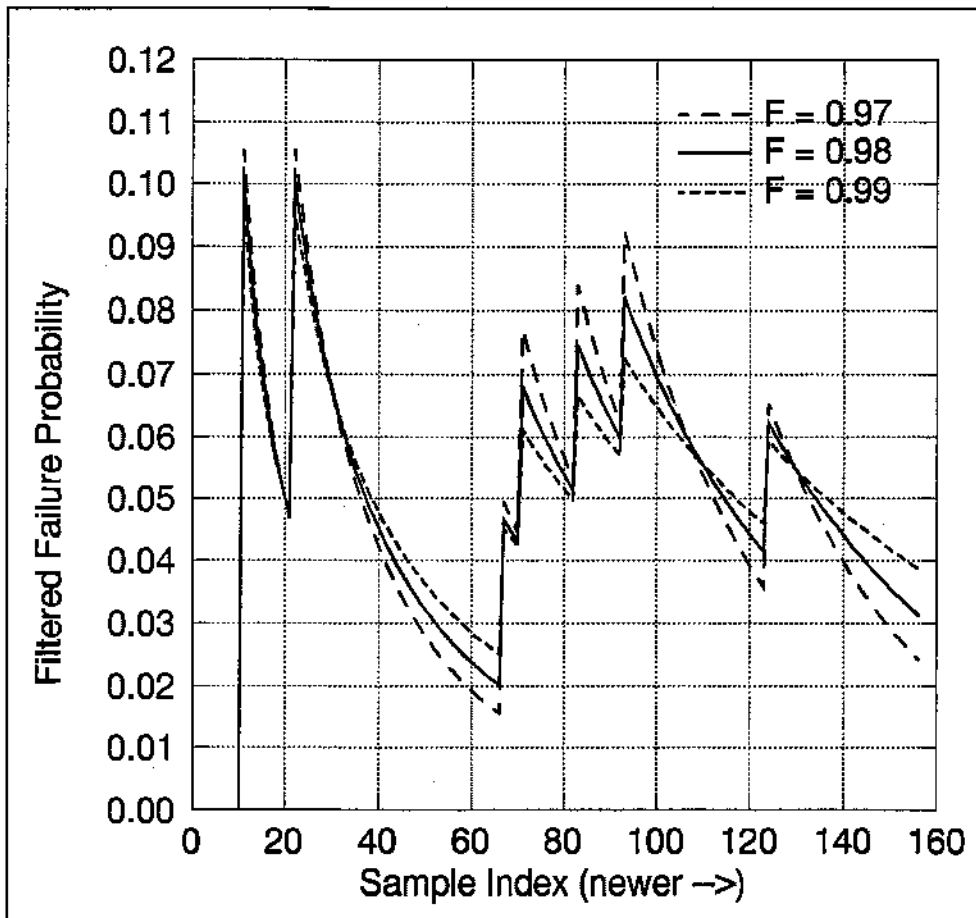


Figure 4. Filter Factor Results for Representative Configurations of Atlas

In summary, it must be recognized that there is no "correct" value for  $F$ , and that it is even difficult to argue generally that one value of  $F$  is better than another. In RTI's view, values of  $F$  below 0.97 place too much emphasis on a relatively small sample of recent launches. Values above 0.99 extend the sample so far back in time that too little emphasis is placed on improvements in design, materials, and operational procedures. In any event, the value chosen for  $F$  is crucial in arriving at a predicted failure probability. For the more conservative, a value of 0.99 can be chosen; the optimistic might chose 0.97.

Since most risk-analysis studies that RTI makes are concerned with the launch area, failure probabilities beyond flight-phase 2 are of minor interest. The overall failure probabilities shown in Table 6 have, with one exception, been extracted from Table 2 for  $F = 0.98$ . Where a best estimate is called for, RTI plans to use these probabilities in future launch-area risk analyses for the 45 SW/SE unless directed otherwise, or until additions to the data samples in Appendix D justify changes.

Table 6. Failure Probabilities for Atlas, Delta, and Titan

Vehicle	Predicted Failure Probability *	
	Flight Phase	Flight Phase
	0 - 1	0 - 2
Atlas	0.022	0.031
Delta	0.010	0.013
Titan	0.040	0.064

\* Exponential filter with  $F = 0.98$

For Delta, the predicted failure probabilities shown in Table 2 for flight-phases 0 - 1 and 0 - 2 are the same, since no second-stage failure has occurred in the 125 flights included in the representative sample. Obviously, this does not mean that the probability of a Delta second-stage failure is zero. As stated earlier, the choice of  $F$  is a judgment matter with the most reasonable range for  $F$  considered to be  $0.97 \leq F \leq 0.99$ . To show a difference in failure probabilities between Delta flight phases, a value of  $F = 0.98$  has been used for flight phases 0 - 1, and 0.99 for flight phases 0 - 2. It is an interesting coincidence that the same value of 0.013 is obtained using  $F = 0.98$  and all Delta configurations (see Table 3). Another way to estimate the Delta second-stage failure probability is to calculate an upper confidence limit at some suitable level for an event that has occurred zero times in 125 trials. At the 80% confidence level, the reliability is at least 0.987, so the failure probability during second-stage burn (flight phases 1.5 - 2) is no bigger than 0.013.

## 5.2 Relative and Absolute Probabilities for Response Modes

For Atlas, Delta, and Titan vehicles, failure-response Modes 1, 2, and 3 are much less likely to occur than Modes 4 and 5. Since the probabilities of occurrence for the less-likely modes may be only one in a thousand or less, such responses may not have occurred at all in the flight tests of representative configurations. In fact, in the combined samples for Atlas, Delta, and Titan, only 16 failures have occurred during flights phases 0 - 2. None of the 16 resulted in response-modes 1, 2, or 3. Because of the small number of failures in the representative configuration samples, the relative probabilities of occurrence for Modes 1 through 5 have been estimated using results from all vehicle configurations and launches shown in Appendix D. The rationale for this approach is that, except for obvious problems that have been corrected, other changes made through the years to improve vehicle reliability have reduced the probabilities of occurrence of all response modes more or less proportionally. The greater significance of more recent vehicle modifications and test results is accounted for by using an exponential filter to estimate overall failure probabilities. Thus, if Mode-1 failures occurred more frequently in the distant past than in recent years, the weighting process reduces the significance of the earlier Mode-1 responses in the relative probability-of-occurrence calculations. As tabulated from Appendix D, the number (count) of failures by response mode and flight phase for Atlas, Delta, Titan, and Eastern-Range Thor launches are given in Table 7 through Table 10. Thor launches

from the Western Range were not included since available performance records were incomplete. The results for the four vehicles are combined in Table 11. Table 12 gives last-occurrence dates by response mode for each launch vehicle.

Table 7. Number of Atlas Failures - All Configurations (532 Flights)

Flight Phase	Failure-Response Mode						3 & 4 Tumble
	1	2	3	4	5	'NA'	
0	0	0	0	0	0	0	0
0-1	7	1	2	38	8	4	11
0-2	7	1	2	66	15	13	19
0-3	7	1	2	86	15	18	25
0-4	7	1	2	89	15	21	27
0-5	7	1	2	89	15	23	27

Table 8. Number of Delta Failures - All Configurations (232 Flights)

Flight Phase	Failure-Response Mode						3 & 4 Tumble
	1	2	3	4	5	'NA'	
0	0	0	0	0	0	0	0
0-1	0	0	0	2	2	5	0
0-2	0	0	0	4	2	10	1
0-3	0	0	0	7	3	12	1
0-4	0	0	0	7	3	13	1
0-5	0	0	0	7	3	15	1

Table 9. Number of Titan Failures - All Configurations (337 Flights)

Flight Phase	Failure-Response Mode						3 & 4 Tumble
	1	2	3	4	5	'NA'	
0	0	0	0	3	0	0	1
0-1	2	2	0	13	1	0	5
0-2	2	2	0	39	5	3	10
0-3	2	2	0	46	5	5	11
0-4	2	2	0	47	5	7	11
0-5	2	2	0	47	5	10	11

Table 10. Number of Eastern-Range Thor Failures (85 Flights)

Flight Phase	Failure-Response Mode						3 & 4 Tumble
	1	2	3	4	5	'NA'	
0	0	0	0	0	0	0	0
0-1	4	1	1	15	4	1	3
0-2	4	1	1	20	5	3	3
0-3	4	1	1	22	5	3	3
0-4	4	1	1	22	5	4	3
0-5	4	1	1	22	5	5	3

Table 11. Number of Failures for All Vehicles (1186 Flights)

Flight Phase	Failure-Response Mode						3 & 4 Tumble
	1	2	3	4	5	'NA'	
0	0	0	0	3	0	0	1
0-1	13	4	3	68	15	11	19
0-2	13	4	3	129	27	29	33
0-3	13	4	3	161	28	38	40
0-4	13	4	3	165	28	45	42
0-5	13	4	3	165	28	53	42

Table 12. Date of Most Recent Failure

Response Mode	Vehicle			
	Atlas	Delta	Titan	Thor *
1	03/02/65	none	12/12/59	04/19/58
2	12/18/81	none	05/01/63	12/30/58
3	04/25/61	none	none	07/21/59
4	08/22/92	05/03/86	10/05/93	03/24//64
5	12/08/80	08/27/69	11/30/65	01/24/62

\* Last Thor launch was 02/23/65

For the reasons advanced previously, an exponential filter has been used to estimate relative probabilities of occurrence for Modes 1 through 5 and the fraction of Mode-3 and Mode-4 failures that tumble while the vehicle is thrusting. The percentage weightings for various data samples are shown in Table 13 for values of F from 0.980 to 0.999. Because of the large size of the composite sample (1186), the filter-control constant of 0.98 used previously to estimate absolute failure probabilities for individual vehicles does not seem suitable for estimating relative probabilities for the individual response modes. Use of 0.98 would effectively place 98.2% of the total weight on the most recent 200 tests thus, in effect, eliminating the earliest 986 tests from the solution. These are the very tests needed to provide an adequate sample of failures from which to estimate relative frequencies of occurrence of the individual response modes.

Table 13. Percentage Weighting for Sample of 1186 Launches

Filter Constant	Last Point	Last 100 Points	Last 200 Points	Last 300 Points	Last 500 Points	Point Ratio Last:First
0.999	0.14	13.7	26.1	37.3	56.7	3.3
0.996	0.40	33.3	55.6	70.6	87.3	$1.2 \times 10^2$
0.995	0.50	39.5	63.5	78.0	92.1	$3.8 \times 10^2$
0.994	0.60	45.3	70.0	83.6	95.1	$1.3 \times 10^3$
0.993	0.70	50.5	75.5	87.9	97.0	$4.2 \times 10^3$
0.992	0.80	55.2	79.9	91.0	98.2	$1.4 \times 10^4$
0.991	0.90	59.5	83.6	93.4	98.9	$4.5 \times 10^4$
0.990	1.00	63.4	86.6	95.1	99.3	$1.5 \times 10^5$
0.980	2.00	86.7	98.2	99.8	99.996	$3.9 \times 10^{11}$

The value of F = 0.999 is considered inappropriate because, as seen in Table 13, the weighting factor applied to the most recent datum is only 3.3 times that applied to the oldest test result from 39 years ago. The most recent 200 and 300 points in the sample comprising 16.8% and 25.2% of the data receive only 26.1% and 37.3% of the total weight. This is not too different from equal weighting of data, which is appropriate only if the relative frequency of occurrence of each response mode has not changed significantly through the years. On the other hand, use of F = 0.99 effectively throws out the oldest 600 to 700 launches that are sorely needed for an adequate sample size.

The results of the filtering process are given in Table 14 for failures during flight phases 0 - 2.

Table 14. Response-Mode Occurrence Percentages

Filter Factor	Response Mode				
	1	2	3	4	5
0.999	7.39	2.27	1.70	73.30	15.34
0.996	2.24	4.35	0.37	80.37	12.67
0.995	1.32	4.92	0.19	82.59	10.98
0.994	0.73	5.26	0.09	84.57	9.35
0.993	0.39	5.37	0.04	86.25	7.95
0.992	0.20	5.31	0.02	87.68	6.78
0.991	0.11	5.13	0.01	88.92	5.84
0.990	0.05	4.87	0.00	90.02	5.06
0.980	0.00	1.86	0.00	96.81	1.33

The results in Table 14 show that the percentages of occurrence for response-modes 2 and 4 are relatively insensitive to filter-factor values, while the percentages for Modes 1, 3, and 5 decrease as filter memory (filter factor) decreases. This suggests that occurrences of Modes 1, 3, and 5 have been decreasing over the years, while Modes 2 and 4 occurrences have not changed much. Although it cannot be argued convincingly

that 0.993 is superior to 0.992 or 0.994, or even values outside this interval, a value of 0.993 was chosen.

This section has thus far described a rationale for selecting a filtering process and filter constant to estimate percentages of occurrence of failure-response modes for Atlas, Delta, and Titan launch vehicles. These are mature launch systems with improved reliability as a result of years of experience and corrections of problems. Although the designs of new launch vehicles may be based to some extent on mature systems, new systems are expected to fail at a higher rate. For vehicles with liquid-propellant stages burning at liftoff, the percentages of occurrence of the various response modes are more likely to be similar to the earlier versions of Atlas, Delta, and Titan than to current vehicles. For lack of any other data, for such new liquid-propellant systems the relative percentages for the five failure-response modes have been calculated using the total combined sample of Atlas, Delta, Titan, and Thor with a filter constant of 0.999 (almost equal weighting).

For new solid-propellant vehicles, use of  $F = 0.999$  results in a Mode-1 percentage that seems much too high. All of the 13 Mode-1 failures in the composite sample (Table 11) involved liquid-propellant vehicles, whereas none of the Atlas, Delta, or Titan configurations with solid-propellant boosters have experienced a Mode-1 response. On the other hand, use of  $F = 0.993$  that is applied for mature launch systems seems to reduce the probability of a Mode-5 response too much, since a Red Tigris vehicle and a Joust vehicle launched at the Cape in 1991 both experienced Mode-5 failure responses (see Section 2). As a compromise between new and mature liquid-propellant vehicles, a value of  $F = 0.996$  has been assumed for new solid-propellant vehicles. The percentages shown in Table 15 for flight phases 0 - 2 have been obtained from Table 14. Similar information for flight phases 0 - 1 are given in Table 16. In future risk studies for the 45 SW/SE, RTI plans to use these relative percentages for mature and new systems.

Table 15. Recommended Response-Mode Percentages for Flight Phases 0 - 2

Response Mode	Mature Launch Systems (F = 0.993)	New Solid Systems (F = 0.996)	New Liquid Systems (F = 0.999)
1	0.4	2.2	7.4
2	5.4	4.3	2.3
3	0.1	0.4	1.7
4	86.2	80.4	73.3
5	7.9	12.7	15.3

Table 16. Recommended Response-Mode Percentages for Flight Phases 0 - 1

Response Mode	Mature Launch Systems (F = 0.993)	New Solid Systems (F = 0.996)	New Liquid Systems (F = 0.999)
1	0.5	3.4	10.7
2	7.4	6.6	4.3
3	0.1	0.6	2.4
4	81.9	74.5	67.0
5	10.1	14.9	15.6

Absolute probabilities of occurrence for response Modes 1 through 5 can be obtained by multiplying the absolute failure probabilities for flight phases 0 - 1 and 0 - 2 (Table 6) by the relative failure probabilities in Table 15 and Table 16. The results are shown in Table 17. Probabilities are listed to six decimal places to show differences, not because all figures are actually significant. To obtain these results, more precise values for relative probabilities of occurrence were used than shown in Table 15 and Table 16.

Table 17. Absolute Failure Probabilities for Response Modes 1 - 5

Vehicle:	Atlas		Delta		Titan	
Flight Phase:	0 - 1 (0-170 sec)	0 - 2 (0-280 sec)	0 - 1 (0-270 sec)	0 - 2 (0-630 sec)	0 - 1 (0-300 sec)	0 - 2 (0-540 sec)
Mode 1	0.000119	0.000121	0.000054	0.000051	0.000216	0.000250
Mode 2	0.001637	0.001665	0.000744	0.000698	0.002976	0.003437
Mode 3	0.000011	0.000012	0.000005	0.000005	0.000020	0.000026
Mode 4	0.018007	0.026738	0.008185	0.011212	0.032740	0.055200
Mode 5	0.002226	0.002465	0.001012	0.001034	0.004048	0.005088
Total	0.022	0.031	0.010	0.013	0.040	0.064

For each vehicle, the absolute probabilities for Modes 1, 2, and 3 differ slightly for flight phases 0 - 1 and 0 - 2. This difference is due to the unequal data weighting produced by the exponential filter. If equal data weighting had been applied, the absolute probabilities for these modes would have been identical as expected, since Modes 1, 2, and 3 cannot occur beyond flight phase 1.

Differences in absolute probabilities for Modes 4 and 5 for flight phases 0 - 1 and 0 - 2 can also be seen in the table. A part of this difference may result from unequal data weighting, but primarily it is due to the obvious fact that fewer Mode 4 and 5 failures have occurred during flight phase 0 - 1 than during the longer span of flight phase 0 - 2.

### 5.3 Relative Probability of Tumble for Response-Modes 3 and 4

Exponential filters with values of F from 0.98 to 0.999 have been used to estimate the percentage of Mode-3 and Mode-4 responses that terminate with a thrusting tumble. Results are given in Table 18 for flight phases 0 - 2 and 0 - 5. For launch-area risk calculations, only flight phases 0 - 2 are of interest. The data sample was a chronological composite of all Atlas, Delta, Titan, and Thor tests and configurations shown in Appendix D. To several decimal places at least, the values in the table are determined entirely from Mode-4 responses, since the last vehicle to experience a Mode-3 response (4/25/61) is weighted out of the solution. The results in Table 18 are based on a total sample size of 1,186 flight tests.

Table 18. Percent of Response Modes 3 and 4 That Tumble

Filter Factor	Flight Phases 0 - 2	Flight Phases 0 - 5
0.999	25.0	25.0
0.996	26.3	27.0
0.993	27.3	28.6
0.990	28.3	30.1
0.980	31.3	34.8

Through flight phase 2, there were 33 tumbles out of a total of 132 Mode-3 and Mode-4 responses. Through flight phase 5, there were 42 tumbles out of 168 Mode-3 and Mode-4 responses.

As seen from Table 13, the smaller the filter factor, the greater the weight placed on recent test data. In view of this, it is apparent from Table 18 that the percentage of Mode-4 responses that end with a thrusting tumble has been increasing gradually. The same conclusion is reached for flight phases 0 - 2 and 0 - 5. In recognition of this gradual increase, in future studies RTI will assume that **approximately one-third of Mode-3 and Mode-4 failure responses end with a thrusting tumble.**

## 6. Shaping Constants Through Simulation

Since adequate test data are not available to establish the Mode-5 shaping constants empirically, other methods are needed for this purpose. It will be recalled that, after vehicle pitchover, any malfunction with the potential to cause a substantial deviation from the intended flight line is, by definition, a Mode-5 failure response. The malfunction need not actually cause a large deviation to be classified as a Mode-5 response. One such class of failures leading to a Mode-5 response has been termed a random-attitude failure. Such responses can result from guidance and control failures that lead to erroneous orientation of the guidance platform or an erroneous spatial target. Another class of failures that can cause sustained deviation away from the flight line is the slow turn, where the engine nozzle, in effect, locks in some fixed position, generally but not necessarily near null. Both types of malfunctions have been investigated in an attempt to estimate numerical values for Mode-5 shaping constants A and B. Basically, the idea is to (1) run a large sample of random-attitude and slow-turn failures, (2) calculate the percentages of impacts in five-degree sectors from 0° to 180°, (3) compare these percentages with those obtained from the Mode-5 impact density function when specific values are assigned to A and B, and (4) assign values to A and B until the best possible fit is obtained between the simulated-turn impacts and the theoretical Mode-5 impacts.

### 6.1 Malfunction Turn Simulations

#### 6.1.1 Random-Attitude Failures

A guidance and control failure leading to a fixed erroneous direction of thrust is termed a random-attitude failure. Such failures represent a subset of possible Mode-5 failure responses. Random-attitude failures can be used to establish the maximum possible region of impact, given that a vehicle has flown normally for a specified period of time. For this purpose RTI has developed a Random-Attitude Failure Impact Point (RAFIP) program written in Fortran (3900 lines of code) for execution on a personal computer.

Using a Monte Carlo approach, program RAFIP first selects a starting time and then a random thrust direction on the attitude sphere, with all directions having the same chance of being chosen. Each Monte-Carlo run is begun using the nominal vehicle position and velocity at the selected start time, assuming an instantaneous change in thrust direction. Thrust is applied continuously in the selected random direction, and the equations of motion are numerically integrated until one of four conditions is satisfied: (1) final stage burnout occurs, (2) the vehicle impacts while thrusting, (3) orbital insertion occurs, (4) the vehicle breaks up due to aerodynamic forces

For conditions (1) and (4), the trajectory is extended to impact using Kepler's equations. For condition (3), an impact point does not exist. The process just described is repeated

for a suitably large sample so the distribution of resulting impact points will, for all practical purposes, represent all possible impact points, irrespective of the actual nature of the failure.

Depending on vehicle breakup characteristics and failure time, a vehicle that experiences a random-attitude failure may break up at the instant of failure, or after a few seconds into the turn, or not at all. In making the calculations, three separate breakup thresholds and a no-breakup case were investigated. With respect to vehicle breakup, the assumption was made that the vehicle would break up if  $q\alpha$  exceeded a specified constant limit, where  $q$  is the dynamic pressure and  $\alpha$  is the total angle of attack. Although the breakup  $q\alpha$  may well be a complicated function of Mach number and other parameters, this simplistic approach was taken.

Random-attitude-failure calculations were made individually for Atlas, Delta, Titan, and LLV1 starting shortly after pitchover and continuing to some convenient time such as a stage burnout when the vehicle could no longer endanger the launch area. Theoretically, the Mode-5 impact density function extends downrange until the instantaneous impact point vanishes. Since this study is concerned with evaluation of density-function parameters for launch-area risk analysis, the random-attitude calculations were stopped at a staging event when the vehicle no longer had sufficient energy to return the impact point to the launch area. Using trajectory data for each vehicle, program RAFIP was run to generate 10,000 impact-point samples at each starting time. Calculations were made at ten-second intervals.

### 6.1.2 Slow-Turn Failures

Certain types of guidance and control failures can cause the thrusting engine to gimbal to null or a near-null position. Such failures can produce what is herein called a slow turn. For various reasons, after an engine is commanded to null it may not thrust precisely through the center of gravity, e.g., structural misalignments, shifting center of gravity, canted nozzles. Since, like random-attitude failures, slow turns constitute a subset of Mode-5 failure responses, they have been investigated using RTI program RAFIP. The following assumptions have been made in making the calculations:

- (1) The effective thrust offset of a "nulled" engine is normally distributed with a zero mean and a standard deviation of  $0.1^\circ$ .
- (2) A fixed thrust offset results in a constant angular acceleration of the airframe, and thus a constant angular acceleration of the thrust vector.
- (3) For small thrust misalignments, the angular acceleration of the airframe is proportional to the angular thrust misalignment.

At each time point, the angular acceleration produced by small thrust offsets was estimated from the malfunction turn data provided to the safety office by the range user. Malfunction turns for the Atlas IIAS were provided for three gimbal angles, the smallest being one degree. For each gimbal angle, the results were plotted as

cumulative angle turned versus time. Since the slope of the curve (i.e., the turning rate) is greatest when the thrust (and thus airframe) is directed at right angles to the velocity vector, the average angular acceleration during the first 90° of rotation was obtained from the equation

$$\theta = \frac{1}{2} \ddot{\theta} t^2 \quad (4)$$

so that

$$\ddot{\theta} = \frac{2 \theta (\text{deg})}{t^2 (\text{sec}^2)} = \frac{180 \text{ deg}}{t^2 \text{ sec}^2} \quad (5)$$

where  $t$  is the elapsed time from the beginning of the tumble turn until the airframe has rotated approximately 90°. If the assumption is made that the angular acceleration is directly proportional to the thrust offset angle (i.e., nozzle deflection), the angular acceleration  $\ddot{\theta}_a$  for any small deflection angle becomes

$$\ddot{\theta}_a = \ddot{\theta} \frac{\delta_a}{\delta} \quad (6)$$

where  $\ddot{\theta}$  is the angular acceleration computed from Eq. (5) for deflection angle  $\delta$  (1° for Atlas IAS), and  $\delta_a$  is some small deflection angle.

Using the Atlas IAS data, angular accelerations  $\ddot{\theta}$  were computed at ten-second intervals from the programming time of 15 seconds to 275 seconds for  $\delta = 1^\circ$ . For each starting time, a normal distribution with zero mean and a standard deviation of 0.1° was sampled to obtain an initial thrust misalignment  $\delta_a$  to substitute in Eq. (6). The resulting angular acceleration  $\ddot{\theta}_a$  was applied throughout the turn. Slow-turn calculations were made in a manner analogous to the random-attitude turns, using the reference trajectory to obtain the starting position and velocity components. The slow turn was assumed to occur in a randomly oriented plane containing the starting velocity vector. Each turn was carried out until one of the four conditions listed in Section 6.1.1 for random-attitude turns was met. For conditions (1) and (4), impact points were calculated and, along with thrusting impacts from condition (2), summed for each five-degree sector from 0° to 175°. At each starting time, 10,000 impact-point calculations were made.

### 6.1.3 Factors Affecting Malfunction-Turn Results

Random-attitude turns and slow turns are only subsets of the totality of Mode-5 failure responses. As discussed earlier in Section 3, other types of behavior following a Mode-5 failure are numerous and largely impossible to categorize, much less simulate. Ideally, impact distributions from all types of Mode-5 responses should be combined before results are compared with those obtained from the theoretical Mode-5 impact

density function. Since this could not be done in general, impacts from only the two types of malfunction turns were considered. Several factors affect the results of the simulations:

- a. **Weighting of turn data:** Both random-attitude and slow-turn simulations were made for Atlas IIAS. In combining impacts from the two data sets, random-attitude turns were assumed to be three times as likely to occur as slow turns. A factor of three was selected since, among the Mode-5 failure responses in the performance summaries for Atlas, Delta, and Titan, random-attitude turns appeared to occur about three times as often as slow turns. In many cases, lack of detailed information made it difficult to decide whether a Mode-5 response should be considered as a random-attitude turn, a slow turn, or some other type of failure. The relative weighting of turns makes little difference, however, since the impact distribution for the two types of turns are similar (as shown later in Figure 5), and since the weighted composite must lie between the two. It was assumed that similar results would be obtained for Delta, Titan, and LLV1, so slow-turn computations were not made for these vehicles, cutting the number of time-consuming simulations in half.
- b. **Breakup  $q\alpha$ :** In the turn calculations, the assumption was made that vehicle breakup would occur if a certain value of  $q\alpha$  was reached. In addition to the no-breakup case which is considered unrealistic, separate runs were made for three constant values of  $q\alpha$ : 5,000, 10,000, and 20,000 deg-lb/ft<sup>2</sup>. As stated previously, the determination of vehicle breakup is, in reality, much more involved than this simplistic approach would suggest. However, to add realism to the malfunction-turn calculations, use of a simple approach seemed better than none at all. For Titan IV, allowable (but not breakup)  $q\alpha$ 's were provided as functions of Mach number. The maximum permissible value and corresponding Mach number for Titan/Centaur, Titan/NUS, and Titan/IUS were, respectively, 6819 deg-lb/ft<sup>2</sup> at Mach No. 0.77, 5332 deg-lb/ft<sup>2</sup> at Mach No. 0.815, and 17,000 deg-lb/ft<sup>2</sup> at Mach No. 0.325. For Atlas, Delta, and LLV1 vehicles, no breakup  $q\alpha$  data were available. The breakup  $q\alpha$ 's used in the calculations bracket the range of permissible  $q\alpha$ 's for the Titan vehicles.
- c. **End time  $T_b$ :** The simulated impact distributions from random-attitude failures and slow turns were compared with impact distributions computed from the Mode-5 theoretical impact-density function. For the comparisons to be meaningful, the value selected for  $T_b$  in the Mode-5 impact-density equation and the stop time for thrusting-turn simulations must be the same. To some extent, the shaping constants A and B derived by fitting the theoretical and simulated impact data depend on  $T_b$ , since the percentage of impacts in each 5° sector depends on  $T_b$ . However, after A and B have been established for a particular  $T_b$ , using a different  $T_b$  in the DAMP calculations has no effect on computed risks provided an adjustment is made in the probability of occurrence of a Mode-5

response. Referring to Eq. (3), the right-hand member must be multiplied by the probability  $p_5$  of a Mode-5 response to obtain absolute probabilities. Except for  $T_b$  itself (and to a slight degree, shaping constants A and B), the quantities in the equation do not depend on  $T_b$ . Thus if  $T_b$  and  $p_5$  are both changed so that  $p_5/(T_b - T_p)$  remains constant, the computed risks are unchanged.

If destruct action (i.e., impact limit lines) is included in the DAMP calculations, the supplemental risks\* resulting from that action must be accounted for. In this case, the termination time has a minor influence on results, since it affects the number of impacts that would occur beyond the impact limit lines without destruct that are forced inside when destruct action is taken. If destruct action is omitted, the value of  $T_b$  is immaterial (i.e., supplemental Mode-5 risks are non-existent) provided that the impact range along the reference trajectory at time  $T_b$  exceeds the range to all targets of interest. (Except in this paragraph, supplemental Mode-5 risks are not addressed in this present report.)

- d. Vacuum calculations: Atmospheric effects were accounted for in determining when vehicle breakup would occur and, to some extent, during each thrusting turn by using accelerations from the nominal trajectory. To reduce computer time and cost of this study, vacuum calculations were made during free fall after vehicle breakup or burnout. Although this increased impact dispersions somewhat, vacuum results should not be drastically different from those obtainable using a maximum-beta piece. In theory at least, different mode-5 shaping constants exist for each debris class. In view of the uncertainties in vehicle breakup conditions and characteristics, and in the overall process of simulating Mode-5 malfunctions, attempts to derive unique shaping constants for each debris class did not seem justified.

#### 6.1.4 Malfunction-Turn Results for Atlas IIAS

For Atlas IIAS, the distribution of impacts for simulated random-attitude turns, slow turns, and a weighted combination (75% random-attitude and 25% slow turn) are shown in Figure 5. Since the impact distribution (i.e., the percentages of impacts in 5° sectors) for the weighted composite was not significantly different from that for random-attitude failures, slow-turn computations were not made for Delta, Titan, and LLVI.

---

\* See Ref. [1], Section 10.

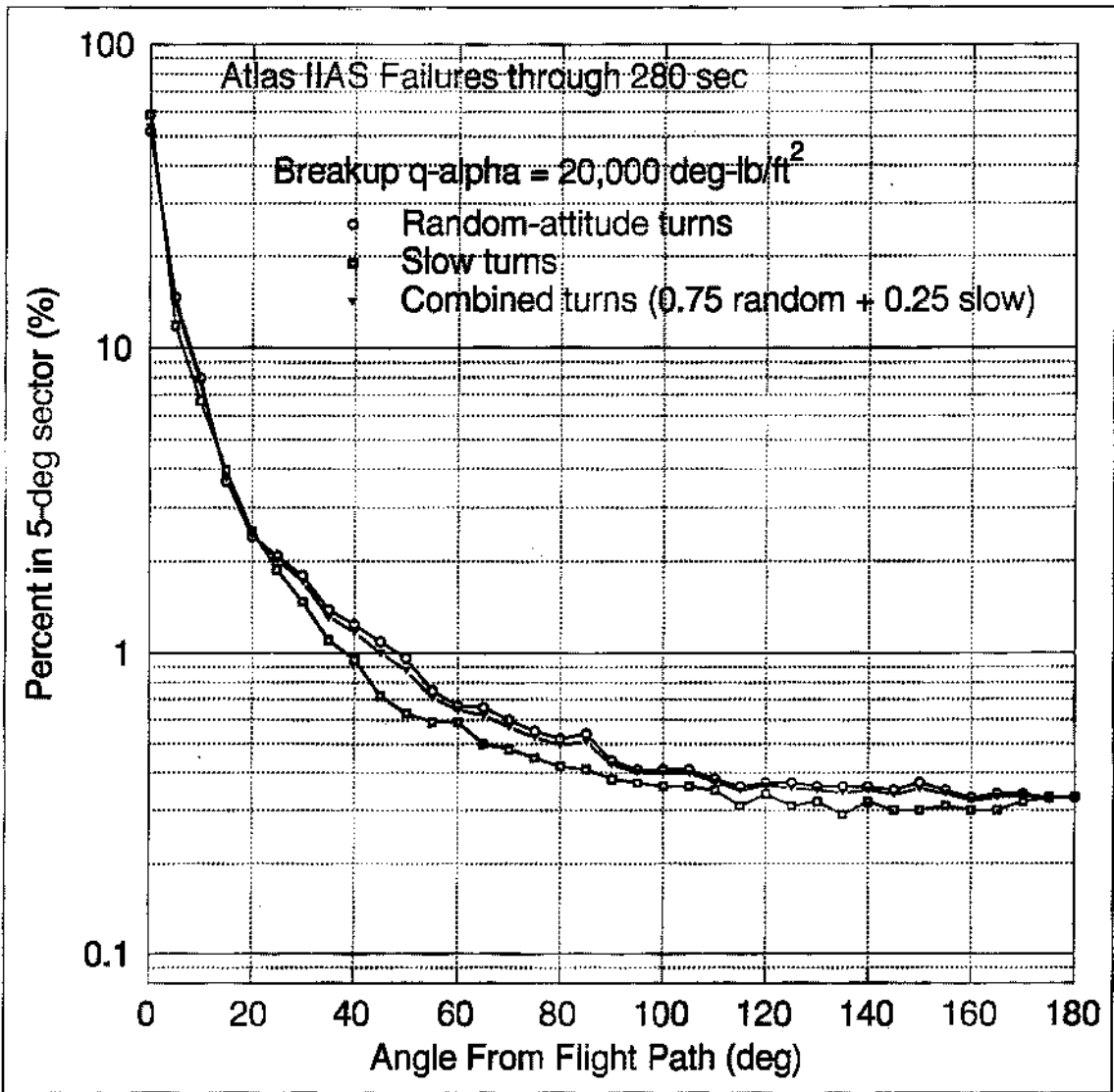


Figure 5. Combined Random-Attitude and Slow-Turn Results

## 6.2 Shaping Constants for Atlas IIAS

### 6.2.1 Optimum Mode-5 Shaping Constants

Since the dynamic pressures that can cause the Atlas IIAS to break up were not available, random-attitude failures were simulated for a no-breakup case and for three breakup  $q\alpha$ 's: 20,000 deg-lb/ft<sup>2</sup>, 10,000 deg-lb/ft<sup>2</sup>, and 5,000 deg-lb/ft<sup>2</sup>. For each case, 270,000 trajectories were run, giving a total of 1,080,000. It turned out that the value chosen for the breakup  $q\alpha$  was critical in determining shaping constant A, since the lower the  $q\alpha$ , the less the thrusting time before breakup, and the higher the percentages of impacts in sectors near the flight line.

For Atlas IIAS, the effects of  $q\alpha$  on breakup are shown in Figure 6 where, for the selected  $q\alpha$ 's, the percentages of random-attitude turns that result in breakup before 280 seconds are plotted against failure time.

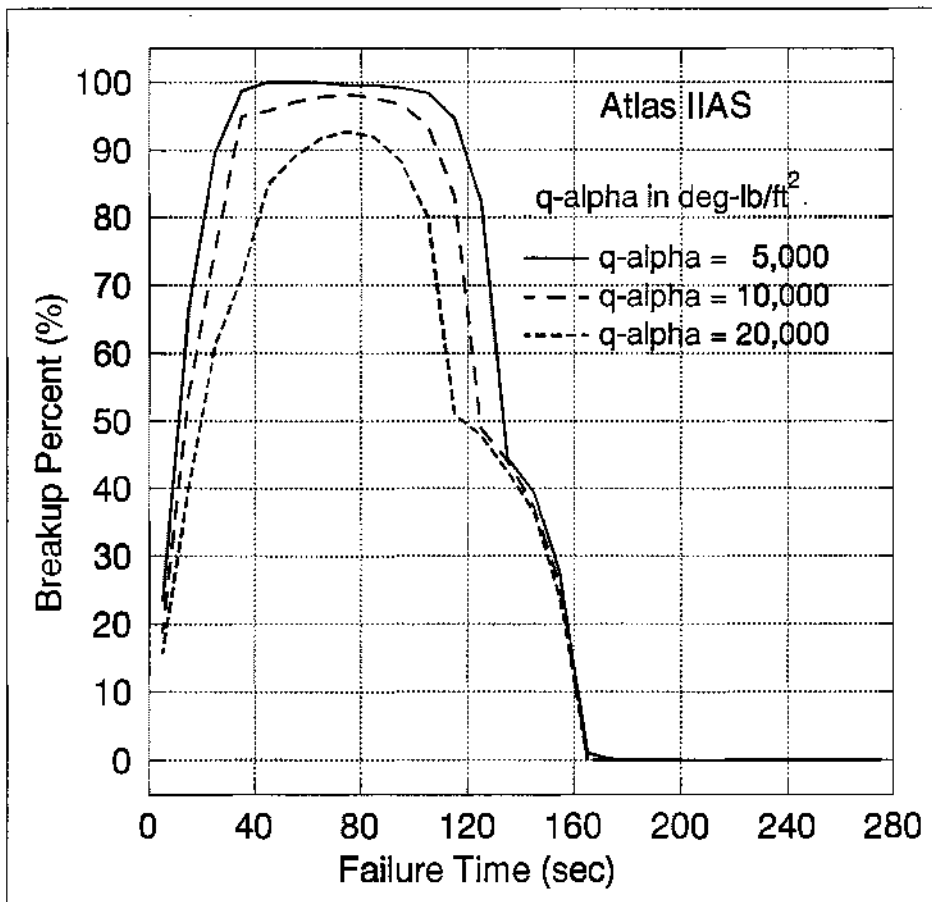


Figure 6. Atlas IIAS Breakup Percentages for Random-Attitude Turns

For failures between 10 and 30 seconds, most breakups do not occur at failure, but later in flight after the vehicle has built up significant velocity. For failures between 40 and 105 seconds, more than 80% breakup occurs, even for  $q\alpha$ 's as high as 20,000 deg-lb/ft<sup>2</sup>.

In this region, breakup occurs at or shortly after vehicle failure. Beyond 170 seconds, the dynamic pressure between failure and 280 seconds stays sufficiently low so that the vehicle remains intact.

The dramatic differences in impact distributions that can result at certain times during flight if the vehicle is subject to aerodynamic breakup can be seen by comparing the impact footprints in Figure 7 and Figure 8. Both patterns show 10,000 impact points from random-attitude failures of the Atlas IIAS at 130 seconds. Figure 7 is for no breakup, and Figure 8 is for a breakup  $q\alpha$  of 5,000 deg-lb/ft<sup>2</sup>.

The data in Table 19 comprise an example of a 270,000-point sample of random-attitude failures run at 10-second intervals from 15 to 275 seconds. (For brevity, only every-other failure time is shown in the table.) Ten thousand impacts are computed at each failure time. Five-degree sectors are identified in the left-hand column. For each time, the number of impacts in each 5° sector is shown in the column for that time. The total number of impacts for all failure times and the percentages of impacts in each sector are given in the last two columns of the table.

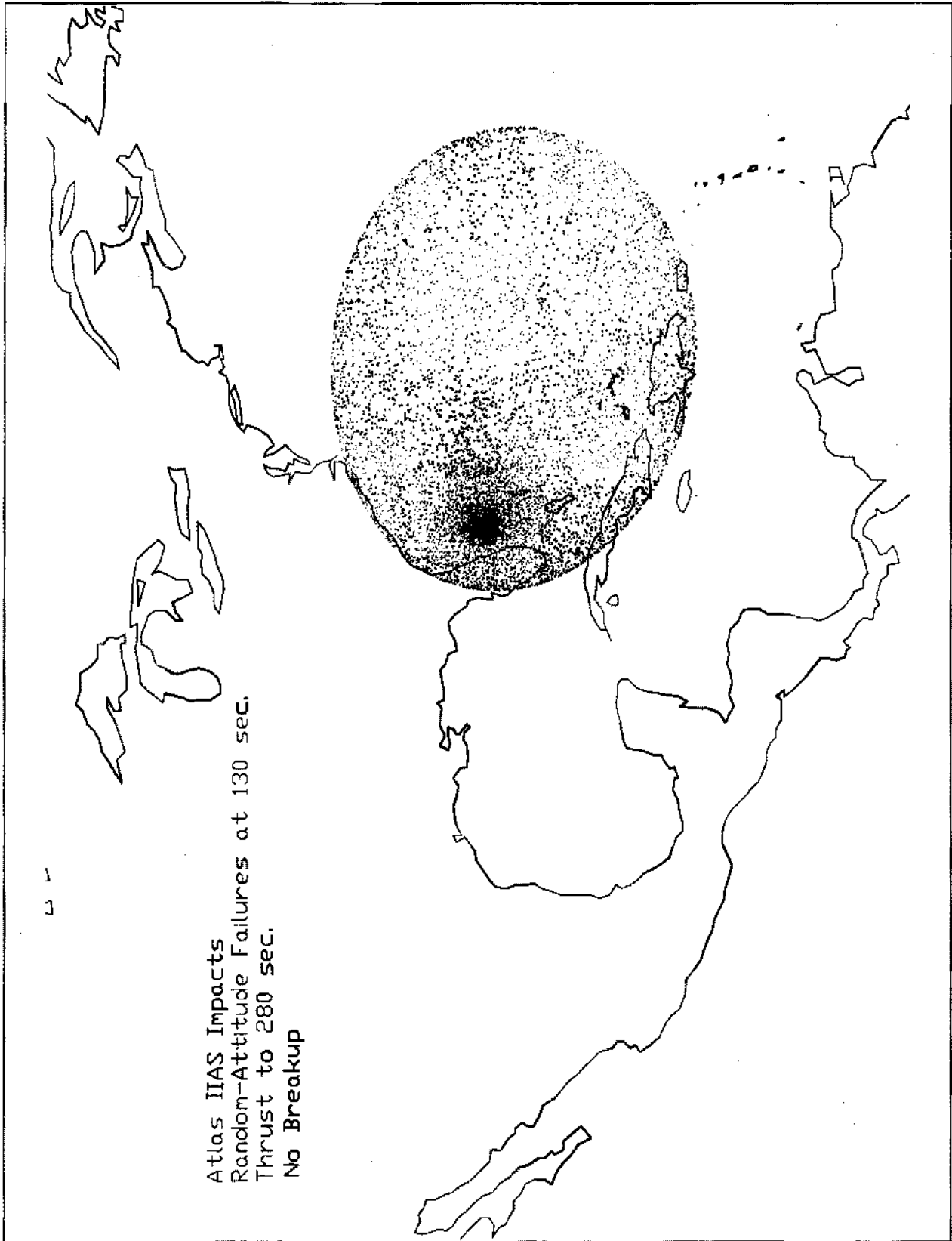


Figure 7. Atlas IIAS Impacts with No Breakup

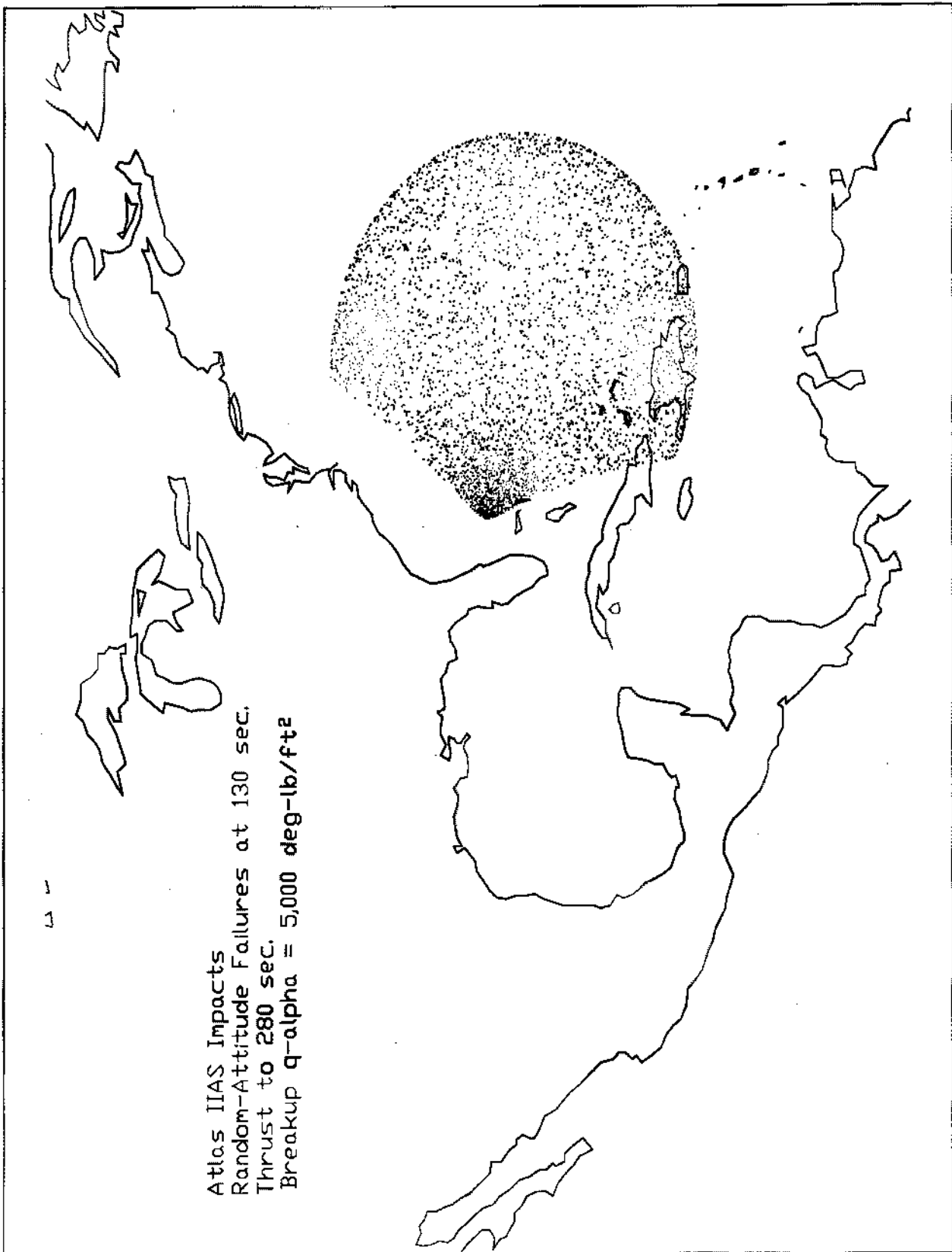


Figure 8. Atlas IIAS Impacts with Breakup

Table 19. Sample Impact Distribution for Atlas IIAS with No Breakup

Ang.	Failure Time (sec)														All	%
	15	35	55	75	95	115	135	155	175	195	215	235	255	275		
0	255	300	411	487	608	835	1107	1843	3333	4092	5386	7906	10000	10000	87746	32.50
5	279	314	388	465	575	808	1082	1762	3065	3827	4206	2094	0	0	38474	14.25
10	261	316	427	495	627	744	975	1652	2820	2081	408	0	0	0	21265	7.88
15	298	329	354	464	558	730	945	1445	782	0	0	0	0	0	12195	4.52
20	274	319	378	421	566	670	845	1292	0	0	0	0	0	0	8875	3.29
25	287	316	349	406	525	641	776	1203	0	0	0	0	0	0	8189	3.03
30	257	339	337	415	452	505	617	800	0	0	0	0	0	0	6893	2.55
35	299	336	381	368	405	506	550	3	0	0	0	0	0	0	5883	2.18
40	275	293	388	374	409	454	520	0	0	0	0	0	0	0	5593	2.07
45	299	298	310	397	366	412	441	0	0	0	0	0	0	0	5285	1.96
50	242	282	331	346	323	352	378	0	0	0	0	0	0	0	4535	1.68
55	280	308	282	303	314	292	331	0	0	0	0	0	0	0	4005	1.48
60	272	308	289	306	293	299	260	0	0	0	0	0	0	0	3827	1.42
65	288	262	279	300	294	286	256	0	0	0	0	0	0	0	3666	1.36
70	250	275	326	281	264	243	205	0	0	0	0	0	0	0	3483	1.29
75	283	261	272	271	238	232	170	0	0	0	0	0	0	0	3321	1.23
80	273	266	249	272	234	194	111	0	0	0	0	0	0	0	3022	1.12
85	287	274	241	242	219	191	96	0	0	0	0	0	0	0	2888	1.07
90	235	285	246	230	226	171	70	0	0	0	0	0	0	0	2778	1.03
95	303	283	280	235	180	136	55	0	0	0	0	0	0	0	2815	1.04
100	292	283	268	215	190	126	49	0	0	0	0	0	0	0	2620	0.97
105	279	254	246	211	200	108	30	0	0	0	0	0	0	0	2571	0.95
110	283	267	237	204	168	114	27	0	0	0	0	0	0	0	2448	0.91
115	261	255	230	178	162	120	18	0	0	0	0	0	0	0	2346	0.87
120	311	263	251	211	167	98	17	0	0	0	0	0	0	0	2321	0.86
125	276	255	225	189	155	62	11	0	0	0	0	0	0	0	2239	0.83
130	266	251	227	195	126	86	8	0	0	0	0	0	0	0	2246	0.83
135	283	259	227	176	128	77	8	0	0	0	0	0	0	0	2221	0.82
140	286	244	184	186	169	63	5	0	0	0	0	0	0	0	2138	0.79
145	305	243	187	180	118	59	8	0	0	0	0	0	0	0	2102	0.78
150	251	225	178	166	128	72	8	0	0	0	0	0	0	0	1895	0.70
155	293	259	199	151	113	68	2	0	0	0	0	0	0	0	2103	0.78
160	253	213	220	177	127	59	6	0	0	0	0	0	0	0	1952	0.72
165	254	242	203	172	115	68	2	0	0	0	0	0	0	0	2008	0.74
170	298	256	195	171	127	60	6	0	0	0	0	0	0	0	2034	0.75
175	312	267	205	140	131	59	5	0	0	0	0	0	0	0	2018	0.75
Total	10000	10000	10000	10000	10000	10000	10000	10000	10000	10000	10000	10000	10000	10000	270000	100.00

In Figure 9, the percentages of impacts in 5° sectors from 0° to 180° have been plotted for Atlas IIAS random-attitude turns out to 280 seconds. (It should be remembered that random-attitude turns are representative of combined random-attitude and slow turns.) For B = 1000, theoretical Mode-5 impact percentages are also plotted in the figure for best-fit values of A obtained by trial and error.

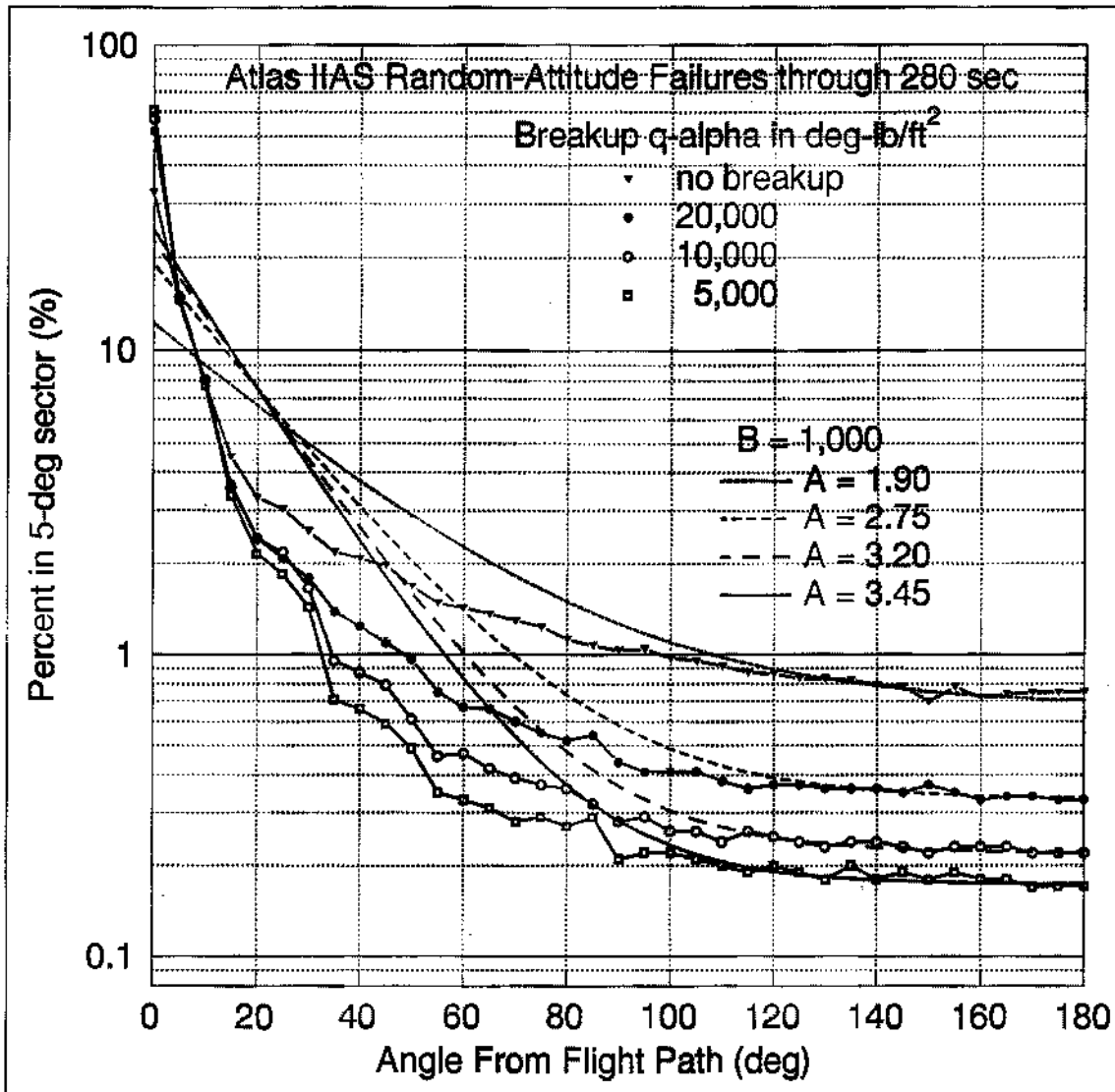


Figure 9. Atlas IIAS Simulation Results with B = 1,000

By observing curve shapes, it can perhaps be seen that no single value of A causes a theoretical impact distribution and a distribution of impacts from random-attitude turns to match closely over the entire range of 5° sectors. Attempts to improve the match on one end of the curve by selecting a different A merely degrades the match on

the other end. It is possible, however, to obtain fairly close agreement over sectors\* from  $\pm 80^\circ$  to  $\pm 180^\circ$ , as seen in Figure 9. Since for Atlas IIAS there are few, if any, significant population centers in the launch area outside these sectors (i.e., within  $\pm 80^\circ$  of the flight line), failure of the curves to match closely near the flight line is of little consequence. If a better data match is considered desirable for computing risks to population centers within  $\pm 80^\circ$  of the flight line (e.g., ships), either a different A can be selected for use with  $B = 1,000$  or other values of A and B can be derived. If only a single value of B is used, no matter what the value, a good match between theoretical and simulated data is not possible over the entire  $180^\circ$  sector for various breakup  $q\alpha$ 's.

Before becoming too concerned about lack of a data match between  $0^\circ$  and  $80^\circ$ , it should be remembered that many types of Mode-5 responses cannot be simulated, so that the malfunction-turn impact distributions plotted in Figure 9 are only a subset of all possible Mode-5 impacts. Based on twelve Mode-5 failure responses for which impact data are available, it is believed that inclusion of the "non-simulatable" Mode-5 responses would considerably improve the match in the sector from  $\pm 10^\circ$  to  $\pm 80^\circ$ . Another mitigating factor is that risks near the flight line are totally dominated by Mode-4 failure responses.

To see how data matching is affected by selecting widely differing values of B, the theoretical Mode-5 impact distributions were computed for  $B = 50,000, 100,000, 500,000,$  and  $5,000,000$ . Best-fit values for A were again determined by trial and error. Results are shown in Figure 10 through Figure 13 along with the same impact distributions for random-attitude turns plotted in Figure 9.

---

\* For other values of B and  $q\alpha$ , close agreement is possible from  $\pm 60^\circ$  to  $\pm 180^\circ$ .

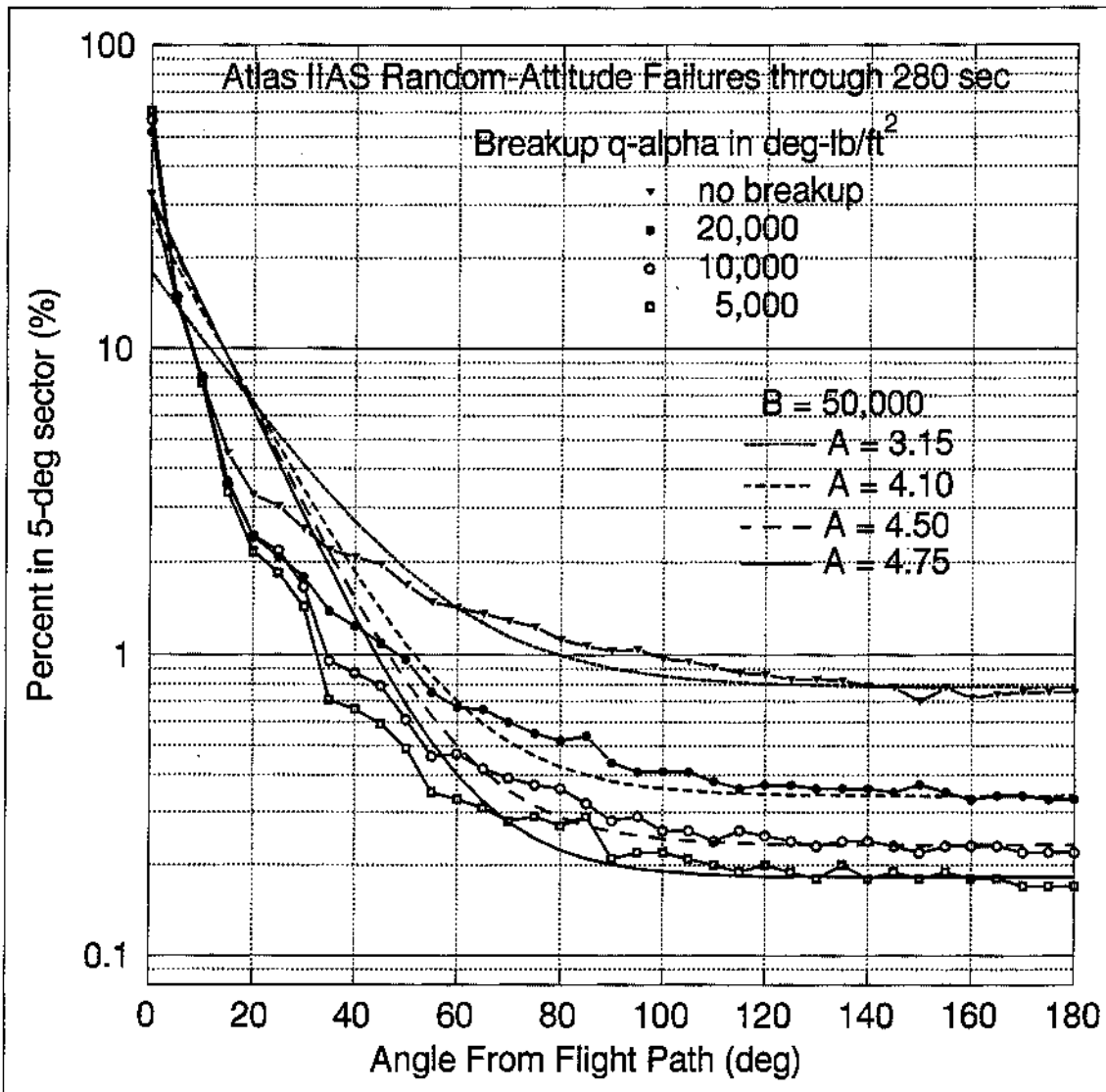


Figure 10. Atlas IIAS Simulation Results with  $B = 50,000$

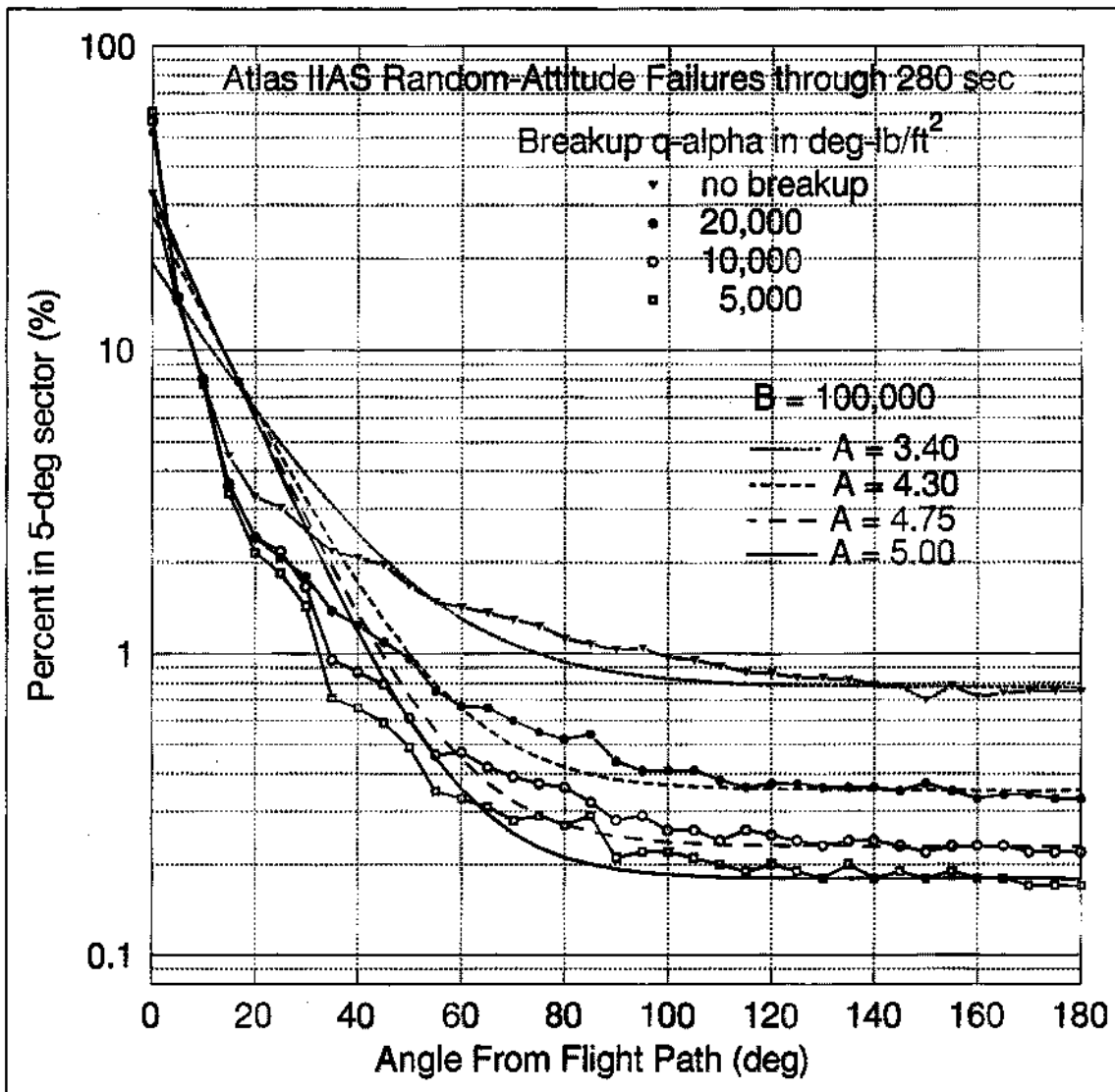


Figure 11. Atlas IIAS Simulation Results with  $B = 100,000$

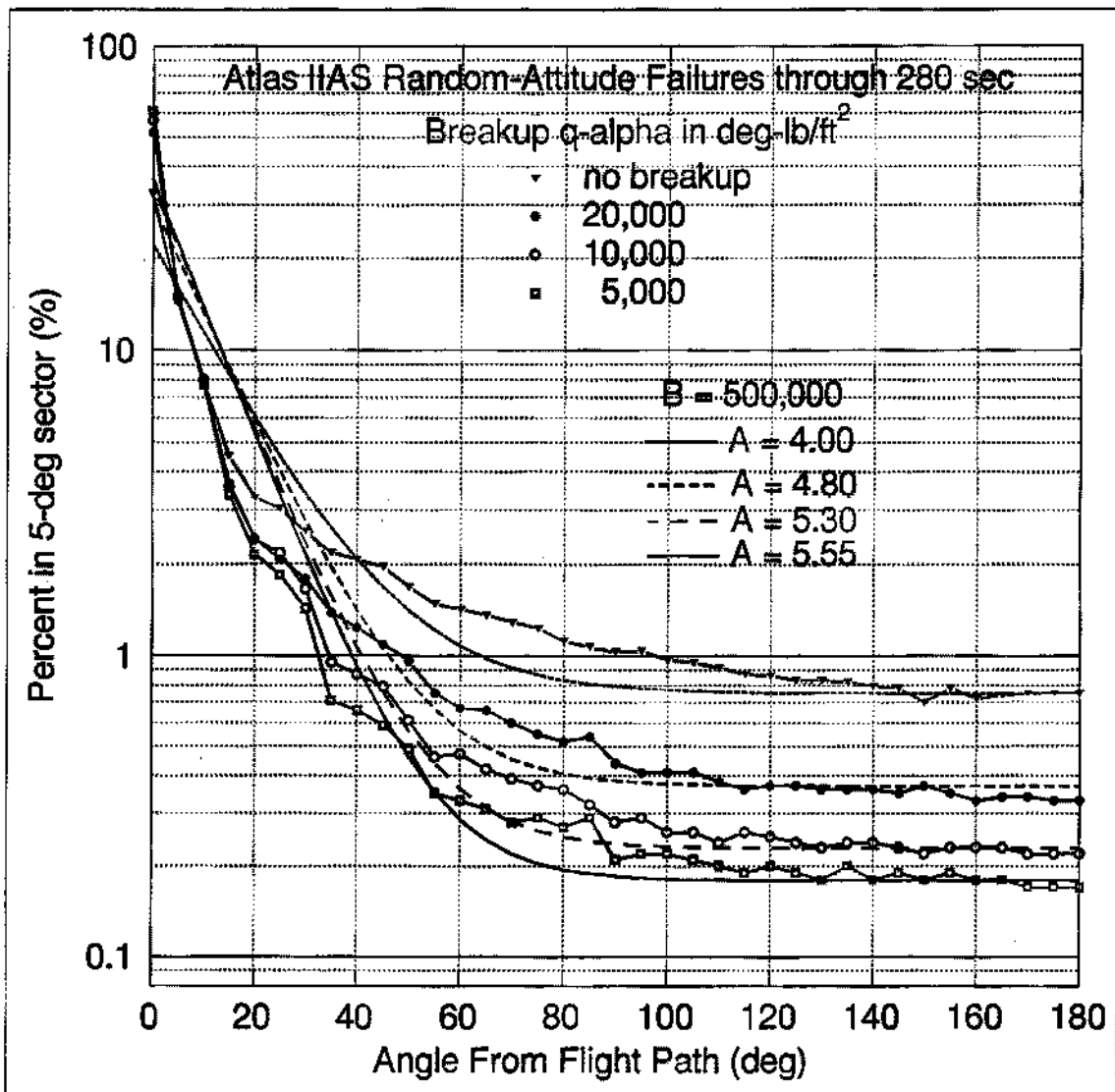


Figure 12. Atlas IIAS Simulation Results with  $B = 500,000$

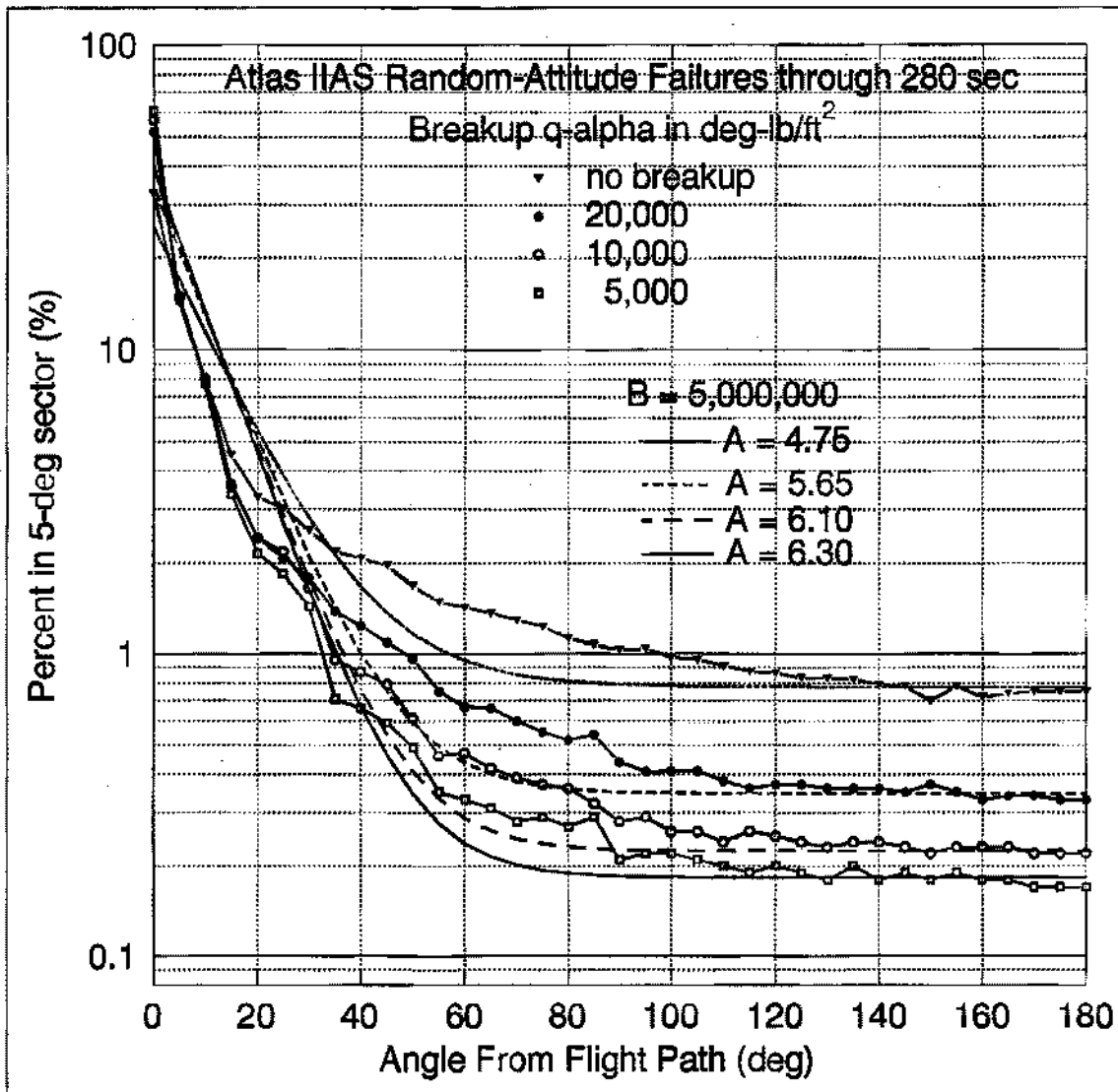


Figure 13. Atlas IIAS Simulation Results with  $B = 5,000,000$

The five values of B and the corresponding best-fit values of A used to compute the Mode-5 distributions shown in Figure 9 through Figure 13 are tabulated in Table 20. It is apparent that the value of A is dependent on both  $q\alpha$  and B. In general, if a larger value of B is selected, a larger value of A is required to effect a fit with the random-attitude-turn data. On the other hand, if the breakup  $q\alpha$  is increased, the required value of A must be decreased. Only  $q\alpha$  is critical since, as shown later, any value of B, together with its corresponding value of A, can be used in the launch-area risk computations if significant targets do not lie within  $\pm 80^\circ$  of the flight line.

Table 20. Shaping Constants for Atlas IIAS

Breakup $q\alpha$ (deg-lb/ft <sup>2</sup> )	B	A
none	1,000	1.90
20,000		2.75
14,000 *		3.00 *
10,000		3.20
5,000		3.45
none	50,000	3.15
20,000		4.10
10,000		4.50
5,000		4.75
none	100,000	3.40
20,000		4.30
10,000		4.75
5,000		5.00
none	500,000	4.00
20,000		4.85
10,000		5.30
5,000		5.55
none	5,000,000	4.75
20,000		5.65
10,000		6.10
5,000		6.30

\* interpolated

Because of the uncertainties in breakup conditions, the values of A for each B in Table 20 have been plotted against  $q\alpha$  in Figure 14. By reading from the plots, a value of A for the five values of B can be obtained for any breakup  $q\alpha$  deemed appropriate between 5,000 and 20,000 deg-lb/ft<sup>2</sup>.

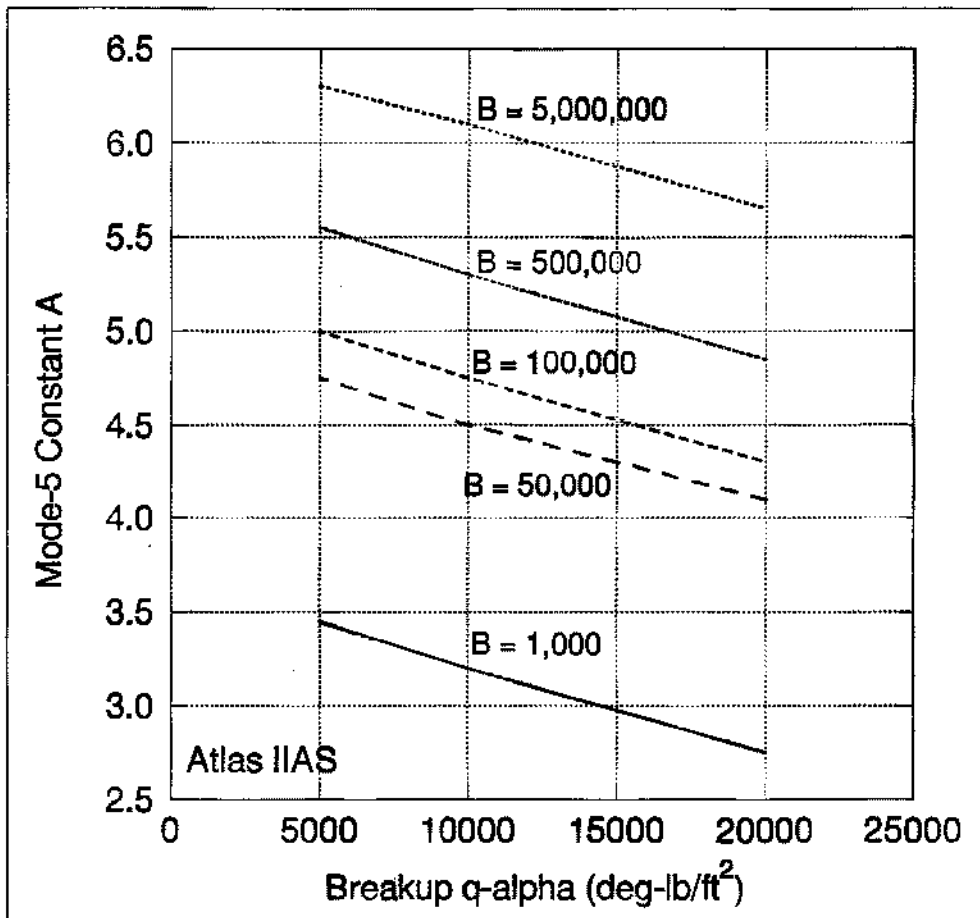


Figure 14. Effects of Breakup  $q\alpha$  on A for Atlas IIAS

### 6.2.2 Launch-Area Mode-5 Risks

The twenty sets of A and B shown in Table 20 were used to compute Mode-5 launch-area risks for population centers inside the impact limit lines for an Atlas IIAS daytime launch of a Telstar-4 payload from Pad 36A. Results of these and two other cases are given in Table 21. The Mode-5  $E_c$  in the first line (old baseline case) of Table 21 is presented for comparison only. It was obtained from data in the first line of Table 45 of an earlier RTI study<sup>[3]</sup>. In Ref. [3], the total Atlas IIAS failure probability for the first two minutes of flight was set at 0.04, with the probability of a Mode-5 failure response assumed to be 0.005. The second line in Table 21 shows the result of a recomputation of the Mode-5 baseline risks, again with  $B = 1000$  and  $A = 3$ , using newly derived values for the total failure probability and for a Mode-5 failure response. For flight phases 0 – 2, a total failure probability of 0.031 was assumed, as extracted from Table 6 for

F = 0.98. The conditional probability of a Mode-5 response was assumed to be 0.08 (from the last line of Table 15), so the absolute probability was  $0.031 \times 0.08 = 0.0025$ . For the remaining cases in Table 21, the same assumptions were made for the total failure probability and for the probability of a Mode-5 response.

Table 21. Shaping Constants and Related Risks for Atlas IIAS

$p_s$	$T_p$ (sec)	Breakup $q\alpha$ (deg-lb/ft <sup>2</sup> )	B	A	Mode-5 $E_c$ ( $\times 10^6$ )
0.005	118	14,000 * (baseline)	1,000	3.00	227
0.0025	280	14,000 * (new $p_s$ & $T_p$ )	1,000	3.00	49.1
0.0025	280	none	1,000	1.90	139.8
		20,000		2.75	73.7
		10,000		3.20	33.4
		5,000		3.45	19.8
0.0025	280	none	50,000	3.15	144.9
		20,000		4.10	75.6
		10,000		4.50	37.1
		5,000		4.75	21.8
0.0025	280	none	100,000	3.40	144.8
		20,000		4.30	79.8
		10,000		4.75	36.1
		5,000		5.00	21.1
0.0025	280	none	500,000	4.00	143.6
		20,000		4.85	79.9
		10,000		5.30	35.9
		5,000		5.55	20.8
0.0025	280	none	5,000,000	4.75	144.8
		20,000		5.65	77.7
		10,000		6.10	34.2
		5,000		6.30	22.0

\* Interpolated from Figure 14

As seen from Table 21, the Mode-5 risks are highly dependent on A and insensitive to the value chosen for B provided a proper choice is made for A. Even for values of B as different as 1,000 and 5,000,000, the Mode-5 risks ( $q\alpha = 5,000$ ) differ by only 12%. This difference drops for all other values of B. In fact, the differences probably have more to do with the choice of A than to any inherent difference in results due to the choice of B. For Atlas IIAS, 24% of the total Mode-5  $E_c$  in the launch area is due to one population center, and 51% of the total  $E_c$  to only five population centers (see page 49 of Ref [3]). If values of A had been chosen so that theoretical distributions and random-attitude-turn distributions more nearly matched for the radial directions to these population centers,

the differences in calculated Mode-5 risks for the different values of B would surely have been less.

Further understanding of why small differences in  $E_c$  exist can be gained by plotting values of the Mode-5 density function computed from Eq. (3). This has been done in Figure 15 for a range of three miles using values of A and B from Table 21 for  $q\alpha = 5,000 \text{ deg-lb/ft}^2$ . Since Eq. (3) does not include a factor to account for the probability of a Mode-5 failure, the values plotted in the figure are conditional impact probabilities per square mile. For the sector from  $120^\circ$  to  $180^\circ$ , which is where most population centers are located, the density-function value for  $B = 5,000,000$  is largest and for  $B = 1,000$  is smallest. Results consistent with this are shown in Table 21, where the largest and smallest  $E_c$ 's are for  $B = 5,000,000$  and  $B = 1,000$ , respectively.

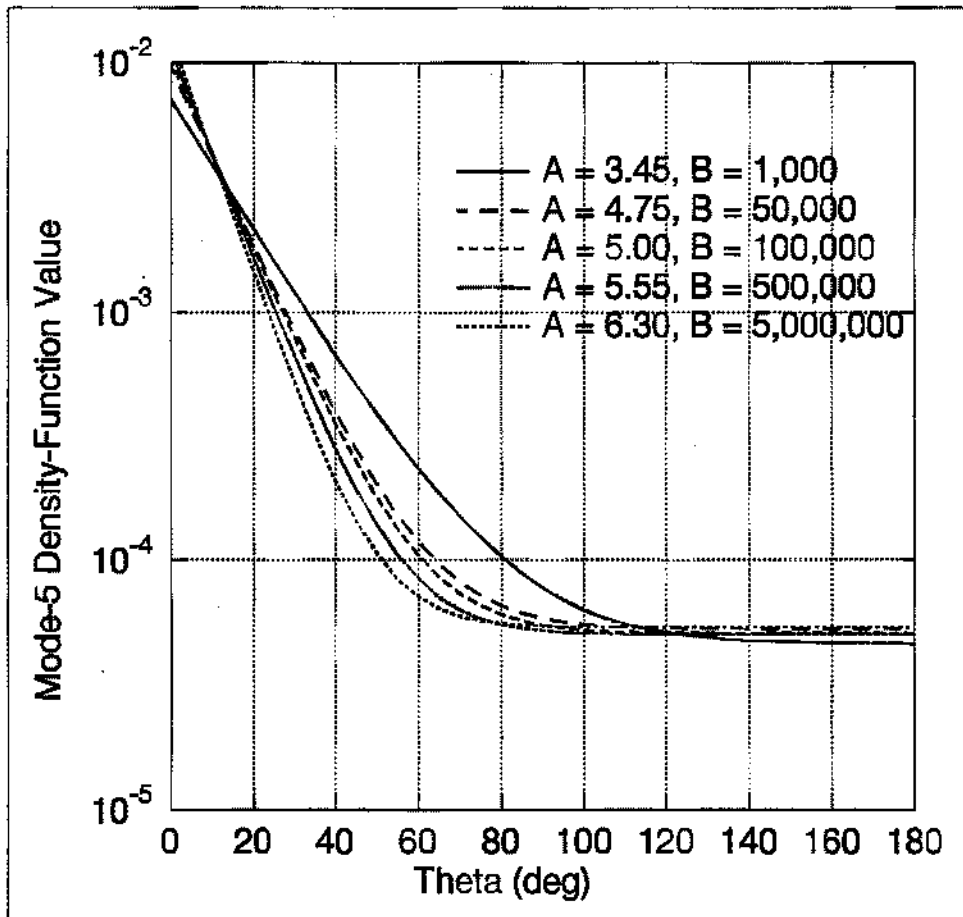


Figure 15. Mode-5 Density-Function Values at Three Miles

### 6.2.3 Effects of Mode-5 Constants on Ship-Hit Contours

In the preceding section, certain values were assigned to B and, by trial and error, best-fit values of A were found. For every breakup  $q\alpha$  and every B, it was possible to find a value of A that produced good agreement between theoretical and simulated impact data over  $5^\circ$  sectors from  $\pm 100^\circ$  to  $\pm 180^\circ$  (see Figure 10 through Figure 13). In some

cases the agreement gradually deteriorated for angles below  $\pm 100^\circ$  while, in other cases, agreement was remarkably good to  $\pm 40^\circ$ . Below this, agreement was generally poor except in a region between  $\pm 3^\circ$  and  $\pm 6^\circ$  where the theoretical and simulated curves crossed.

As pointed out previously, for Atlas pad locations at the Cape essentially all significant population centers (except ships) are located in the sectors from  $\pm 100^\circ$  to  $\pm 180^\circ$ . Thus any B with the corresponding best-fit value of A can be used to compute launch-area risks, irrespective of the assumed breakup  $q\alpha$ . In unusual cases at the Cape or at other launch locations, population centers may be located outside sectors of good agreement for some B's. If such situations arise, a value of B should be used in the risk calculations that produces the best fit over the largest sector possible, generally  $\pm 40^\circ$  to  $\pm 180^\circ$ . The values of B producing this result are listed in Table 22 as functions of breakup conditions.

Table 22. Best-Fit Conditions for Atlas IIAS

Breakup Conditions	B	A
none	50,000	3.15
20,000	100,000	4.30
10,000	100,000	4.75
5,000	5,000,000	6.30

Although the selected values of A produce poor agreement in the sectors from  $0^\circ$  to  $\pm 40^\circ$ , this does not mean that good agreement in this region is impossible. Instead, it means that the value of A required to produce good agreement in the  $\pm 40^\circ$  sectors will produce poor agreement elsewhere. In special situations where the only population centers of interest are within  $\pm 40^\circ$  of the flight line, other values of A can be derived for use in the risk calculations.

From a practical standpoint, the effort required to find a value of A that produces a better fit within  $\pm 40^\circ$  or so of the flight line is unnecessary. Within this sector, the Mode-4 failure response, which is almost 11 times more likely to occur than a Mode-5 response, totally dominates the computed risks. As verification, the DAMP program was run for the Atlas IIAS vehicle, and ship-hit contours plotted for three vastly different pairs of A's and B's. The results are shown in Figure 16 through Figure 21, where the total failure probability during the first two minutes of flight was assumed to be 0.04, and the probabilities of Mode-4 and Mode-5 responses were 0.033 and 0.005, respectively. For each A and B, ship-hit contours were computed for Mode 5 alone, and then for all response modes. As expected, some downrange extension occurred in the Mode-5 contours as the value of A was increased, since the higher the value of A, the more concentrated impacts are near the flight line. When all response modes were included in the calculations, contour differences were almost imperceptible, showing the total dominance of Mode 4. If the calculations were remade with a Mode-4

response 10.9\* instead of 6.6 ( $0.033 \div 0.005 = 6.6$ ) times as likely as a Mode-5 response, the differences in contours would be even less.

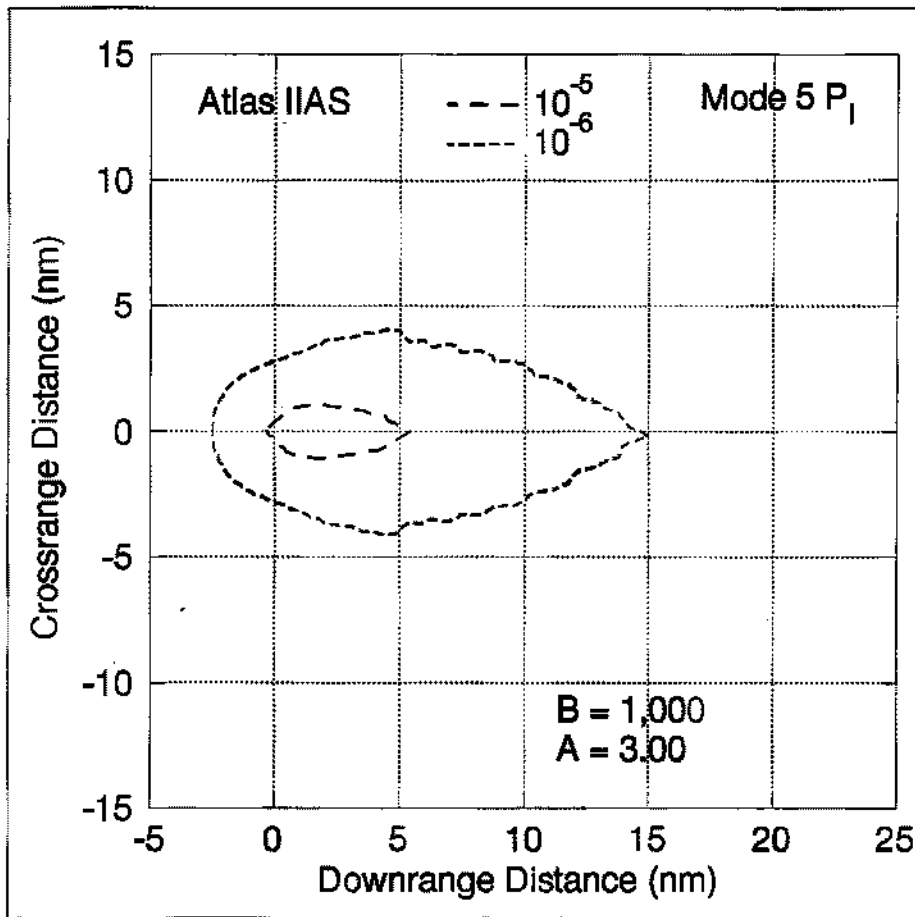


Figure 16. Atlas IIAS Mode-5 Ship-Hit Contours with A = 3.00

\* From Table 15,  $86.2 \div 7.9 = 10.9$ .

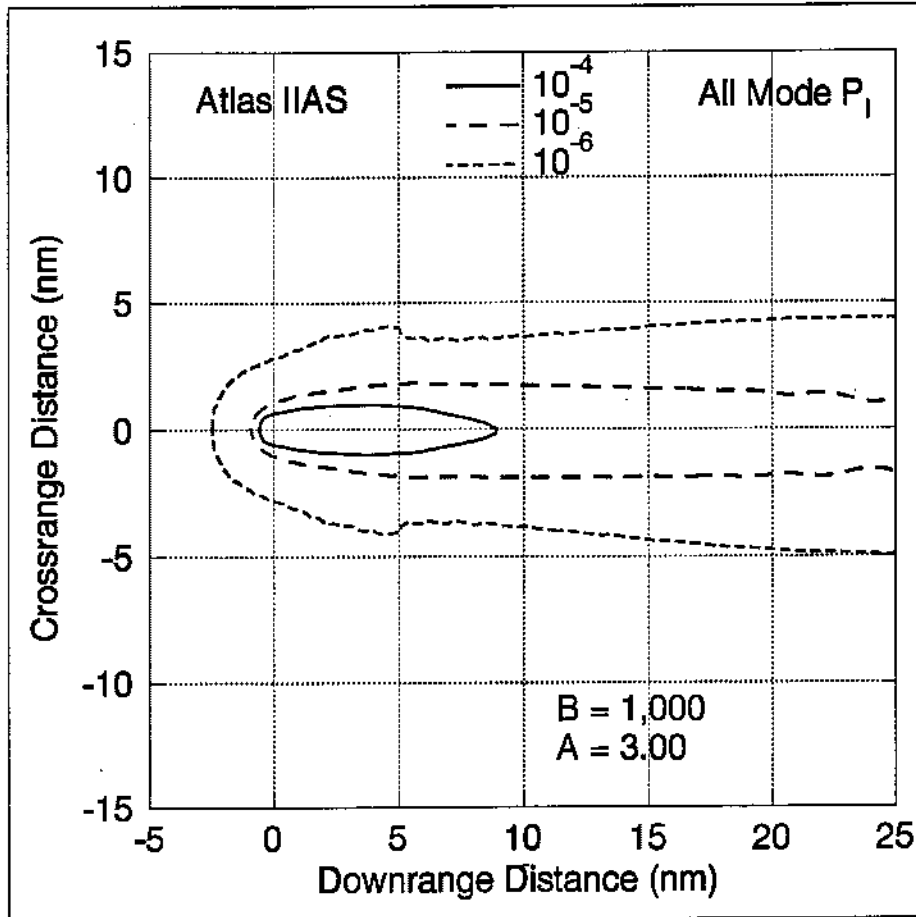


Figure 17. Atlas IIAS All-Mode Ship-Hit Contours with A = 3.00

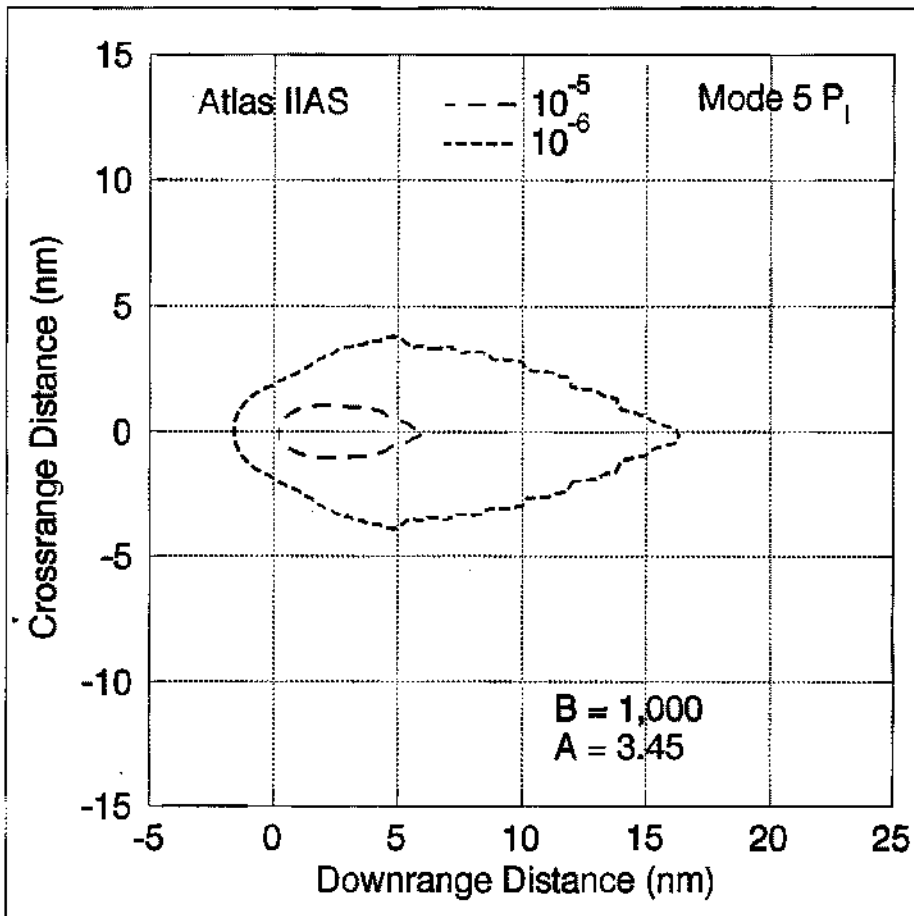


Figure 18. Atlas IIAS Mode-5 Ship-Hit Contours with A = 3.45

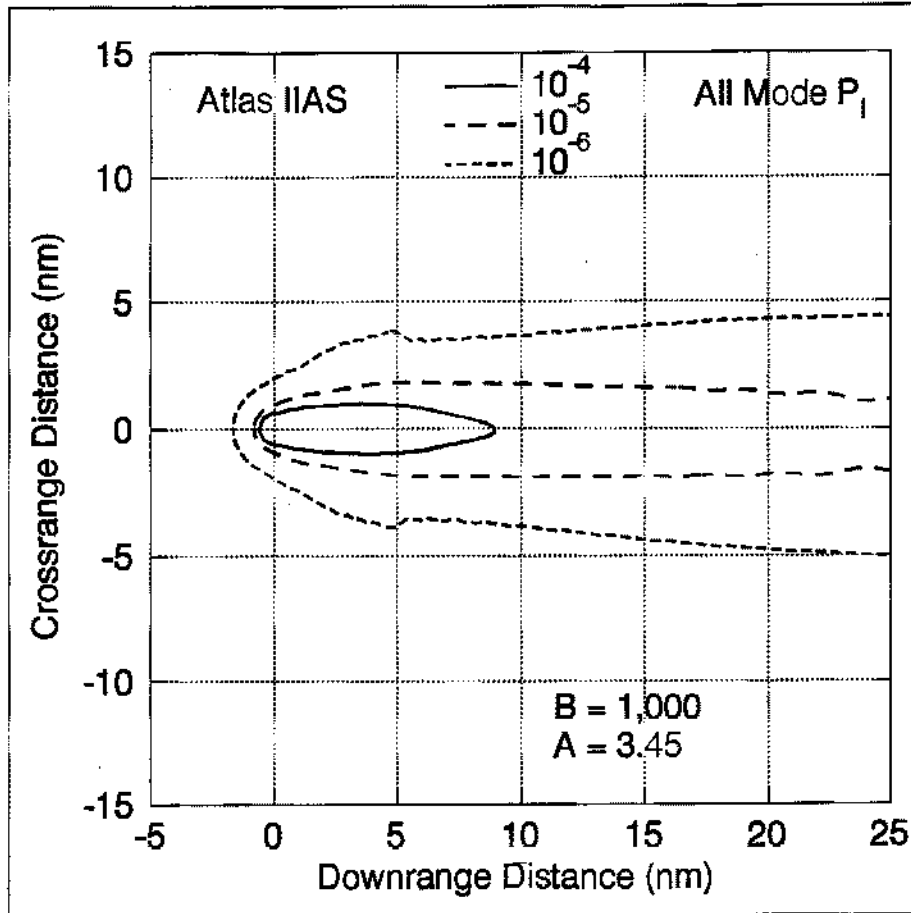


Figure 19. Atlas IIAS All-Mode Ship-Hit Contours with A = 3.45

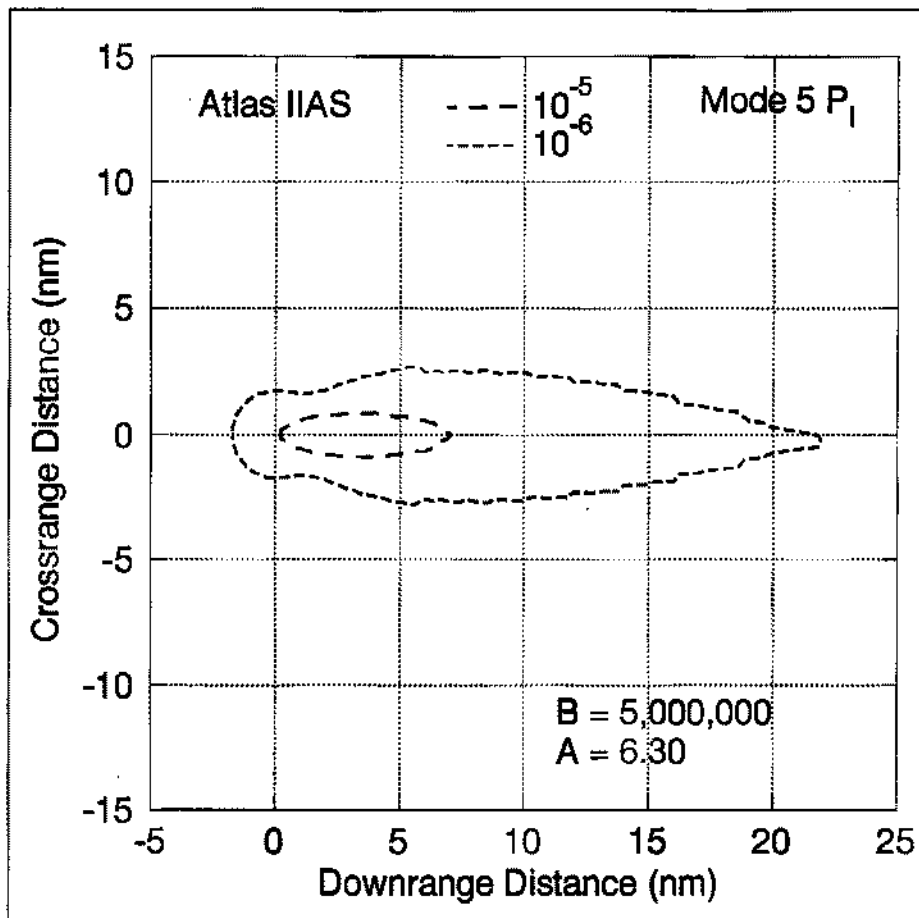


Figure 20. Atlas IIAS Mode-5 Ship-Hit Contours with A = 6.30

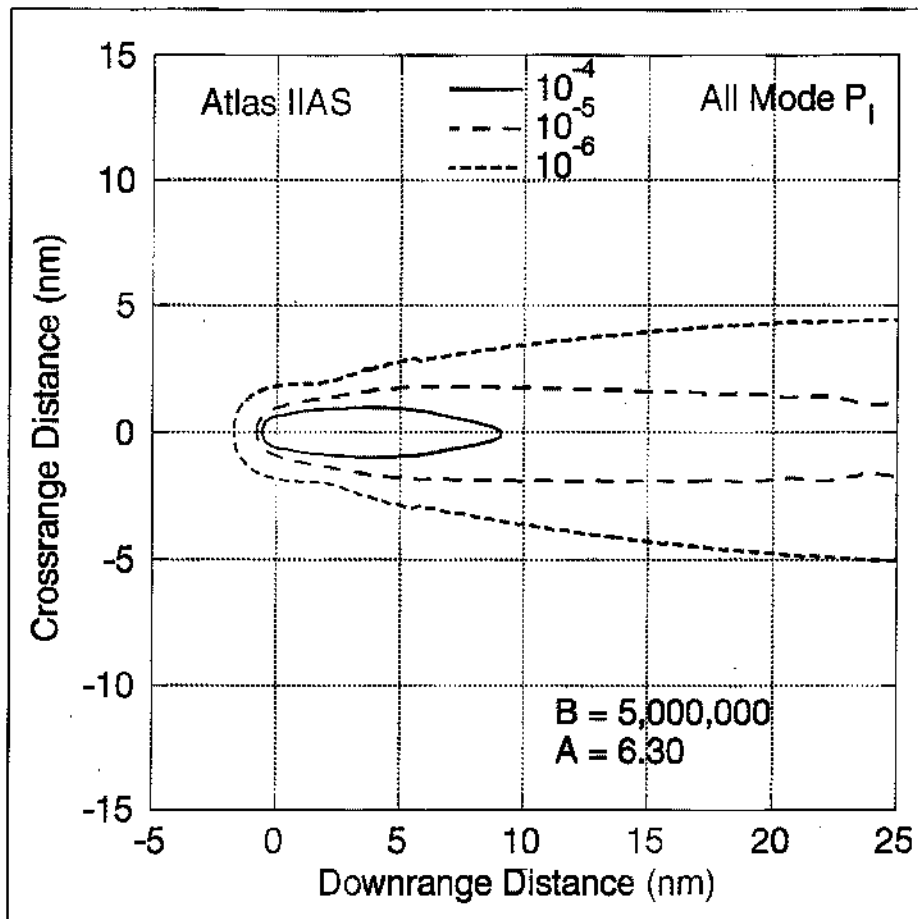


Figure 21. Atlas IIAS All-Mode Ship-Hit Contours with A = 6.30

#### 6.2.4 Range Distributions of Theoretical and Simulated Impacts

Earlier discussions had to do with how well the angular part of the Mode-5 impact density function could be made to agree with angular data derived from simulated random-attitude turns. A similar procedure was used to test agreement between the range part of the Mode-5 impact density function and the simulated data. For this purpose, beginning at 15 seconds random-attitude turns were made at 2-second intervals out to 279 seconds, assuming no breakup and breakup  $q\alpha$ 's of 5,000 and 20,000 deg-lb/ft<sup>2</sup>. At each time, 2,000 trajectories and impact points were computed, giving a total sample of 266,000 for each breakup condition. For each impact point, the range from the pad was computed, and the total number of impacts calculated in 10-mile range intervals out to 350 miles. Impacts beyond this range were placed in a single range category. The percentage of impacts in each range interval was then computed and plotted as shown in Figure 22.

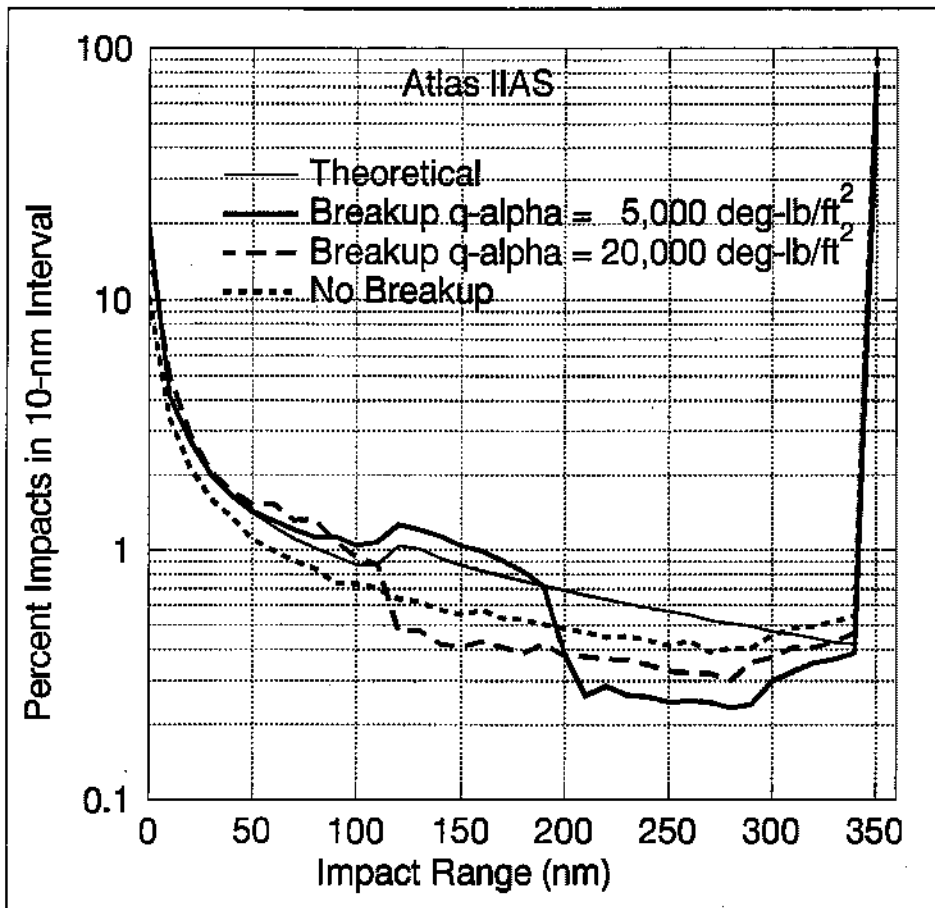


Figure 22. Impact-Range Distributions

Theoretical impact percentages for the same 10-mile range intervals were obtained by integrating the Mode-5 impact-density function [Eq. (3)] between the angle limits of zero and  $\pi$ , and between the range limits of  $R_1$  and  $R_2$ , and doubling the results. The percentages are plotted in Figure 22. As pointed out in more detail at the end of Appendix B, the percentage of impacts in any range interval is independent of the values of A and B.

Figure 22 shows that the range impact distributions for theoretical Mode-5 impacts and random-attitude failures for breakup  $q\alpha$ 's between 5,000 and 20,000 deg-lb/ft<sup>2</sup> are in excellent agreement out to 50 miles. Theoretical percentages and random-attitude percentages for  $q\alpha = 5,000$  deg-lb/ft<sup>2</sup> (considered to be the most realistic value) are in good agreement out to 190 miles. Beyond that the differences appear fairly large, magnified as they are by the logarithmic scale, although the maximum absolute difference is only 0.4%. The steep rise in all curves at 350 miles is artificially created by lumping all impacts beyond 350 miles into one range interval instead of 10-mile intervals.

### 6.3 Shaping Constants for Delta-GEM

Although less extensive, the computations made and graphs plotted to establish Mode-5 shaping constants for Delta parallel those described in Section 6.2 for Atlas IIAS. The approach may be summarized as follows:

- (1) Calculate impact points from 10,000 simulated random-attitude turns made at 10-second intervals from programming time at 6 seconds until staging at 270 seconds (260,000 simulations total). The impact points from these turns, which produce impact results similar to slow turns, are assumed to be representative of the totality of Mode-5 impacts.
- (2) Determine the percentages of impacts in  $5^\circ$  sectors from  $0^\circ$  to  $180^\circ$ .
- (3) For assumed values of A and B, compute the percentages of impacts in the same  $5^\circ$  sectors from the theoretical Mode-5 impact-density function.
- (4) By trial and error, find values of A and B that provide a best fit between the simulated and theoretical impact data.

### 6.3.1 Optimum Mode-5 Shaping Constants

The percentage of Delta vehicles that break up during simulated random-attitude turns are plotted against failure time in Figure 23. The same breakup  $q\alpha$ 's used in the Atlas IIAS calculations were used here. It can be seen from the figure that over 50% of the vehicles break up, either immediately or eventually, if a turn begins between about 10 and 115 seconds.

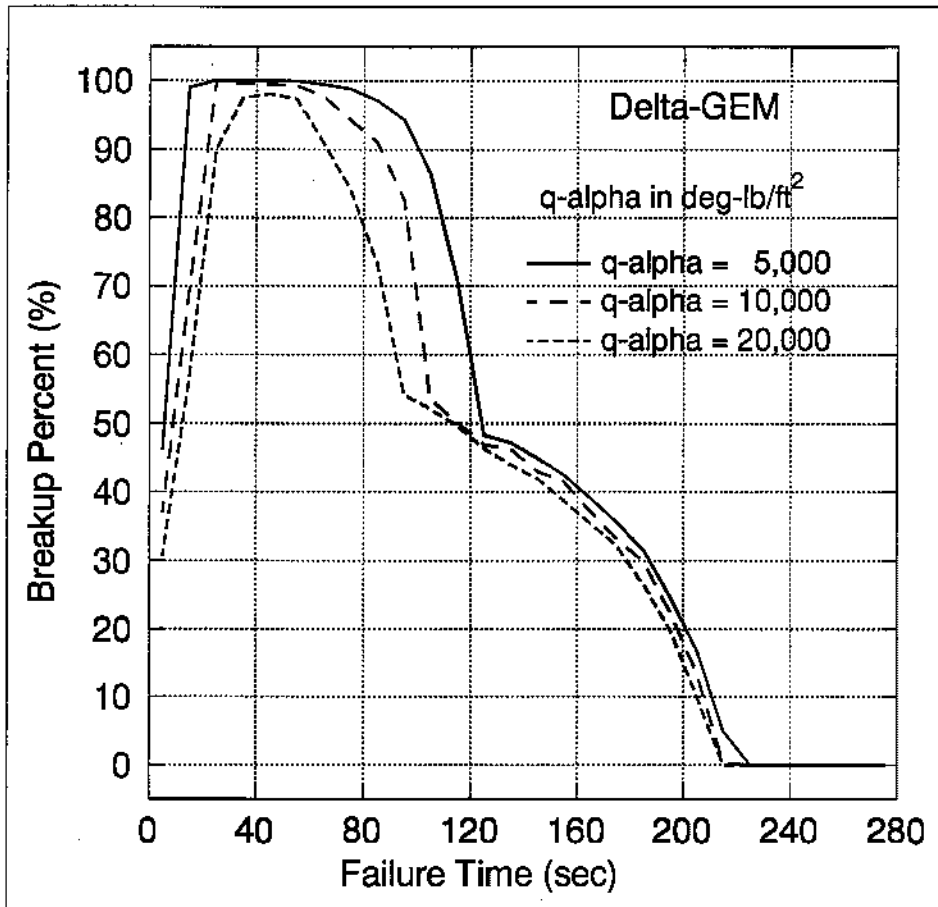


Figure 23. Delta-GEM Breakup Percentages

Figure 24 shows the percentages of malfunction-turn impacts in 5° sectors for no breakup and for breakup  $q\alpha$ 's of 20,000, 10,000, and 5,000 deg-lb/ft<sup>2</sup>. For  $B = 1,000$ , theoretical Mode-5 impacts are also plotted using best-fit values of  $A$ . This value of  $B$  was chosen since it is currently used by RTI in making launch-area risk studies for the 45th Space Wing. In the sectors from  $\pm 80^\circ$  to  $\pm 180^\circ$ , where most of the population centers are located, fairly good data fits were possible for all breakup  $q\alpha$ 's except 5,000 deg-lb/ft<sup>2</sup>. No value of  $A$  could be found to produce a good fit with  $B = 1,000$ . The bottom plot in Figure 25 shows that an excellent fit between malfunction-turn and theoretical data is possible for  $q\alpha = 5,000$  deg-lb/ft<sup>2</sup> if a different choice of  $B$  is made.

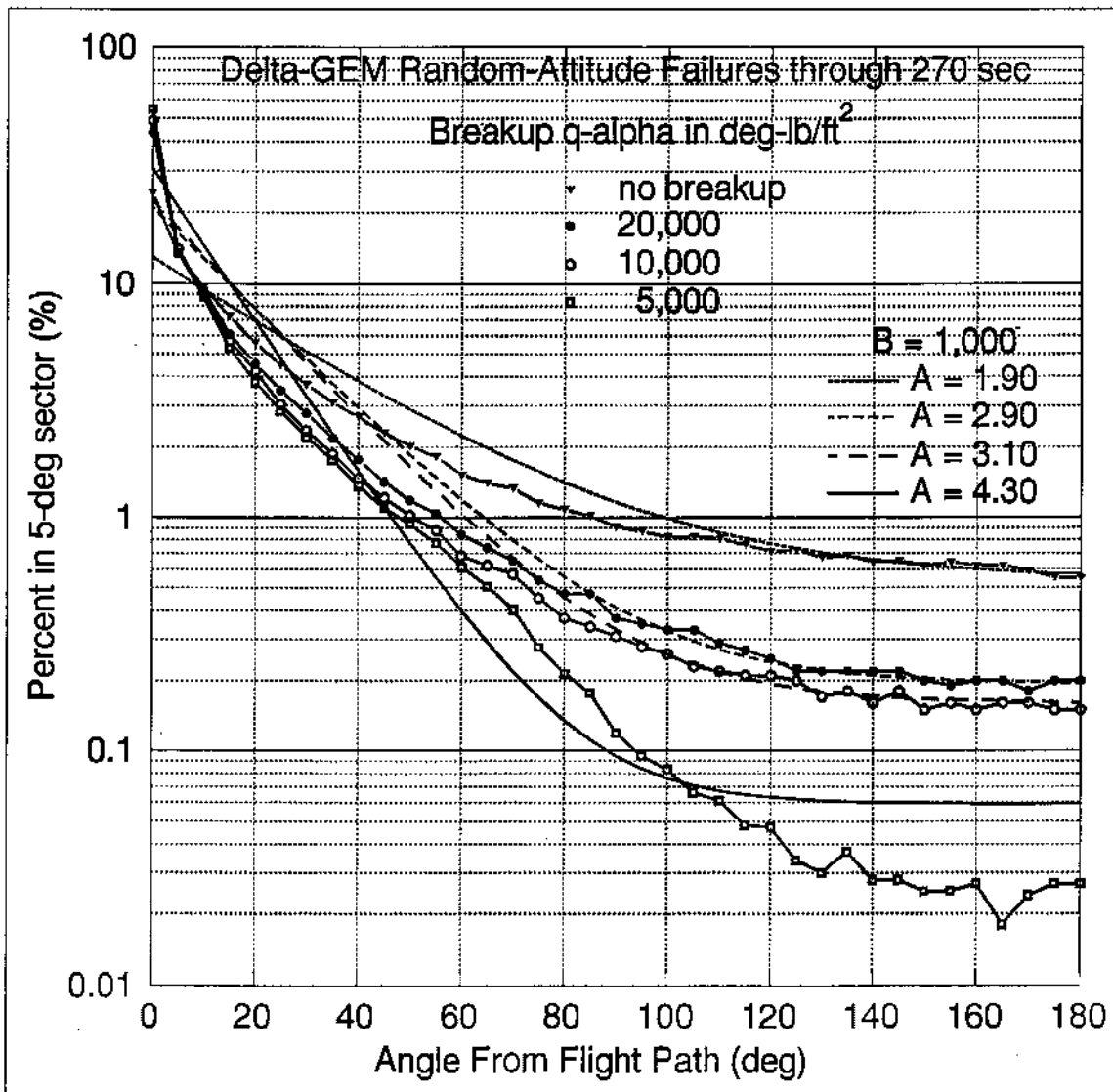


Figure 24. Delta-GEM Simulation Results with  $B = 1,000$

The simulated impact percentages plotted in Figure 25 are identical with those shown in Figure 24. The theoretical percentages in Figure 25 were obtained by trying various combinations of B and A until the best possible fit was obtained in the sectors from  $\pm 60^\circ$  to  $\pm 180^\circ$ . From these plots it seems apparent that a reasonable fit between malfunction-torn and theoretical Mode-5 impact data can be found for any  $q\alpha$  between 5,000 and 20,000 deg-lb/ft<sup>2</sup>.

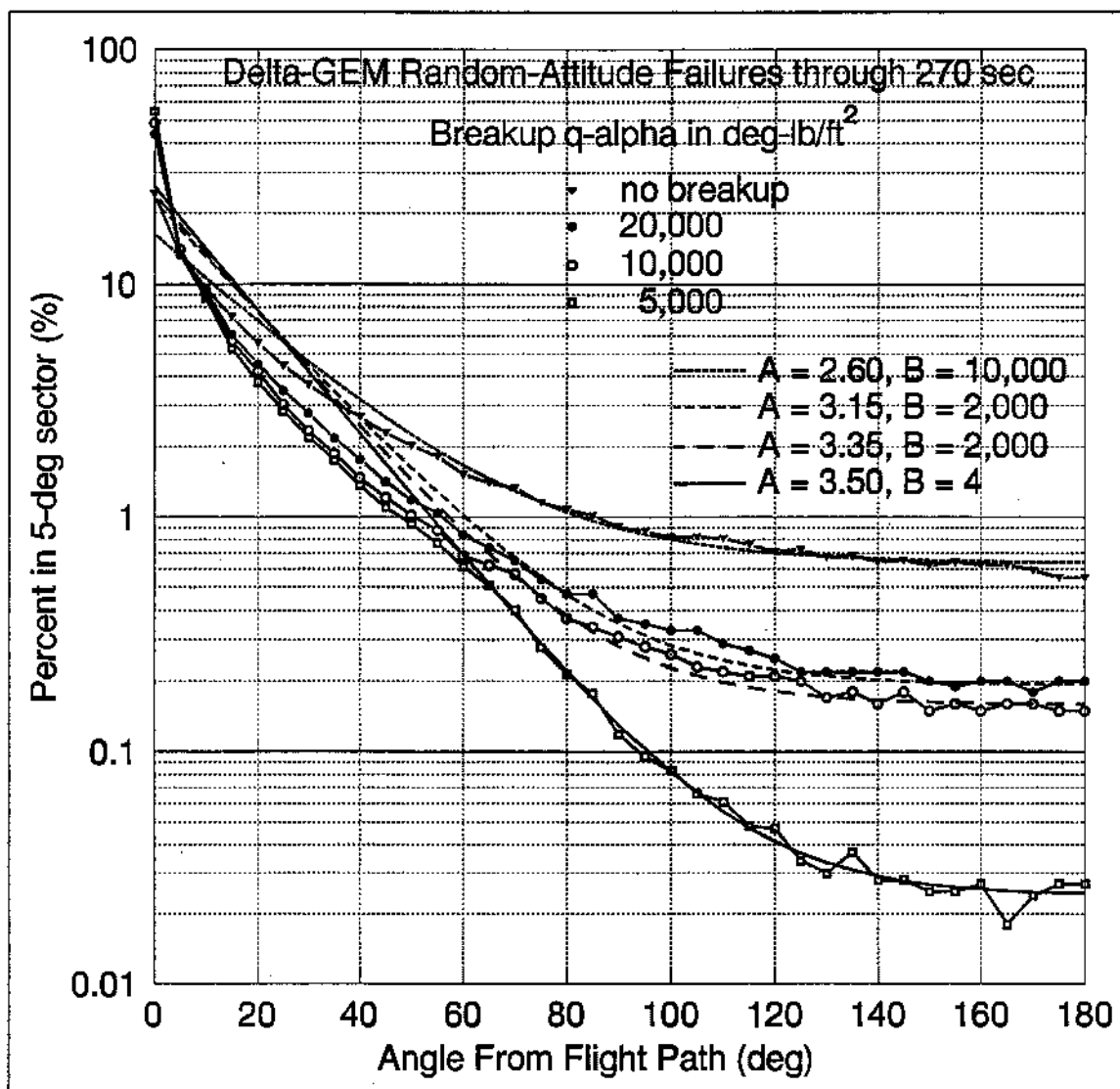


Figure 25. Delta-GEM Simulation Results with Best-Fit Shaping Constants

### 6.3.2 Launch-Area Mode-5 Risks

Using values of A and B from Figure 24 and Figure 25, program DAMP was run to compute Mode-5 launch-area risks for population centers inside the impact limit lines for a Delta-GEM/GPS-10 daytime launch from Pad 17A. Results from these and two other cases are shown in Table 23. The Mode-5  $E_c$  in the first line (old baseline case) is presented for comparison. It was obtained from the first line of Table 55 of an earlier RTI study<sup>31</sup>. In that study, the total Delta failure probability during the first 130 seconds of flight was set at 0.02, with the probability of a Mode-5 response assumed to be 0.0025. The second line in Table 23 shows the result of a recomputation of the Mode-5 risks, again with  $B = 1,000$  and  $A = 3$ , using failure probabilities derived earlier in this report. From Table 6 and Table 15, the failure probability during flight phases 0 - 2 is 0.013, and the relative frequency of occurrence of a Mode-5 response is 0.08. The absolute probability of a Mode-5 response thus becomes  $0.013 \times 0.08 \cong 0.001$ .

Table 23. Shaping Constants and Related Risks for Delta-GEM

$p_s$	$T_b$ (sec)	Breakup $q\alpha$ (deg-lb/ft <sup>2</sup> )	B	A	Mode-5 $E_c$ ( $\times 10^4$ )	
0.0025	130	12,000 * (baseline)	1,000	3.00	394	
0.001	270	12,000 * (new $p_s$ & $T_b$ )	1,000	3.00	88.8	
0.001	270	none	1,000	1.90	220.0	
		20,000		2.90	104.4	
		10,000		3.10	74.1	
		5,000		4.30	5.2	
0.001	270	none	10,000	2.60	224.4	
		20,000		2,000	3.15	102.4
		10,000		2,000	3.35	72.0
		5,000		4	3.50	5.1

\* Interpolated from data contained in Figure 24

As in the case of Atlas, Table 23 again shows that the risks in the launch area are highly dependent on  $q\alpha$  and thus on A, but relatively insensitive to changes in B if a proper value is selected for A. For example, if  $q\alpha = 10,000$ , the computed risks for  $B = 1,000$  ( $A = 3.10$ ) and  $B = 2,000$  ( $A = 3.35$ ) differ by less than 3%. For the no-breakup cases where  $B = 1,000$  and then 10,000, the computed risks in the launch area differ by less than 2%.

Launch-area risks are highly dependent on the vehicle's capability to withstand aerodynamic forces. Except early in flight, low-strength vehicles generally break up quickly after a malfunction turn begins. The later such turns occur, the more likely pieces are to impact downrange of the launch point, thus lessening risks to uprange populations. The effects of vehicle strength on risk are clearly seen in Table 23 where,

for example, the risks are over 20 times as great if the vehicle's breakup  $q\alpha$  is 20,000 rather than 5,000 deg-lb/ft<sup>2</sup>.

#### 6.4 Shaping Constants for Titan IV

Mode-5 shaping constants for Titan IV were developed as described in Section 6.3 for Delta, except that a total of 290,000 simulations were run between the programming time of 18 seconds and staging at 300 seconds. The percentage of vehicles that break up during simulated random-attitude turns are plotted against failure time in Figure 26. The same  $q\alpha$ 's used with Atlas and Delta were used here, and similar breakup results were obtained.

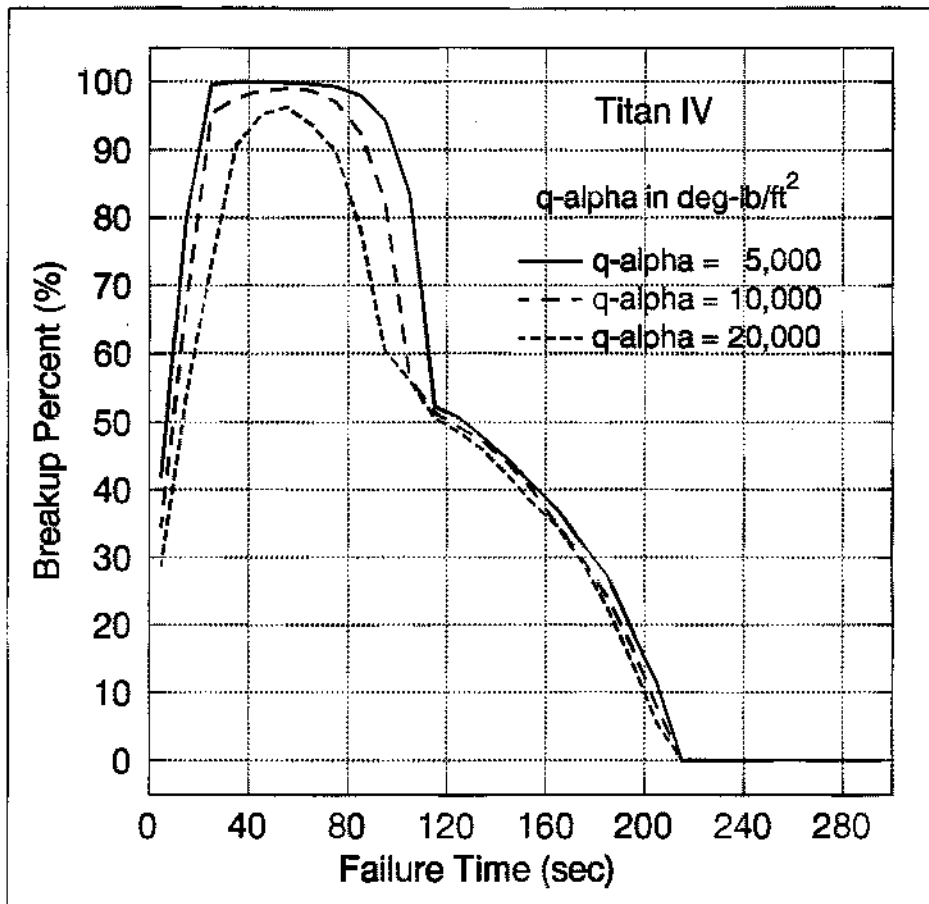


Figure 26. Titan IV Breakup Percentages

Figure 27 shows the percentages of malfunction-turn impacts in 5° sectors for no breakup and for breakup  $q\alpha$ 's of 20,000, 10,000, and 5,000 deg-lb/ft<sup>2</sup>. For  $B = 1,000$ , theoretical Mode-5 impact distributions are also plotted in the figure using best-fit values of  $A$ . This value of  $B$  was chosen since it is currently used by RTI in making launch-area risk studies for 45 SW/SE. Within the sectors from  $\pm 60^\circ$  to  $\pm 180^\circ$ , where most population centers are located, data fits are reasonably good. As seen in the next figure, the divergence for the no-breakup case can be greatly reduced by selecting other values for  $B$  and  $A$ .

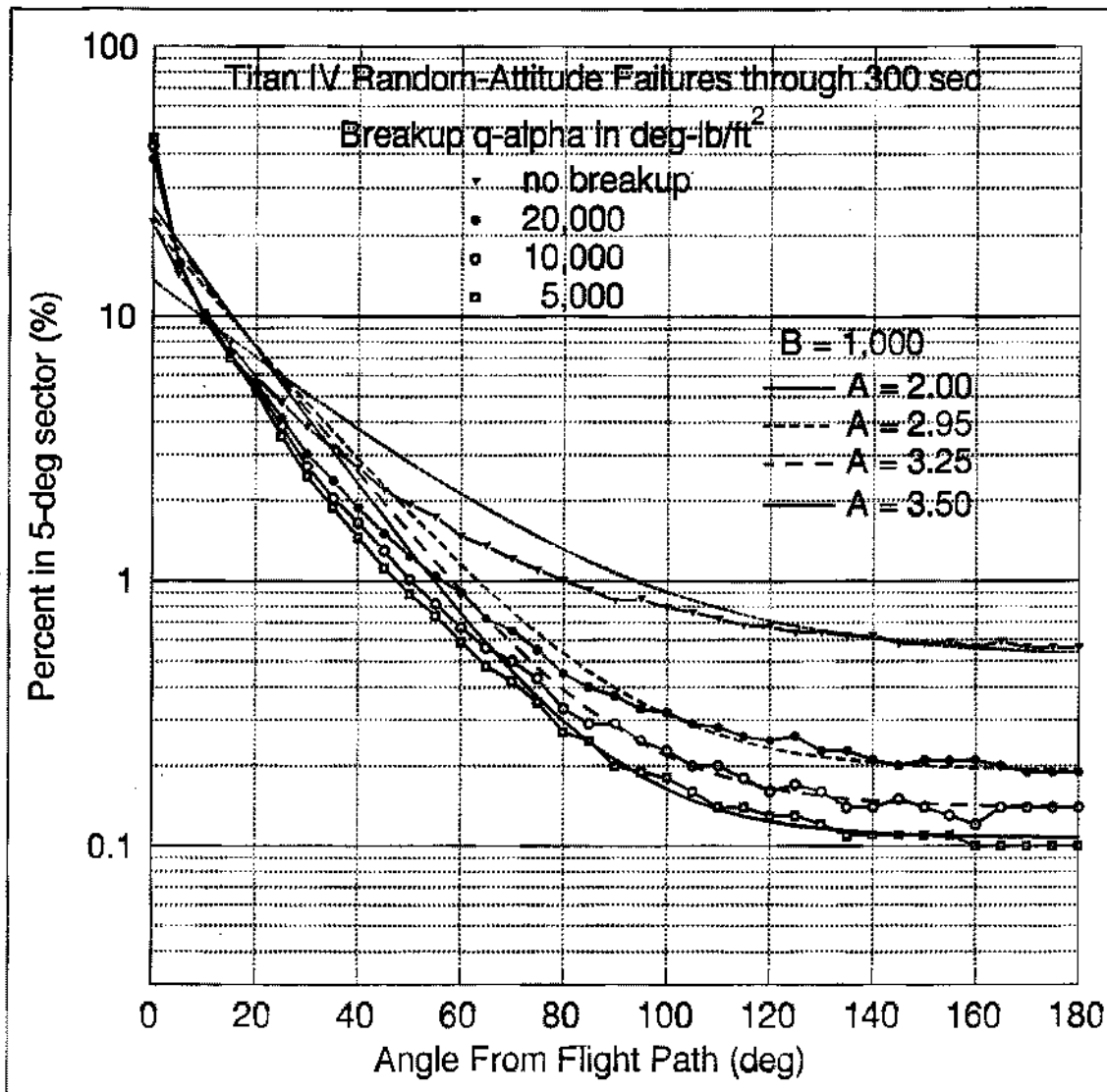


Figure 27. Titan Simulation Results with  $B = 1,000$

The simulated impact distributions plotted in Figure 28 are identical to those shown in Figure 27. The theoretical Mode-5 percentages were obtained by testing various combinations of B and A until a good fit between the simulated malfunction-turn results and theoretical impact-distribution data was obtained in the sectors from  $\pm 60^\circ$  to  $\pm 180^\circ$ . Although somewhat better fits may be possible for the lower breakup  $q\alpha$ 's, the effort to find them did not seem worthwhile, since the A's and B's shown in the figure produced fits that were more than adequate in the sectors where the population centers are located.

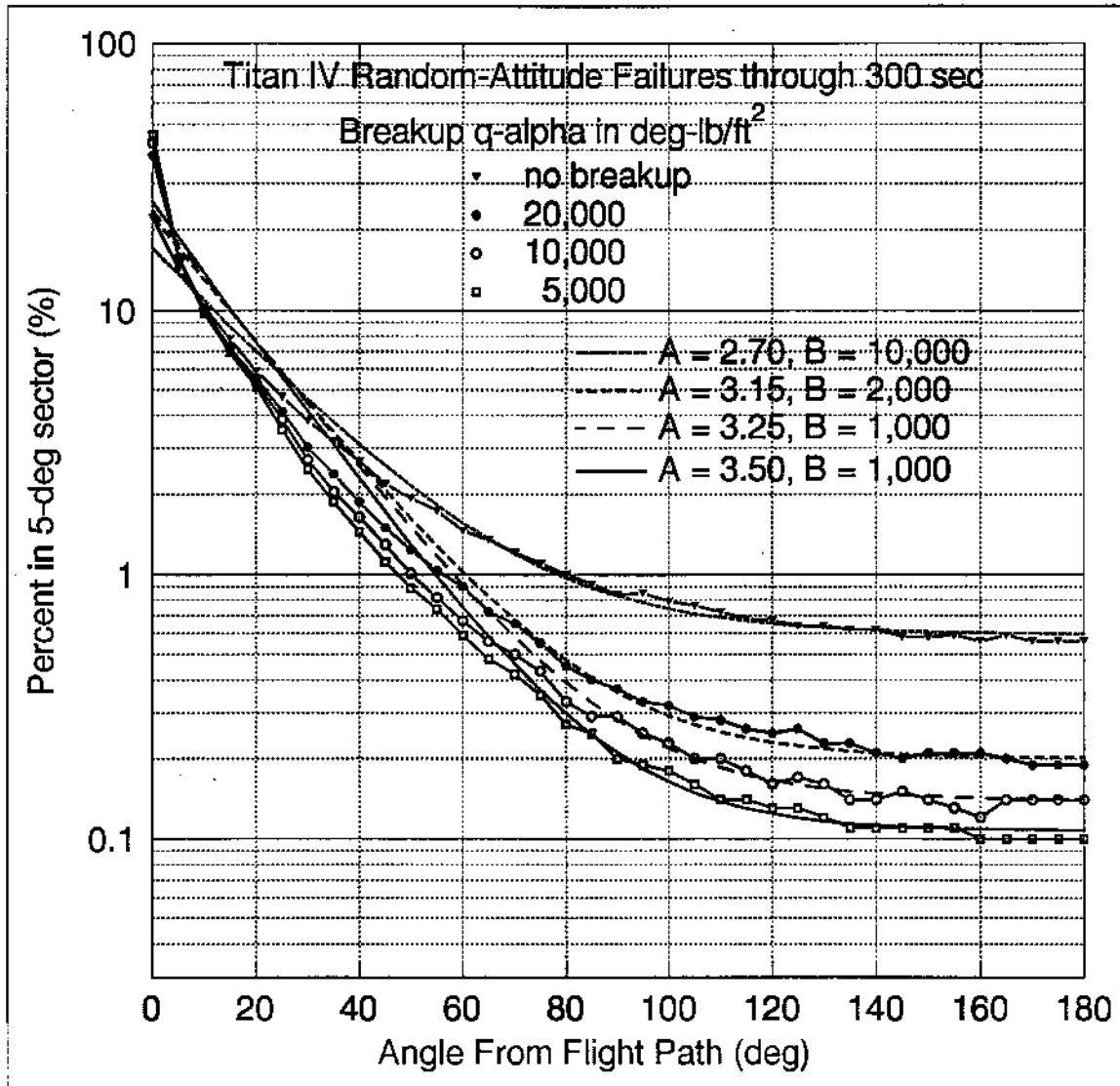


Figure 28. Titan Simulation Results with Best-Fit Shaping Constants

The best-fit values of B and A shown in Figure 27 and Figure 28 are tabulated for convenient reference in Table 24. For breakup  $q\alpha$ 's of 10,000 and 5,000 deg-lb/ft<sup>2</sup>, the currently-used value of B = 1,000 provided a better data fit than other values of B that were investigated.

Table 24. Shaping Constants for Titan IV

$T_b$ (sec)	Breakup $q\alpha$ (deg-lb/ft <sup>2</sup> )	B	A
300	none	1,000	2.00
	20,000		2.95
	10,000		3.25
	5,000		3.50
300	none	10,000	2.70
	20,000	2,000	3.15
	10,000	1,000	3.25
	5,000	1,000	3.50

Risk calculations in the launch area were not made for Titan IV.

## 6.5 Shaping Constants for LLV1

Shaping constants for LLV1 were developed as described in Section 6.3 for Delta, except that a total of 290,000 simulations were made between the programming time of 1 second and staging at 290 seconds. The percentages of vehicles that break up during simulated random-attitude turns are plotted in Figure 29. As expected, the results are similar to those shown previously for Atlas, Delta, and Titan although, due to its higher acceleration, the rapid drop-off from near 100% breakup occurs at an earlier time for the LLV1 than for the other vehicles.

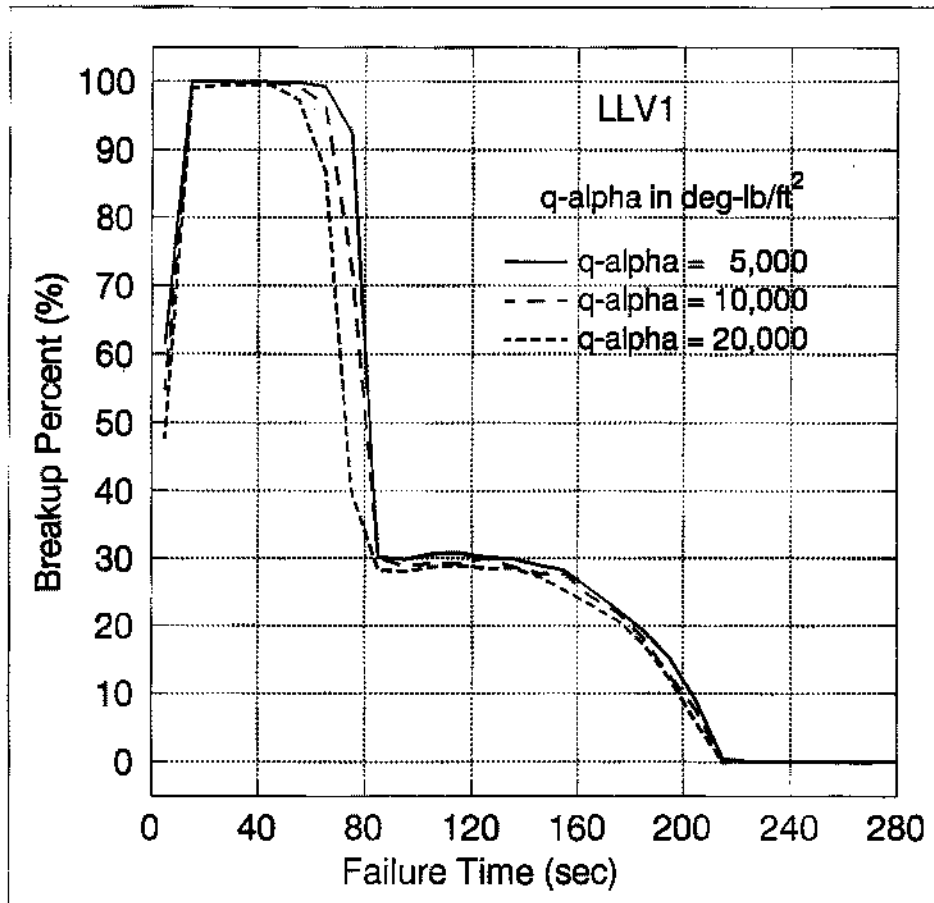


Figure 29. LLV1 Breakup Percentages

Figure 30 shows the percentage of malfunction-turn impacts in 5° sectors for no breakup, and for breakup  $q\alpha$ 's of 20,000, 10,000, and 5,000 deg-lb/ft<sup>2</sup>. The three breakup  $q\alpha$ 's produced impact distributions that were surprisingly similar, possibly due to the vehicle's higher acceleration. Theoretical Mode-5 impact distributions are also plotted in the figure for  $B = 1,000$  and best-fit values of  $A$ . This value of  $B$  was chosen since it is currently used by RTI in making launch-area risk studies for 45 SW/SE. For all except the no-breakup case, values of  $A$  were found that produced good fits between the malfunction-turn and Mode-5 impact distributions in the sectors from  $\pm 60^\circ$  to  $\pm 180^\circ$ .

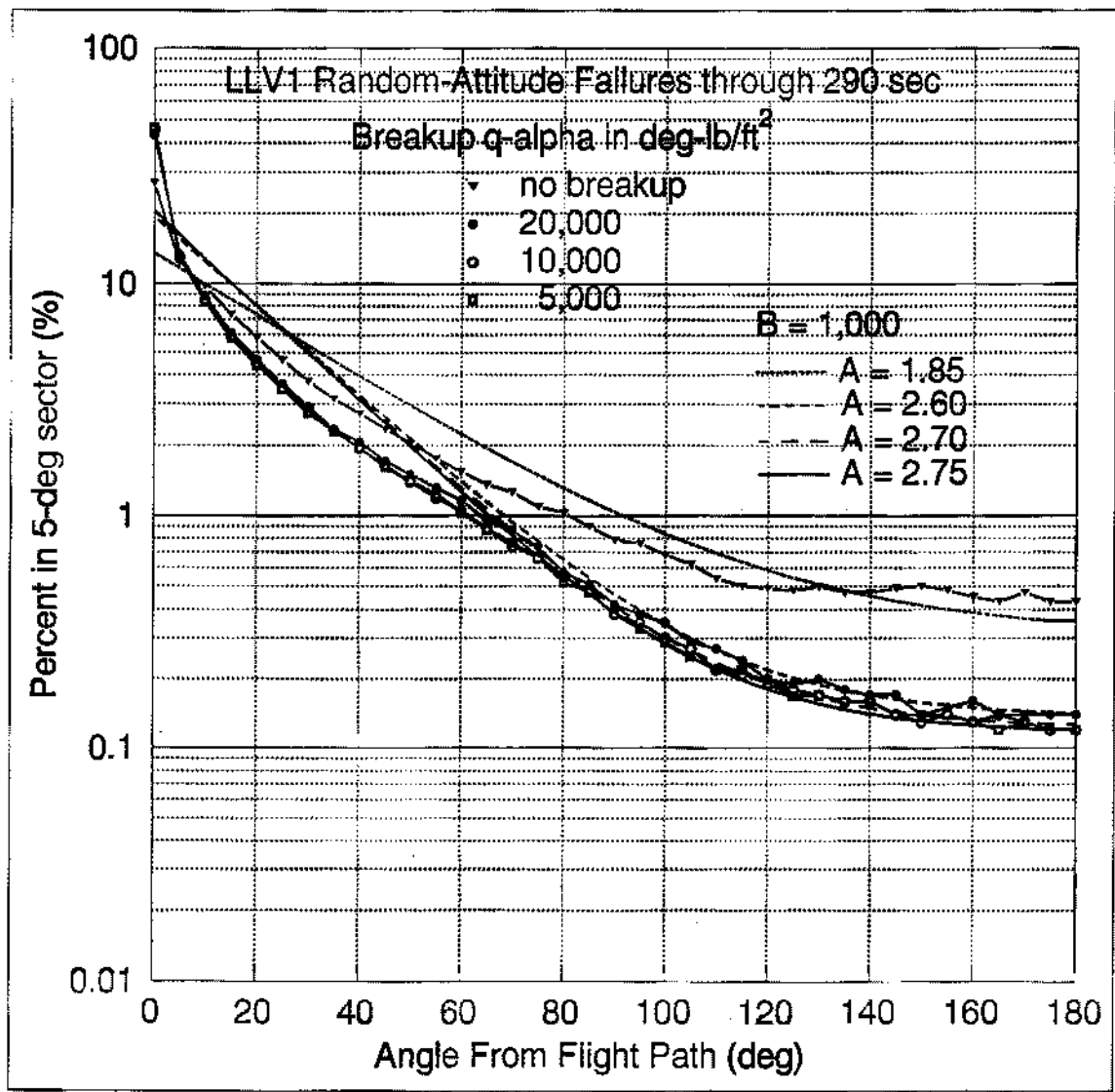


Figure 30. LLV1 Simulation Results with  $B = 1,000$

Figure 31 shows that a good fit for the no-breakup case is possible if higher values of B and A are used. The simulated malfunction-turn impact distributions for the breakup cases plotted in this figure are identical with those in Figure 30. Since the theoretical percentages for B = 1,000 produced excellent fits, these values were simply replotted in Figure 31. For the no-breakup case, various combinations of B and A were tried before arriving at the plot shown in the figure.

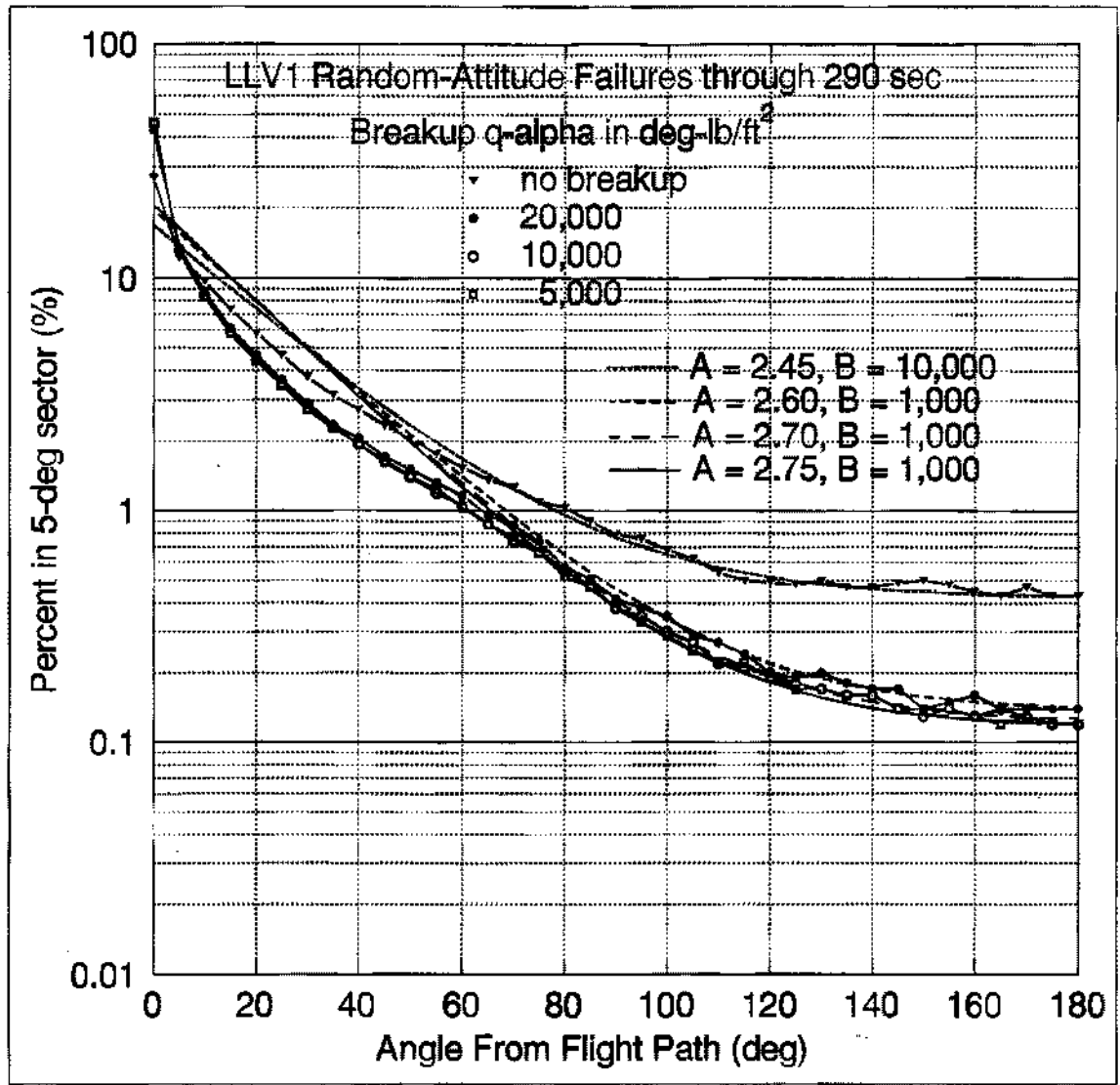


Figure 31. LLV1 Simulation Results with Best-Fit Shaping Constants

The best-fit values of B and A from Figure 30 and Figure 31 have been listed for convenient reference in Table 25. It is interesting to note that, for all breakup conditions, the currently-used value of B = 1,000 provided a better data fit than any other B that was investigated.

Table 25. Shaping Constants for LLV1

$T_b$ (sec)	Breakup $q\alpha$ (deg-lb/ft <sup>2</sup> )	B	A
290	none	1,000	1.85
	20,000		2.60
	10,000		2.70
	5,000		2.75
290	none	10,000	2.45
	20,000	1,000	2.60
	10,000	1,000	2.70
	5,000	1,000	2.75

No launch-area risk calculations were made for LLV1.

### 6.6 Shaping Constants for Other Launch Vehicles

Procedures for developing Mode-5 shaping constants A and B are fully described in this report. For Atlas, Delta, Titan, and LLV1, best-fit values of A were derived for four breakup conditions (1) for the currently-used value of B = 1,000, and (2) for optimum-fit values of B. For any new launch vehicle requiring risk calculations, the same procedures should be followed to obtain suitable values for A and B.

As an alternative and less time-consuming process, values of A and B can be estimated by comparing the new vehicle with one of the four vehicles referred to above and listed in Table 26. If the configuration and trajectory of the new vehicle and one of the listed vehicles are similar, values of A and B shown in the table for that vehicle and the assumed breakup condition can be used. There may, of course, be no similarity between the new vehicle and any of the listed vehicles. In that event and depending on assumed breakup conditions, one of the mean values shown in the last row of the table can be selected until better values can be developed.

Table 26. Summary of A Values for B = 1,000

Vehicle	IP Range (nm) at 30 sec	Breakup $q\alpha$ (deg-lb/ft <sup>2</sup> )			
		5,000	10,000	20,000	None
Atlas IAS	0.3	3.45	3.20	2.75	1.90
Delta-GEM	5.2	4.30	3.10	2.90	1.90
Titan IV	1.9	3.50	3.25	2.95	2.00
LLV1	33.4	2.75	2.70	2.60	1.85
Other vehicles		3.5	3.1	2.8	1.9

## 7. Potential Future Investigations

Because of contract limitations on funds and the deadline for publishing the report, certain interesting facets of the Mode-5 modeling process could not be fully investigated. Several such issues are listed below in considered order of importance:

- (1) Effects on shaping constants A and B of using more precise breakup ( $q\alpha$ ) conditions during malfunction-turn simulations.
- (2) Effects on shaping constants A and B (and thus overall risks) if different values of  $T_b$  are used in computing theoretical and simulated impacts (e.g.,  $T_b$  corresponding to burnout of zero, first, and second stages).
- (3) Effects on shaping constants A and B if drag is accounted for in computing free-fall impact points after a malfunction turn. (Shaping constants could be determined for maximum, minimum, and intermediate ballistic coefficients, then interpolated for other values. This more accurate approach would ultimately require extensive modifications to DAMP.)
- (4) Effects on shaping constants A and B if sectors smaller than  $5^\circ$  are used to compare theoretical and simulated impact data (e.g.,  $1^\circ$  or  $2^\circ$ ).
- (5) Effects on relative failure probabilities for solid-propellant vehicles if unclassified solid-propellant vehicles or declassified test results are used in the historical data samples (e.g., Pershing, Polaris, Poseidon, Trident).

Other tasks that should be performed at some point in the future include:

- (a) Update absolute failure probabilities for Atlas, Delta, Titan, and perhaps other vehicles.
- (b) Develop suitable shaping constants A and B for new vehicles. (In this regard, see Section 6.6)

## 8. Summary

In RTI's risk-computation program DAMP, vehicle failures per se are not considered. Instead each catastrophic failure is assumed to produce one of five failure responses, and it is these response modes that are modeled in DAMP. Although most catastrophic failures result in impacts near the flight line, less likely malfunctions may cause debris to fall either uprange or well away from the flight line. In DAMP, vehicle failures with this potential are, for the most part, classified as Mode-5 failure responses. The resulting impacts are modeled by a rather formidable-looking density function that includes two shaping constants (A and B) that strongly influence the nature of the impact-density function. To obtain absolute probabilities (or risks), the function must be multiplied by a probability-of-occurrence factor ( $p_s$ ). The primary purpose of this study was to determine the best values for A, B, and  $p_s$  for various vehicle programs. Other objectives not explicitly included in the statement of work were to develop absolute failure probabilities for Atlas, Delta, and Titan and to derive relative probabilities of occurrence for the five failure-response modes in DAMP.

Although some risk analyses may ignore unlikely failure-response modes, Section 2 demonstrates the need for a Mode-5 response - or some similar response - through brief descriptions of actual vehicle flights. Section 3 and Appendix B provide the reader with a fuller understanding of the nature and intricacies of the Mode-5 impact-density function. Together, they show how density-function shaping is affected by values of A and B, and in particular how the Atlas IAS launch-area risk contours change if the value of A is changed.

Section 4 is a philosophical discussion of methods of assessing vehicle failure probability (or reliability). Two approaches are discussed, one strictly empirical, the other a parts-analysis method that involves the assignment of failure probabilities to individual parts, components, and systems. Although difficulties exist with both approaches, the empirical method was chosen to estimate both absolute and relative failure probabilities.

As the first step in estimating failure probabilities empirically, performance histories were gathered, summarized, and tabulated (Appendix D) by launch date for Atlas, Delta, and Titan vehicle launches from the Eastern and Western Ranges, and for Thor launches from the Eastern Range. Obtaining this information, and assigning response modes and associated flight phases for each failure consumed a large portion of the effort expended on this task.

A filtering (i.e., data weighting) technique was selected (see Section 5.1 and Appendix C) and applied to the launch failure data to estimate overall failure probabilities by flight phase (see Section D.1.3) for Atlas, Delta, and Titan vehicles. The recommended failure probabilities are based on test results involving only those vehicle configurations that are considered to be representative of current launch

configurations (see Section D.1.4). The results, summarized previously in Table 6 of Section 5.1, are repeated here in Table 27. Flight phases 0 - 1 go from liftoff through first-stage or booster cutoff, while flight phase 2 extends through second-stage or sustainer cutoff. Although failure probabilities for all flight phases are listed in Table 2, only malfunctions during flight phases 0 through 1 have significant effects on launch-area risks.

Table 27. Failure Probabilities for Atlas, Delta, and Titan

Vehicle	Predicted Failure Probability	
	Flight Phase 0 - 1	Flight Phase 0 - 2
Atlas	0.022	0.031
Delta	0.010	0.013
Titan	0.040	0.064

Absolute overall failure probabilities for Atlas, Delta, and Titan were based only on flight results from "representative" vehicle configurations. Because of the small number of failures in the individual representative samples, test results for all configurations (including Thor) were combined into a single sample and filtered to estimate relative failure probabilities for the five failure-response modes in program DAMP (see Section 5.2). The results for flight phases 0 - 2 and 0 - 1, together with recommended values for new launch systems, were summarized in Table 15 and Table 16, respectively, and are repeated here in Table 28 and Table 29.

Table 28. Recommended Response-Mode Percentages for Flight Phases 0 - 2

Response Mode	Mature Launch Systems (F = 0.993)	New Solid Systems (F = 0.996)	New Liquid Systems (F = 0.999)
1	0.4	2.2	7.4
2	5.4	4.3	2.3
3	0.1	0.4	1.7
4	86.2	80.4	73.3
5	7.9	12.7	15.3

Table 29. Recommended Response-Mode Percentages for Flight Phases 0 - 1

Response Mode	Mature Launch Systems (F = 0.993)	New Solid Systems (F = 0.996)	New Liquid Systems (F = 0.999)
1	0.5	3.4	10.7
2	7.4	6.6	4.3
3	0.1	0.6	2.4
4	81.9	74.5	67.0
5	10.1	14.9	15.6

For Atlas, Delta, and Titan, absolute probabilities for the individual response modes were obtained by multiplying absolute failure probabilities from Table 27 by the relative probabilities shown in the second columns of Table 28 and Table 29. The results, presented originally in Table 17, are repeated below in Table 30. To obtain

these results, the relative probabilities used were more precise than those given in Table 28 and Table 29. No pretense is made that all figures in Table 30 are actually significant.

Table 30. Absolute Failure Probabilities for Response Modes 1 - 5

Vehicle:	Atlas		Delta		Titan	
	0 - 1 (0-170 sec)	0 - 2 (0-280 sec)	0 - 1 (0-270 sec)	0 - 2 (0-630 sec)	0 - 1 (0-300 sec)	0 - 2 (0-540 sec)
Mode 1	0.000119	0.000121	0.000054	0.000051	0.000216	0.000250
Mode 2	0.001637	0.001665	0.000744	0.000698	0.002976	0.003437
Mode 3	0.000011	0.000012	0.000005	0.000005	0.000020	0.000026
Mode 4	0.018007	0.026738	0.008185	0.011212	0.032740	0.055200
Mode 5	0.002226	0.002465	0.001012	0.001034	0.004048	0.005088
Total	0.022	0.031	0.010	0.013	0.040	0.064

The same chronological composite sample used to estimate relative failure probabilities for the failure-response modes was used to estimate the conditional probability that a Mode-3 or Mode-4 response terminates with a rapid tumble. This was found to be about one-third (see Section 5.3).

Because the empirical data were insufficient to determine Mode-5 density-function shaping constants A and B, an alternate approach was used. Basically, for each of four vehicles (Atlas, Delta, Titan, and LLV1), Mode-5 failure responses were simulated at a series of failure times. The simulated malfunctions investigated were random-attitude turns and slow turns. At each time, 10,000 impact points were computed. The percentages of impacts in 5° sectors from 0° (downrange) to 180° (uprange) were determined. These were compared with the percentages obtained in the same sectors from the theoretical Mode-5 impact-density function when specific values were assigned to A and B. By trial and error, values of A and B producing a good match between the two sets of percentages were established (see Section 6). After best-fit values were determined, the impact percentages for Atlas IIAS in 10-mile range increments were checked to verify that the range part of the Mode-5 impact-density function was consistent with impact ranges resulting from 266,000 simulated Mode-5 failure responses (see Section 6.2.4).

Since the impact distributions resulting from simulated malfunction turns were highly dependent upon the dynamic pressure ( $q\alpha$ ) assumed to cause vehicle breakup, shaping constants A and B were likewise dependent on breakup assumptions. Three breakup  $q\alpha$ 's and a no-breakup case were investigated by simulating 270,000 malfunction turns for each of the four conditions. Although a  $q\alpha$  of 5,000 deg-lb/ft<sup>2</sup> is considered most likely applicable for Atlas, Delta, and Titan, shaping constants for all breakup conditions were provided earlier in Section 6.

Traditionally, a value of  $B = 1,000$  has been used by the 45 SW/SE in ship-hit calculations, and by RTI in performing launch-area risk analyses for the 45 SW/SE. Using this value of  $B$ , for each vehicle values of  $A$  were found that produced a good match between simulated and theoretical data. The results for  $q\alpha = 5,000, 10,000,$  and  $20,000$  deg-lb/ft<sup>2</sup> are given in Table 31. As discussed earlier in the report, no single value of  $A$  could be found that produced a good fit over the entire 180° sector, although with one exception a good match did exist in the uprange portion of the sector from about  $\pm 90^\circ$  to  $\pm 180^\circ$ . For launches from Cape Canaveral, most population centers are located in this uprange sector. For any launch-area population centers located in the downrange sector, the risks are almost surely dominated by the Mode-4 failure response.

Table 31. Summary of A Values for  $B = 1,000$

Vehicle	Flight Phase	$T_b$ (sec)	Breakup $q\alpha$ (deg-lb/ft <sup>2</sup> )		
			5,000	10,000	20,000
Atlas IIAS	0 - 2	280	3.45	3.20	2.75
Delta-GEM	0 - 1	270	4.30	3.10	2.90
Titan IV	0 - 1	300	3.50	3.25	2.95
LLV1	0 - 2	290	2.75	2.70	2.60
Other vehicles	---	---	3.5	3.1	2.8

Other values of  $B$  were investigated to find combinations of  $B$  and  $A$  that provided the best possible data fits over the largest possible portion of the  $0^\circ$  to  $180^\circ$  sector. Although no combinations of  $A$  and  $B$  could be found that produced good fits for the entire 180° sector, the values shown in Table 32 extended the fit from the uprange direction to within about  $40^\circ$  of the downrange direction.

Table 32. Summary of Optimum Mode-5 Shaping Constants

Vehicle	Flight Phase	$T_b$ (sec)	Breakup $q\alpha$ (deg-lb/ft <sup>2</sup> )	$B$	$A$
Atlas	0 - 2	280	5,000	5,000,000	6.30
Delta	0 - 1	270	5,000	4	3.50
Titan	0 - 1	300	5,000	1,000	3.50
LLV1	0 - 2	290	5,000	1,000	2.75

Launch-area risk calculations were made for Atlas and Delta to ascertain the effects of using radically different values of  $A$  and  $B$  in the Mode-5 impact-density function. For example, for a breakup  $q\alpha$  of 5,000 deg-lb/ft<sup>2</sup>, values of  $A = 3.45$  and  $B = 1,000$  from Table 31 and  $A = 6.30$  and  $B = 5,000,000$  from Table 32 were used to determine total Mode-5 launch-area risks for an Atlas IIAS launch from Complex 36. The total risks differed by about 10%. (Other results for Atlas IIAS are given in Table 21, and for Delta in Table 23.) Other calculations for Atlas and Delta show that the value of  $B$  is not

important in the launch-area risk calculations provided an appropriate value of A is selected.

Since a good data match within  $\pm 40^\circ$  of the flight line was not found, the effect of this on ship-hit calculations was investigated. It was discovered that the values chosen for A and B made no significant difference, since the risks to shipping near the flight line are totally dominated by the Mode-4 failure response (see Section 6.2.3).

Mode-5 baseline risks for Atlas and Delta were recomputed using newly derived values for (1) shaping constants A and B, (2) the overall vehicle failure probability, and (3) the relative probabilities of occurrence of the individual failure-response modes. Results were then compared with baseline risks computed in prior RTI studies. For Atlas, Mode-5 launch-area risks were reduced by a factor between 3 to 11, the exact value depending on the assumed breakup  $q_0$  for the vehicle. For Delta, the reduction factor was between 4 and 75, with the exact value again depending on assumed breakup conditions.

## Appendix A. Failure Response Modes in Program DAMP

In program DAMP, no attempt is made to model vehicle behavior for failure of specific systems and components. A list of such failures and possible behaviors for any vehicle would be extensive, and variations from vehicle to vehicle would complicate the modeling process, or make it almost impossible. Instead, failure *responses* are modeled in DAMP without regard to the specific failure that causes the response. There are only six possible response modes in DAMP, five for failures, and one to model the behavior of a normal vehicle. The six vehicle-response modes are described in layman's language as follows; technical descriptions are provided in Ref. [1].

**Mode 1:** Vehicle topples over or falls back on the launch point after a rise of, at most, a few feet. Propellants deflagrate or explode with some assumed TNT equivalency.

**Mode 2:** Vehicle loses control at or shortly after liftoff, with all flight directions equally likely. Destruct is transmitted as soon as erratic flight is confirmed, usually no later than six to twelve seconds after launch. For each vehicle, a latest destruct time is established that is used in computing the maximum impact distance for pieces, given that a Mode-2 response has occurred.

**Mode 3:** Vehicle fails to pitch-program normally, producing near-vertical flight while thrusting at normal levels. Vehicle may tumble rapidly out of control at any point during vertical flight resulting in spontaneous breakup, or may be destroyed when destruct criteria are violated. The mode is terminated by destruct action if the vehicle reaches the so-called "straight-up" time without programming. This time varies with launch vehicle and with mission, but usually occurs (at Cape Canaveral Air Station) between 30 and 70 seconds after launch.

**Mode 4:** Vehicle flies within normal limits until some malfunction terminates thrust, causes spontaneous breakup, or results in destruct by flight-control personnel. Breakup may or may not be preceded by a rapid tumble while the vehicle is still thrusting but, in any event, vehicle debris and components impact near the intended flight line.

**Mode 5:** Vehicle may impact in any direction from the launch point within its range capability. At any range, impacts are most likely to occur along the flight line, becoming less likely as the angular deviation from the flight line increases. As the impact range increases, weighting is progressively increased to favor the downrange direction. In any fixed direction, the impact probability decreases as the impact range increases. Flight may terminate spontaneously due to complete loss of vehicle stability or because of destruct action. Outside the launch area, any malfunction with the potential to cause a substantial deviation from the intended flight direction is classified as a Mode-5 failure response. By definition, Mode-5

responses begin at vehicle pitch-over or programming for vertically-launched missiles, and at liftoff for those not launched vertically.

**Mode 6:** Unlike impacts from response Modes 1 through 5, Mode-6 impacts result from normal flights and normal impacts of separated stages and components. Jettisoned components are assumed to be non-explosive. For each impacting stage or component, a mean point of impact and bivariate-normal impact dispersions in downrange and crossrange components are assumed. The impact dispersions include the effects of variations in vehicle performance, drag uncertainties, and winds.

Of the five failure-response modes, only Mode 5 is modeled to allow for the possibility of failure of the flight termination system, since vehicles experiencing other failure responses tend to impact within the impact limit lines. In DAMP, risk computations for Modes 2 through 4 are based on the assumption that the flight termination system is successfully employed when required. Failure responses originally classified as Mode 2, 3, or 4 may be reclassified as Mode 5 if the flight termination system fails or subsequent vehicle performance does not conform with the original response-mode definition. Risks associated with vehicle failure responses accompanied by a failure of the flight termination system are assumed to be adequately modeled in DAMP by Mode 5.

The five failure-response modes modeled in DAMP are sufficient to account for all anomalous impacts in the estimation of risks. However, some vehicle failures and anomalous behaviors have an effect on mission success without increasing risks to people and property on the ground. These behaviors have been assigned **Mode NA** (not applicable) in the response-mode column of the launch-history tables in Appendix D.

## Appendix B. Shaping-Constant Effects on Mode-5 Impact Distributions

The values chosen for shaping constants A and B that appear in the Mode-5 impact-density function [Eq. (3)] have a significant effect on the angular distribution of impacts about the launch point. This Appendix shows the effects of A and B on (1) the ratio of impacts along the downrange line to any other radial through the launch point, and (2) the percentages of impacts in various sectors relative to the downrange line.

Following the procedures outlined in Section 9.7 of Reference [1], it is interesting to observe the effects of varying the constants A and B. This is done in terms of a so-called f-ratio, which is expressed in Ref. [1] as Eq. (9.19), and is repeated here:

$$f\text{-ratio} = \frac{e^{A\pi} + \frac{B}{R}}{e^{A\phi} + \frac{B}{R}} \quad (7)$$

The ratio shows how much more likely impact is to occur along the flight line (where  $\phi = \pi$ ) than along some other radial line that makes an angle  $\theta$  ( $\theta = \pi - \phi$ ) with the flight line. Table 33 and Table 34 present f-ratios for values of A = 2.5, 3.0, 3.5, and 4.0, and B = 1000 for impact ranges from one to 25 miles. Table 35 and Table 36 show the effects of halving and doubling the constant B for a fixed value of A = 3.0.

Before citing numerical examples, it should be emphasized that the data in Table 33 through Table 36 are derived from the primary Mode-5 impact-density function and, as such, they indicate likelihood ratios for the location of the secondary Mode-5 density functions. A secondary function, it will be remembered, describes the dispersion of a debris class about the impact point of the mean piece in the class. Thus, referring to Table 34 with A = 3.0, it can be seen that the secondary impact-density function for a debris class is 4.7 times more likely to be centered 10 miles downrange along the flight line ( $\theta = 0^\circ$ ) than 10 miles from the launch point along a radial line that makes a  $30^\circ$  angle with the flight line. As another example, the secondary function (i.e., the impact point for the mean piece in a debris class) is 82.2 times more likely to be located 25 miles downrange along the flight line than 25 miles crossrange ( $\theta = 90^\circ$ ), and assuming no destruct action, that it is  $303.2/82.2 = 3.7$  times more likely to be located 25 miles crossrange than 25 miles uprange ( $\theta = 180^\circ$ ).

Table 33. Effect on f-Ratio of Varying Mode-5 Constant A (B = 1000) - Part 1

180 - $\phi$	R = 1 nm				R = 5 nm			
	A = 2.5	A = 3.0	A = 3.5	A = 4.0	A = 2.5	A = 3.0	A = 3.5	A = 4.0
0	1.0	1.0	1.0	1.0	1.0	1.0	1.0	1.0
5	1.2	1.3	1.3	1.4	1.2	1.3	1.4	1.4
10	1.3	1.6	1.8	2.0	1.5	1.7	1.8	2.0
15	1.5	2.0	2.4	2.8	1.8	2.2	2.5	2.8
20	1.7	2.5	3.3	4.0	2.2	2.8	3.4	4.0
25	1.9	3.1	4.3	5.6	2.6	3.6	4.6	5.7
30	2.1	3.7	5.8	7.9	3.1	4.5	6.1	8.1
35	2.3	4.5	7.6	11.1	3.7	5.8	8.3	11.4
40	2.5	5.3	9.8	15.5	4.3	7.3	11.1	16.1
45	2.6	6.2	12.6	21.5	4.9	9.2	14.9	22.8
50	2.8	7.0	15.9	29.5	5.7	11.4	19.9	32.1
55	2.9	7.9	19.7	40.2	6.4	14.1	26.3	45.1
60	3.0	8.7	24.0	53.8	7.2	17.1	34.7	63.1
65	3.1	9.5	28.5	70.7	7.9	20.6	45.2	87.8
70	3.2	10.2	33.1	91.0	8.6	24.3	58.2	121.4
75	3.3	10.8	37.6	113.9	9.3	28.5	73.8	166.3
80	3.3	11.3	41.8	138.6	10.0	32.5	92.1	224.8
85	3.4	11.7	45.5	163.6	10.5	36.5	112.6	299.2
90	3.4	12.1	48.7	187.4	11.1	40.4	134.7	390.1
95	3.4	12.3	51.4	208.9	11.5	44.1	157.4	496.7
100	3.5	12.6	53.5	227.2	11.9	47.3	179.9	615.2
105	3.5	12.7	55.2	242.2	12.3	50.2	200.9	739.7
110	3.5	12.9	56.5	254.1	12.5	52.7	219.9	862.9
115	3.5	13.0	57.6	263.1	12.8	54.7	236.4	977.7
120	3.5	13.1	58.3	270.0	13.0	56.4	250.2	1079.0
125	3.5	13.2	58.9	275.0	13.2	57.8	261.4	1164.0
130	3.5	13.2	59.4	278.6	13.3	58.9	270.4	1232.6
135	3.6	13.3	59.7	281.2	13.4	59.8	277.4	1286.0
140	3.6	13.3	59.9	283.1	13.5	60.5	282.8	1326.5
145	3.6	13.3	60.1	284.5	13.6	61.1	286.9	1356.7
150	3.6	13.3	60.2	285.4	13.6	61.5	290.0	1378.8
155	3.6	13.3	60.3	286.1	13.7	61.8	292.3	1394.8
160	3.6	13.4	60.4	286.6	13.7	62.1	294.1	1406.3
165	3.6	13.4	60.5	286.9	13.7	62.3	295.4	1414.6
170	3.6	13.4	60.5	287.2	13.8	62.4	296.3	1420.5
175	3.6	13.4	60.5	287.3	13.8	62.6	297.0	1424.7
180	3.6	13.4	60.5	287.5	13.8	62.6	297.6	1427.6

Table 34. Effect on f-Ratio of Varying Mode-5 Constant A (B = 1000) - Part 2

180 - $\phi$	R = 10 nm				R = 25 nm			
	A = 2.5	A = 3.0	A = 3.5	A = 4.0	A = 2.5	A = 3.0	A = 3.5	A = 4.0
0	1.0	1.0	1.0	1.0	1.0	1.0	1.0	1.0
5	1.2	1.3	1.4	1.4	1.2	1.3	1.4	1.4
10	1.5	1.7	1.8	2.0	1.5	1.7	1.8	2.0
15	1.9	2.2	2.5	2.8	1.9	2.2	2.5	2.8
20	2.3	2.8	3.4	4.0	2.3	2.8	3.4	4.0
25	2.8	3.6	4.6	5.7	2.9	3.7	4.6	5.7
30	3.4	4.7	6.2	8.1	3.6	4.8	6.2	8.1
35	4.1	6.0	8.4	11.5	4.4	6.1	8.4	11.5
40	4.9	7.7	11.3	16.2	5.3	7.9	11.4	16.3
45	5.8	9.8	15.3	23.0	6.5	10.2	15.5	23.1
50	6.8	12.4	20.5	32.4	7.9	13.2	20.9	32.7
55	8.0	15.7	27.5	45.8	9.6	16.9	28.3	46.2
60	9.3	19.7	36.7	64.5	11.5	21.6	38.1	65.4
65	10.7	24.4	48.8	90.6	13.7	27.5	51.2	92.3
70	12.1	29.9	64.3	126.7	16.2	34.8	68.7	130.2
75	13.5	36.3	84.1	176.4	19.0	43.8	91.7	183.1
80	15.0	43.4	108.6	243.9	22.1	54.5	121.8	256.9
85	16.4	51.1	138.4	333.9	25.4	67.3	160.6	358.9
90	17.8	59.1	173.5	451.4	28.8	82.2	209.9	498.3
95	19.0	67.3	213.3	600.5	32.4	98.9	271.3	686.6
100	20.1	75.3	256.8	782.9	35.9	117.3	345.7	936.0
105	21.2	82.9	302.1	996.3	39.4	137.0	433.3	1258.3
110	22.1	89.8	347.2	1233.5	42.7	157.2	532.8	1662.1
115	22.9	96.0	390.2	1482.5	45.9	177.4	641.3	2148.4
120	23.5	101.4	429.4	1728.6	48.7	196.9	754.5	2707.0
125	24.1	106.0	463.6	1957.9	51.3	215.0	867.2	3315.0
130	24.6	109.9	492.6	2159.9	53.5	231.5	974.6	3939.0
135	25.0	113.0	516.4	2329.5	55.5	245.9	1072.3	4542.1
140	25.3	115.5	535.5	2466.0	57.2	258.3	1158.0	5092.0
145	25.6	117.6	550.4	2572.4	58.6	268.8	1230.3	5567.4
150	25.8	119.2	562.0	2653.1	59.9	277.4	1289.7	5959.9
155	26.0	120.5	570.8	2713.1	60.9	284.5	1337.3	6271.7
160	26.1	121.5	577.5	2757.1	61.7	290.1	1374.6	6512.1
165	26.3	122.2	582.5	2789.0	62.4	294.6	1403.5	6693.0
170	26.4	122.8	586.3	2812.0	63.0	298.2	1425.6	6826.7
175	26.4	123.3	589.1	2828.4	63.4	301.0	1442.3	6924.4
180	26.5	123.7	591.2	2840.1	63.8	303.2	1454.9	6994.9

Table 35. Effect on f-Ratio of Varying Mode-5 Constant B (A = 3) - Part 1

180 - $\phi$	R = 1 nm			R = 5 nm		
	B = 500	B = 1000	B = 2000	B = 500	B = 1000	B = 2000
0	1.0	1.0	1.0	1.0	1.0	1.0
5	1.3	1.3	1.2	1.3	1.3	1.3
10	1.6	1.6	1.5	1.7	1.7	1.7
15	2.1	2.0	1.9	2.2	2.2	2.1
20	2.7	2.5	2.3	2.8	2.8	2.7
25	3.4	3.1	2.7	3.6	3.6	3.4
30	4.2	3.7	3.1	4.7	4.5	4.3
35	5.2	4.5	3.6	6.0	5.8	5.4
40	6.4	5.3	4.1	7.7	7.3	6.6
45	7.7	6.2	4.5	9.8	9.2	8.1
50	9.2	7.0	5.0	12.4	11.4	9.8
55	10.8	7.9	5.3	15.7	14.1	11.7
60	12.4	8.7	5.7	19.7	17.1	13.7
65	14.1	9.5	6.0	24.4	20.6	15.8
70	15.8	10.2	6.2	29.9	24.3	17.8
75	17.3	10.8	6.4	36.3	28.5	19.9
80	18.7	11.3	6.6	43.4	32.5	21.8
85	20.0	11.7	6.7	51.1	36.5	23.5
90	21.1	12.1	6.8	59.1	40.4	25.0
95	22.0	12.3	6.9	67.3	44.1	26.3
100	22.8	12.6	7.0	75.3	47.3	27.5
105	23.4	12.7	7.0	82.9	50.2	28.4
110	23.9	12.9	7.1	89.8	52.7	29.1
115	24.3	13.0	7.1	96.0	54.7	29.7
120	24.6	13.1	7.1	101.4	56.4	30.2
125	24.9	13.2	7.1	106.0	57.8	30.6
130	25.1	13.2	7.1	109.9	58.9	30.9
135	25.3	13.3	7.2	113.0	59.8	31.2
140	25.4	13.3	7.2	115.5	60.5	31.3
145	25.5	13.3	7.2	117.6	61.1	31.5
150	25.5	13.3	7.2	119.2	61.5	31.6
155	25.6	13.3	7.2	120.5	61.8	31.7
160	25.6	13.4	7.2	121.5	62.1	31.8
165	25.7	13.4	7.2	122.2	62.3	31.8
170	25.7	13.4	7.2	122.8	62.4	31.8
175	25.7	13.4	7.2	123.3	62.6	31.9
180	25.7	13.4	7.2	123.7	62.6	31.9

Table 36. Effect on f-Ratio of Varying Mode-5 Constant B (A = 3) - Part 2

180 - $\phi$	R = 10 nm			R = 25 nm		
	B = 500	B = 1000	B = 2000	B = 500	B = 1000	B = 2000
0	1.0	1.0	1.0	1.0	1.0	1.0
5	1.3	1.3	1.3	1.3	1.3	1.3
10	1.7	1.7	1.7	1.7	1.7	1.7
15	2.2	2.2	2.2	2.2	2.2	2.2
20	2.8	2.8	2.8	2.8	2.8	2.8
25	3.7	3.6	3.6	3.7	3.7	3.6
30	4.7	4.7	4.5	4.8	4.8	4.7
35	6.1	6.0	5.8	6.2	6.1	6.0
40	7.9	7.7	7.3	8.0	7.9	7.8
45	10.2	9.8	9.2	10.4	10.2	9.9
50	13.0	12.4	11.4	13.4	13.2	12.7
55	16.7	15.7	14.1	17.3	16.9	16.1
60	21.2	19.7	17.1	22.3	21.6	20.3
65	26.9	24.4	20.6	28.7	27.5	25.3
70	33.9	29.9	24.3	36.8	34.8	31.3
75	42.3	36.3	28.3	47.0	43.8	38.5
80	52.3	43.4	32.5	59.7	54.5	46.6
85	63.9	51.1	36.5	75.4	67.3	55.5
90	77.1	59.1	40.4	94.5	82.2	65.2
95	91.7	67.3	44.1	117.4	98.9	75.3
100	107.3	75.3	47.3	144.4	117.3	85.5
105	123.5	82.9	50.2	175.4	137.0	95.4
110	139.7	89.8	52.7	210.1	157.2	104.7
115	155.4	96.0	54.7	247.9	177.4	113.3
120	170.1	101.4	56.4	287.7	196.9	120.9
125	183.5	106.0	57.8	328.3	215.0	127.5
130	195.3	109.9	58.9	368.2	231.5	133.1
135	205.5	113.0	59.8	406.3	245.9	137.7
140	214.1	115.5	60.5	441.4	258.3	141.5
145	221.2	117.6	61.1	472.8	268.8	144.6
150	227.0	119.2	61.5	500.3	277.4	147.1
155	231.7	120.5	61.8	523.6	284.5	149.0
160	235.4	121.5	62.1	543.2	290.1	150.5
165	238.4	122.2	62.3	559.3	294.6	151.7
170	240.7	122.8	62.4	572.3	298.2	152.7
175	242.5	123.3	62.6	582.7	301.0	153.4
180	244.0	123.7	62.6	591.0	303.2	154.0

The f-ratios in Table 33 and Table 34 (also in Table 35 and Table 36) have been plotted in Figure 32 for  $A = 3.0$  and  $B = 1000$ . Reading from the 10-mile plot for  $\theta = 90^\circ$ , it can be seen that a vehicle experiencing a Mode-5 response is about 60 times more likely to impact along the flight line than along the 90-degree radial. Essentially the same value (actually 59.1) appears in Table 34.

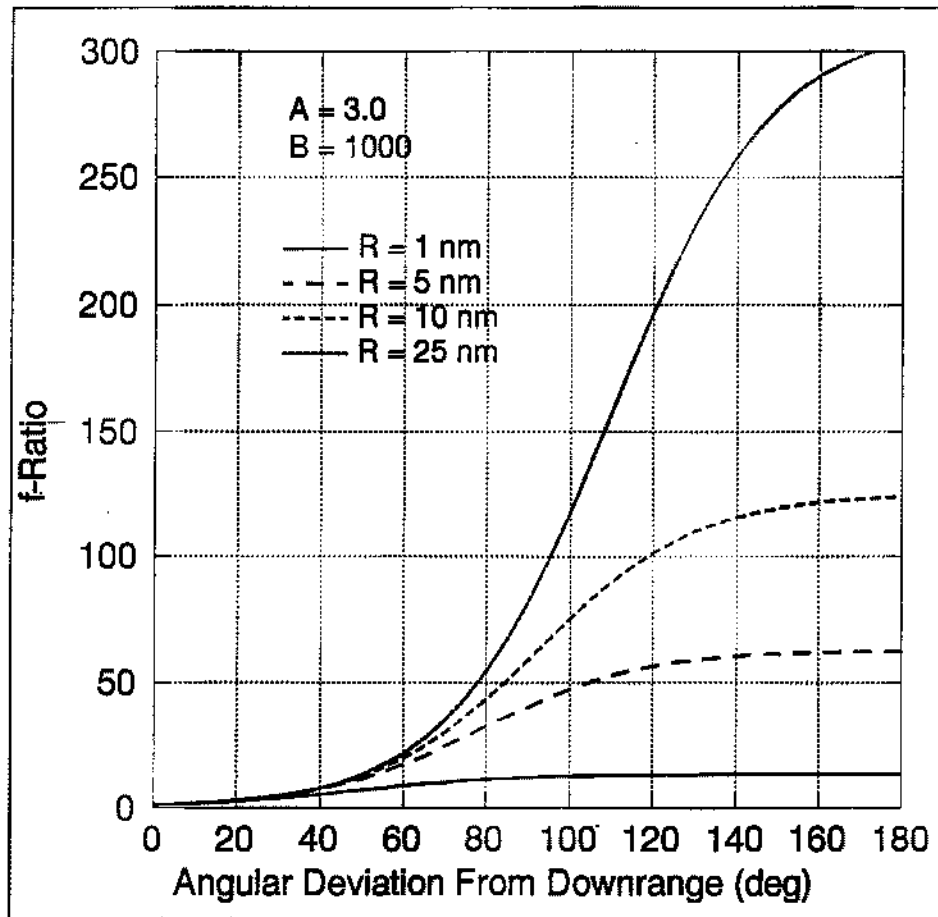


Figure 32. f-Ratios for Ranges from 1 to 25 Miles

There are other ways to show how the value chosen for A affects the Mode-5 impact density function. For five values of A, the plots in Figure 33 show the percentages\* of Atlas IIAS impacts that lie between the flight line and any radial line through the launch point that makes an angle  $\theta$  with respect to the flight line. If  $A = 3.0$ , it can be seen that approximately 46% of all Mode-5 impacts lie between  $0^\circ$  and  $20^\circ$ . If A is 4.0, the percentage of impacts between  $0^\circ$  and  $20^\circ$  increases to about 64%.

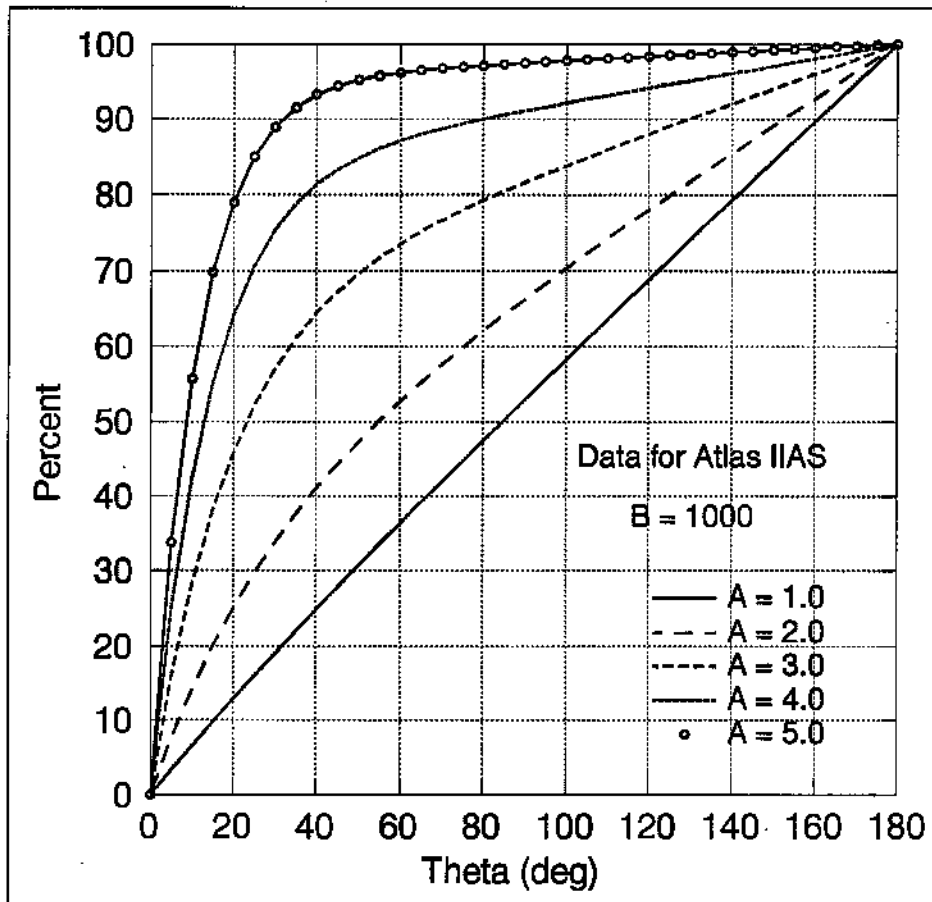


Figure 33. Percentage of Impacts Between Flight Line and Any Radial

\* The Mode-5 impact density function must be integrated numerically to arrive at the values plotted in Figure 33. Since the quantity  $\bar{R}$  that appears in the density function is trajectory dependent, somewhat different curves would be obtained for other trajectories and vehicles.

Another way to show how the value of A affects Mode-5 impacts is illustrated in Figure 34. For the same values of A used previously in Figure 33, the graphs in Figure 34 show the percentages of impacts in any 5° sector between radials that make angles of  $\theta^\circ$  and  $(\theta + 5)^\circ$  with respect to the flight line. It is interesting to note that if A is set equal to 1.0 with B = 1,000, impacts in all 5° sectors are approximately the same, thus resulting in an impact-density function that is essentially uniform in direction.

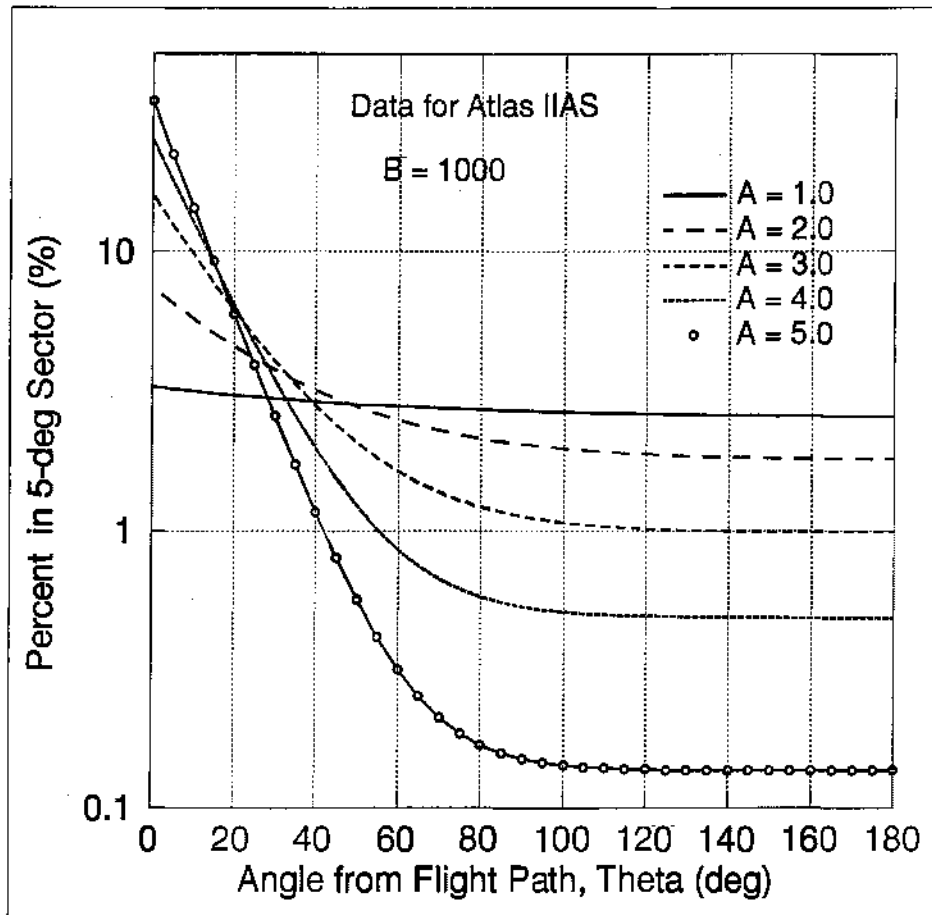


Figure 34. Percentage of Impacts in 5-Degree Sectors

For A = 1, the Mode-5 impact-density function is essentially the same as a density function formerly used in the Launch Risk Analysis (LARA) Program at the Western Range to model gross azimuth failures. This response mode was called the Gross Flight Deviation Failure (GFDF) mode. In LARA the range and azimuth portions of the GFDF density function were assumed to be independent. Impact azimuths were uniformly distributed, while the range density function can be represented as

$$f(R) = \frac{P}{T_b R} \quad (8)$$

where  $p$  is the probability of occurrence of the GFDF mode,  $T_b$  is the stage burn time, and  $\dot{R}$  is the rate of change of the impact range. The function cannot be applied early in flight before programming when  $\dot{R}$  is essentially zero. The range portion of the Mode-5 impact-density function used in DAMP reduces to essentially the same form. If Eq. (3) is integrated between the limits of zero and  $\pi$ , the conditional Mode-5 density function reduces to

$$f(R) = \frac{1}{(T_b - T_p)\dot{R}} \quad (9)$$

where  $T_p$  is the programming time, and  $T_b$  and  $\dot{R}$  are as previously defined. To obtain absolute values,  $f(R)$  must of course be multiplied by the probability of occurrence of a Mode-5 failure response.

Although the GFDF density function may be a suitable model for random-attitude failures occurring at or a few seconds after programming, the performance histories in Appendix D indicate that such failures are no more likely to occur at programming than at any other time. Thus, there appears to be no need for including a GFDF mode per se in the risk calculations, since all random-attitude failures are accounted for by the Mode-5 density function. However, if for some obscure reason inclusion of a GFDF response mode is desired, two approaches are possible: (1) run the GFDF mode separately in DAMP (by using Mode-5 with  $A = 1$ ) while zeroing out all other response modes; (2) modify DAMP to handle two separate Mode-5 density functions, each with its own values of  $A$  and  $B$ . Obviously approach (2) is much more involved and time consuming to implement.

Although it may not be obvious, the probability of impact in any annular range interval obtained by integrating the Mode-5 density function between the interval boundaries is independent of the values assigned to  $A$  and  $B$ . If Eq. (3) is integrated between the angle limits of zero and  $\pi$  (and only for these limits), the  $A$ 's and  $B$ 's cancel leaving the probability of impact between  $R_1$  and  $R_2$  as a function of impact range alone. With a change of variable, the probability of impacting between  $R_1$  and  $R_2$  becomes a simple function of time (see pages 84 and 85 of Ref. [1] for details).

## Appendix C. Filter Characteristics

Estimating launch-vehicle failure probabilities using empirical launch data is an uncertain process when the sample size is small and the data are obtained from an evolving system. One approach that may be used to estimate failure probabilities is to perform a least-squares fit to trial outcome values (0 = success, 1 = failure). For mature launch vehicles, failure probabilities have decreased markedly from their early experimental days. For new programs, empirical data may be scant or nonexistent.

One decision that must be made involves the type of function to fit to the data. The true nature of the failure-rate function may be unknown or extremely complex, or there may be insufficient data to estimate a complex function. The easiest calculation is made when a constant failure-rate function is assumed. However, available data appear to indicate that failure rates decrease as a program matures, at least up to a point. If it can be assumed that launch-vehicle failure probabilities decrease over time (i.e., as the number of launches increases), then some non-constant function (perhaps linear or exponential) can be chosen for the fit, or the data weighted as a function of time. In estimating Atlas reliability, General Dynamics<sup>69</sup> chose the latter option by adopting the Duane model. This model is based on the assumption that the mean number of launches between failures increases when causes of failure are corrected. Although this may be the case up to a point, eventually reliability seems to level off at a fairly constant value. Consequently, for mature programs RTI has chosen to fit the failure-rate function to a constant. Such a fit can be based on simple least squares using a fixed-length sliding-window filter to allow for changes in the estimated value over time, or on a least squares fit with unequal weighting.

If a constant function is fit to a set of data using least squares with equal weighting of data, the solution is given by the mean:

$$\bar{X} = \frac{1}{n} \sum_{i=1}^n x_i \quad (10)$$

Consider the following example:

$$\begin{aligned} x_1 &= 6 \\ x_2 &= 5 \\ x_3 &= 7 \end{aligned}$$

Then,

$$\bar{X} = \frac{6+5+7}{3} = \frac{18}{3} = 6 \quad (11)$$

Recursively,

$$\begin{aligned}\bar{X}_n &= \bar{X}_{n-1}(1-a_n) + x_n(a_n) \\ \bar{X}_n &= \bar{X}_{n-1} + a_n(x_n - \bar{X}_{n-1})\end{aligned}\tag{12}$$

For the equally-weighted case, the recursive filter factor  $a_n = 1/n$ .

Using the same example, with  $\bar{X}_0 = 0$ ,

$$\begin{aligned}\bar{X}_1 &= x_1 = 6 \\ \bar{X}_2 &= \bar{X}_1 + \frac{1}{2}(x_2 - \bar{X}_1) = 6 + \frac{1}{2}(5 - 6) = 5.5 \\ \bar{X}_3 &= \bar{X}_2 + \frac{1}{3}(x_3 - \bar{X}_2) = 5.5 + \frac{1}{3}(7 - 5.5) = 6.0\end{aligned}\tag{13}$$

In general terms, this recursive formulation of the least squares solution is called an expanding-memory filter, as opposed to a sliding-window or fixed-length filter. In an expanding-memory filter, the solution is always based on the entire data set. In the equally-weighted case, all data points have an equal influence on the solution, regardless of their locations in the sequence.

It can be seen that in the limit as  $n$  becomes very large,  $a_n$  approaches zero. That is, each data point in the sequence is accorded a decreased weight due to the increased number of points being fit. If the data being fit should actually describe a constant, this is exactly what is desired. Normally, however, the function that the data should fit is unknown, and a constant function is used merely as an approximation to smooth or edit the data. What is desired is a recursive least squares fit that assigns a decreasing weight to data of increasing age, so the fit de-weights data points used in earlier recursions.

In a fading-memory filter, the weighting factor decreases as time recedes into the past, so that the importance of any given datum will decrease as the age of the datum increases. An example of such a filter is one in which each datum is weighted by its count or index number in the sequence:

$$\bar{X}_n = \frac{\sum_{i=1}^n i x_i}{\sum_{i=1}^n i}\tag{14}$$

Using the same numerical example as before, where  $x_1 = 6$ ,  $x_2 = 5$ , and  $x_3 = 7$ ,

$$\bar{X} = \frac{1 \cdot 6 + 2 \cdot 5 + 3 \cdot 7}{1 + 2 + 3} = \frac{37}{6} = 6.17\tag{15}$$

For the recursive form of this filter, where each datum is weighted by its position in the chronological sequence, the recursive filter factor for the  $n^{\text{th}}$  point is given by

$$a_n = \frac{n}{\sum_{i=1}^n i} = \frac{2n}{n(n+1)} = \frac{2}{n+1} \quad (16)$$

Using Eq. (12),

n = 1	a <sub>1</sub> = 1	$\bar{X}_1 = x_1 = 6$	(17)
n = 2	a <sub>2</sub> = $\frac{2}{3}$	$\bar{X}_2 = 6 + \frac{2}{3}(5-6) = 5.33$	
n = 3	a <sub>3</sub> = $\frac{1}{2}$	$\bar{X}_3 = 5.33 + \frac{1}{2}(7-5.33) = 6.17$	

The "memory" (i.e., importance) of older data in this filter fades at a rate dictated by the filter. In this case, the 50<sup>th</sup> value is 50 times more important than the first, and the 100<sup>th</sup> value is twice as important as the 50<sup>th</sup> and 100 times more important than the first.

The exponentially-weighted filter provides the analyst with more flexibility. This filter uses  $F^i$  as a weighting factor, where the filter-control constant  $F$  is a value chosen between zero and one, and  $i$  is the "age-count" of the  $i^{\text{th}}$  data point. For this filter,  $i = 0$  now designates the current or latest data point,  $i = 1$  designates the immediately preceding or next-to-last data point, etc., so the data points are indexed in reverse chronological order starting with zero. The weighted least-squares solution is

$$\bar{X}_n = \frac{\sum_{i=0}^{n-1} F^i x_{n-i}}{\sum_{i=0}^{n-1} F^i} \quad (18)$$

Using  $F = 0.9$  and the same example as before,

$$\begin{aligned} \bar{X}_3 &= \frac{F^0 x_3 + F^1 x_2 + F^2 x_1}{F^0 + F^1 + F^2} \\ &= \frac{(.9)^0(7) + (.9)^1(5) + (.9)^2(6)}{(.9)^0 + (.9)^1 + (.9)^2} \\ &= \frac{7 + 4.5 + 4.86}{2.71} = \frac{16.36}{2.71} = 6.04 \end{aligned} \quad (19)$$

The weighting of each data point for sample sizes up to 300 is shown in Figure 35 for values of  $F$  from 0.8 to 1.0. For  $F = 1$ , all points in the sample are weighted equally. For

$F = 0.8$ , only the most recent 25 or so data points contribute to the final result, since all older data points are essentially weighted out of the solution.

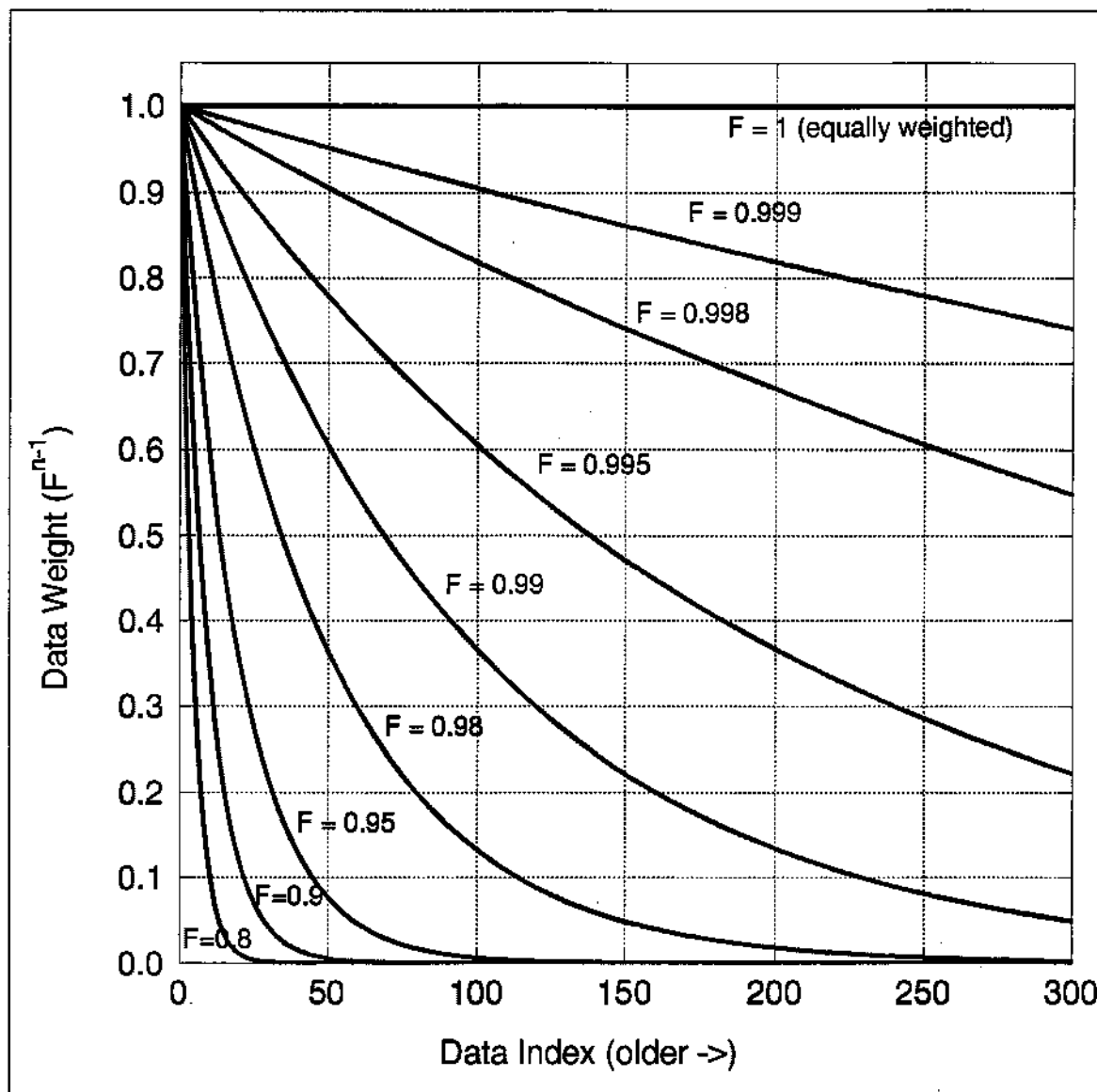


Figure 35. Exponential Weights for Fading-Memory Filters

For the exponentially-weighted fading-memory filter, it can be shown that the recursive filter factor used in Eq. (12) is

$$a_n = \frac{1-F}{1-F^n} \quad (20)$$

Since  $0 \leq F \leq 1$ ,  $a_n$  in Eq. (20) does not approach zero as  $n$  approaches infinity (as the other two filters do), but instead approaches the value  $(1 - F)$ . If  $F = 0$ , then  $a_n = 1$  for all  $n$ , the filter has no memory at all, and the filtered value always equals the last measurement. In the limit as  $F$  approaches one, L'Hospital's rule can be applied to

show that  $a_n$  approaches  $1/n$ , the filter-factor value for the equally-weighted case, and the filter memory no longer fades. For values of  $F$  between zero and one, the rate at which the filter memory fades decreases as  $F$  increases. The analyst can control the rate at which the filter memory fades by selecting an appropriate value of  $F$ .

As the number of points  $n$  increases, the value of  $a_n$  used in the recursive exponential-filter equation decreases continuously as it asymptotically approaches  $1 - F$ . For any given  $n$ , a larger  $a_n$  means more emphasis is placed on the current data point and less on previous points. That is, the larger the recursive filter factor  $a_n$ , the faster the filter memory fades. Filter factors for sample sizes up to 300 points are shown in Figure 36 for six different filters. Early in the data-index count ( $n$  less than 30), the filter based on index-number weighting has the fastest fading memory, since for 30 data points or fewer the filter has the largest filter factors. After 160 points or so, the index-weighted filter fades at a slower rate than the exponential filter with  $F = 0.99$ . Consequently, users of index-count-based fading filters frequently calculate a filter factor for some maximum value of  $n$  that is then applied to all subsequent data points as well. For example, if a maximum count of about 180 is used for  $n$ , this filter from that point on will behave similarly to the exponentially-fading filter with  $F = 0.99$ .

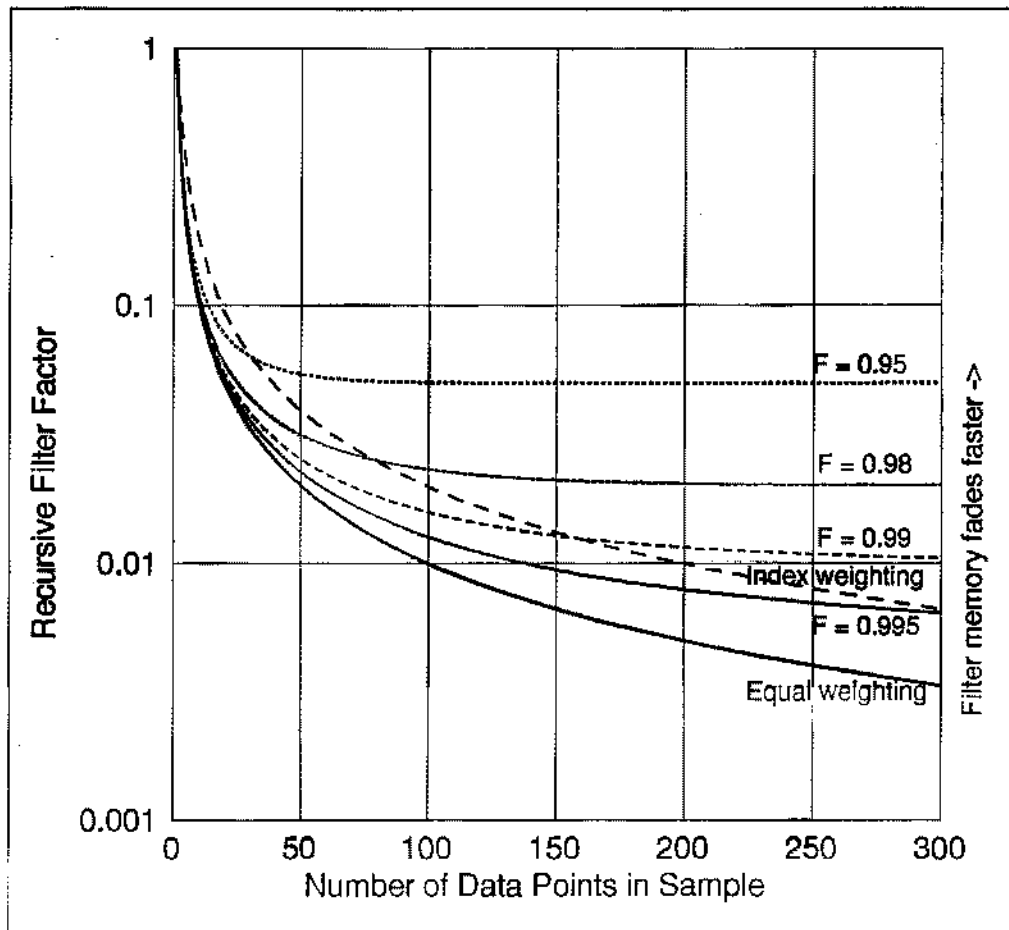


Figure 36. Recursive Filter Factor for Last Data Point

The fading-memory recursive filter, defined by Eqs. (12) and (20), can be applied to launch test results to estimate failure probability. For this application the values to be filtered are the test outcomes, with 0 representing a successful launch, and 1 representing a failure or anomalous behavior. Given a series of outcomes, the filtered result after each launch in the series represents the estimate of failure probability at that point. Filtered results for two filter-control constants are shown in Table 37 for a hypothetical series of ten launches for which all but the second and fourth flights were successful.

Table 37. Filter Application for Failure Probability

Index	Outcome	F = 0.98		F = 0.90	
		Filter factor, $a_n$	Fail. Prob.	Filter factor, $a_n$	Fail. Prob.
1	0	1.0000	0.0	1.0000	0.0
2	1	0.5051	0.5051	0.5263	0.5263
3	0	0.3401	0.3333	0.3690	0.3321
4	1	0.2576	0.5051	0.2908	0.5263
5	0	0.2082	0.3999	0.2442	0.3978
6	0	0.1752	0.3299	0.2132	0.3129
7	0	0.1517	0.2798	0.1917	0.2529
8	0	0.1340	0.2423	0.1756	0.2085
9	0	0.1203	0.2132	0.1632	0.1745
10	0	0.1093	0.1899	0.1535	0.1477

In this example, estimated failure probabilities are shown for two values of the filter constant that force the filter to fade at two different rates. After ten launches the estimated failure probability using  $F = 0.98$  is 0.1899. For the faster fading-memory filter ( $F = 0.90$ ), the result is 0.1477. Both estimates are less than that obtained by equal weighting, since the two failures occurred early in the sequence. Note that after four launches (2 successes and 2 failures) both filtered estimates exceed 0.5, since one of the two failures occurred during the fourth flight.

If the 1's and 0's used in the example to represent failures and successes were reversed, the same filter would provide estimates of probability of success.

## Appendix D. Launch and Performance Histories

### D.1 Basic Data

In support of the empirical approach to use post-test results to estimate future vehicle failure rates, the performance histories for Atlas, Delta, Titan, and Thor missiles/vehicles were studied. Results are summarized in Appendix D as follows:

Appendix D.2: Atlas Launch and Performance History

Appendix D.3: Delta Launch and Performance History

Appendix D.4: Titan Launch and Performance History

Appendix D.5: Thor Launch and Performance History

The histories include all Atlas, Delta, and Titan launches from the Eastern and Western Ranges prior to 1 September 1996. For Thor, only Eastern Range launches are included, since this summary was completed before it was decided not to use Thor results in predicting failure probabilities for Delta. The Atlas, Titan, and Thor summaries include both weapons systems tests and space flights, while the Delta summary includes only space flights.

For each vehicle, each section of the appendix is divided into two parts:

- (1) A tabular summary listing all launches in chronological order by sequence number, a mission identifier, launch date, vehicle configuration, launch range, the failure-response mode to which any failure has been assigned, the flight phase in which the failure or anomalous behavior occurred, and a configuration flag (0 or 1) indicating whether the vehicle is sufficiently representative of current vehicles to be included in the data sample used to predict vehicle reliability.
- (2) A brief narrative – necessarily brief in most cases due to lack of information – describing the general nature of the failure or the behavior of the vehicle after failure, or the effects of the failure on flight parameters.

#### D.1.1 Data Sources

The vehicle performance summaries and histories were collected primarily from the following sources:

- (1) "Eastern Range Launches, 1950 - 1994, Chronological Summary", 45th Space Wing History Office.<sup>[7]</sup>
- (2) Extension to (1) updating the launch summary through 30 December 1995.<sup>[8]</sup>
- (3) "Vandenberg AFB Launch Summary", Headquarters 30th Space Wing, Office of History, Launch Chronology, 1958 - 1995.<sup>[9]</sup>

- (4) "Spacelift Effective Capacity: Part 1 - Launch Vehicle Projected Success Rate Analysis", Draft prepared by Booz•Allen & Hamilton, Inc. 19 February 1992, prepared for Air Force Space Command Launch Services Office.<sup>[4]</sup>
- (5) Isakowitz, Steven J., (updated by Jeff Samella), *International Reference Guide to Space Launch Systems*, Second Edition, published and distributed by AIAA in 1995.<sup>[10]</sup>
- (6) Smith, O. G., "Launch Systems for Manned Spacecraft", Draft, July 23, 1991.<sup>[11]</sup>
- (7) "Comparison of Orbit Parameters - Table 1", prepared by McDonnell Douglas Space Systems Company, Delta launches through 4 Nov 95.<sup>[12]</sup>
- (8) Missiles/Space Vehicle Files, 45th Space Wing, Wing Safety, Mission Flight Control and Analysis (SEO), 1957 through 1995.<sup>[13]</sup>
- (9) Missile Launch Operations Logs, 30th Space Wing, copies provided via ACTA, Inc., (Mr. James Baeker), 1963 through 1995.<sup>[14]</sup>
- (10) "Titan IV, America's Silent Hero", published by Lockheed Martin in *Florida Today*, 13 Nov 95.<sup>[15]</sup>
- (11) "Atlas Program Flight History" (through April 1965), General Dynamics Report EM-1860, 26 April 1965.<sup>[16]</sup>
- (12) Fenske, C. W., "Atlas Flight Program Summary", Lockheed Martin, April 1995.<sup>[17]</sup>
- (13) Brater, Bob, "Launch History", Lockheed Martin FAX to RTI, March 13, 1996.<sup>[18]</sup>
- (14) Several USAF Accident/Incident Reports for Atlas and Titan failures.<sup>[19]</sup>
- (15) Quintero, Andrew H., "Launch Failures from the Eastern Range Since 1975", Aerospace memo, February 25, 1996, provided to RTI by Bill Zelinsky.<sup>[20]</sup>
- (16) Set of "Titan Flight Anomaly/Failure Summary" since 1959, received from Lockheed Martin, April 4, 1996.<sup>[21]</sup>
- (17) Chang, I-Shih, "Space Launch Vehicle Failures (1984 - 1995)", Aerospace Report No. TOR-96(8504)-2, January 1996.<sup>[22]</sup>

There were numerous discrepancies in the source data, particularly with regard to launch date and vehicle configuration. Some sources apparently list launch dates in local time, others use Greenwich time, and in some cases the same source may use both with no indication of which is which. Most of the launch dates shown in Appendix D agree with those in the Eastern Range and Western Range summaries published by the respective History offices. Since the dates on these summaries are not consistently local or Greenwich, neither are the dates listed in Appendix D. Although launch dates are

used to order the vehicle tests for filtering, whether the dates are inconsistently in local or Greenwich times is inconsequential. In most cases, the ordering is not affected by a one-day change in launch date. In rare cases where the order of two launches might be inadvertently reversed, the filtering calculations are unaffected if the interchanged flights are both failures or both successes. Even when this is not the case, the effect on the final results for samples greater than one-hundred is negligible.

Configuration discrepancies also existed in the source data as, for example, the listing of the same Atlas vehicle as a IIA in one source and as a IIAS in another. In rare cases, a launch may have been called a success in one document and a failure in another, with little or no data provided to make it clear whether the difference in classification was due to error or different success criteria. Although a considerable effort was made to eliminate errors and discrepancies in Appendix D, there can be no assurance that the effort was 100% successful.

#### D.1.2 Assignment of Failure-Response Modes

In the tabular historical summaries in Appendix D, the column labeled "Response Mode" refers to the failure-response modes in program DAMP. The numbers 1 through 5 in this column correlate with the failure-response modes described in Appendix A. The letter "T" following either a "3" or "4" indicates that the vehicle executed a thrusting tumble before breakup or destruct. An "NA" (i.e., not applicable) appearing in the column means that some anomalous behavior caused stages or components to impact outside their normal impact areas without necessarily failing the flight, or that the anomalous behavior resulted in an unplanned orbit that may or may not have interfered with mission objectives. If the response-mode column is blank, either the flight was a success, or there was no information in the data sources to indicate otherwise.

In some cases where the data sources contained only sketchy or incomplete information, assignment of the response mode involved some speculation. Mostly, this situation arose in trying to decide between response modes 4 and 5 or between modes 4 and 4T or, in rare cases, what mode to assign when the vehicle response did not exactly fit any of the response-mode definitions.

#### D.1.3 Assignment of Flight Phase

The number shown in the "Flight Phase" column in the tabular summaries of Appendix D indicates the phase of vehicle flight in which the failure or anomalous behavior occurred. Definitions of flight phase are given in Table 38. The assigned numbers are arbitrary, but were chosen in a way that suggests the vehicle stage that failed or the stage that was thrusting when the failure occurred.

Table 38. Flight-Phase Definitions

Flight Phase	Description
0	SRM auxiliary thrust phase
1	First-stage thrust phase if no auxiliary SRM's carried, or First-stage thrust phase after SRM separation
1.5	Attitude-control phase after first-stage thrust phase or between first and second-thrust phases
2	Second-stage thrust phase
2.5	Attitude-control phase after second thrust phase or between second and third-thrust phases
3	Third-stage thrust phase, or third thrust phase if second stage is restartable
3.5	Attitude-control phase after third thrust phase or between third and fourth thrust phases
4	Fourth thrust phase, or Upper stage/payload thrust phase
5	Attitude control phase after Flight Phase 4, or orbital phase

In some cases, two flight phases are listed opposite an entry, e.g., 2 and 5. This means that some failure or anomalous behavior occurred during the second-stage thrusting period that did not prevent the attainment of an orbit, but did result in an abnormal final orbit. Other somewhat arbitrary decisions were necessary in assigning a flight phase when an expended stage failed to separate, or an upper stage failed to ignite. If, for example, the first and second stages failed to separate, any of flight phase 1, 1.5, or 2 could be assigned, depending on the exact cause of the failure. The detailed information needed to make the proper choice was sometimes lacking.

Table 39 is provided to assist in understanding how flight phases were assigned for Atlas, Delta/Thor, and Titan vehicles.

Table 39. Flight Phases by Launch Vehicle

Flight Phase	Atlas	Delta/Thor	Titan
0	Castor burn	Castor/GEM burn	SRM solo
1	Atlas booster	First-stage burn	Stage 1
1.5	Booster separation	Vernier solo - Sep 1/2	Stage-1 separation
2	Sustainer	Second-stage burn	Stage 2
2.5	Vernier/ACS solo	Coast between stg 2/3	Vernier solo
3	Agena/Centaur	Third-stage burn	TS/Centaur/IUS
3.5	-	Coast after stg 3	-
4	Second burn	Second burn	Second burn
5	Orbit	Orbit	Orbit

#### D.1.4 Representative Configurations

The last column in the tables in Appendix D indicates whether the vehicle configuration is considered sufficiently similar to current and future vehicles for the test result to be included in the representative data sample used to predict absolute reliability. A "1" in the column indicates that the test result is included, while a "0" indicates that it is excluded. There are likely to be differences of opinion about which past configurations are representative and which are not. In determining which to include, RTI has relied entirely on the Booz•Allen & Hamilton report<sup>141</sup> referred to earlier. When faced with the same problem, Booz•Allen established the following criteria for deciding whether past configurations were sufficiently similar to current configurations:

- (1) **Genealogy:** Is the current system a direct or indirect derivative of the historical configuration?
- (2) **Operations:** Is the current system operated in the same manner as the historical configurations (e.g., ICBM versus space-launch vehicle)?
- (3) **Composition:** Does the current system use the same types of elements (i.e., SRMs, upper stage, etc.)?

Based on these criteria and other factors, Booz•Allen decided to use test results from flights of the following vehicle configurations to predict future success rates:

**Atlas:** SLV-3 and later configurations to include SLV-3A, SLV-3C, SLV-3D, G, H, I, II, IIA, IIAS. (Excluded: Atlas A, B, C, LV-3A, 3B, 3C, D, E, F)

**Delta:** 291X and later configurations to include 391X, 392X, 492X, 592X, 692X, 792X.

**Titan:** Titan IIIC and later configurations to include IIIB, IIID, IIIE, 34B, 34D, III/CT, IV, II-SLV.

## D.2 Atlas Launch and Performance History

Atlas space-launch vehicles, originally manufactured by General Dynamics and currently by Lockheed Martin, derived from the Atlas ICBM series developed in the 1950s. The primary one-and-one-half-stage vehicle played a major role in early lunar exploration activities (the unmanned Ranger, Lunar Orbiter, and Surveyor programs), and planetary probes (Mariner and Pioneer). Table 40 shows a summary of Atlas configurations since the beginning of the program.<sup>[10]</sup>

Table 40. Summary of Atlas Vehicle Configurations

Configuration	Description
A	ICBM single-stage test vehicle
B, C	ICBM 1½-stage test vehicle
D	ICBM and later space-launch vehicle
E, F	First an ICBM (1960), then a reentry test vehicle (1964), then a space-launch vehicle (1968)
LV-3A	Same as D except Agena upper stage
LV-3B	Same as D except man-rated for Project Mercury
SLV-3	Same as LV-3A except reliability improvements
SLV-3A	Same as SLV-3 except stretched 117 inches
LV-3C	Integrated with Centaur D upper stage
SLV-3C	Same as LV-3C except stretched 51 inches
SLV-3D	Same as SLV-3C except Centaur uprated to D-1A and Atlas electronics integrated with Centaur (no longer radio guided)
G	Same as SLV-3D but Atlas stretched 81 inches
H	Same as SLV-3D except with E/F avionics and no Centaur
I	Same as G except strengthened for 14-ft payload fairing, ring laser gyro added
II	Same as I except Atlas stretched 108 inches, engines uprated, hydrazine roll-control added, verniers deleted, Centaur stretched 36 inches
IIA	Same as II except Centaur RL-10s engines uprated to 20K lbs thrust and 6.5 seconds Isp increase from extendible RL-10 nozzles
IIAS	Same as IIA except 4 Castor IVA strap-on SRMs added

Atlas A, B, and C were developmental ICBMs. Atlas D, E, and F configurations were deployed as operational ICBMs during the 1960s. During that time, some Atlas Ds were modified as space-launch vehicles in the LV series: LV-3A, 3B, and 3C. The Standardized Launch Vehicle (SLV) series derived from a need to reduce lead times in transforming Atlas missiles to space-launch vehicles. The SLV series began with the SLV-3 vehicle, which used an Agena upper stage. The G and H vehicles evolved from the SLV series. Eventually the I, II, IIA, and IIAS configurations were developed with the aim of also supporting commercial launches.

Atlas vehicles are fueled by a mixture of liquid oxygen and kerosene (RP-1). The latest IAS configuration also incorporates Castor IVA solid-rocket motors. The early Atlas core vehicle included a sustainer, verniers, and two booster engines, all ignited prior to liftoff. In the Atlas II, IIA, and IAS vehicles, the vernier engines have been replaced by a hydrazine roll-control system. Of the four Castor SRBs on the IAS, two are ground lit and two are air lit some 60 seconds later. Atlas vehicles are now typically integrated with the Centaur upper stage vehicle that is fueled with liquid oxygen and liquid hydrogen. Earlier flights used an Agena upper stage.

The entire Atlas history through 1995 is depicted rather compactly in bar-graph form in Figure 37. The solid-block portion of each bar indicates the number of launches during the calendar year for which vehicle performance was entirely normal, in so far as could be determined. The clear white parts forming the tops of most bars show the number of launches that were either failures or flights where the launch vehicle experienced some sort of anomalous behavior. Every launch with an entry in the response mode column in Table 41 falls in this category. Such behavior did not necessarily prevent the attainment of some, or even all, mission objectives.

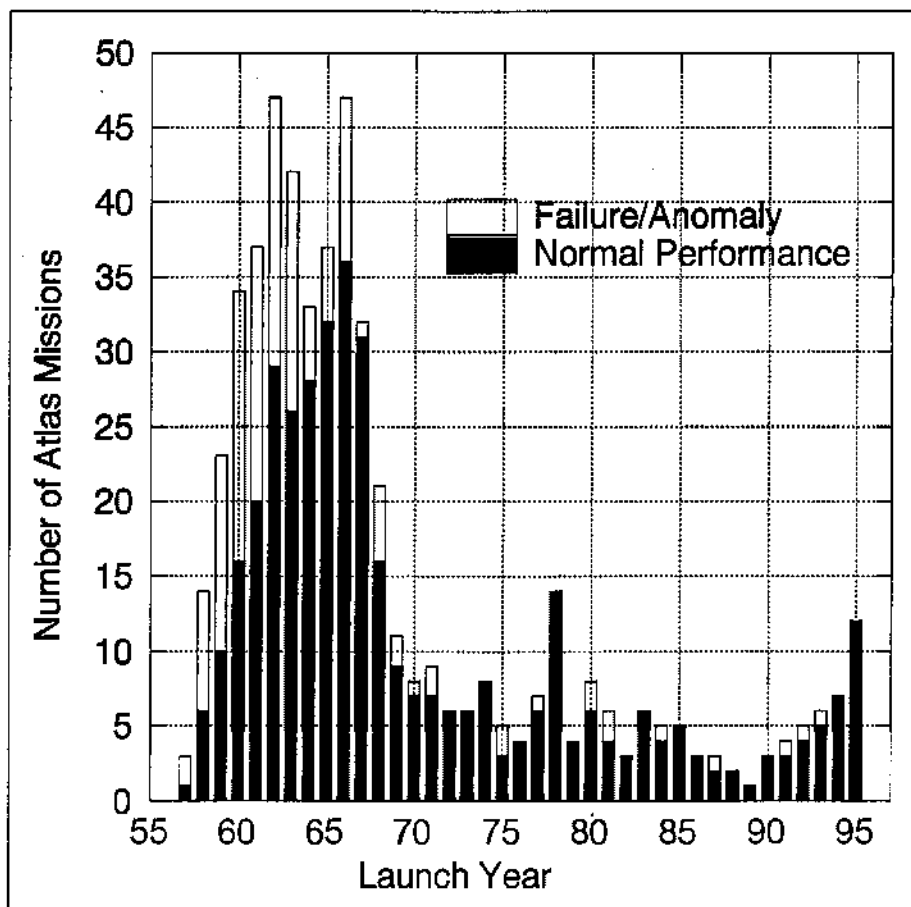


Figure 37. Atlas Launch Summary

## D.2.1 Atlas Launch History

The data in Table 41 summarize the flight performance of all Atlas and Atlas-boosted space-vehicle launches since the program began in June 1957. A launch sequence number is provided in the first column, a mission ID and launch date in columns 2 and 3. The vehicle configuration or Atlas booster number is given in the fourth column, while the fifth column shows whether the launch took place from the Eastern or Western Range. The last three columns in the table show, respectively, the response mode assigned by RTI to any failure or anomalous behavior that occurred, the flight phase in which it occurred, and whether the vehicle configuration is considered representative for the purposes of predicting future Atlas reliability. Launches through sequence number 532 were used in the filtering process to estimate failure rate.

Table 41. Atlas Launch History

No.	Mission/ID	Launch Date	Vehicle Configuration	Test Range	Response Mode	Flight Phase	Rep. Conf.
1	Weapons System (WS)	06/11/57	4A	ER	4T	1	0
2	WS	09/25/57	6A	ER	4	1	0
3	WS	12/17/57	12A	ER			0
4	WS	01/10/58	10A	ER			0
5	WS	02/07/58	13A	ER	4	1	0
6	WS	02/20/58	11A	ER	4T	1	0
7	WS	04/05/58	15A	ER	4	1	0
8	WS	06/03/58	16A	ER			0
9	WS	07/19/58	3B	ER	4T	1	0
10	WS	08/02/58	4B	ER			0
11	WS	08/28/58	5B	ER	4	2.5	0
12	WS	09/14/58	8B	ER	4	2.5	0
13	WS	09/18/58	6B	ER	4	1	0
14	WS	11/17/58	9B	ER	4	2	0
15	WS	11/28/58	12B	ER			0
16	SCORE	12/18/58	10B LV-3A/AGENA	ER			0
17	WS	12/23/58	3C	ER			0
18	WS	01/15/59	13B	ER	5	1	0
19	WS	01/27/59	4C	ER	5	2	0
20	WS	02/04/59	11B	ER			0
21	WS	02/20/59	5C	ER	4	2	0
22	WS	03/18/59	7C	ER	4	1	0
23	WS	04/14/59	3D	ER	4	1	0
24	WS	05/18/59	7D	ER	4	1	0
25	WS	06/06/59	5D	ER	4	2	0
26	WS	07/21/59	8C	ER			0
27	WS	07/28/59	11D	ER			0
28	WS	08/11/59	14D	ER			0
29	WS	08/24/59	11C	ER			0
30	MERCURY (test)	09/09/59	10D LV-3B	ER	4	2	0
31	DESERT HEAT	09/09/59	12D	WR			0

No.	Mission/ID	Launch Date	Vehicle Configuration	Test Range	Response Mode	Flight Phase	Rep. Conf.
32	WS	09/16/59	17D	ER	4	2.5	0
33	WS	10/06/59	18D	ER			0
34	WS	10/09/59	22D	ER			0
35	WS	10/29/59	26D	ER	4	2.5	0
36	WS	11/04/59	28D	ER	NA	2	0
37	WS	11/24/59	15D	ER	NA	2.5	0
38	ABLE (PIONEER)	11/26/59	20D LV-3A/AGENA	ER	4	1	0
39	WS	12/08/59	31D	ER			0
40	WS	12/18/59	40D	ER			0
41	WS	01/06/60	43D	ER			0
42	WS	01/26/60	44D	ER			0
43	DUAL EXHAUST	01/26/60	6D	WR	4	2 & 2.5	0
44	WS	02/11/60	49D	ER			0
45	MIDAS I	02/26/60	29D LV-3A/AGENA A	ER	4	2.5	0
46	WS	03/08/60	42D	ER	4	2.5	0
47	WS	03/10/60	51D	ER	1	1	0
48	WS	04/07/60	48D	ER	1	1	0
49	QUICK START	04/22/60	25D	WR			0
50	LUCKY DRAGON	05/06/60	23D	WR	3	1	0
51	WS	05/20/60	56D	ER			0
52	MIDAS II	05/24/60	45D LV-3A/AGENA A	ER			0
53	WS	06/11/60	54D	ER			0
54	WS	06/22/60	62D	ER	4	2.5	0
55	WS	06/27/60	27D	ER			0
56	WS	07/02/60	60D	ER	4	2	0
57	TIGER SKIN	07/22/60	74D	WR	5	1	0
58	MERCURY 1	07/29/60	50D LV-3B	ER	4	1	0
59	WS	08/09/60	32D	ER			0
60	WS	08/12/60	66D	ER			0
61	GOLDEN JOURNEY	09/12/60	47D	WR	4	2	0
62	WS	09/16/60	76D	ER			0
63	WS	09/19/60	79D	ER			0
64	ABLE 5 (PIONEER)	09/25/60	80D LV-3A/AGENA	ER	4T	2.5 & 3	0
65	HIGH ARROW	09/29/60	33D	WR	4	1	0
66	WS	10/11/60	3E	ER	5	2	0
67	Gibson Girl	10/11/60	57D LV-3A/AGENA A	WR	NA	3 & 5	0
68	DIAMOND JUBILEE	10/12/60	81D	WR	4	1	0
69	WS	10/13/60	71D	ER			0
70	WS	10/22/60	55D	ER			0
71	WS	11/15/60	83D	ER			0
72	WS	11/29/60	4E	ER	5	2	0
73	ABLE 5B (PIONEER)	12/15/60	91D LV-3A/AGENA	ER	4	1	0
74	HOT SHOT	12/16/60	99D	WR			0
75	WS	01/23/61	90D	ER			0
76	WS	01/24/61	8E	ER	5	2	0
77	Jawhawk Jamboree	01/31/61	70D LV-3A/AGENA A	WR	NA	2	0

No.	Mission/ID	Launch Date	Vehicle Configuration	Test Range	Response Mode	Flight Phase	Rep. Conf.
78	MERCURY 2	02/21/61	67D LV-3B	ER			0
79	WS	02/24/61	9E	ER			0
80	WS	03/13/61	13E	ER	4	2	0
81	WS	03/24/61	16E	ER	4	1.5	0
82	MERCURY 3	04/25/61	100D LV-3B	ER	3	1	0
83	WS	05/12/61	12E	ER			0
84	LITTLE SATIN	05/24/61	95D	WR			0
85	WS	05/26/61	18E	ER			0
86	SURE SHOT	06/07/61	27E	WR	4	1	0
87	WS	06/22/61	17E	ER	4	1	0
88	WS	07/06/61	22E	ER			0
89	Polar Orbit (Midas III)	07/12/61	97D, LV-3A/AGENA B	WR			0
90	WS	07/31/61	21E	ER			0
91	WS	08/08/61	2F	ER			0
92	NEW NICKEL	08/22/61	101D	WR			0
93	RANGER 1	08/23/61	111D LV-3A/AGENA	ER	NA	4	0
94	WS	09/08/61	26E	ER	4	2	0
95	First Motion (Samos III)	09/09/61	106D LV-3A/AGENA B	WR	1	1	0
96	MERCURY 4	09/13/61	88D LV-3B	ER			0
97	WS	10/02/61	25E	ER			0
98	WS	10/05/61	30E	ER			0
99	Big Town (Midas IV)	10/21/61	105D LV-3A/AGENA B	WR	NA	2	0
100	WS	11/10/61	32E	ER	4T	1	0
101	RANGER 2	11/18/61	117D LV-3A/AGENA	ER	NA	4	0
102	WS	11/22/61	4F	ER			0
103	Round Trip (Samos IV)	11/22/61	108D LV-3A/AGENA B	WR	4T	2	0
104	MERCURY 5	11/29/61	93D LV-3B	ER			0
105	BIG PUSH	11/29/61	53D	WR			0
106	WS	12/01/61	35E	ER			0
107	BIG CHIEF	12/07/61	82D	WR			0
108	WS	12/12/61	5F	ER	5	2	0
109	WS	12/19/61	36E	ER			0
110	WS	12/20/61	6F	ER	4T	2	0
111	Ocean Way (Samos V)	12/22/61	114D LV-3A/AGENA B	WR	NA	2	0
112	BLUE FIN	01/17/62	123D	WR			0
113	BLUE MOSS	01/23/62	132D	WR			0
114	RANGER 3	01/26/62	121D LV-3A/AGENA B	ER	NA	2 & 5	0
115	WS	02/13/62	40E	ER			0
116	BIG JOHN	02/16/62	137D	WR	NA	1.5	0
117	MERCURY 6	02/20/62	109D, LV-3B	ER			0
118	CHAIN SMOKER	02/21/62	52D	WR	4	1	0
119	SILVER SPUR	02/28/62	66E	WR	4T	1.5 & 2	0
120	Loose Tooth	03/07/62	112D, LV-3A/AGENA B	WR			0
121	CURRY COMB I	03/23/62	134D	WR			0
122	WS	04/09/62	11F	ER	1	1	0
123	Night Hunt	04/09/62	110D LV-3A/AGENA B	WR	NA	1	0

No.	Mission/ID	Launch Date	Vehicle Configuration	Test Range	Response Mode	Flight Phase	Rep. Conf.
124	CURRY COMB II	04/11/62	129D	WR			0
125	RANGER 4	04/23/62	133D, LV-3A/AGENA B	ER			0
126	Dainty Doll	04/26/62	118D, LV-3A/AGENA B	WR			0
127	BLUE BALL	04/27/62	140D	WR			0
128	AC-1 (SUBORBITAL)	05/08/62	104D LV-3C/CENT. D	ER	4	1	0
129	CANNONBALL FLYER	05/11/62	127D	WR			0
130	MERCURY 7	05/24/62	107D, LV-3B	ER			0
131	Rubber Gun	06/17/62	115D, LV-3A/AGENA B	WR	4	3	0
132	ALL JAZZ	06/26/62	21D	WR			0
133	LONG LADY	07/12/62	141D	WR			0
134	EXTRA BONUS	07/13/62	67E	WR	4	2 & 2.5	0
135	Armored Car	07/18/62	120D, LV-3A/AGENA B	WR			0
136	FIRST TRY	07/19/62	13D	WR			0
137	MARINER 1 (VENUS)	07/22/62	145D LV-3A/AGENA B	ER	5	2	0
138	HIS NIBS	08/01/62	15F	WR			0
139	Air Scout	08/05/62	124D, LV-3A/AGENA B	WR			0
140	PEG BOARD	08/09/62	8D	WR			0
141	PEG BOARD II	08/09/62	87D	WR	4	2.5	0
142	CRASH TRUCK	08/10/62	57F	WR	5	1	0
143	WS	08/13/62	7F	ER			0
144	MARINER 2 (VENUS)	08/27/62	179D LV-3A/AGENA B	ER	NA	2	0
145	WS	09/19/62	8F	ER			0
146	BRIAR STREET	10/02/62	4D	WR	4	2	0
147	MERCURY 8	10/03/62	113D, LV-3B	ER			0
148	RANGER 5	10/18/62	215D LV-3A/AGENA B	ER	NA	5	0
149	WS	10/19/62	14F	ER			0
150	CLOSED CIRCUITS	10/26/62	159D	WR			0
151	WS	11/07/62	16F	ER			0
152	After Deck	11/11/62	128D, LV-3A/AGENA B	WR			0
153	ACTION TIME	11/14/62	13F	WR	4	1	0
154	WS	12/05/62	21F	ER			0
155	DEER PARK	12/12/62	161D	WR			0
156	Bargain Counter	12/17/62	131D, LV-3A/AGENA B	WR	4T	1	0
157	OAK TREE	12/18/62	64E	WR	4T	1	0
158	FLY HIGH	12/22/62	160D	WR	4	2	0
159	BIG SUE	01/25/63	39D	WR	4	1	0
160	FAINT CLICK	01/31/63	176D	WR			0
161	FLAG RACE	02/13/63	182D	WR			0
162	PITCH PINE	02/28/63	188D	WR			0
163	ABRES-1	03/01/63	134F	ER			0
164	TALL TREE 3	03/09/63	102D	WR	5	1	0
165	TALL TREE 2	03/11/63	64D	WR			0
166	TALL TREE 1	03/15/63	46D	WR	4T	2	0
167	TALL TREE 5	03/15/63	63F	WR			0
168	LEADING EDGE	03/16/63	193D	WR	4T	2	0
169	KENDALL GREEN	03/21/63	83F	WR	4	2.5	0

No.	Mission/ID	Launch Date	Vehicle Configuration	Test Range	Response Mode	Flight Phase	Rep. Conf.
170	TALL TREE 4	03/23/63	52F	WR	4	1	0
171	BLACK BUCK	04/24/63	65E	WR	NA	2.5	0
172	ABRES-2	04/26/63	135F	ER			0
173	Damp Clay	05/09/63	119D, LV-3A/AGENA B	WR			0
174	MERCURY 9	05/15/63	130D, LV-3B	ER			0
175	DOCK HAND	06/04/63	62E	WR			0
176	HARPOON GUN	06/12/63	198D	WR			0
177	Big Four	06/12/63	139D, LV-3A/AGENA B	WR	4T	1	0
178	GO BOY	07/03/63	69E	WR			0
179	Fish Pool	07/12/63	201D, LV-3A/AGENA D	WR			0
180	Damp Duck	07/18/63	75D, LV-3A/AGENA B	WR			0
181	SILVER DOLL	07/26/63	24E	WR	4	2	0
182	BIG FLIGHT	07/30/63	70E	WR			0
183	COOL WATER I	07/31/63	143D	WR			0
184	PIPE DREAM	08/24/63	72E	WR			0
185	COOL WATER II	08/28/63	142D	WR			0
186	Fixed Fee	09/06/63	212D, LV-3A/AGENA D	WR			0
187	COOL WATER III	09/06/63	63D	WR	4	1	0
188	COOL WATER IV	09/11/63	84D	WR	4T	2.5	0
189	FILTER TIP	09/25/63	71E	WR	4T	2	0
190	HOT RUM	10/03/63	45F	WR	1	1	0
191	COOL WATER V	10/07/63	163D	WR	4	1	0
192	VELA 1 & 2	10/16/63	197D, LV-3A/AGENA D	ER			0
193	Hay Bailer	10/25/63	224D, LV-3A/AGENA D	WR			0
194	ABRES-3	10/28/63	136F	ER	4T	2	0
195	HICKORY HOLLOW	11/04/63	232D	WR			0
196	COOL WATER VI	11/13/63	158D	WR	4	1	0
197	AC-2	11/27/63	126D, LV-3C/CENTAUR D	ER			0
198	LENS COVER	12/18/63	233D	WR			0
199	Rest Easy	12/18/63	227D, LV-3A/AGENA D	WR			0
200	DAY BOOK	12/18/63	109F	WR			0
201	RANGER 6	01/30/64	199D, LV-3A/AGENA B	ER			0
202	BLUE BAY	02/12/64	48E	WR	4	2	0
203	Upper Octane	02/25/64	285D, LV-3A/AGENA D	WR			0
204	ABRES-4	02/25/64	5E	ER			0
205	Ink Blotter	03/11/64	296D, LV-3A/AGENA D	WR			0
206	ABRES-5	04/01/64	137F	ER			0
207	HIGH BALL	04/03/64	3F	WR	1	1	0
208	PROJECT FIRE	04/14/64	263D, LV-3A/AGENA D	ER			0
209	Anchor Dan	04/23/64	351D, LV-3A/AGENA D	WR			0
210	Big Fred	05/19/64	350D, LV-3A/AGENA D	WR			0
211	IRON LUNG	06/18/64	243D	WR			0
212	AC-3	06/30/64	135D, LV-3C/CENT. D	ER	4	3	0
213	Quarter Round	07/06/64	352D, LV-3A/AGENA D	WR			0
214	VELA 3 & 4	07/17/64	216D, LV-3A/AGENA D	ER			0
215	RANGER 7	07/28/64	250D, LV-3A/AGENA D	ER			0

No.	Mission/ID	Launch Date	Vehicle Configuration	Test Range	Response Mode	Flight Phase	Rep. Conf.
216	KNOCK WOOD	07/29/64	248D	WR			0
217	LARGE CHARGE	08/07/64	110F	WR			0
218	Big Sickle	08/14/64	7101, SLV-3A/AGENA D	WR			1
219	GALLANT GAL	08/27/64	57E	WR	4	2	0
220	BIG DEAL	08/31/64	36F	WR			0
221	OGO-1	09/04/64	195D, LV-3A/AGENA B	ER			0
222	BUTTERFLY NET	09/15/64	245D	WR			0
223	BUZZING BEE	09/22/64	247D	WR			0
224	Slow Pace	09/23/64	7102, SLV-3/AGENA D	WR			1
225	Busy Line	10/08/64	7103, SLV-3/AGENA D	WR			1
226	Boon Decker	10/23/64	353D, LV-3A/AGENA D	WR			0
227	MARINER 3	11/05/64	289D, LV-3A/AGENA D	ER	4	4	0
228	MARINER 4	11/28/64	288D, LV-3A/AGENA D	ER			0
229	BROOK TROUT	12/01/64	210D	WR			0
230	OPERA GLASS	12/04/64	300D	WR			0
231	Battle Royal	12/04/64	7105, SLV-3/AGENA D	WR			1
232	AC-4	12/11/64	146D, LV-3C/CENTAUR D	ER			0
233	STEP OVER	12/22/64	111F	WR			0
234	PILOT LIGHT	01/08/65	106F	WR			0
235	PENCIL SET	01/12/65	166D	WR			0
236	Beaver's Dam	01/21/65	172D/ABRES	WR	4	2 & 3	0
237	Sand Lark	01/23/65	7106, SLV-3/AGENA D	WR			1
238	RANGER 8	02/17/65	196D, LV-3A/AGENA B	ER			0
239	DRAG BAR	02/27/65	211D	WR			0
240	PORK BARREL	03/02/65	301D	WR			0
241	AC-5	03/02/65	166D, LV-3C/CENT. D	ER	1	1	0
242	Ship Rail	03/12/65	7104, SLV-3/AGENA D	WR			1
243	ANGEL CAMP	03/12/65	154D	WR			0
244	RANGER 9	03/21/65	204D, LV-3A/AGENA B	ER			0
245	FRESH FROG	03/26/65	297D	WR			0
246	Air Pump	04/03/65	7401, SLV-3/AGENA D	WR			1
247	FLIP SIDE	04/06/65	150D	WR			0
248	Dwarf Tree	04/28/65	7107, SLV-3/AGENA D	WR			1
249	PROJECT FIRE	05/22/65	264D, LV-3A/AGENA D	ER			0
250	Bottom Land	05/27/65	7108, SLV-3/AGENA D	WR			1
251	Tennis Match	05/27/65	68D/ABRES	WR	4	1	0
252	OLD FOGY	06/03/65	177D	WR			0
253	LEA RING	06/08/65	299D	WR			0
254	STOCK BOY	06/10/65	302D	WR			0
255	Worn Face	06/25/65	7109, SLV-3/AGENA D	WR			1
256	BLIND SPOT	07/01/65	59D	WR			0
257	White Pine	07/12/65	7112, SLV-3/AGENA D	WR	4 & 5	2 & 3	1
258	VELA 5 & 6	07/20/65	225D, LV-3A/AGENA D	ER			0
259	Water Tower	08/03/65	7111, SLV-3/AGENA D	WR			1
260	PIANO WIRE	08/04/65	183D	WR			0
261	SEA TRAMP	08/05/65	147F	WR			0

No.	Mission/ID	Launch Date	Vehicle Configuration	Test Range	Response Mode	Flight Phase	Rep. Conf.
262	AC-6	08/11/65	151D, LV-3C/CENTAUR D	ER			0
263	TONTO RIM	08/26/65	61D	WR			0
264	WATER SNAKE	09/29/65	125D	WR			0
265	Log Fog	09/30/65	7110, SLV-3/AGENA D	WR			1
266	Seething City	10/05/65	34D/ABRES	WR			0
267	GTV-6	10/25/65	5301, SLV-3/AGENA D	ER	4	3	1
268	Shop Degree	11/08/65	7113, SLV-3/AGENA D	WR			1
269	WILD GOAT	11/29/65	200D	WR			0
270	TAG DAY	12/20/65	85D	WR			0
271	Blanket Party	01/19/66	7114, SLV-3/AGENA D	WR			1
272	YEAST CAKE	02/10/66	305D	WR			0
273	LONELY MT.	02/11/66	86D	WR			0
274	Mucho Grande	02/15/66	7115, SLV-3/AGENA D	WR			1
275	SYCAMORE RIDGE	02/19/66	73D	WR			0
276	ETERNAL CAMP	03/04/66	303D	WR	5	1	0
277	GTV-8	03/16/66	5302, SLV-3/AGENA D	ER			1
278	Dumb Dora	03/18/66	7116, SLV-3/AGENA D	WR			1
279	WHITE BEAR	03/19/66	304D	WR	5	2	0
280	Bronze Bell	03/30/66	72D	WR			0
281	AC-8	04/07/66	184D, LV-3C/CENT. D	ER	4T	4	0
282	OAO-1	04/08/66	5001, SLV-3/AGENA D	ER			0
283	Shallow Stream	04/19/66	7117, SLV-3/AGENA D	WR			1
284	CRAB CLAW	05/03/66	208D	WR	4T	1	0
285	SUPPLY ROOM	05/13/66	98D	WR			0
286	Pump Handle	05/14/66	7118, SLV-3/AGENA D	WR			1
287	GTV-9	05/17/66	5303, SLV-3/AGENA D	ER	5	1	1
288	SAND SHARK	05/26/66	41D	WR			0
289	SURVEYOR-1 (AC-10)	05/30/66	290D, LV-3C/CENTAUR D	ER			0
290	GTV-9A	06/01/66	5304, SLV-3/AGENA D	ER			1
291	Power Drill	06/03/66	7119, SLV-3/AGENA D	WR			1
292	OGO-3	06/06/66	5601, SLV-3/AGENA B	ER			1
293	Mama's Boy	06/09/66	7201, SLV-3/AGENA D	WR			1
294	ENEER PANEL	06/10/66	96D	WR	4	2.5	0
295	GOLDEN MT.	06/26/66	147D	WR			0
296	HEAVY ARTILLERY	06/30/66	298D	WR			0
297	Snake Creek	07/12/66	7120, SLV-3/AGENA D	WR			1
298	Stony Island	07/13/66	58D/ABRES	WR	NA	3	0
299	GTV-10	07/18/66	5305, SLV-3/AGENA D	ER			1
300	BUSY RAMROD	08/08/66	149F	WR	4	2	0
301	LUNAR ORBITER 1	08/10/66	5801, SLV-3/AGENA D	ER			1
302	Silver Doll	08/16/66	7121, SLV-3/AGENA D	WR			1
303	Happy Mt.	08/19/66	7202, SLV-3/AGENA D	WR			1
304	GTV-11	09/12/66	5306, SLV-3/AGENA D	ER			1
305	Taxi Driver	09/16/66	7123, SLV-3/AGENA D	WR			1
306	SURVEYOR 2 (AC-7)	09/20/66	194D, LV-3C/CENT. D	ER	NA	5	0
307	Dwarf Killer	10/05/66	7203, SLV-3/AGENA D	WR			1

No.	Mission/ID	Launch Date	Vehicle Configuration	Test Range	Response Mode	Flight Phase	Rep. Conf.
308	LOW HILL	10/11/66	115F	WR	4	1	0
309	Gleaming Star	10/12/66	7122, SLV-3/AGENA D	WR			1
310	AC-9	10/26/66	174D, LV-3C/CENT. D	ER	NA	2	0
311	Red Caboose	11/02/66	7124, SLV-3/AGENA D	WR			1
312	LUNAR ORBITER 2	11/06/66	5802, SLV-3/AGENA D	ER			1
313	GTV-12	11/11/66	5307, SLV-3/AGENA D	ER			1
314	Busy Mermaid	12/05/66	7125, SLV-3/AGENA D	WR			1
315	ATS-B	12/06/66	5101, SLV-3/AGENA D	ER			1
316	Busy Panama	12/11/66	89D/ABRES	WR			0
317	Busy Peacock	12/21/66	7001, SLV-3/AGENA D	WR			1
318	BUSY STEPSON	01/17/67	148F	WR	NA	2.5	0
319	BUSY NIECE	01/22/67	35D	WR			0
320	Busy Party	02/02/67	7126, SLV-3/AGENA D	WR			1
321	LUNAR ORBITER 3	02/04/67	5803, SLV-3/AGENA D	ER			1
322	BUSY BOXER	02/13/67	121F	WR			0
323	Giant Chief	03/05/67	7002, SLV-3/AGENA D	WR			1
324	LITTLE CHURCH	03/16/67	151F	WR			0
325	ATS-A	04/05/67	5102, SLV-3/AGENA D	ER			1
326	BUSY SUNRISE	04/07/67	38D	WR			0
327	SURVEYOR 3 (AC-12)	04/17/67	292D, LV-3C/CENTAUR D	ER			0
328	Busy Tournament	04/19/67	7003, SLV-3/AGENA D	WR			1
329	LUNAR ORBITER 4	05/04/67	5804, SLV-3/AGENA D	ER			1
330	BUSY PIGSKIN	05/19/67	119F	WR			0
331	Busy Camper	05/22/67	7127, SLV-3/AGENA D	WR			1
332	Busy Wolf	06/04/67	7128, SLV-3/AGENA D	WR			1
333	BUCK TYPE	06/09/67	122F	WR			0
334	MARINER 5 (VENUS)	06/14/67	5401, SLV-3/AGENA D	ER			1
335	ABRES (AFSC)	07/06/67	65D	WR			0
336	SURVEYOR 4 (AC-11)	07/14/67	291D, LV-3C/CENTAUR D	ER			0
337	ABRES (AFSC)	07/22/67	114F	WR			0
338	AFSC	07/27/67	92D/ABRES	WR			0
339	BREAD HOOK	07/29/67	150F	WR			0
340	LUNAR ORBITER 5	08/01/67	5805, SLV-3/AGENA D	ER			1
341	SURVEYOR 5 (AC-13)	09/08/67	5901C, SLV-3/CENTAUR D	ER			1
342	ABRES (AFSC)	10/11/67	69D	WR			0
343	ABRES (AFSC)	10/14/67	118F	WR			0
344	ABRES (AFSC)	10/27/67	81F	WR	4T	1	0
345	ATS-C	11/05/67	5103, SLV-3/AGENA D	ER			1
346	SURVEYOR 6 (AC-14)	11/07/67	5902C, SLV-3C/CENTAUR D	ER			1
347	ABRES (AFSC)	11/07/67	94D	WR			0
348	ABRES (AFSC)	11/10/67	113F	WR			0
349	ABRES (AFSC)	12/21/67	117F	WR			0
350	SURVEYOR 7 (AC-15)	01/07/68	5903C, SLV-3C/CENTAUR D	ER			1
351	ABRES (AFSC)	01/31/68	94F	WR			0
352	ABRES (AFSC)	02/26/68	116F	WR			0
353	OGO-E	03/04/68	5602A, SLV-3A/AGENA D	ER			1

No.	Mission/ID	Launch Date	Vehicle Configuration	Test Range	Response Mode	Flight Phase	Rep. Conf.
354	ABRES (AFSC)	03/06/68	74E	WR			0
355	AFSC	04/06/68	107F/ABRES	WR			0
356	ABRES (AFSC)	04/18/68	77E	WR			0
357	ABRES (AFSC)	04/27/68	78E	WR			0
358	ABRES (AFSC)	05/03/68	95F	WR	5	1	0
359	ABRES (AFSC)	06/01/68	89F	WR			0
360	ABRES (AFSC)	06/22/68	86F	WR			0
361	ABRES (AFSC)	06/29/68	32F	WR			0
362	AFSC	07/11/68	75F/ABRES	WR			0
363	DOD (AA-27)	08/06/68	SLV-3A/AGENA D	ER			1
364	ATS-D (AC-17)	08/10/68	5104C, SLV-3C/CENTAUR D	ER	NA	4	1
365	AFSC	08/16/68	7004, SLV-3/BURNER II	WR	4	3	1
366	ABRES (AFSC)	09/25/68	99F	WR			0
367	ABRES (AFSC)	09/27/68	84F	WR			0
368	ABRES (AFSC)	11/16/68	56F	WR	4T	2.5	0
369	ABRES (AFSC)	11/24/68	60F	WR			0
370	OAO-A2 (AC-16)	12/07/68	5002C, SLV-3C/CENTAUR D	ER			1
371	ABRES (AFSC)	01/16/69	70F	WR			0
372	MARINER 6 (MARS) (AC-20)	02/24/69	5403C, SLV-3C/CENTAUR D	ER	NA	1	1
373	AFSC	03/17/69	104F/ABRES	WR			0
374	MARINER 7 (MARS) (AC-19)	03/27/69	5105C, SLV-3C/CENTAUR D	ER			1
375	DOD (AA-28)	04/12/69	SLV-3A/AGENA D	ER			1
376	ATS-E (AC-18)	08/12/69	5402C, SLV-3C/CENTAUR D	ER			1
377	ABRES (AFSC)	08/20/69	112F	WR			0
378	ABRES (AFSC)	09/16/69	100F	WR			0
379	ABRES (AFSC)	10/10/69	98F	WR	4	1	0
380	ABRES (AFSC)	12/03/69	44F	WR			0
381	ABRES (AFSC)	12/12/69	93F	WR			0
382	ABRES (AFSC)	02/08/70	96F	WR			0
383	ABRES (AFSC)	03/13/70	28F	WR			0
384	ABRES (AFSC)	05/30/70	91F	WR			0
385	ABRES (AFSC)	06/09/70	92F	WR			0
386	DOD (AA-29)	06/19/70	SLV-3A/AGENA D	ER			1
387	DOD (AA-30)	08/31/70	SLV-3A/AGENA D	ER			1
388	OAO-B (AC-21)	11/30/70	5003C, SLV-3C/CENTAUR D	ER	4	2	1
389	ABRES (AFSC)	12/22/70	105F	WR			0
390	INTELSAT IV F-2 (AC-25)	01/25/71	5005C, SLV-3C/CENTAUR D	ER			1
391	ABRES (AFSC)	04/05/71	85F	WR			0
392	MARINER 8 (MARS) (AC-24)	05/08/71	5405C, SLV-3C/CENTAUR D	ER	4T	3	1
393	MARINER 9 (MARS) (AC-23)	05/30/71	5404C, SLV-3C/CENTAUR D	ER			1
394	ABRES (AFSC)	06/29/71	103F	WR			0
395	AFSC	08/06/71	76F	WR			0
396	ABRES (AFSC)	09/01/71	74F	WR			0
397	DOD (AA-31)	12/04/71	SLV-3A/AGENA D	ER	4	1	1
398	INTELSAT IV F-3 (AC-26)	12/19/71	5006C, SLV-3C/CENTAUR D	ER			1
399	INTELSAT IV F-4 (AC-28)	01/22/72	5008C, SLV-3C/CENTAUR D	ER			1

No.	Mission/ID	Launch Date	Vehicle Configuration	Test Range	Response Mode	Flight Phase	Rep. Conf.
400	PIONEER 10 (AC-27)	03/02/72	5007C, SLV-3C/CENTAUR D	ER			1
401	INTELSAT IV F-5 (AC-29)	06/13/72	5009C, SLV-3C/CENTAUR D	ER			1
402	OAO-C (AC-22)	08/21/72	5004C, SLV-3C/CENTAUR D	ER			1
403	AFSC	10/02/72	102F/BURNER II	WR			0
404	DOD (AA-32)	12/20/72	SLV-3A/AGENA D	ER			1
405	DOD (AA-33)	03/06/73	SLV-3A/AGENA D	ER			1
406	PIONEER 11 (AC-30)	04/05/73	5011D, SLV-3D/CENT D-1A	ER			1
407	INTELSAT IV F-7 (AC-31)	08/23/73	5010D, SLV-3D/CENT D-1A	ER			1
408	ABRES (AFSC)	08/29/73	78F	WR			0
409	ACE	09/30/73	108F	WR			0
410	MARINER 10 (AC-34)	11/03/73	5014D, SLV-3D/CENT D-1A	ER			1
411	SFT-1	03/06/74	73F	WR			0
412	ACE	03/23/74	97F	WR			0
413	SFT-2	05/01/74	64F	WR			0
414	SFT-3	06/28/74	82F	WR			0
415	NTS-1	07/13/74	69F	WR			0
416	ACE	09/08/74	80F	WR			0
417	ABRES (AFSC)	10/12/74	31F	WR			0
418	INTELSAT IV F-8 (AC-32)	11/21/74	5012D, SLV-3D/CENT D-1A	ER			1
419	INTELSAT IV F-6 (AC-33)	02/20/75	5015D, SLV-3D/CENT D-1A	ER	4T	2	1
420	AFSC	04/12/75	71F	WR	4	1	0
421	INTELSAT IV F-1 (AC-35)	05/22/75	5018D, SLV-3D/CENT D-1A	ER			1
422	DOD (AA-34)	06/18/75	SLV-3A/AGENA	ER			1
423	INTELSAT IVA F-1 (AC-36)	09/25/75	5016D, SLV-3D/CENT D-1A	ER			1
424	INTELSAT IVA F-2 (AC-37)	01/29/76	5017D, SLV-3D/CENT D-1A	ER			1
425	AFSC	04/30/76	F	WR			0
426	COMSTAR D-1 (AC-38)	05/13/76	5020D, SLV-3D/CENT D-1A	ER			1
427	COMSTAR D-2 (AC-40)	07/22/76	5022D, SLV-3D/CENT D-1A	ER			1
428	DOD (AA-35)	05/23/77	SLV-3A/AGENA	ER			1
429	INTELSAT IVA F-4 (AC-39)	05/26/77	5019D, SLV-3D/CENT D-1A	ER			1
430	NTS-2	06/23/77	65F	WR			0
431	HEAO-A (AC-45)	08/12/77	5025D, SLV-3D/CENT D-1A	ER			1
432	INTELSAT IVA F-5 (AC-43)	09/29/77	5701D, SLV-3D/CENT D-1A	ER	4T	1	1
433	AFSC	12/08/77	F	WR			0
434	DOD (AA-36)	12/11/77	SLV-3A/AGENA D	ER			1
435	INTELSAT IVA F-3 (AC-46)	01/06/78	5026D, SLV-3D/CENT D-1A	ER			1
436	FLTSATCOM-A (AC-44)	02/09/78	5024D, SLV-3D/CENT D-1A	ER			1
437	NDS-1	02/22/78	64F	WR			0
438	INTELSAT IVA F-6 (AC-48)	03/31/78	5028D, SLV-3D/CENT D-1A	ER			1
439	DOD (AA-37)	04/07/78	SLV-3A/AGENA D	ER			1
440	NDS-2	05/13/78	49F	WR			0
441	PIONEER (VENUS) (AC-50)	05/20/78	5030D, SLV-3D/CENT D-1A	ER			1
442	SEASAT A	06/26/78	23F/AGENA D	WR			0
443	COMSTAR D-3 (AC-41)	06/29/78	5021D, SLV-3D/CENT D-1A	ER			1
444	PIONEER (VENUS) (AC-51)	08/08/78	5031D, SLV-3D/CENT D-1A	ER			1
445	NAVSTAR III	10/06/78	47F	WR			0

No.	Mission/ID	Launch Date	Vehicle Configuration	Test Range	Response Mode	Flight Phase	Rep. Conf.
446	TIROS N	10/13/78	29F	WR			0
447	HEAO-B (AC-52)	11/13/78	5032D, SLV-3D/CENT D-1A	ER			1
448	NAVSTAR IV	12/10/78	39F	WR			0
449	STP-78-1	02/24/79	27F	WR			0
450	FLTSATCOM-B (AC-47)	05/04/79	5027D, SLV-3D/CENT D-1A	ER			1
451	NOAA-A	06/27/79	25F	WR			0
452	HEAO-C (AC-53)	09/20/79	5033D, SLV-3D/CENT D-1A	ER			1
453	FLTSATCOM-C (AC-49)	01/17/80	5029D, SLV-3D/CENT D-1A	ER			1
454	NAVSTAR V	02/09/80	35F	WR			0
455	AFSC	03/03/80	F	WR			0
456	NAVSTAR VI	04/26/80	34F	WR			0
457	NOAA-B	05/29/80	19F	WR	NA	1	0
458	FLTSATCOM-D (AC-57)	10/31/80	5037D, SLV-3D/CENT D-1A	ER			1
459	INTELSAT IV F-2 (AC-54)	12/06/80	5034D, SLV-3D/CENT D-1A	ER			1
460	AFSC	12/08/80	68E	WR	5	1	0
461	COMSTAR D (AC-42)	02/21/81	5023D, SLV-3D/CENT D-1A	ER			1
462	INTELSAT V (AC-56)	05/23/81	5036D, SLV-3D/CENT D-1A	ER			1
463	NOAA-C	06/23/81	87F	WR			0
464	FLTSATCOM-E (AC-59)	08/06/81	5039D, SLV-3D/CENT D-1A	ER	NA	1 & 5	1
465	INTELSAT V F-3 (AC-55)	12/15/81	5035D, SLV-3D/CENT D-1A	ER			1
466	NAVSTAR VII	12/18/81	76E	WR	2	1	0
467	INTELSAT V F-4 (AC-58)	03/05/82	5038D, SLV-3D/CENT D-1A	ER			1
468	INTELSAT V F-5 (AC-60)	09/28/82	5040D, SLV-3D/CENT D-1A	ER			1
469	DMSP F-6	12/20/82	60E	WR			0
470	AFSC	02/09/83	H	WR			1
471	NOAA-E	03/28/83	73E	WR			0
472	INTELSAT V F-6 (AC-61)	05/19/83	5041D, SLV-3D/CENT D-1A	ER			1
473	AFSC	06/09/83	H	WR			1
474	NAVSTAR VIII	07/14/83	75E/PAM-D	WR			0
475	DMSP F-7	11/17/83	58E	WR			0
476	AFSC	02/05/84	H	WR			1
477	INTELSAT V F-9 (AC-62)	06/09/84	5042G/CENT D-1A	ER	4T	4	1
478	NAVSTAR IX	06/13/84	42E/PAM-D	WR			0
479	NAVSTAR X	09/08/84	14E/PAM-D	WR			0
480	NOAA-F	12/12/84	39E	WR			0
481	GEOSTA-A	03/12/85	41E	WR			0
482	INTELSAT V F-10 (AC-63)	03/22/85	5043G/CENT D-1A	ER			1
483	INTELSAT V F-11 (AC-64)	06/30/85	5044G/CENT D-1A	ER			1
484	INTELSAT V F-12 (AC-65)	09/28/85	5045G/CENT D-1A	ER			1
485	NAVSTAR XI	10/08/85	55E	WR			0
486	AFSC	02/09/86	H	WR			1
487	NOAA-G	09/17/86	52E	WR			0
488	FLTSATCOM F-7 (AC-66)	12/05/86	5046G/CENT D-1A	ER			1
489	FLTSATCOM F-6 (AC-67)	03/26/87	5048G/CENT D-1A	ER	4T	1	1
490	AFSC	05/15/87	H	WR			1
491	DMSP F-8	06/19/87	59E	WR			0

No.	Mission/ID	Launch Date	Vehicle Configuration	Test Range	Response Mode	Flight Phase	Rep. Conf.
492	DMSP F-9	02/02/88	54E	WR			0
493	NOAA-H	09/24/88	63E	WR			0
494	FLTSATCOM F-8 (AC-68)	09/25/89	5047G/CENT D-1A	ER			1
495	P87-2	04/11/90	28E/ALT 3A	WR			0
496	CRRES (AC-69)	07/25/90	5049 I/CENT I	ER			1
497	DMSS 10	12/01/90	61E	WR			0
498	BS-3H COMSAT (AC-70)	04/18/91	5050 I/CENT I	ER	4T	3	1
499	NOAA-D	05/14/91	50E	WR			0
500	DMSP F-11	11/28/91	53E	WR			0
501	EUTELSAT (AC-102)	12/07/91	8102 II/CENT I	ER			1
502	DSCS III (AC-101)	02/11/92	8101 II/CENT I	ER			1
503	GALAXY 5 (AC-72)	03/14/92	5052 I/CENT	ER			1
504	INTELSAT K (AC-105)	06/10/92	8105 IIA/CENT	ER			1
505	DSCS III (AC-103)	07/02/92	8103 II/CENT	ER			1
506	GALAXY 1R (AC-71)	08/22/92	5051 I/CENT	ER	4T	3	1
507	UHF FOLLOW ON-1 (AC-74)	03/25/93	5054 I/CENT	ER	NA	2 & 5	1
508	DSCS III (AC-104)	07/19/93	8104 II/CENT	ER			1
509	NOAA-I	08/09/93	34E	WR			0
510	UHF F/O-2 (AC-75)	09/03/93	5055 I/CENT	ER			1
511	DSCS III (AC-106)	11/28/93	8106 II/CENT	ER			1
512	TELSTAR 4 (AC-108)	12/16/93	8201 IIAS/CENT	ER			1
513	GOES-1 (AC-73)	04/13/94	5053 I/CENT	ER			1
514	UHF F/O-3 (AC-76)	06/24/94	5056 I/CENT	ER			1
515	DIRECT TV (AC-107)	08/03/94	8107 IIA/CENT	ER			1
516	DMSP F-12	08/29/94	20E	WR			0
517	INTELSAT VII (AC-111)	10/06/94	8202 IIAS/CENT	ER			1
518	ORION (AC-110)	11/29/94	8109 IIA/CENT	ER			1
519	NOAA-J	12/30/94	11E	WR			0
520	INTELSAT 704-2 (AC-113)	01/10/95	8203 IIAS/CENT	ER			1
521	EHF F/O-4 (AC-112)	01/29/95	8110 II/CENT	ER			1
522	INTELSAT VII (AC-115)	03/22/95	8204 IIAS/CENT	ER			1
523	DMSP F-13	03/24/95	45E	WR			0
524	MSAT (AC-114)	04/07/95	8111 IIA/CENT	ER			1
525	GOES-J (AC-77)	05/23/95	I/CENT	ER			1
526	EHF F/O-5 (AC-116)	05/31/95	II/CENT	ER			1
527	DSCS III (AC-118)	07/31/95	IIA/CENT	ER			1
528	JCSAT (AC-117)	08/29/95	IIAS/CENT	ER			1
529	EHF F/O-6 (AC-119)	10/22/95	II/CENT	ER			1
530	SOLAR OBSERV. (AC-121)	12/02/95	IIAS/CENT	ER			1
531	GALAXY IIIR (AC-120)	12/15/95	IIA/CENT	ER			1
532	PALAPA-C (AC-126)	01/31/96	IIAS/CENT	ER			1
533	INMARSAT-3 (AC-122)	04/03/96	IIA/CENT	ER			1
534	SAX (AC-78)	04/30/96	I/CENT	ER			1
535	UHF F7 (AC-125)	07/25/96	II/CENT	ER			1

## D.2.2 Atlas Failure Narratives

The following narratives provide the available details about each Atlas failure since the beginning of the Atlas program. The narratives are numbered to match the flight-sequence numbers in Section D.2.1.

1. 4A, 11 June 57, Response Mode 4T, Flight Phase 1: Flight appeared normal for 24.7 seconds when drop in fuel supply to B2 engine produced a drop in performance and shutdown. Both engines moved to hardover in pitch to compensate for thrust asymmetry. The B1 engine failed at 27 seconds. A fuel fire was observed in aft end after thrust was lost. The missile continued to rise, reaching an altitude of 9,800 feet at 38 seconds. Missile was destroyed by safety officer 50.1 seconds after liftoff. Thrust unit and other hardware impacted about 1/4 mile south of launch pad (105° flight azimuth).
2. 6A, 25 Sep 57, Response Mode 4, Flight Phase 1: Flight appeared normal until about 32.5 seconds after liftoff, when performance level of both engines dropped to 35% of normal. Both engines shut down at 37 seconds. Missile was destroyed at 63 seconds. Loss of thrust was due to loss of LOX regulator in the booster gas generator. Major components impacted about 8000 feet downrange and 1000 feet right of flight line.
5. 13A, 7 Feb 58, Response Mode 4, Flight Phase 1: The B2 turbopump and engine stopped operating about 118 seconds due either to loss of LO<sub>2</sub> regulator reference pressure or a control-system failure. The B1 engine ceased to operate 0.3 second later. Failure was attributed to shorting of a vernier engine feedback transducer due to aerodynamic heating. Propellant sloshing that began building up at about 100 seconds led to missile instability. Vehicle broke up at 167 seconds. Impact occurred about 280 miles downrange and about 3 miles crossrange.
6. 11A, 20 Feb 58, Response Mode 4T, Flight Phase 1: Vernier engine was hardover from 51.9 seconds to 89.4 seconds, then returned to null until 104 seconds, then went hardover again. Other systems appeared normal until 109.6 seconds, when divergent oscillations began in rate-gyro outputs and engine positions. All engines reached stops by 114.3 seconds and continued thereafter to oscillate between stops until loss of thrust at 124.8 seconds. Vehicle breakup occurred one second later. Probable cause of oscillation was a component failure in flight control system. Vehicle impacted about 105 miles downrange and 8 miles right of flight line.
7. 15A, 5 Apr 58, Response Mode 4, Flight Phase 1: Booster engines shut down prematurely at 105.3 seconds (instead of planned 127 seconds) due to B1 turbopump failure. Since B1 chamber pressure drives the gas generator, the B2 turbopump and engine also stopped. Impact was 180 miles downrange and slightly left of flight line.

9. 3B, 19 July 58, Response Mode 4T, Flight Phase 1: Random failure of yaw rate gyro caused violent maneuvers resulting in rupture of LO<sub>2</sub> tank, engine shutdown, and a fire near the lube oil drain. Missile broke up about 42 seconds with impact about 2 miles downrange and 0.4 miles crossrange left.
11. 5B, 28 Aug 58, Response Mode 4, Flight Phase 2.5: Missile was normal to SECO. After SECO, failure of hydraulic system caused loss of vernier engine control. Warhead impacted close to intended target.
12. 8B, 14 Sep 58, Response Mode 4, Flight Phase 2.5: Warhead impacted close to target although control was lost after SECO due to failure of vernier-engine hydraulic system.
13. 6B, 18 Sep 58, Response Mode 4, Flight Phase 1: Except for a late-opening sustainer fuel valve, flight was apparently normal until 80.8 seconds, when the B1 turbopump failed. Performance of the B1 engine and the axial acceleration dropped sharply at about 81.7 seconds, and the B2 system shut down about 0.1 seconds later. The sustainer and vernier engines continued to operate normally until 82.9 seconds, when the missile exploded. Impact was about 25 miles downrange and about 0.6 miles right of the flight line.
14. 9B, 17 Nov 58, Response Mode 4, Flight Phase 2: The flight was terminated at 227.6 seconds by premature fuel depletion caused either by failure of the propulsion utilization system or by a tanking error. Missile impacted near the flight line about 2300 miles downrange, some 850 miles short of target.
18. 13B, 15 Jan 59, Response Mode 5, Flight Phase 1: The vehicle appeared normal for the first 50-60 seconds, at which time it was obscured by clouds. It was probably normal until about 100 seconds, but prelaunch removal of the mainframe telemetry system prevented a precise determination. Beginning about 101 seconds, various erratic pitch, yaw, and roll rates and oscillations were noted with accompanying drops in acceleration and velocity. These rates become excessive at 106.6 seconds. At 121 seconds, the nosecone telemetry system showed that yaw and pitch rates abruptly increased, and this condition existed until reentry at 281 seconds. All thrusting apparently stopped between 121 and 123 seconds. The missile impacted about 170 miles downrange and 7.5 miles left.
19. 4C, 27 Jan 59, Response Mode 5, Flight Phase 2: Since the guidance system was inoperative throughout, the flight path was controlled by the pre-programmed flight control system. Impact was about 80 miles long and 30 miles left of target point.
21. 5C, 20 Feb 59, Response Mode 4, Flight Phase 2: After a normal booster phase, missile exploded at 173 seconds (BECO at 149.2 sec) apparently due to loss of fuel-tank pressure and subsequent rupture of LOX/fuel-tank bulkhead. Impact was about 1000 miles downrange and 6 miles left.

22. 7C, 18 Mar 59, Response Mode 4, Flight Phase 1: Booster engines shut down prematurely at 129.4 seconds, but booster section was not jettisoned until the near-normal time of 153 seconds. Guidance was inoperative. Since the sustainer engine could not gimbal before booster separation, the autopilot was unable to stabilize the missile after BECO. The sustainer shut down about 40 seconds before propellant depletion. The reentry vehicle spin rockets fired prematurely at 86.3 seconds after liftoff.
23. 3D, 14 Apr 59, Response Mode 4, Flight Phase 1: Performance of B2 engine dropped 36% at launch, resulting in a violent pitch as missile left the launcher. Flight control system corrected missile attitude, and flight continued at reduced thrust until a more violent explosion tore the thrust section away from the missile at 26.1 seconds. The sustainer continued operating with decreased thrust until shutdown by the safety officer at 36 seconds. Debris impacted about 3000 feet from launch point.
24. 7D, 18 May 59, Response Mode 4, Flight Phase 1: Failure in pneumatic system resulted in missile explosion at 65 seconds. A temporary failure of the thrust-structure fairing at liftoff strained the pneumatic lines and disconnects, resulting in leaks in the pneumatic system.
25. 5D, 6 June 59, Response Mode 4, Flight Phase 2: Either structural damage at booster staging or failure of the booster staging valve to close resulted in a fuel leak and explosion at 159.3 seconds. Impact occurred near the flight line about 780 miles downrange.
30. 10D (Mercury), 9 Sep 59, Response Mode 4, Flight Phase 2: Booster section failed to jettison resulting in a final velocity about 3000 ft/sec low and an impact range about 500 miles short of target.
32. 17D, 16 Sep. 59, Response Mode 4, Flight Phase 2.5: Flight was considered a success since impact was within two miles of target point. However, failure of the vernier hydraulic package resulted in loss of missile control during the vernier solo phase.
35. 26D, 29 Oct 59, Response Mode 4, Flight Phase 2.5: Vernier solo phase was unstable in pitch due to loss of thrust from V2 vernier engine. The V2 engine lost chamber pressure during booster jettison. Impact was about 14 miles short and out of splash net.
36. 28D, 4 Nov 59, Response Mode NA, Flight Phase 2: The flight was normal, but was terminated prematurely when the range-safety impact-predictor system failed.
37. 15D, 24 Nov 59, Response Mode NA, Flight Phase 2.5: Flight was normal, except the reentry vehicle failed to arm or separate.

38. 20D (Able IV), 26 Nov 59, Response Mode 4, Flight Phase 1: Third and fourth stages and payload broke off about 47 seconds. Atlas flight was normal and second stage ignited properly after Atlas SECO.
43. 6D (Dual Exhaust), 26 Jan 60, Response Mode 4, Flight Phase 2 and 2.5: At 175 seconds, as a result of a full-scale positive yaw command generated for five seconds, the missile stabilized on an erroneous heading. When a range-rate flag was lost 20 seconds later, the differentiated range-rate data substituted for measured data corrected the erroneous azimuth by generating a full-scale negative yaw command. The substituted data resulted in slightly erratic steering and a premature VECO signal that was not acted upon. The verniers were subsequently cutoff by the backup signal.
45. 29D (Midas I), 26 Feb 60, Response Mode 4, Flight Phase 2.5: Flight was normal until firing of the retro rockets after Atlas separation. An explosion at this time, probably due to activation of the Agena inadvertent separation destruct system, destroyed both the Atlas vehicle and the Agena.
46. 42D, 8 Mar 60, Response Mode 4, Flight Phase 2.5: Flight was considered a success although failure of the vernier hydraulic system resulted in loss of attitude control during the vernier solo phase.
47. 51 D, 10 Mar 60, Response Mode 1, Flight Phase 1: Due to combustion instability, an explosion occurred in the B1 chamber before missile movement. Missile was destroyed at 2.5 seconds after 2-inch motion when main propellants ignited.
48. 48D, 7 Apr 60, Response Mode 1, Flight Phase 1: Missile was destroyed in launch stand during launch attempt, apparently due to combustion instability in the B2 thrust chamber.
50. 23D (Lucky Dragon), 6 May 60, Response Mode 3, Flight Phase 1: An inoperative pitch gyro caused pitch instability, and resulted in destruct at 25.6 seconds.
54. 62D, 22 June 60, Response Mode 4, Flight Phase 2.5: Vernier engines were cutoff by autopilot backup when guidance discrete was not sent. Impact was 18 miles long.
56. 60D, 2 July 60, Response Mode 4, Flight Phase 2: Depletion of helium bottle pressure led to low sustainer and vernier engine thrust, and eventually early shutdown of engines. Impact was 40 miles short of target.
57. 74D (Tiger Skin), 22 July 60, Response Mode 5, Flight Phase 1: A pitchover rate that was 69% above the nominal rate resulted in vehicle breakup at 69.2 seconds.

58. 50D (Mercury), 29 July 60, Response Mode 4, Flight Phase 1: Flight appeared normal till 57.6 seconds when missile broke up apparently due to a rupture of the forward section of the LO<sub>2</sub> tank.
61. 47D (Golden Journey), 12 Sep 60, Response Mode 4, Flight Phase 2: Flight was apparently normal until about 222 seconds, when missile acceleration began to decay. A LOX regulator failure caused low sustainer performance and insufficient velocity to reach target. Impact was about 535 miles short.
64. 80D (Able V/Pioneer), 25 Sep 60, Response Mode 4T, Flight Phase 2.5 and 3: Atlas performed normally except for failure of vernier engines to cut off. Flight was not successful since the Agena chamber pressure stabilized at 70% of normal shortly after ignition. Stage then apparently tumbled before cutting off 30 seconds early. Third-stage spun up and stabilized in a nose-down attitude.
65. 33D (High Arrow), 29 Sep 60, Response Mode 4, Flight Phase 1: The booster engines cut off prematurely and failed to separate from sustainer. The missile remained intact, but failed to achieve the desired range because of the added booster weight.
66. 3E, 11 Oct 60, Response Mode 5, Flight Phase 2: Sustainer hydraulic pressure began to decay at 41 seconds and dropped to zero at 62 seconds. Sustainer began tumbling at booster staging when control was essentially lost. Thrust continued for about 18 seconds moving the impact point some 270 miles farther downrange and 27 miles crossrange. The missile exploded at 155 seconds.
67. 57D (LV-3A)/Agena A (Gibson Girl), 11 Oct 60, Response Mode NA, Flight Phase 3 and 5: Atlas performance was satisfactory. An umbilical failed to release properly from the Agena at liftoff, resulting in loss of pneumatic supply to the Agena attitude control system. A satisfactory orbit was not achieved. Guidance beacon failed at 106 seconds resulting in autopilot flight.
68. 81D (Diamond Jubilee), 12 Oct 60, Response Mode 4, Flight Phase 1: Overpressurization of the LOX tank resulted in tank rupture and vehicle breakup at 71.6 seconds.
72. 4E, 29 Nov 60, Response Mode 5, Flight Phase 2: Sustainer hydraulic pressure lost at 41 seconds. Missile tumbled shortly after booster staging. Sustainer thrust terminated at about 150 seconds, some 22 seconds after BECO. During the sustainer solo phase, the impact point moved about 120 miles downrange and 44 miles crossrange.
73. 91D, 15 Dec 60, Response Mode 4, Flight Phase 1: Vehicle performed normally till about 66.7 seconds, when a blast-band failure apparently resulted in rupture of the forward section of the LOX tank. The upper stages separated at this time, but the Atlas engines continued thrusting until 71 seconds. Control was lost between

72 and 73 seconds, and a final explosion occurred at 74 seconds. Impact was about 8 miles downrange and one mile crossrange.

76. 8E, 24 Jan 61, Response Mode 5, Flight Phase 2: Missile stability was lost at about 161 seconds, some 30 seconds after BECO, probably due to failure of the servo-amplifier power supply. The sustainer engine shut down at 248 seconds, and the vernier engines about 10 seconds later. Impact occurred 1316 miles downrange and 215 miles crossrange.
77. 70D (LV-3A)/Agena A (Jawhawk Jamboree), 31 Jan 61, Response Mode NA, Flight Phase 2: Flight was considered successful although loss of rate lock at 222 seconds caused slightly erratic steering during the last 20 seconds of Atlas sustainer thrusting flight and failure of vehicle to pitch over during the vernier solo period.
80. 13E, 13 Mar 61, Response Mode 4, Flight Phase 2: Sustainer main fuel valve remained in the full open position throughout flight, resulting in fuel depletion and premature shutdown of sustainer engine at 251 seconds.
81. 16E, 24 Mar 61, Response Mode 4, Flight Phase 1.5: Due to depletion of helium-bottle pressure, booster section failed to jettison, leading to fuel depletion and impact far short of target.
82. 100D (Mercury 3), 25 Apr 61, Response Mode 3, Flight Phase 1: Flight was terminated at 40 seconds by RSO when vehicle failed to perform roll and pitch-over maneuvers, apparently due to failure of the autopilot programmer. The malfunction was attributed to a plastic coating on the connector pins within the programmer, causing an open circuit. Major debris impacted about 1800 feet downrange and 6100 feet crossrange left.
86. 27E (Sure Shot), 7 June 61, Response Mode 4, Flight Phase 1: Apparent combustion instability caused an explosion and missile destruction 3.86 seconds after liftoff.
87. 17E, 22 June 61, Response Mode 4, Flight Phase 1: Missile destroyed itself at 101.5 seconds due to failure of flight-control system. Pitch rate was about 1.55 times normal. Just before breakup at 66,000 feet altitude, missile had pitched over almost 90° due to higher than normal pitch rate, producing excessive heating and aerodynamic loads. At breakup, flight path was nearly horizontal. Impact was about 64 miles downrange.
93. 111D(Ranger-1), 23 Aug 61, Response Mode NA, Flight Phase 4: The Agena achieved a normal parking orbit. Flight continued normally until Agena second burn. During the restart sequence the fuel valve failed to open so only oxygen was pumped into the thrust chamber. Apogee of final orbit was only slightly above the normal circular parking-orbit altitude.

94. 26E, 8 Sep 61, Response Mode 4, Flight Phase 2: Sustainer engine shut down prematurely during the booster jettison sequence. Most probable cause was drop in fuel flow to the gas generator. The vernier engines continued to burn for about 28 seconds after the sustainer shut down. Vernier thrust decayed at 137 seconds, guidance platform tumbled at 163 seconds. The missile remained intact until at least 470 seconds, when data were lost. Impact was about 525 miles downrange.
95. 106D (LV-3A)/Agena B (First Motion), 9 Sep 61, Response Mode 1, Flight Phase 1: Failure of an umbilical to eject allowed a commit/stop-power signal to reach the missile. Lack of electrical power 0.265 seconds after liftoff caused the vehicle to fall back on the launch pad after a rise of about 18 inches.
99. 105D (LV-3A)/Agena B (Big Town), Midas IV, 21 Oct 61, Response Mode NA, Flight Phase 2: Flight was regarded as a success, since the Agena compensated for Atlas anomalies. Atlas roll control was lost at 186 seconds, resulting in a roll rate of over 40° per second at Agena separation. Control in pitch and yaw was maintained. A LOX leak affected sustainer performance just before SECO and throughout the vernier phase.
100. 32E, 10 Nov 61, Response Mode 4T, Flight Phase 1: Sustainer engine shut down 0.7 seconds after liftoff. Although a fire appeared in the thrust section at 19 seconds, booster engines maintained stability until 24.5 seconds, when the B2 engine performance began to decay. All control was lost after this point, and the missile was destroyed by the RSO at 35 seconds. Impact was about 2500 feet downrange and 320 feet crossrange.
101. 117D (Ranger-2), 18 Nov 61, Response Mode NA, Flight Phase 4: The Atlas booster functioned normally. A parking orbit was attained during the Agena first burn although roll control was not maintained due to failure of the roll gyro. When control gas was depleted, missile lost stability and began to tumble. Second Agena burn lasted only one second.
103. 108D (LV-3A)/Agena B (Round Trip), 22 Nov 61, Response Mode 4T, Flight Phase 2: Flight was not successful since vehicle failed to achieve orbit. Loss of pitch control at 244 seconds was attributed to aerodynamic heating. At Agena separation the Atlas had pitched up 145°.
108. 5F, 12 Dec 61, Response Mode 5, Flight Phase 2: A failure in the inertial guidance system of 1.06 seconds duration caused the existing inertial X velocity to be inserted in the Z-velocity channel. As a result, the missile impacted 575 miles short and 30 miles left of target.
110. 6F, 20 Dec 61, Response Mode 4T, Flight Phase 2: Flight appeared normal until staging. During booster jettison, sustainer and vernier hydraulic pressure began to decay, leading to complete loss of sustainer yaw and pitch control at 229 and 232 seconds, respectively. Missile began tumbling at about 226 seconds.

Sustainer engine shut down at 282 seconds. Missile impacted 1300 miles downrange and 18 miles crossrange.

111. 114D (LV-3A)/Agena B (Ocean Way), 22 Dec 61, Response Mode NA, Flight Phase 2: Flight was considered successful although a failure in the flight programmer prevented the SECO signal from cutting off the sustainer engine. Sustainer burned an additional 2.5 seconds to propellant depletion producing excess Atlas velocity.
114. 121 D (Ranger 3), 26 Jan 62, Response Mode NA, Flight Phase 2 and 5: Failure of pulse beacon in guidance system at 49 seconds caused sustainer to burn to LOX depletion, resulting in a 300 ft/sec overspeed. Due to malfunction of pulse beacon at 49 seconds, no guidance steering commands or discretives were given. Booster was cut off by backup signal from accelerometer, sustainer by fuel depletion. Due to excess speed, spacecraft passed 22,000 miles in front of moon, and primary mission objective was not met. All other Atlas and Agena systems performed as planned.
116. 137D (Big John), 16 Feb 62, Response Mode NA, Flight Phase 1.5: Flight was considered successful, although RV did not separate properly.
118. 52D (Chain Smoke), 21 Feb 62, Response Mode 4, Flight Phase 1: A fire in the engine compartment resulted in shutdown of all engines at 60 seconds and vehicle explosion at 72 seconds.
119. 66E (Silver Spur), 28 Feb 62, Response Mode 4T, Flight Phase 1.5 and 2: Loss of helium-bottle pressure resulted in failure to jettison booster engines and premature vernier-engine cutoff at 131.5 seconds. Cutoff of verniers resulted in loss of roll control. Vehicle exploded at 295 seconds.
122. 11F, 9 Apr 62, Response Mode 1, Flight Phase 1: An explosion in thrust section at 0.9 seconds after about 6 feet of motion was followed by a further explosion in the propellant tanks and total missile destruction at 1.2 seconds.
123. 110D (LV-3A)/Agena B (Night Hunt), Midas, 9 Apr 62, Response Mode NA, Flight Phase 1: An autopilot malfunction prevented sufficient pitchover during booster and sustainer phase resulting in improper SECO conditions and an improper orbit.
128. 104D, 8 May 62, Response Mode 4, Flight Phase 1: Flight appeared normal until about 45 seconds when weather shield shifted. Further shocks occurred at 50 seconds with loss of weather shield. Booster-engine cutoff was initiated at 55 seconds. Missile destroyed itself at 57 seconds due to breakup of Centaur upper stage. Recorded impact was 8500 feet downrange and 8200 feet crossrange.

131. LV-3A/Agena B (Rubber Gun), 17 June 62, Response Mode 4, Flight Phase 3: Although Atlas performance was satisfactory, the mission was apparently a failure. No other data available.
134. 67E (Extra Bonus), 13 July 62, Response Mode 4, Flight Phase 2 and 2.5: A LOX leak in the high-pressure line apparently froze sustainer control components. Residual sustainer thrust after cutoff continued for some 30 seconds, causing a 120-mile overshoot.
137. 145D (Mariner R-1), 22 July 62, Response Mode 5, Flight Phase 2: Booster stage and flight appeared normal until after booster staging at guidance enable at about 157 seconds. Operation of guidance rate beacon was intermittent. Due to this and faulty guidance equations, erroneous guidance commands were given based on invalid rate data. Vehicle deviations became evident at 172 seconds and continued throughout flight with a maximum yaw deviation of 60° and pitch deviation of 28° occurring at 270 seconds. The vehicle deviated grossly from the planned trajectory in azimuth and velocity, and executed abnormal maneuvers in pitch and yaw. The missile was destroyed by the RSO at 293.5 seconds, some 12 seconds after SECO.
141. 87D (Peg Board II), 9 Aug 62, Response Mode 4, Flight Phase 2.5: Failure of the sustainer/vernier hydraulic system to maintain system pressure prevented normal operation during the vernier solo phase.
142. 57F (Crash Truck), 10 Aug 62, Response Mode 5, Flight Phase 1: The roll program failed. The missile was destroyed by the RSO at 68 seconds.
144. 179D (Mariner R-2), 27 Aug 62, Response Mode NA, Flight Phase 2: Flight was successful although roll control was lost during the period from 140 seconds to 190 seconds due to erratic performance of vernier engine #2. Before and after this time interval, vernier #2 and all other Atlas and Agena systems performed normally.
146. 4D (Briar Street), 2 Oct 62, Response Mode 4, Flight Phase 2: The missile self-destructed at 183 seconds. The vernier engines shut down prematurely at 46 seconds. Subsequently, closure of the vernier bleed valves led to excessively high sustainer performance and premature shutdown at 181.3 seconds.
148. 215 D (Ranger-5), 18 Oct 62, Response Mode NA, Flight Phase 5: Flight was regarded as successful although failure in the ground control system 35 minutes after launch prevented accomplishment of primary lunar impact and study mission. The guidance rate beacon failed at 94.6 seconds but backup differentiated tracking data kept the vehicle within normal limits.
153. 13F (Action Time), 14 Nov 62, Response Mode 4, Flight Phase 1: The flight was terminated when sustainer and vernier engines shut down prematurely at

94.3 seconds. A thrust-section fire before 20 seconds apparently failed the lube oil system, which led to cessation of propellant flow.

156. 131D LV-3A/Agema B (Bargain Counter), 17 Dec 62, Response Mode 4T, Flight Phase 1: Mission failed because of an Atlas hydraulic failure. Missile lost stability at 77.5 seconds, then rolled clockwise, pitched down and yawed left before breaking up at about 80.5 seconds.
157. 64E (Oak Tree), 18 Dec 62, Response Mode 4T, Flight Phase 1: The B2 engine failed at 37.1 seconds as a result of lubrication loss to the pinion gear. Booster engine shutdown resulted in a violent rolling yaw maneuver that caused missile breakup followed by an explosion at about 38 seconds.
158. 160D (Fly High), 22 Dec 62, Response Mode 4, Flight Phase 2: Due to noisy data, range safety limits in the automatic cutoff system were exceeded, causing generation of an all-engines-cutoff signal. As a result, the vernier engines were cut off about 10 seconds early, and the reentry vehicle was about 12.3 miles short.
159. 39D (Big Sue), 25 Jan 63, Response Mode 4, Flight Phase 1: Propulsion system performance was unsatisfactory after 78 seconds, when booster engine performance started to decay. Booster engines shut down shortly after this, probably as a result of excessive heating in the gas-generator regulator. The sustainer operated normally until at least 106 seconds, with shutdown occurring sometime between 106 and 126 seconds. Breakup occurred about 300 seconds. Missile apparently impacted about 100 miles downrange.
164. 102D (Tall Tree 3), 9 Mar 63, Response Mode 5, Flight Phase 1: A flight-control malfunction occurred at about 15 seconds at the start of the pitch program. The missile pitched excessively, reaching 310° and an altitude of 5,000 feet at 33.5 seconds when it broke up. Debris impacted close to pad.
166. 64D (Tall Tree 1), 15 Mar 63, Response Mode 4T, Flight Phase 2: A sustainer hydraulic-system failure at 83.5 seconds resulted in loss of sustainer engine control by 86 seconds and loss of vernier control at 99 seconds. Missile control was maintained by the booster engines until booster cutoff, when lack of sustainer and vernier control caused the missile to roll clockwise, pitch up, and yaw left. Sustainer thrust decayed at 131 seconds, and the missile began tumbling at 136.6 seconds. Missile self-destructed at 146 seconds with impact point about 600 miles downrange.
168. 193D (Leading Edge), 16 Mar 63, Response Mode 4T, Flight Phase 2: Loss of B2 pitch feedback signal at 103.5 seconds resulted in loss of vehicle stability. Missile tumbled, then self-destructed at about 270 seconds.
169. 83F (Kendall Green), 21 Mar 63, Response Mode 4, Flight Phase 2.5: A defective solder joint apparently led to two instances of erroneous velocity computations in

the x and z velocity channels. As a result, the missile impacted about 12 miles short and 0.2 miles right of target.

170. 52F (Tall Tree 4), 23 Mar 63, Response Mode 4, Flight Phase 1: Missile self-destructed at about 91 seconds for unknown reasons. Impact was near the flight line about 120 miles downrange.
171. 65E (Black Buck), 24 Apr 63, Response Mode NA, Flight Phase 2.5: Vernier hydraulic-system pressure was lost at 301 seconds, resulting in loss of vernier-engine control during the vernier solo phase. The reentry vehicle impact point was not perceptibly affected by this malfunction.
176. 139D LV-3A/Agena B (Big Four), 12 Jun 63: Response Mode 4T, Flight Phase 1: Flight appeared normal until about 88.4 seconds when, due to a hydraulic failure, the vehicle made a violent right and down maneuver. The missile broke up five seconds later at 93.4 seconds.
181. 24E (Silver Doll), 26 July 63, Response Mode 4, Flight Phase 2: Spurious voltage transients caused premature pressurization of the vernier solo tanks at 101.3 seconds, and premature sustainer engine shut down just after booster separation at 141 seconds.
187. 63D (Cool Water III), 6 Sep 63, Response Mode 4, Flight Phase 1: All systems performed satisfactorily till 110 seconds, when the sustainer/vernier hydraulic pressure dropped from 3080 to 490 psig. The failure resulted in premature shutdown of the sustainer engine at 136 seconds. Booster-engine cutoff occurred normally at 140.3 seconds, and the booster was successfully jettisoned. The impact point occurred about 620 miles downrange.
188. 84D (Cool Water IV), 11 Sep 63, Response Mode 4T, Flight Phase 2.5: Flight seemed normal through SECO, although the pneumatic precharge to the vernier solo accumulator was lost at 96.6 seconds. Due to this failure, missile stability was lost near the start of the vernier solo phase. The R/V probably failed to separate.
189. 71E (Filter Tip), 25 Sep 63, Response Mode 4T, Flight Phase 2: Visual observers reported a boat-tail fire, radical oscillations in yaw, and rough running booster and sustainer engines. Failure of the sustainer hydraulic system during the staging sequence resulted in loss of missile stability at 140 seconds. Sustainer and vernier engines shut down at about 267 seconds with the impact point about 600 miles downrange.
190. 45F (Hot Rum), 3 Oct 63, Response Mode 1, Flight Phase 1: The B-1 booster-engine fuel valve failed to open during the start sequence, so the engine did not ignite. Missile toppled over and exploded.

191. 163D (Cool Water V), 7 Oct 63, Response Mode 4, Flight Phase 1: Flight was normal up to about 73 seconds when the missile exploded. Suspected cause was intermediate bulkhead reversal/rupture due to insufficient helium pressure.
194. 136F (ABRES), 28 Oct 63, Response Mode 4T, Flight Phase 2: After a normal booster phase and staging, failure of sustainer hydraulic system resulted in loss of sustainer control and stability at 138 seconds. Sustainer and vernier engines shut down at 260 seconds, some 28 seconds early. The R/V impacted about 507 miles downrange.
196. 158D (Cool Water VI), 13 Nov 63, Response Mode 4, Flight Phase 1: The trajectory was low throughout flight. The sustainer/vernier hydraulic pressure was lost at 112.7 seconds, followed by missile self-destruct at about 118 seconds when the vacuum impact point was about 280 miles downrange and on azimuth.
202. 48E (Blue Bay), 12 Feb 64, Response Mode 4, Flight Phase 2: The booster engine shut down at 119.5 seconds, and the sustainer engine shut down prematurely at 198.8 seconds. Impact was near the flight line about 635 miles downrange.
207. 3F (High Ball), 3 Apr 64, Response Mode 1, Flight Phase 1: Missile was destroyed on the pad when the B1 booster engine failed to ignite.
212. 135D (AC-3), 30 June 64, Response Mode 4, Flight Phase 3: The Centaur engines shut down early, apparently due to a hydraulic coupling failure that led to a failure in the propellant system. Impact was about 2340 miles downrange.
219. 57E (Gallant Gal), 27 Aug 64, Response Mode 4, Flight Phase 2: Missile experienced an early SECO with no vernier burn thereafter due to a guidance-system malfunction. Impact was about 88 miles short and 0.4 miles right of target.
227. 289D (Mariner-3), 5 Nov 64, Response Mode 4, Flight Phase 4: A short second burn of the Agena prevented attainment of the desired orbit, and resulted in a heliocentric orbit.
232. 146D, 11 Dec 64, Response Mode NA, Flight Phase 5: Flight was completely normal through Centaur first burn. During the coast phase, liquid hydrogen vented through the vent valve caused vehicle instability and tumbling. By second engine firing, insufficient liquid hydrogen remained at boost-pump sump to sustain normal combustion.
236. 172D/ABRES (Beaver's Dam), 21 Jan 65: Response Mode 4, Flight Phase 2 and 3: The Atlas apparently performed normally, except that the sustainer shut down 1.35 seconds early. The OV1-1 failed to separate from the Atlas and thus failed to put the spacecraft in orbit.

240. 156D, 2 Mar 65, Response Mode 1 Flight Phase 1: At 0.36 seconds booster fuel-pump pressure dropped due to a fuel pre valve failure, booster lost thrust, fell back on launch pad, and was destroyed at 3.26 seconds.
251. 68D/ABRES (Tennis Match), 27 May 65: Response Mode 4, Flight Phase 1: A failure in the booster gas-generator loop resulted in decreasing booster performance after 116 seconds. The impact point stopped moving at 122 seconds when an explosion occurred in the thrust section. Further vehicle breakup occurred at 218 seconds. Destruct was sent at 293 seconds. Debris impacted close to the intended ground track.
257. SLV-3/Agenda D (White Pine), 12 Jul 65: Response Mode 4 & 5, Flight Phase 2 & 3: Flight was normal until booster engines cutoff at 131 seconds. As a result of a circuit board failure caused by excessive vibrations, the sustainer also shutdown at BECO. The Atlas booster engines did not separate immediately from the sustainer, but did so some 50 seconds later after the event timer recycled. The Agenda subsequently separated and ignited at about 198 seconds, creating wild uprange movements on the IP display by 255 seconds. Destruct was sent at 257 seconds.
267. SLV-3 (GTV-6), 25 Oct 65, Response Mode 4, Flight Phase 3: The flight was a failure although all Atlas objectives were achieved. The Agenda startup appeared normal, but the engine shut down after about one second of operation, Propellants ceased flowing but the helium pressurization system continued to pressurize the propellant tanks until they burst.
276. 303D (Eternal Camp), 4 Mar 66, Response Mode 5, Flight Phase 1: Although track and rate lock were lost at 88 seconds, missile appeared normal till about 112 seconds when skyscreen operator reported that vehicle was spiraling. A hydraulic system failure occurred during the staging sequence, resulting in loss of vehicle stability at 153 seconds and sustainer engine shutdown at 194 seconds. The impact point initially appeared to stop about 800 miles downrange, well beyond the booster impact point. At about this time or shortly thereafter, telemetry indicated rapidly varying pitch, roll, and yaw rates and shutdown of sustainer and vernier engines. Final impact was estimated to be 976 miles downrange and 3° left of the nominal track.
279. 304D (White Bear), 19 Mar 66, Response Mode 5, Flight Phase 2: The reentry vehicle impacted 82 miles beyond the target point when the head suppression valve failed to close at SECO. The LOX tank thus vented through the sustainer chamber, adding impulse in the process.
281. 184D (AC-8), 7 Apr 66, Response Mode 4T, Flight Phase 4: Flight appeared normal until second Centaur burn. Both Centaur engines started but one could not

maintain thrust. Thrust imbalance resulted in tumbling, followed by fuel starvation, and early thrust termination.

284. 208D (Crab Claw), 3 May 66, Response Mode 4T, Flight Phase 1: High engine-compartment temperatures were first noted at 41 seconds. The sustainer pitch-actuator feedback-loop failed open at 136 seconds, a few seconds before planned BECO. The flight appeared normal to the safety officer until about this time when roll and pitch rates increased. The IIP apparently stopped about 155 seconds, although General Dynamics reported that vehicle stability was not lost until 216 seconds. Shutdown of sustainer and vernier engines occurred at 235 seconds. Suspected cause of malfunction was excessive heating in the boat-tail section.
287. SLV-3 (GTA-9), 17 May 66, Response Mode 5, Flight Phase 1: Vehicle became unstable when B2 pitch control was lost at 121 seconds. Loss of pitch control resulted in a pitch-down maneuver much greater than 90°. Guidance control was lost at 132 seconds. After BECO, the vehicle stabilized in an abnormal attitude. Although the vehicle did not follow the planned trajectory, SECO (at 280 seconds), VECO (at 298 seconds), and Agena separation occurred normally from programmer commands.
294. 96D (Vener Panel), 10 Jun 66, Response Mode 4, Flight Phase 2.5: The reentry vehicle undershot the target by 20 miles when the vernier engines shut down early. Failure was caused by an abnormal decay of control-bottle helium pressure.
298. 58D/ABRES (Stony Island), 13 July 66: Response Mode NA, Flight Phase 3: Flight was regarded as a success, although one of two OV's failed to orbit when it impacted the structure door which had not been opened.
300. 149F (Busy Ramrod), 8 Aug 66, Response Mode 4, Flight Phase 2: The sustainer engine shut down 27 seconds early due to fuel depletion caused by an unfavorable ratio of propellant usage during the booster stage. Verniers burned to fuel depletion.
306. 194D (AC-7), 20 Sep 66, Response Mode NA, Flight Phase 5: Atlas Centaur performance was normal, but Surveyor spacecraft lost stability on the way to the moon.
308. 115F (Low Hill), 11 Oct 66, Response Mode 4, Flight Phase 1: The missile was normal till about 85 seconds when it appeared to lose thrust and breakup. Several major pieces impacted 32 to 40 miles downrange near the intended flight line.
310. 174D (AC-9), 26 Oct 66, Response Mode NA, Flight Phase 2: Although Atlas pressurization system anomaly caused decaying sustainer engine performance and early SECO, no mission objectives were compromised.

318. 148F (Busy Stepson), 17 Jan 67, Response Mode NA, Flight Phase 2.5: Flight was normal except that reentry vehicle failed to separate.
344. 81F (ABRES/AFSC), 27 Oct 67, Response Mode 4T, Flight Phase 1: Although various anomalous events occurred early in flight, the missile appeared to follow the intended trajectory till about 24 seconds. Diverging roll oscillations actually began about 21.4 seconds, and pitch and roll stability were lost by 24.8 seconds. By 27.9 seconds, the vehicle was tumbling about 6.5 degrees per second in pitch and yaw, and 12 degrees per second in roll. By 30 seconds, the vehicle lost all thrust and began to break up. Fuel cutoff and destruct were sent at 35 and 39 seconds, respectively.
358. 95F (ABRES/AFSC), 3 May 68, Response Mode 5, Flight Phase 1: Immediately after liftoff the telemetered roll and yaw rates indicated that the missile was erratic. During the first 10 seconds of flight the missile yawed hard to the left. It then began a hard yaw to the right, crossed over the flight line and continued toward the right destruct line. Shortly thereafter the missile apparently pitched up violently and the IIP began moving back toward the beach. The missile was destructed at about 45 seconds when the altitude was about 14,000 feet and the downrange distance about 9 miles. Major pieces impacted less than a mile offshore, indicating uprange movement of the impact point during the last part of thrusting flight.
364. 5104C AC-17 (ATS-D), 10 Aug 68, Response Mode NA, Flight Phase 4: A normal parking orbit was achieved, but when Centaur restart was attempted, thrust could not be maintained because of inoperative boost pumps. Frozen H<sub>2</sub>O<sub>2</sub> line was the apparent root cause.
365. 7004 SLV-3/Burner II/Agena D (AFSC), 16 Aug 68: Response Mode 4, Flight Phase 3: Atlas performance was normal. The vehicle failed to achieve orbit because the protective shroud surrounding the second stage failed to separate.
368. 56F (ABRES/AFSC), 16 Nov 68, Response Mode 4T, Flight Phase 2.5: Flight was normal through SECO. The missile then lost attitude control, executing a hard yaw rate turn throughout and beyond the vernier solo phase.
372. 5403C AC-20 (Mariner 6 Mars), 24 Feb 69, Response Mode NA, Flight Phase 1: Early Atlas BECO due to staging accelerometer failure was compensated for by extended Atlas sustainer and Centaur burns. Mission was successful.
379. 98F (ABRES/AFSC), 10 Oct 69, Response Mode 4, Flight Phase 1: The missile appeared normal until about 66 seconds when the sustainer engine shut down prematurely. The booster engine apparently continued normally to BECO. At about 255 seconds the payload SPDS engine ignited. Destruct was sent at 272 seconds.

388. 5003C AC-21 (OAO-B), 30 Nov 70, Response Mode 4, Flight Phase 2: Since the nose fairing failed to separate, Centaur did not have enough energy to make orbit. Payload impacted in Africa.
392. 5405C AC-24 (Mariner 8 Mars), 8 May 71, Response Mode 4T, Flight Phase 3: Mission requirements were not met. The Atlas boost phase was normal. Shortly after Centaur main-engine start, pitch stabilization was lost due to failure of the rate gyro or an electrical failure in the pitch channel of the flight control system. The vehicle began an accelerated nose-down tumbling motion that subsequently resulted in early and erratic main-engine shutdown due to propellant starvation.
397. SLV-3A (Agena), 4 Dec 71, Response Mode 4, Flight Phase 1: Sustainer engine turbine damage during engine start resulted in hot gas leaks and eventual failure of thrust-section hardware. Vehicle broke up at 87 seconds.
419. 5015D AC-33 (Intelsat IV F-6), 20 Feb 75, Response Mode 4T, Flight Phase 2: The Atlas booster-section electrical disconnect failed at booster staging. The harness was pulled apart, so flight-control avionics was unable to maintain vehicle stability. Missile appeared normal until the IP stopped at 200 seconds. Precautionary destruct was sent at 414 seconds.
420. 71F (AFSC), 12 Apr 75: Response Mode 4, Flight Phase 1: Although an abnormal overpressure occurred at the base of the missile 620 msec before liftoff, the vehicle appeared normal until about 45 seconds when sustainer manifold and fuel-pump pressures began dropping. By 61 seconds, both the sustainer and vernier engines had shut down. Booster engines continued thrusting until about 123 seconds when the IIP stopped moving and radar operator reported multiple pieces. The breakup apparently resulted from an external explosion in the flame bucket that damaged the thrust section. Destruct was sent at 303 seconds when missile elevation dropped to 5°.
432. 5701D AC-43 (Intelsat IVA F-5), 29 Sep 77, Response Mode 4T, Flight Phase 1: A leak in the booster hot-gas generator at 2.3 seconds resulted in a fire in the thrust section at 36.5 seconds. The vehicle went into a violent maneuver at 54.9 seconds, failing the structure. The Atlas exploded at 55.8 seconds, leaving the Centaur intact. The Centaur was destroyed by the RSO at 61.7 seconds.
457. 19F (NOAA-B), 29 May 80: Response Mode NA, Flight Phase 1: Failure of turbopump seal allowed fuel to enter the gear box resulting in 21% low thrust by the B1 booster engine. The payload was inserted into an abnormal orbit and the mission was lost.
460. 68E, 8 Dec 80: Response Mode 5, Flight Phase 1: Flight appeared normal until 102.7 seconds when the lube oil pressure on the B2 booster engine suddenly dropped. At 120.1 seconds, the engine shut down, followed 385 msec later by guidance shutdown of the B1 engine. The asymmetric thrust during shutdown

caused yaw and roll rates that the flight control system could not correct. As a result, attitude control was lost and the thrusting sustainer pivoted the missile to a retrofire attitude before the vehicle could be stabilized. After the booster package was jettisoned, the missile was stabilized and decelerating in the retrofire mode by 148 seconds. The sustainer continued thrusting in this attitude until 282.9 seconds when reentry heating apparently caused sustainer shutdown and vehicle breakup.

464. 5039D AC-59 (FLTSATCOM), 6 Aug 81, Response Mode NA, Flight Phase 1 and 5: The basic mission was accomplished although three increasingly severe shock events were recorded at 56.2, 70.7, and 120.8 seconds. The structural damage sustained by the spacecraft severely limited on-orbit operations.
466. 76E (NAVSTAR VII), 18 Dec 81: Response Mode 2, Flight Phase 1: Shortly after clearing the launch tower at an altitude of about two tower heights, the thrust performance of the B1 engine began to decay. The engine was shut down completely by 7.4 seconds. The unbalanced thrust caused the missile to pitch over to the right, and travel horizontally for about one second. It then pitched toward the ground. A small explosion occurred about one-third of the way down, followed by a larger explosion when the missile impacted the ground directly behind the launch pad about 19 seconds after liftoff. Cause of the engine failure was plugging of the gas-generator fuel-cooling parts that resulted in a gas-generator burn-through.
477. 5042G AC-62 (Intelsat V), 9 Jun 84, Response Mode 4T, Flight Phase 4: Performance was normal until an abnormal shock event occurred at Atlas/Centaur separation. Subsequent data indicated that a Centaur oxygen tank leak resulted in a loss of 1483 pounds of LOX during Centaur first burn. The leak resulted in the LOX tank pressure falling below the LH2 tank pressure, which led to collapse of the intermediate bulkhead during the coast phase. Bulkhead collapse caused unexpected tumbling forces during coast. The Centaur engines restarted after coast, but burned for only 6 or 7 seconds of a planned 90-second burn.
489. 5048G AC-67 (FLTSATCOM F-6), 26 Mar 87, Response Mode 4T, Flight Phase 1: Vehicle performance was normal till 48.4 seconds, when the vehicle was struck by lightning. As a result, the guidance computer commanded a hard right turn which caused vehicle breakup due to inertial and aerodynamic loads. RSO sent destruct at 70.7 seconds.
498. 5050 AC-70 (BS-3H COMSAT), 18 Apr 91, Response Mode 4T, Flight Phase 3: Atlas performance was normal. Although both Centaur main engines began the start sequence properly, the C-1 turbo-machinery decelerated and stopped, leaving the C-1 engine thrust at the ignition level. Air entering through the stuck-open check valve liquefied and froze in the LH2 pump and gear box of the C-1

engine, thus preventing the engine from achieving full thrust. Due to the resulting thrust imbalance, the vehicle tumbled out of control. Destruct was sent some 80 seconds after Centaur ignition.

506. 5051 AC-71 (Galaxy 1R), 22 Aug 92, Response Mode 4T, Flight Phase 3: A Centaur engine check valve stuck open allowing air into the turbopumps. Air entering through the stuck-open check valve liquefied and froze in the LH2 pump and gear box of the C-1 engine, which prevented the engine from achieving full thrust. Destruct was sent by the RSO about 193 seconds after Centaur ignition. This is the same failure experienced by AC-70 launched on 18 Apr 91.
507. 5054 AC-74 (UHF Follow On-1), 25 Mar 93, Response Mode NA, Flight Phase 2 and 5: The flight was considered successful although below normal Atlas performance resulted in a low spacecraft apogee (5000 nm vice planned 9225 nm). The perigee altitude was near nominal at 120 nm. A loose screw that allowed the oxygen regulator to go out of adjustment caused booster-engine thrust to drop to 65% of nominal at 103 seconds. The booster engines remained attached to the sustainer, which flew to propellant depletion. These events led to depletion shutdown of the Centaur stage 22 seconds early.

### D.3 Delta Launch and Performance History

The Delta launch-vehicle family originated in 1959 with a NASA contract to Douglas Aircraft Company, now McDonnell Douglas Corporation. The Delta, using components from USAF's Thor IRBM program and USN's Vanguard launch-vehicle program, was operational 18 months later. On May 13, 1960, the first Delta was launched from Cape Canaveral with a 179-pound Echo-I passive communications satellite. In the intervening years, the Delta has evolved to meet the ever-increasing demands of its payloads – including weather, scientific, and communications satellites. Each Delta modification corresponded to an increase in payload capacity. Table 42 shows a summary of Delta configurations since the beginning of the program.<sup>[10]</sup>

The Delta 7925, the latest vehicle in the series, is a three-stage liquid-propellant vehicle with nine solid-propellant strap-on booster motors. For propellants, the Delta uses RP-1 and liquid oxygen in Stage 1, and nitrogen tetroxide and aerazine 50 in Stage 2. Stage 3 consists of a Payload Assist Module (PAM) with a solid-propellant motor. The strap-on boosters are Hercules graphite epoxy motors (GEMs) using HTPB-type solid propellant. At liftoff, the liquid-propellant Stage-1 engine and six of the nine GEMs are ignited. The remaining three GEMs are ignited some 65 seconds later.

Table 42. Summary of Delta Vehicle Configurations

Configuration	Description
Delta	Stg. 1: Modified Thor. MB-3 Blk I engine Stg. 2: Vanguard AJ10-118 propulsion system Stg. 3: Vanguard X-248 motor
A	Stg. 1: Engine replaced with MB-3 Blk II
B	Stg. 2: Tanks lengthened; higher energy oxidizer used
C	Stg. 3: Replaced with Scout X-258 motor PLF: Bulbous replaced low drag
D	Stg. 0: Added 3 Thor-developed SRMs (Castor I)
E	Stg. 0: Castor II replaced Castor I Stg. 1: MB-3 Blk III replaced Blk II Stg. 2: Propellant tank diameters increased Stg. 3: Replaced with USAF-developed FW-4 motor PLF: Fairing enlarged to 65-inch diameter
J	Stg. 3: TE-364-3 used
L, M, N	Stg. 1: Tanks lengthened, RP-1 tank diameter increased Stg. 3: Varied: FW-4 (L), TE-364-3 (M), none (N)
M-6, N-6	Stg. 0: Six Castor IIs employed
900	Stg. 0: No Castor IIs employed Stg. 2: Replaced with Transtage AJ10-118F engine
1604	Stg. 0: Six Castor IIs employed Stg. 3: Replaced with TE-364-4

Configuration	Description
1910, 1913, 1914	Stg. 0: Nine Castor IIs employed Stg. 3: Varied: none (1910), TE-364-3 (1913), TE-364-4 (1914) PLF: 96-inch diameter replaced 65-inch
2310, 2313, 2314	Stg. 0: Three Castor IIs employed Stg. 1: RS-27 replaced MB-3 Stg. 2: TR-201 engine replaced AJ10-118F Stg. 3: Varied: none (2310), TE-364-3 (2313), TE-364-4 (2314)
2910, 2913, 2914	Stg. 0: Nine Castor IIs employed Stg. 3: Varied: none (2910), TE-364-3 (2913), TE-364-4 (2914)
3910, 3913, 3914	Stg. 0: Nine Castor IVs replaced Castor IIs Stg. 3: Varied: none or PAM (3910), TE-364-3 (3913), TE-364-4 (3914)
3920, 3924	Stg. 2: AJ10-118K engine replaced TR-201 Stg. 3: Varied: none or PAM (3920), TE-364-4 (3924)
4920	Stg. 0: Castor IVA replaced Castor IV Stg. 1: MB-3 replaced RS-27
5920	Stg. 1: RS-27 replaced MB-3
6925	Stg. 1: Tanks lengthened 12 feet Stg. 3: STAR 48B motor used PLF: Bulbous 114-inch diameter used
7925	Stg. 0: GEM replaced Castor IVA Stg. 1: RS-27A replaced RS-27

The entire Delta history through 1995 is depicted rather compactly in bar-graph form in Figure 38. The solid-block portion of each bar indicates the number of launches during the calendar year for which vehicle performance was entirely normal, in so far as could be determined. The clear white parts forming the tops of most bars show the number of launches that were either failures or flights where the launch vehicle experienced some sort of anomalous behavior. Every launch with an entry in the response-mode column in Table 43 falls in this category. Such behavior did not necessarily prevent the attainment of some, or even all, mission objectives.

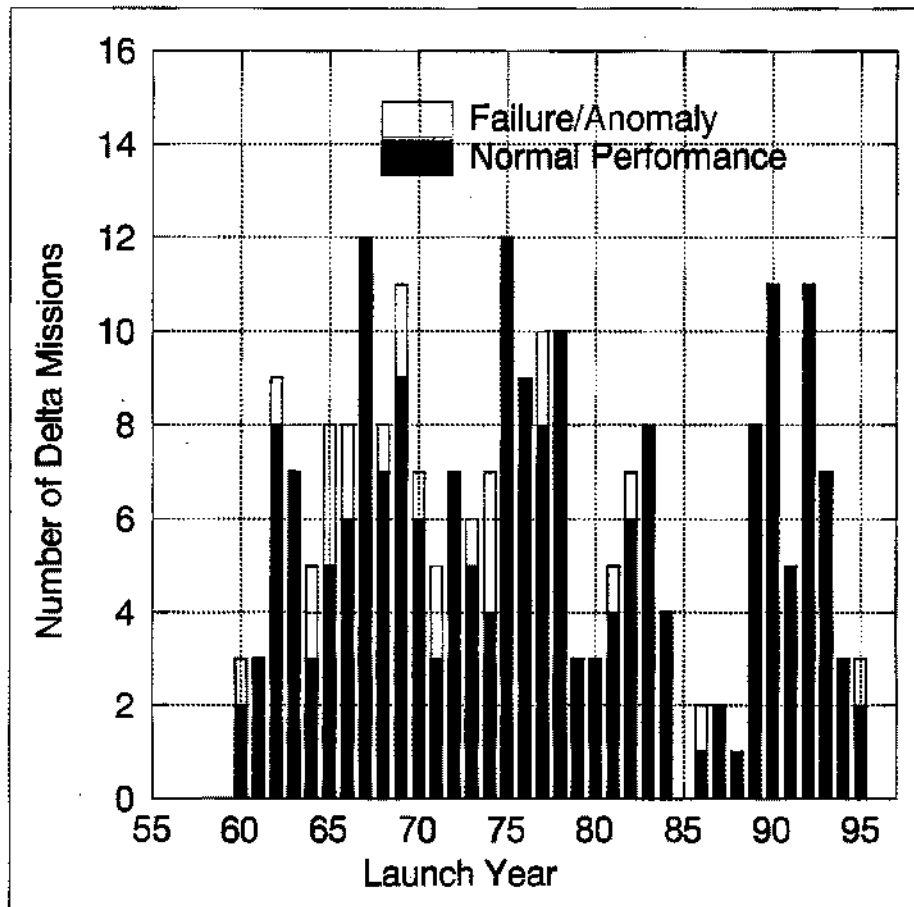


Figure 38. Delta Launch Summary

### D.3.1 Delta Launch History

The data in Table 43 summarizes all Delta and Delta-boosted space-vehicle launches since the program began. A launch sequence number is provided in the first column. A launch ID and date are provided in columns 2 and 3. The fourth column indicates the vehicle configuration. The fifth column indicates the launch range. The sixth column indicates the failure-response mode (1 through 5 and NA) that RTI has determined best describes the failure that occurred. For Mode 3 or 4 failures, a suffix of 'T' indicates the vehicle tumbled. Successful launches are indicated by a blank in the Response-Mode column. The seventh column indicates the operational flight phase during which the failure occurred. The last column indicates whether the vehicle configuration is representative of those being launched today. Launches through sequence number 232 were used in the filtering process to estimate failure rate.

Table 43. Delta Launch History

No.	Mission/ID	Launch Date	Vehicle Configuration	Test Range	Response Mode	Flight Phase	Rep. Conf.
1	ECHO I	05/13/60	DM-19	ER	4	2.5	0
2	ECHO IA	08/12/60	DM-19	ER			0
3	TIROS A2	11/23/60	DM-19	ER			0
4	P-14	03/25/61	DM-19	ER			0
5	TIROS A3	07/12/61	DM-19	ER			0
6	S-3	08/15/61	DM-19	ER			0
7	TIROS D	02/08/62	DM-19	ER			0
8	S-16	03/07/62	DM-19	ER			0
9	S-51	04/26/62	DM-19	ER			0
10	TIROS E	06/19/62	DM-19	ER	NA	5	0
11	TSX-1	07/10/62	DM-19	ER			0
12	TIROS F	09/18/62	DM-19	ER			0
13	S-3A	10/02/62	DSV-3A	ER			0
14	S-3B	10/27/62	DSV-3A	ER			0
15	RELAY A-15	12/13/62	DSV-3B	ER			0
16	SYNCOM A-25	02/13/63	DSV-3B	ER			0
17	S-6	04/02/63	DSV-3B	ER			0
18	TSX-2	05/07/63	DSV-3B	ER			0
19	TIROS G	06/19/63	DSV-3B	ER			0
20	SYNCOM A-26	07/26/63	DSV-3B	ER			0
21	IMP A	11/26/63	DSV-3C	ER			0
22	TIROS H	12/21/63	DSV-3B	ER			0
23	RELAY A-16	01/21/64	DSV-3B	ER			0
24	S-66	03/19/64	DSV-3B	ER	4	3	0
25	SYNCOM A-27	08/19/64	DSV-3D	ER			0
26	IMP-B	10/03/64	DSV-3C	ER	NA	5	0
27	S-3C	12/21/64	DSV-3C	ER			0
28	TIROS I	01/22/65	DSV-3C	ER	NA	2 & 5	0
29	OSO-B	02/03/65	DSV-3C	ER			0
30	COMSAT #1	04/06/65	DSV-3D	ER			0

No.	Mission/ID	Launch Date	Vehicle Configuration	Test Range	Response Mode	Flight Phase	Rep. Conf.
31	IMP-C	05/29/65	DSV-3C	ER			0
32	TIROS OT-1	07/01/65	DSV-3C	ER			0
33	OSO-C	08/25/65	DSV-3C	ER	4	2.5	0
34	GEOS A	11/06/65	DSV-3E	ER	NA	2 & 5	0
35	PIONEER A	12/16/65	DSV-3E	ER			0
36	TIROS OT-3	02/03/66	DSV-3C	ER			0
37	TIROS OT-2	02/28/66	DSV-3E	ER			0
38	AE-B	05/25/66	DSV-3C	ER	NA	2 & 5	0
39	AIMP-D	07/01/66	DSV-3E	ER	NA	2.5 & 5	0
40	PIONEER-B	08/17/66	DSV-3E	ER			0
41	TOS	10/02/66	DSV-3E	WR			0
42	INTELSAT II (F-1)	10/26/66	DSV-3E	ER			0
43	BIOS-A	12/14/66	DSV-3G	ER			0
44	INTELSAT II (F-2)	01/11/67	DSV-3E	ER			0
45	TOS	01/26/67	DSV-3E	WR			0
46	OSO-E1	03/08/67	DSV-3C	ER			0
47	INTELSAT II (F-3)	03/22/67	DSV-3E	ER			0
48	TOS D	04/20/67	DSV-3E	WR			0
49	IMP-F	05/24/67	DSV-3E	WR			0
50	AIMP-E	07/19/67	DSV-3E	ER			0
51	BIOS-B	09/07/67	DSV-3G	ER			0
52	INTELSAT II (F-4)	09/27/67	DSV-3E	ER			0
53	OSO-D	10/18/67	DSV-3C	ER			0
54	TOS-C	11/10/67	DSV-3E	WR			0
55	PIONEER-C	12/13/67	DSV-3E	ER			0
56	GEOS-B	01/11/68	DSV-3E	WR			0
57	RAE-A	07/04/68	DSV-3E	WR			0
58	TOS-E	08/16/68	DSV-3L	WR			0
59	INTELSAT III-A	09/18/68	DSV-3L	ER	5	1	0
60	PIONEER-D	11/08/68	DSV-3E	ER			0
61	HEOS-A	12/05/68	DSV-3E	ER			0
62	TOS-F	12/15/68	DSV-3L	WR			0
63	INTELSAT III-C	12/18/68	DSV-3L	ER			0
64	OSO-F	01/22/69	DSV-3C	ER			0
65	ISIS-A	01/30/69	DSV-3E	WR			0
66	INTELSAT III-B	02/05/69	DSV-3L	ER			0
67	TOS-G	02/26/69	DSV-3E	ER			0
68	INTELSAT III-D	05/21/69	DSV-3L	ER			0
69	IMP-G	06/21/69	DSV-3E	WR			0
70	BIOS-D	06/29/69	DSV-3L	ER			0
71	INTELSAT III-E	07/26/69	DSV-3L	ER	5	3 & 5	0
72	OSO-G	08/09/69	DSV-3L	ER			0
73	PIONEER-E	08/27/69	DSV-3L	ER	5	1	0
74	IDCSP/A-A	11/22/69	DSV-3L	ER			0
75	INTELSAT III-F	01/14/70	DSV-3L	ER			0
76	TIROS-M	01/23/70	DSV-3L	WR			0

No.	Mission/ID	Launch Date	Vehicle Configuration	Test Range	Response Mode	Flight Phase	Rep. Conf.
77	NATO-A	03/20/70	DSV-3L	ER			0
78	INTELSAT III-G	04/22/70	DSV-3L	ER	NA	1 & 5	0
79	INTELSAT III-H	07/23/70	DSV-3L	ER			0
80	IDCSP/A-B	08/19/70	DSV-3L	ER			0
81	ITOS-A	12/11/70	DSV-3L	WR			0
82	NATO-B	02/03/71	DSV-3L	ER			0
83	IMP-I	03/13/71	DSV-3L	ER			0
84	ISIS-B	04/01/71	DSV-3E	WR			0
85	OSO-H	09/29/71	DSV-3L	ER	NA	2 & 5	0
86	ITOS-B	10/21/71	DSV-3L	WR	4	2	0
87	HEOS-A2	01/31/72	DSV-3L	WR			0
88	TD-1	03/11/72	DSV-3L	WR			0
89	ERTS-A	07/23/72	900	WR			0
90	IMP-H	09/22/72	1604	ER			0
91	ITOS-D	10/15/72	300	WR			0
92	TELESAT-A	11/10/72	1914	ER			0
93	NIMBUS-E	12/10/72	900	WR			0
94	TELESAT-B	04/20/73	1914	ER			0
95	RAE-B	06/10/73	1913	ER			0
96	ITOS-E	07/16/73	300	WR	4T	2	0
97	IMP-J	10/26/73	1604	ER			0
98	ITOS-F	11/06/73	300	WR			0
99	AE-C	12/16/73	1900	WR			0
100	SKYNET IIA	01/19/74	2313	ER	NA	4 & 5	0
101	WESTAR-A	04/13/74	2914	ER	NA	1	1
102	SMS-A	05/17/74	2914	ER	NA	1 & 5	1
103	WESTAR-B	10/10/74	2914	ER			1
104	ITOS-G	11/15/74	2310	WR			0
105	SKYNET-IIB	11/22/74	2313	ER			0
106	SYMPHONIE-A	12/18/74	2914	ER			1
107	ERTS-B	01/22/75	2910	WR			1
108	SMS-B	02/06/75	2914	ER			1
109	GEOS-C	04/09/75	1410	WR			0
110	TELESAT-C	05/07/75	2914	ER			1
111	NIMBUS-F	06/12/75	2910	WR			1
112	OSO-I	06/21/75	1910	ER			0
113	COS-B	08/08/75	2913	WR			1
114	SYMPHONIE-B	08/26/75	2914	ER			1
115	AE-D	10/06/75	2910	WR			1
116	GOES-A	10/16/75	2914	ER			1
117	AE-E	11/19/75	2910	ER			1
118	RCA-SATCOM-A	12/12/75	3914	ER			1
119	CTS	01/17/76	2914	ER			1
120	MARISAT-A	02/19/76	2914	ER			1
121	RCA-SATCOM-B	03/26/76	3914	ER			1
122	NATO-III A	04/22/76	2914	ER			1

No.	Mission/ID	Launch Date	Vehicle Configuration	Test Range	Response Mode	Flight Phase	Rep. Conf.
123	LAGEOS	05/04/76	2913	WR			1
124	MARISAT-B	06/10/76	2914	ER			1
125	PALAPA-A	07/08/76	2914	ER			1
126	ITOS-E2	07/29/76	2310	WR			0
127	MARISAT-C	10/14/76	2914	ER			1
128	NATO IIIB	01/27/77	2914	ER			1
129	PALAPA-B	09/10/77	2914	ER			1
130	ESRO-GEOS	04/20/77	2914	ER	NA	2.5 & 5	1
131	GOES-B	06/16/77	2914	ER			1
132	GMS	07/14/77	2914	ER			1
133	SIRIO	08/25/77	2313	ER			0
134	OTS	09/13/77	3914	ER	4	1	1
135	ISEE A/B	10/22/77	2914	ER			1
136	METEOSAT-F1	11/22/77	2914	ER			1
137	CS	12/14/77	2914	ER			1
138	IUE	01/26/78	2914	ER			1
139	L&SAT-C	03/05/78	2910	WR			1
140	BSE	04/07/78	2914	ER			1
141	OTS-2	05/11/78	3914	ER			1
142	GOES-C	06/19/78	2914	ER			1
143	ESRO-GEOS2	07/14/78	2914	ER			1
144	ISEE-C	08/12/78	2914	ER			1
145	NIMBUS-G	10/24/78	2910	WR			1
146	NATO IIIC	11/19/78	2914	ER			1
147	TELESAT-D	12/16/78	3914	ER			1
148	SCATHA	01/30/79	2914	ER			1
149	WESTAR-C	08/09/79	2914	ER			1
150	RCA-C	12/07/79	3914	ER			1
151	SMM	02/14/80	3910	ER			1
152	GOES-D	09/09/80	3914	ER			1
153	SBS-A	11/15/80	3910 PAM	ER			1
154	GOES-E	05/22/81	3914	ER			1
155	DE	08/03/81	3913	WR	NA	2 & 5	1
156	SBS-B	09/24/81	3910 PAM	ER			1
157	SME	10/06/81	2310	WR			0
158	RCA-D	11/20/81	3910 PAM	ER			1
159	RCA-C'	01/15/82	3910 PAM	ER			1
160	WESTAR-IV	02/26/82	3910 PAM	ER			1
161	INSAT-IA	04/10/82	3910 PAM	ER			1
162	WESTAR-V	06/09/82	3910 PAM	ER	NA	1	1
163	L&SAT-D	07/16/82	3920	WR			1
164	TELESAT-F	08/26/82	3920 PAM	ER			1
165	RCA-E	10/27/82	3924	ER			1
166	IRAS	01/26/83	3910	WR			1
167	RCA-F	04/11/83	3924	ER			1
168	GOES-F	04/28/83	3914	ER			1

No.	Mission/ID	Launch Date	Vehicle Configuration	Test Range	Response Mode	Flight Phase	Rep. Conf.
169	EXOSAT	05/26/83	3914	WR			1
170	GALAXY-A	06/28/83	3920 PAM	ER			1
171	TELSTAR-3A	07/28/83	3920 PAM	ER			1
172	RCA-G	09/08/83	3924	ER			1
173	GALAXY-B	09/22/83	3920 PAM	ER			1
174	L&SAT-D'	03/01/84	3920	WR			1
175	AMPTE	08/16/84	3924	ER			1
176	GALAXY-C	09/21/84	3920 PAM	ER			1
177	NATO-IIID	11/14/84	3914	ER			1
178	GOES-G	05/03/86	3914	ER	4	1	1
179	DELTA 180	09/05/86	3920	ER			1
180	GOES-H	02/26/87	3924	ER			1
181	PALAPA B2-P	03/20/87	3920 PAM	ER			1
182	DELTA 181	02/08/88	3910	ER			1
183	NAVSTAR II-1	02/14/89	6925	ER			1
184	DELTA STAR	03/24/89	3920	ER			1
185	NAVSTAR II-2	06/10/89	6925	ER			1
186	NAVSTAR II-3	08/18/89	6925	ER			1
187	BSB-R1	08/27/89	4925	ER			1
188	NAVSTAR II-4	10/21/89	6925	ER			1
189	OOBE	11/18/89	5920	WR			1
190	NAVSTAR II-5	12/11/89	6925	ER			1
191	NAVSTAR II-6	01/24/90	6925	ER			1
192	LOSAT	02/14/90	6920-8	ER			1
193	NAVSTAR II-7	03/26/90	6925	ER			1
194	PALAPA B-2R	04/13/90	6925	ER			1
195	ROSAT	06/01/90	6920-10	ER			1
196	INSAT-1D	06/11/90	4925	ER			1
197	NAVSTAR II-8	08/02/90	6925	ER			1
198	BSB-R2	08/18/90	6925	ER			1
199	NAVSTAR II-9	10/01/90	6925	ER			1
200	INMARSAT-2F1	10/30/90	6925	ER			1
201	NAVSTAR II-10	11/26/90	7925	ER			1
202	NATO IVA	01/07/91	7925	ER			1
203	INMARSAT-2F2	03/08/91	6925	ER			1
204	ASC-2	04/12/91	7925	ER			1
205	AURORA II	05/29/91	7925	ER			1
206	NAVSTAR II-11	07/03/91	7925	ER			1
207	NAVSTAR II-12	02/23/92	7925	ER			1
208	NAVSTAR II-13	04/09/92	7925	ER			1
209	PALAPA B4	05/13/92	7925-8	ER			1
210	EUVE	06/07/92	6920-10	ER			1
211	NAVSTAR II-14	07/07/92	7925	ER			1
212	GEOTAIL	07/24/92	6925	ER			1
213	SATCOM C4	08/31/92	7925	ER			1
214	NAVSTAR II-15	09/09/92	7925	ER			1

No.	Mission/ID	Launch Date	Vehicle Configuration	Test Range	Response Mode	Flight Phase	Rep. Conf.
215	COPERNIKUS	10/12/92	7925	ER			1
216	NAVSTAR II-16	11/22/92	7925	ER			1
217	NAVSTAR II-17	12/18/92	7925	ER			1
218	NAVSTAR II-18	02/03/93	7925	ER			1
219	NAVSTAR II-19	03/30/93	7925	ER			1
220	NAVSTAR II-20	05/13/93	7925	ER			1
221	NAVSTAR II-21	06/26/93	7925	ER			1
222	NAVSTAR II-22	08/30/93	7925	ER			1
223	NAVSTAR II-23	10/26/93	7925	ER			1
224	NATO IVB	12/08/93	7925	ER			1
225	GALAXY I-R	02/19/94	7925-8	ER			1
226	NAVSTAR II-24	03/10/94	7925	ER			1
227	WIND	11/01/94	7925-10	ER			1
228	KOREASAT	08/05/95	7925	ER	NA	1 & 5	1
229	RADAR SAT	11/04/95	7920-10	ER			1
230	X-RAY EXPLORER	12/30/95	7920A-10	ER			1
231	KOREASAT-2	01/14/96	7925	ER			1
232	NEAR	02/17/96	7925-8	ER			1
233	POLAR	02/24/96	7925-10	WR			1
234	GPS-7	03/27/96	7925-8	ER			1
235	MSX	04/24/96	7920-10	WR			1
236	GALAXY 1X	05/24/96	7925A	ER			1
237	GPS-26	07/16/96	7925-9.5	ER			1

### D.3.2 Delta Failure Narratives

The following narratives provide available details about each Delta failure since the beginning of the Delta program. The narratives are numbered to match the flight-sequence numbers in Section D.3.1.

1. Echo I, 13 May 60, Response Mode 4, Flight Phase 2.5: Attitude control lost during second stage coast period. Third stage spun up, but did not fire.
10. Tiros E, 19 June 62, Response Mode NA, Flight Phase 5: The flight was considered a success, although failure of the BTL guidance system resulted in a propellant-depletion shutdown of the second stage. The apogee of the final orbit was 175 miles above the planned value and well outside the three-sigma limit of 76 miles.
24. S-66, 19 Mar 64, Response Mode 4, Flight Phase 3: Spacecraft did not attain orbit. Third-stage burn of X-248 motor was interrupted after 23 seconds of a planned 42-second burn period.
26. Imp B, 3 Oct 64, Response Mode NA, Flight Phase 5: The flight was considered a partial success, although it failed to reach the desired orbital altitude. The apogee was some 52,590 miles below the planned value of 110,000 miles, but perigee was within 3 miles of the desired value of 105 miles.
28. Tiros I, 22 Jan 65, Response Mode NA, Flight Phase 2 and 5: Loss of WECO guidance during second-stage burn caused second stage to burn to oxygen depletion. As a result, spacecraft was inserted into an elliptical rather than a circular orbit.
33. OSO-C, 25 Aug 65, Response Mode 4, Flight Phase 2.5: Third stage ignited after spin up but before separation from second-stage spin table. Payload did not orbit.
34. GEOS A, 6 Nov 65, Response Mode NA, Flight Phase 2 and 5: The flight was considered a success, although failure of the BTL guidance system during second-stage powered flight led to a propellant-depletion shutdown of the stage. Actual apogee was 436 miles too high, and well outside the three-sigma limit.
38. AE-B, 25 May 66, Response Mode NA, Flight Phase 2 and 5: Due to WECO guidance failure (ground system locked on side lobe), second stage burned to propellant depletion, some 12 seconds longer than expected. As a result, the orbital apogee was 800 miles higher than planned.
39. AIMP-D, 1 July 66, Response Mode NA, Flight Phase 2.5 and 5: Although an alternate mission was accomplished, primary objectives could not be achieved because excess velocity imparted to the spacecraft prevented insertion of the

spacecraft into a lunar orbit. Possible cause was malfunction of the coast-control system after third-stage spinup and separation.

59. Intelsat III A, 18 Sep 68, Response Mode 5, Flight Phase 1: Due to loss of rate gyro, undamped pitch oscillations began at 20 seconds. Vehicle began a series of violent maneuvers at 59 seconds. During the 13-second period while these maneuvers continued, the vehicle pitched down some 270°, then up 210°, and then made a large yaw to the left. At 72 seconds the vehicle regained control and flew stably in a down and leftward direction until 100 seconds. At this time, with the main engine against the pitch and yaw stops, the destabilizing aerodynamic forces became so large that quasi-control could no longer be maintained. The first stage broke up at 103 seconds. The second stage was destroyed by the RSO at 110.6 seconds. Major pieces impacted about 12 miles downrange and 2 miles left of the flight line.
71. Intelsat III E, 26 July 69, Response Mode NA, Flight Phase 3 and 5: Unknown but anomalous third-stage performance inserted payload into an erroneous orbit. Apogee was some 17,000 miles too low and orbital inclination was 1.5° above planned 28.8°
73. Pioneer E, 27 Aug 69, Response Mode 5, Flight Phase 1: First-stage hydraulics system failed a few seconds before burnout (MECO). The vehicle pitched down, yawed left, rolled counterclockwise driving all gyros off limits, and then tumbled. Second-stage separation and ignition occurred while the vehicle was out of control. After about 20 seconds, the second stage regained control in a yaw-right, pitch-up attitude. The vehicle flew stably in this attitude for about 240 seconds until destroyed by the safety officer at T+484 seconds.
78. Intelsat III G, 22 Apr 70, Response Mode NA, Flight Phase 1 and 5: The flight was considered a success, although low first-stage velocity resulted in a propellant-depletion shutdown of the second stage. As a result, the actual apogee was some 2,220 miles below the planned value of 195,400 miles, and well outside three-sigma limits.
85. OSO-H, 29 Sep 71, Response Mode NA, Flight Phase 2 and 5: Stage-2 hydraulic-system failure caused faulty control during second-stage burn. Spacecraft injected initially into an elliptical orbit, but was later maneuvered into a more satisfactory orbit although perigee was still about 93 miles below the planned value.
86. ITOS-B (WTR), 21 Oct 71, Response Mode 4, Flight Phase 2: Contamination in the oxygen vent valve apparently prevented its proper operation throughout flight. This led to bulkhead rupture during second-stage burn and loss of vehicle control.

96. ITOS-E (WTR), 16 July 73, Response Mode 4T, Flight Phase 2: Pump-motor failure during second-stage burn at 490 seconds resulted in loss of hydraulic pressure, loss of attitude control, and vehicle tumbling.
100. Skynet IIA, 19 Jan 74, Response Mode NA, Flight Phase 4 and 5: Flight was within normal limits until impact point passed through Africa gate. During the second burn of the second stage, a short circuit in the second-stage electronics package resulted in an improper spacecraft orbit. The satellite reentered the earth's atmosphere five days later on 24 Jan 74.
101. WESTAR-B, 13 Apr 74, Response Mode NA, Flight Phase 1: One solid-rocket motor carried to MECO, but mission was still a complete success.
102. SMS-A, 17 May 74, Response Mode NA, Flight Phase 1 and 5: Mission was a partial success, although low first-stage velocity resulted from a liquid oxygen pressure line failure, and a booster shroud that snagged before fully jettisoning. Apogee was some 1,767 miles below the planned value, and well outside three-sigma limits.
130. ESRO-GOES, 20 Apr 77, Response Mode NA, Flight Phase 2.5 and 5: Due possibly to a short circuit in the second stage or failure in one of the two explosive bolts that hold the stage 2/3 clamp band together, the third stage separated prematurely from the second stage while spinning at only two rpms instead of the normal 97 rpms. As a result, coning during third-stage burn resulted in a spacecraft apogee nearly 13,000 miles low, and far outside three-sigma limits.
134. OTS, 13 Sep 77, Response Mode 4, Flight Phase 1: Core vehicle exploded at 57 seconds due to a burn through on the forward end of the #1 Castor IV motor.
155. DE, 3 Aug 81, Response Mode NA, Flight Phase 2 and 5: Flight was considered a success, although a 260-pound deficiency in fuel loading led to a premature propellant-depletion shutdown of the second burn of the second stage and degradation of final orbit. The inertial velocity at SECO was 240 ft/sec lower than planned. Final apogee was some 855 miles too low and well outside three-sigma limits.
162. WESTAR-V, 9 June 82, Response Mode NA, Flight Phase 1: Booster performance was low but mission was a success. Apogee and perigee were within three-sigma limits.
178. GOES-G, 3 May 86, Response Mode 4, Flight Phase 1: An electrical short in a control circuit in first-stage relay box caused premature main-engine shutdown at 71 seconds. Vehicle then tumbled and was broken up by aerodynamic forces. RSO sent destruct at approximately 91 seconds.

228. Koreasat, 5 Aug 95, Response Mode NA, Flight Phase 1 and 5: One of three air-ignited strap-on GEMs did not separate because of a malfunction in the separation explosive transfer system. Failure to drop a GEM motor resulted in depletion of second-stage propellants. Although perigee was close to nominal, the apogee was 3,450 nm below the planned value and far outside the 3-sigma limits.

#### **D.4 Titan Launch and Performance History**

The Titan family of launch vehicles was established in 1955, when the Air Force awarded the Martin Company a contract to build a heavy-duty space system. Titan I was the nation's first two-stage ICBM and the first to be silo-based. It proved many structural and propulsion techniques that were later incorporated into Titan II. The Titan II was a heavy-duty missile using storable propellants that became a man-rated space booster for NASA's Gemini program. Today the Titan II is returning as a space-launch vehicle with the old ICBMs converted to deliver payloads to orbit. Titan III was the outgrowth of propulsion technology developed in both Titan II and Minuteman ballistic-missile programs.

Today's Titan vehicles (II, III, and IV) are derived from the earlier Titans. In 1984, the DOD called for a space-launch system that would complement the Space Shuttle to ensure access to space for certain national-security payloads. The Titan IV program began as a short-term program for ten launches from Cape Canaveral Air Station. However, after the Challenger accident in 1986, the program has grown to 41 vehicles. With the off-loading of DOD payloads from Shuttle, Titan IV has become DOD's main access to space for many of its heavy payloads. Design of the Titan II Space Launch Vehicle (SLV) began at the same time as that for Titan IV. Titan II SLV was developed from refurbished Titan II ICBMs incorporating technology and hardware from the Titan III program.

Shortly after the Challenger accident in 1986, when the US government decided to offload commercial payloads from the Space Shuttle, Martin Marietta announced plans to develop a Titan III commercial launch vehicle with its own funds. The commercial Titan III is derived from the Titan 34D with a stretched second stage and a bulbous shroud for dual or dedicated payloads. The first commercial Titan III was launched with two communications satellites in December 1989. Table 44 shows a summary of Titan space-vehicle configurations since Gemini.<sup>[10]</sup>

Table 44. Summary of Titan Vehicle Configurations

Configuration	Description
II Gemini	Titan II ICBM converted to a man-rated vehicle
IIIA	Same as Titan II Gemini except stretched stages 1 and 2, and an integral Transtage upper stage
IIIB	Same as IIIA except Agena upper stage instead of Transtage
34B	Same as IIIA except stretched stage 1
IIIC	Same as IIIA with added 5-segment SRMs
IIID	Same as IIIC except no upper stage
IIIE	Same as IIID except Centaur upper stage and 14-foot diameter PLF
34D	Same as 34B with added 5½-segment SRMs. Uses either Transtage or IUS upper stage
II SLV	Refurbished II ICBM with 10-foot diameter PLF
III Commercial	Same as 34D except stretched stage 2, single or dual carrier, enhanced liquid-rocket engines, and 13.1-foot diameter PLF. Can use PAM-D2, Transtage, or TOS upper stage
IV	Same as 34D except stretched stages 1 and 2, 7-segment SRM or 3-segment SRMU, and 16.7-foot diameter PLF. Can use IUS or Centaur upper stage

The entire Titan history through 1995 is depicted rather compactly in bar-graph form in Figure 39. The solid-block portion of each bar indicates the number of launches during the calendar year for which vehicle performance was entirely normal, in so far as could be determined. The clear white parts forming the tops of most bars show the number of launches that were either failures or flights where the launch vehicle experienced some sort of anomalous behavior. Every launch with an entry in the response mode column in Table 45 falls in this category. Such behavior did not necessarily prevent the attainment of some, or even all, mission objectives.

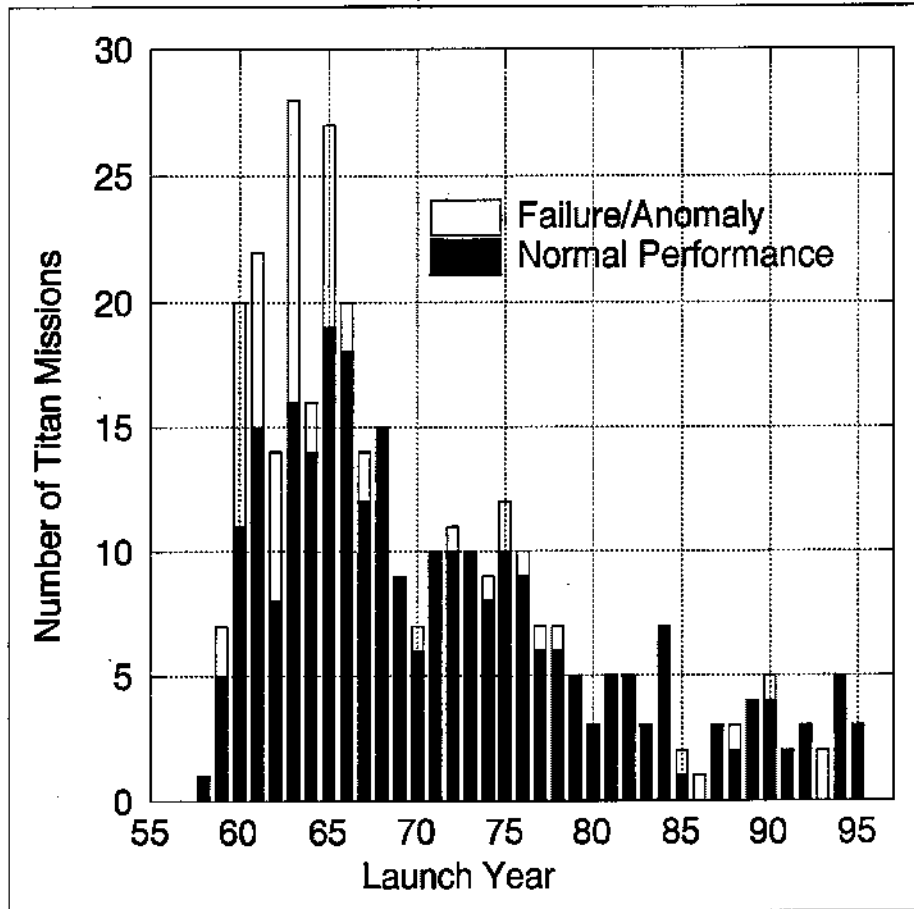


Figure 39. Titan Launch Summary

### D.4.1 Titan Launch History

The data in Table 45 summarizes all Titan and Titan-boosted space-vehicle launches since the program began. A launch sequence number is provided in the first column. A launch ID and date are provided in columns 2 and 3. The fourth column indicates the vehicle configuration. The fifth column indicates the launch range. The sixth column indicates the failure-response mode (1 through 5 and NA) that RTI has determined best describes the failure that occurred. For Mode 3 or 4 failures, a suffix of 'T' indicates the vehicle tumbled. Successful launches are indicated by a blank in the Response-Mode column. The seventh column indicates the operational flight phase during which the failure occurred. The last column indicates whether the vehicle configuration is representative of those being launched today. Launches through sequence number 337 were used in the filtering process to estimate failure rate.

Table 45. Titan Launch History

No.	Mission/ID	Launch Date	Vehicle Configuration	Test Range	Response Mode	Flight Phase	Rep. Conf.
1	Weapons System (WS)	12/20/58	I (A-1)	ER			0
2	WS	02/03/59	I (A-2)	ER			0
3	WS	02/06/59	I (A-3)	ER			0
4	WS	02/25/59	I (A-5)	ER			0
5	WS	04/03/59	I (A-4)	ER			0
6	WS	05/04/59	I (A-6)	ER			0
7	WS	08/14/59	I (B-5)	ER	1	1	0
8	WS	12/12/59	I (C-3)	ER	1	1	0
9	WS	02/02/60	I (B-7A)	ER			0
10	WS	02/05/60	I (C-4)	ER	4T	1	0
11	WS	02/24/60	I (G-4)	ER			0
12	WS	03/08/60	I (C-1)	ER	4	2	0
13	WS	03/22/60	I (G-5)	ER	4	2.5	0
14	WS	04/08/60	I (C-5)	ER	4	2	0
15	WS	04/21/60	I (G-6)	ER			0
16	WS	04/28/60	I (C-6)	ER			0
17	WS	05/13/60	I (G-7)	ER			0
18	WS	05/27/60	I (G-9)	ER			0
19	WS	06/24/60	I (G-10)	ER			0
20	WS	07/01/60	I (J-2)	ER	2	1	0
21	WS	07/28/60	I (J-4)	ER	4	1	0
22	WS	08/10/60	I (J-7)	ER	4	2	0
23	WS	08/30/60	I (J-5)	ER			0
24	WS	09/28/60	I (J-8)	ER			0
25	WS	09/29/60	I (G-8)	ER	4	1	0
26	WS	10/07/60	I (J-3)	ER			0
27	WS	10/24/60	I (J-6)	ER			0
28	WS	12/20/60	I (J-9)	ER	4	2	0
29	WS	01/20/61	I (J-10)	ER	4	2	0
30	WS	02/10/61	I (J-11)	ER			0

No.	Mission/ID	Launch Date	Vehicle Configuration	Test Range	Response Mode	Flight Phase	Rep. Conf.
31	WS	02/20/61	I (J-13)	ER			0
32	WS	03/03/61	I (J-12)	ER	4	2	0
33	WS	03/28/61	I (J-14)	ER			0
34	WS	03/31/61	I (J-15)	ER	4	1	0
35	SILVER SADDLE	05/03/61	I	WR			0
36	WS	05/23/61	I (J-16)	ER			0
37	WS	06/24/61	I (M-1)	ER	4T	2	0
38	WS	07/20/61	I (J-18)	ER			0
39	WS	07/25/61	I (M-2)	ER			0
40	WS	08/03/61	I (J-19)	ER			0
41	WS	09/06/61	I (J-17)	ER			0
42	WS	09/07/61	I (M-3)	ER	5	2	0
43	BIG SAM	09/23/61	I (SM-2)	WR			0
44	WS	09/28/61	I (J-20)	ER			0
45	WS	10/06/61	I (M-4)	ER	5	2	0
46	WS	10/24/61	I (J-21)	ER			0
47	WS	11/21/61	I (J-22)	ER			0
48	WS	11/29/61	I (M-5)	ER			0
49	WS	12/13/61	I (J-23)	ER			0
50	WS	12/15/61	I (M-6)	ER	4	2	0
51	DOUBLE MARTINI	01/20/62	I (SM-4)	WR	4	2	0
52	WS	01/29/62	I (M-7)	ER			0
53	BLUE GANDER	02/23/62	I (SM-18)	WR	4	2	0
54	WS (first Titan II)	03/16/62	II (N-2)	ER			0
55	SILVER TOP	05/04/62	I (SM-34)	WR			0
56	WS	06/07/62	II (N-1)	ER	4	2	0
57	WS	07/11/62	II (N-6)	ER			0
58	WS	07/25/62	II (N-4)	ER	4	2	0
59	WS	09/12/62	II (N-5)	ER			0
60	TIGHT BRACELET	10/06/62	I (SM-35)	WR			0
61	WS	10/12/62	II (N-9)	ER			0
62	WS	10/26/62	II (N-12)	ER			0
63	YELLOW JACKET	12/05/62	I (SM-11)	WR	4T	2	0
64	WS	12/06/62	II (N-11)	ER	4	1	0
65	WS	12/19/62	II (N-13)	ER			0
66	WS	01/10/63	II (N-15)	ER	4	2	0
67	TEN MEN	01/29/63	I (SM-8)	WR			0
68	WS	02/06/63	II (N-16)	ER	4	2	0
69	AWFUL TIRED	02/16/63	II	WR	4T	1	0
70	WS	03/21/63	II (N-18)	ER	4T	2.5	0
71	YOUNG BLOOD	03/30/63	I (SM-3)	WR			0
72	HALF MOON	04/04/63	I	WR			0
73	RAMP ROOSTER	04/13/63	I (SM-1)	WR			0
74	WS	04/19/63	II (N-21)	ER	4	2	0
75	DINNER PARTY	04/27/63	II	WR			0
76	MARES TAIL	05/01/63	I	WR	2	1	0

No.	Mission/ID	Launch Date	Vehicle Configuration	Test Range	Response Mode	Flight Phase	Rep. Conf.
77	WS	05/09/63	II (N-14)	ER	4	2	0
78	FLYING FROG	05/13/63	II (N-19)	WR			0
79	WS	05/24/63	II (N-17)	ER			0
80	WS	05/29/63	II (N-20)	ER	4	1	0
81	THREAD NEEDLE	06/20/63	II (N-22)	WR	5	2	0
82	SILVER SPUR	07/16/63	I (SM-24)	WR	4	2	0
83	HIGH RIVER	08/15/63	I (SM-7)	WR			0
84	WS	08/21/63	II (N-24)	ER			0
85	POLAR ROUTE	08/30/63	I (SM-56)	WR	4	2.5	0
86	DAILY MAIL	09/17/63	I (SM-83)	WR			0
87	TAR TOP	09/23/63	II (N-23)	WR			0
88	WS	11/01/63	II (N-25)	ER			0
89	FIRE TRUCK	11/09/63	II (N-27)	WR	4T	1	0
90	FACT RIDE	11/14/63	I (SM-68)	WR			0
91	WS	12/12/63	II (N-29)	ER			0
92	USEFUL TASK	12/16/63	II (N-28)	WR			0
93	WS	01/15/64	II (N-31)	ER			0
94	RED SAILS	01/23/64	II (N-26)	WR			0
95	SAFE CONDUCT	02/17/64	II	WR			0
96	WS	02/26/64	II (N-32)	ER			0
97	APPLE PIE	03/13/64	II (N-30)	WR			0
98	WS	03/23/64	II (N-33)	ER			0
99	SV: GEMINI GT-1	04/08/64	II (G-1)	ER			0
100	WS	04/09/64	II (N-34)	ER			0
101	COBRA SKIN	07/30/64	II (B-28)	WR			0
102	DOUBLE TALLEY	08/11/64	II (B-9)	WR			0
103	GENTLE ANNIE	08/13/64	II (B-7)	WR			0
104	SV (first Titan III)	09/01/64	IIIA (65-210)/Trans.	ER	4	4	0
105	BLACK WIDOW	10/02/64	II (B-1)	WR			0
106	HIGH RIDER	11/04/64	II (B-32)	WR			0
107	WEST WIND I	12/08/64	I (SM-85)	WR	5	1	0
108	SV	12/10/64	IIIA (65-209)/Trans.	ER			0
109	WEST WIND III	01/14/65	I (SM-33)	WR	4	2	0
110	SV: GEMINI GT-2	01/19/65	II (G-2)	ER			0
111	SV: LES-1	02/11/65	IIIA (65-211)/Trans.	ER			0
112	WEST WIND II	03/05/65	I (SM-80)	WR	4	2	0
113	SV: GEMINI GT-3	03/23/65	II (G-3)	ER			0
114	ARTIC SUN	03/24/65	II (B-60)	WR			0
115	BEAR HUG	04/16/65	II (B-45)	WR			0
116	CARD DECK	04/30/65	II (B-54)	WR	4	1	0
117	SV: LES-2	05/06/65	IIIA (65-214)/Trans.	ER			0
118	FRONT SIGHT	05/21/65	II (B-51)	WR			0
119	SV: GEMINI GT-4	06/03/65	II (G-4)	ER			0
120	GOLD FISH	06/14/65	II (B-22)	WR	4	2.5	0
121	SV: DUMMY PAYLOAD	06/18/65	IIIC (65-215)/Trans.	ER			1
122	BUSY BEE	06/30/65	II (B-30)	WR			0

No.	Mission/ID	Launch Date	Vehicle Configuration	Test Range	Response Mode	Flight Phase	Rep. Conf.
123	LONG BALL	07/21/65	II (B-62)	WR			0
124	MAGIC LAMP	08/16/65	II (B-8)	WR			0
125	SV: GEMINI GT-5	08/21/65	II (G-5)	ER			0
126	NEW ROLE	08/25/65	II (B-19)	WR			0
127	BOLD GUY	09/21/65	II (B-58)	WR	4	2	0
128	SV: OV-2, LCS-5	10/15/65	IIIC (65-212)/Trans.	ER	NA	4 & 5	1
129	POWER BOX	10/20/65	II (B-33)	WR			0
130	RED WAGON	11/27/65	II (B-20)	WR			0
131	CROSS FIRE	11/30/65	II (B-4)	WR	5	2	0
132	SV: GEMINI GT-7	12/04/65	II (G-7)	ER			0
133	SV: GEMINI GT-6A	12/15/65	II (G-6)	ER			0
134	SV: LES-3,4, OSCAR 4	12/21/65	IIIC (66-001)/Trans.	ER	NA	5	1
135	SEA ROVER	12/22/65	II (B-73)	WR	4T	2	0
136	WINTER ICE	02/03/66	II (B-87)	WR			0
137	BLACK HAWK	02/17/66	II (B-61)	WR			0
138	SV: GEMINI GT-8	03/16/66	II (G-8)	ER			0
139	CLOSE TOUCH	03/25/66	II (B-16)	WR			0
140	GOLD RING	04/05/66	II (B-50)	WR			0
141	LONG LIGHT	04/20/66	II (B-55)	WR			0
142	SILVER BULLET	05/24/66	II (B-91)	WR	4	2.5	0
143	SV: GEMINI GT-9A	06/03/66	II (G-9)	ER			0
144	SV: IDCSP	06/16/66	IIIC (66-004)/Trans.	ER			1
145	SV: GEMINI GT-10	07/18/66	II (G-10)	ER			0
146	GIANT TRAIN	07/22/66	II (B-95)	WR			0
147	DAILY MAIL	07/29/66	IIIB/AGENA D (23B)	WR			1
148	SV-IDCSP	08/26/66	IIIC (66-005)/Trans.	ER	4T	0	1
149	SV: GEMINI GT-11	09/12/66	II (G-11)	ER			0
150	BLACK RIVER	09/16/66	II (B-40)	WR			0
151	BUSY SCHEME	09/28/66	IIIB/AGENA D (23B)	WR			1
152	SV-OAR/OV	11/03/66	IIIC (66-002)/Trans.	ER			1
153	SV: GEMINI GT-12	11/11/66	II (G-12)	ER			0
154	BUBBLE GIRL	11/24/66	II (B-68)	WR			0
155	BUSY SKYROCKET	12/14/66	IIIB/AGENA D (23B)	WR			1
156	SV-IDCSP/LES/DATS	01/18/67	IIIC (66-006)/Trans.	ER			1
157	BUSY PALEFACE	02/24/67	IIIB/AGENA D (23B)	WR			1
158	GIFT HORSE	03/17/67	II (B-76)	WR			0
159	GLAMOUR GIRL	04/12/67	II (B-81)	WR	4T	2	0
160	BUSY TAILOR	04/26/67	IIIB/AGENA D (23B)	WR	4	2	1
161	SV-VELA/RSCH	04/28/67	IIIC (66-003)/Trans.	ER			1
162	BUSY PLAYMATE	06/20/67	IIIB/AGENA D (23B)	WR			1
163	BUGGY WHEEL	06/23/67	II (B-70)	WR			0
164	SV-IDCSP	07/01/67	IIIC (66-007)/Trans.	ER			1
165	AFSC	08/16/67	IIIB/AGENA D (23B)	WR			1
166	GLOWING BRIGHT	09/11/67	II (B-21)	WR			0
167	AFSC	09/19/67	IIIB/AGENA D (23B)	WR			1
168	AFSC	10/25/67	IIIB/AGENA D (23B)	WR			1

No.	Mission/ID	Launch Date	Vehicle Configuration	Test Range	Response Mode	Flight Phase	Rep. Conf.
169	AFSC	12/05/67	IIIB/AGENA D (23B)	WR			1
170	AFSC	01/18/68	IIIB/AGENA D (23B)	WR			1
171	GLORY TRIP 4T	02/28/68	II (B-88)	WR			0
172	AFSC	03/13/68	IIIB/AGENA D (23B)	WR			1
173	GLORY TRIP 10T	04/02/68	II (B-36)	WR			0
174	AFSC	04/17/68	IIIB/AGENA D (23B)	WR			1
175	AFSC	06/05/68	IIIB/AGENA D (23B)	WR			1
176	GLORY TRIP 8T	06/12/68	II (B-82)	WR			0
177	SV-IDCSP	06/13/68	IIIC (86-009)/Trans.	ER			1
178	AFSC	08/06/68	IIIB/AGENA D (23B)	WR			1
179	GLORY TRIP 18T	08/21/68	II (B-53)	WR			0
180	AFSC	09/10/68	IIIB/AGENA D (23B)	WR			1
181	SV-LES/OV	09/26/68	IIIC (65-213)/Trans.	ER			1
182	AFSC	11/06/68	IIIB/AGENA D (23B)	WR			1
183	GLORY TRIP 26T	11/19/68	II (B-3)	WR			0
184	AFSC	12/04/68	IIIB/AGENA D (23B)	WR			1
185	AFSC	01/22/69	IIIB/AGENA D (23B)	WR			1
186	SV-TAC COM	02/09/69	IIIC-17/Trans.	ER			1
187	AFSC	03/04/69	IIIB/AGENA D (23B)	WR			1
188	AFSC	04/15/69	IIIB/AGENA D (23B)	WR			1
189	GLORY TRIP 39T	05/20/69	II	WR			0
190	SV-VELA/OV	05/23/69	IIIC-15/Trans.	ER			1
191	AFSC	06/03/69	IIIB/AGENA D (23B)	WR			1
192	AFSC	08/23/69	IIIB/AGENA D (23B-1)	WR			1
193	AFSC	10/24/69	IIIB/AGENA D (23B-2)	WR			1
194	AFSC	01/14/70	IIIB/AGENA D (23B-3)	WR			1
195	SV-VELA	04/08/70	IIIC-18/Trans.	ER			1
196	AFSC	04/15/70	IIIB/AGENA D (23B-4)	WR			1
197	AFSC	06/25/70	IIIB/AGENA D (23B-5)	WR			1
198	AFSC	08/18/70	IIIB/AGENA D (23B-6)	WR			1
199	AFSC	10/23/70	IIIB/AGENA D (23B-7)	WR			1
200	SV-DOD	11/06/70	IIIC-19/Trans.	ER	NA	3.5 & 5	1
201	AFSC	01/21/71	IIIB/AGENA D (23B-8)	WR			1
202	AFSC	03/20/71	IIIB/AGENA D (33B-1)	WR			1
203	AFSC	04/22/71	IIIB/AGENA D (23B-9)	WR			1
204	SV-DOD	05/05/71	IIIC-20/Trans.	ER			1
205	AFSC	06/15/71	IIID (23D-1)	WR			1
206	M1-17	06/20/71	II (B-12)	WR			0
207	AFSC	08/12/71	IIIB/AGENA D (24B-1)	WR			1
208	M2-1	08/27/71	II (B-100)	WR			0
209	AFSC	10/23/71	IIIB/AGENA D (24B-2)	WR			1
210	SV-DOD	11/02/71	IIIC-21/Trans.	ER			1
211	AFSC	01/20/72	IIID (23D-2)	WR			1
212	AFSC	02/16/72	IIIB/AGENA D (33B-2)	WR	4	3	1
213	SV-DOD	03/01/72	IIIC-22/Trans.	ER			1
214	AFSC	03/17/72	IIIB/AGENA D (24B-3)	WR			1

No.	Mission/ID	Launch Date	Vehicle Configuration	Test Range	Response Mode	Flight Phase	Rep. Conf.
215	AFSC	05/20/72	IIIB/AGENA D (24B-4)	WR			1
216	M2-10	05/24/72	II (B-46)	WR			0
217	AFSC	07/07/72	IIID (23D-5)	WR			1
218	AFSC	09/01/72	IIIB/AGENA D (24B-5)	WR			1
219	AFSC	10/10/72	IIID (23D-3)	WR			1
220	M2-14	10/11/72	II (B-78)	WR			0
221	AFSC	12/21/72	IIIB/AGENA D (24B-6)	WR			1
222	AFSC	03/09/73	IIID (23D-6)	WR			1
223	AFSC	05/16/73	IIIB/AGENA D (24B-7)	WR			1
224	SV-DSP	06/12/73	IIIC-24/Trans.	ER			1
225	AFSC	06/26/73	IIIB/AGENA D (24B-9)	WR			1
226	AFSC	07/13/73	IIID (23D-7)	WR			1
227	AFSC	08/21/73	IIIB/AGENA D (33B-3)	WR			1
228	AFSC	09/27/73	IIIB/AGENA D (24B-8)	WR			1
229	M2-27	10/05/73	II	WR			0
230	AFSC	11/10/73	IIID (23D-8)	WR			1
231	SV-DSCS	12/13/73	IIIC-26/Trans.	ER			1
232	SV-VIKING	02/11/74	IIIE/CENT. D-1T (TC-1)	ER	4	3	1
233	AFSC	02/13/74	IIIB/AGENA D (24B-10)	WR			1
234	M2-31	03/01/74	II	WR			0
235	AFSC	04/10/74	IIID (23D-9)	WR			1
236	SV-ATS-F	05/30/74	IIIC-9/Trans.	ER			1
237	AFSC	06/06/74	IIIB/AGENA D (24B-11)	WR			1
238	AFSC	08/14/74	IIIB/AGENA D (24B-12)	WR			1
239	AFSC	10/29/74	IIID (23D-4)	WR			1
240	SV-HELIOS-A (TC-2)	12/10/74	IIIE/CENT-1T (23E-2)	ER			1
241	SOFT-1	01/09/75	II	WR			0
242	AFSC	03/09/75	IIIB/AGENA D (34B-1)	WR			1
243	AFSC	04/18/75	IIIB/AGENA D (24B-14)	WR			1
244	SV-DSCS	05/20/75	IIIC-7/Trans.	ER	NA	2.5	1
245	AFSC	06/08/75	IIID (23D-10)	WR			1
246	DG-2	08/07/75	II	WR			0
247	SV-Viking/Mars (TC-4)	08/20/75	IIIE/CENT. D-1T (23E-4)	ER			1
248	SV-Viking/Mars (TC-3)	09/09/75	IIIE/CENT. D-1T (23E-3)	ER			1
249	AFSC	10/09/75	IIIB/AGENA D (24B-10)	WR			1
250	AFSC	12/04/75	IIID (23D-13)	WR			1
251	DG-4	12/04/75	II	WR			0
252	SV-DSP	12/14/75	IIIC-29/Trans.	ER	NA	5	1
253	SV-HELIOS-B (TC-5)	01/15/76	IIIE/CENT. D-1T (23E-5)	ER			1
254	SV-LES/SOLRAD	03/14/76	IIIC-30/Trans.	ER			1
255	AFSC	03/22/76	IIIB/AGENA D (23B-18)	WR			1
256	AFSC	06/02/76	IIIB/AGENA D (34B-5)	WR			1
257	SV-DSP	06/25/76	IIIC-28/Trans.	ER			1
258	ITF-1	06/27/76	II	WR			0
259	AFSC	07/08/76	IIID (23D-14)	WR			1
260	AFSC	08/06/76	IIIB/AGENA D (34B-6)	WR			1

No.	Mission/ID	Launch Date	Vehicle Configuration	Test Range	Response Mode	Flight Phase	Rep. Conf.
261	AFSC	09/15/76	IIIB/AGENA D (24B-17)	WR	NA	2	1
262	AFSC	12/19/76	IIID (23D-15)	WR			1
263	SV-DSP	02/06/77	IIIC-23/Trans.	ER			1
264	AFSC	03/13/77	IIIB/AGENA D (24B-19)	WR			1
265	SV-DSCS	05/12/77	IIIC-32/Trans.	ER			1
266	AFSC	06/27/77	IIID (23D-17)	WR			1
267	SV-VOYAGER (TC-7)	08/20/77	IIIE/CENT. D-1T (23E-7)	ER			1
268	SV-VOYAGER (TC-6)	09/05/77	IIIE/CENT. D-1T (23E-6)	ER	NA	2	1
269	AFSC	09/23/77	IIIB/AGENA D (24B-23)	WR			1
270	AFSC	02/24/78	IIIB/AGENA D (34B-2)	WR			1
271	AFSC	03/16/78	IIID (23D-20)	WR			1
272	SV-DSCS	03/25/78	IIIC-35/Trans.	ER	4T	2	1
273	SV-DOD	06/10/78	IIIC-33/Trans.	ER			1
274	AFSC	06/14/78	IIID (23D-18)	WR			1
275	AFSC	08/04/78	IIIB/AGENA D (34B-7)	WR			1
276	SV-DSCS	12/13/78	IIIC-36/Trans.	ER			1
277	AFSC	03/16/79	IIID (23D-21)	WR			1
278	AFSC	05/28/79	IIIB/AGENA D (24B-25)	WR			1
279	SV-DSP	06/10/79	IIIC-23C-13/Trans.	ER			1
280	SV-DOD	10/01/79	IIIC-23C-16/Trans.	ER			1
281	SV-DSCS	11/21/79	IIIC-23C-19/Trans.	ER			1
282	AFSC	02/06/80	IIID (23D-19)	WR			1
283	AFSC	06/18/80	IIID (23D-16)	WR			1
284	AFSC	12/13/80	IIIB/AGENA D (34B-3)	WR			1
285	AFSC	02/28/81	IIIB/AGENA D (24B-24)	WR			1
286	SV-DOD	03/16/81	IIIC-23C-22/Trans.	ER			1
287	AFSC	04/24/81	IIIB/AGENA D (34B-8)	WR			1
288	AFSC	09/03/81	IIID (23D-22)	WR			1
289	SV-DOD	10/31/81	IIIC-23C-21/Trans.	ER			1
290	AFSC	01/21/82	IIIB/AGENA D (24B-26)	WR			1
291	SV-DOD	03/06/82	IIIC-23C-20/Trans.	ER			1
292	AFSC	05/11/82	IIID (23D-24)	WR			1
293	SV-DSCS	10/30/82	34D-01/US	ER			1
294	AFSC	11/17/82	IIID (23D-23)	WR			1
295	AFSC	04/15/83	IIIB/AGENA D (24B-27)	WR			1
296	AFSC	06/20/83	34D-5	WR			1
297	AFSC	07/31/83	IIIB/AGENA D (34B-9)	WR			1
298	SV-DOD	01/31/84	34D-10/Trans.	ER			1
299	SV-DOD	04/14/84	34D-11/Trans.	ER			1
300	AFSC	04/17/84	IIIB/AGENA D (24B-28)	WR			1
301	AFSC	06/25/84	34D-4	WR			1
302	AFSC	08/28/84	IIIB/AGENA D (34B-4)	WR			1
303	AFSC	12/04/84	34D-6	WR			1
304	SV-DOD	12/22/84	34D-13/Trans.	ER			1
305	AFSC	02/07/85	IIIB/AGENA D (34B-10)	WR			1
306	AFSC	08/28/85	34D-7	WR	4T	1	1

No.	Mission/ID	Launch Date	Vehicle Configuration	Test Range	Response Mode	Flight Phase	Rep. Conf.
307	AFSC	04/18/86	34D-9	WR	4	0	1
308	AFSC	02/11/87	IIIB/AGENA D (34B-11)	WR			1
309	AFSC	10/26/87	34D-15	WR			1
310	SV-DOD	11/29/87	34D-8/Trans.	ER			1
311	SV-DOD	09/02/88	34D-3/Trans.	ER	NA	5	1
312	AFSC	09/05/88	II/SLV (23G-1)	WR			1
313	AFSC	11/06/88	34D-14	WR			1
314	SV-DOD	05/10/89	34D-16/Trans.	ER			1
315	SV (first T-IV)	06/14/89	IV-1/IUS	ER	NA	1	1
316	SV-DOD	09/04/89	34D-2/Trans.	ER			1
317	AFSC	09/05/89	II/SLV (23G-2)	WR			1
318	SV-JAPAN/UK	01/01/90	III	ER			1
319	SV-INTELSAT VI	03/14/90	III	ER	NA	2,5 & 5	1
320	SV-DOD	06/08/90	IV-4	ER			1
321	SV-INTELSAT VI	06/23/90	III	ER			1
322	SV-DOD	11/13/90	IV-6/IUS	ER			1
323	AFSC	03/08/91	IV	WR			1
324	AFSC	11/17/91	IV	WR			1
325	AFSC	04/25/92	II/SLV	WR			1
326	SV-MARS OBS.	09/25/92	III	ER			1
327	AFMC	11/28/92	IV	WR			1
328	AFMC	08/02/93	IV (K-11)	WR	4	0	1
329	LANDSAT 6	10/05/93	II/SLV	WR	4	2	1
330	CLEMENTINE	01/25/94	II/SLV	WR			1
331	SV-MILSTAR	02/07/94	TIV-CENTAUR (K-10)	ER			1
332	SV-DOD	05/03/94	TIV-CENTAUR (K-7)	ER			1
333	SV-DOD	08/27/94	TIV-CENTAUR (K-9)	ER			1
334	SV-DOD	12/22/94	IV-IUS (K-14)	ER			1
335	SV-DOD	05/14/95	TIV-CENTAUR (K-23)	ER			1
336	SV-DOD	07/10/95	TIV-CENTAUR (K-19)	ER			1
337	SV-MILSTAR	11/06/95	TIV-CENTAUR (K-21)	ER			1
338	DOD	04/24/96	TIV-CENTAUR (K-18)	ER			1
339	DOD	07/02/96	TIV-NUS (K2)	ER			1

#### D.4.2 Titan Failure Narratives

The following narratives provide available details about each Titan failure since the beginning of the Titan I program in 1959. The narratives are numbered to match the flight-sequence numbers in Section D.4.1.

7. B-5, 14 Aug 59, Response Mode 1, Flight Phase 1: Umbilicals were prematurely pulled from missile resulting in engine shutdown and impact on pad.
8. C-3, 12 Dec 59, Response Mode 1, Flight Phase 1: Missile destroyed itself just before liftoff.
10. C-4, 5 Feb 60, Response Mode 4T, Flight Phase 1: While pitch program was in progress, a structural failure occurred in transition section. Nose cone broke off, and missile lost aerodynamic stability. Shortly after, an explosion and fire destroyed the missile.
12. C-1, 8 Mar 60, Response Mode 4, Flight Phase 2: Failure of gas-generator valve to open prevented Stage-II ignition.
13. G-5, 22 Mar 60, Response Mode 4, Flight Phase 2.5: Premature shut down of vernier engines resulted in impact 38 miles short of target.
14. C-5, 8 Apr 60, Response Mode 4, Flight Phase 2: Although Stage-I performance was low, Stage II successfully separated and ignited. All data were lost about 50 seconds later, apparently due to malfunction of Stage II turbopump.
20. J-2, 1 Jul 60, Response Mode 2, Flight Phase 1: Shortly after launch, hydraulic power to engine actuators was lost so control could not be maintained. The missile veered northwest and pitched down (Flight azimuth was 105.97°). Missile was destroyed by RSO 11 seconds after liftoff.
21. J-4, 28 July 60, Response Mode 4, Flight Phase 1: Stage I thrusting flight was terminated prematurely at 101 seconds (Nominal, 136 seconds). Stage II engine did not start, apparently because the auxiliary turbopumps did not receive sufficient head pressure to effect a successful start.
22. J-7, 10 Aug 60, Response Mode 4, Flight Phase 2: Stage II engine shutdown 0.17 seconds early and solo vernier operation did not occur. Impact was 107 miles short of target.
25. G-8, 29 Sep 60, Response Mode 4, Flight Phase 1: Stage I shut down prematurely when a low-level sensor malfunctioned and ceased to be locked out. Stage II performed properly but shutdown prematurely due to propellant depletion. The impact was some 3600 miles short of the 8700-mile target point.

28. J-9, 20 Dec 60, Response Mode 4, Flight Phase 2: No Stage-II ignition due to failure of gas generator to start.
29. J-10, 20 Jan 61, Response Mode 4, Flight Phase 2: No Stage-II operation due to erroneous signal that appeared at umbilical disconnect. Impact some 420 miles downrange.
32. J-12, 3 Mar 61, Response Mode 4, Flight Phase 2: Stage-II terminated prematurely after 54-second burn, apparently due to failure of pump drive assembly. Impact was 730 miles downrange.
34. J-15, 31 Mar 61, Response Mode 4, Flight Phase 1: Booster shut down prematurely at 74 seconds. Missile subsequently tumbled and broke up.
37. M-1, 24 Jun 61, Response Mode 4T, Flight Phase 2: Stage II engine shut down prematurely after 12 seconds of operation due to loss of Stage II hydraulic power. Loss of hydraulic power occurred during Stage I flight, so failure led to loss of control of sustainer and vernier actuators, producing excessive missile motion and tumbling.
42. M-3, 7 Sep 61, Response Mode 5, Flight Phase 2: A transient in guidance computer at 218.35 seconds (SECO at 297.7 seconds) caused impact 20 miles short and 2.8 miles left of target.
45. M-4, 6 Oct 61, Response Mode 5, Flight Phase 2: A one-bit error in the W velocity accumulation caused impact 86 miles short and 14 miles right of target.
50. M-6, 15 Dec 61, Response Mode 4, Flight Phase 2: Start signal for Stage II was not generated. Stage II did not ignite.
51. I, 20 Jan 62, Response Mode 4, Flight Phase 2: Missile self-destructed, apparently after Stage 2 failed to ignite. A backup automatic fuel-cutoff signal was sent at 248 Seconds.
53. I, 23 Feb 62, Response Mode 4, Flight Phase 2: Missile self-destructed, apparently after Stage 2 failed to ignite. A backup automatic fuel cutoff signal was sent at 240 Seconds.
56. N-1, 7 Jun 62, Response Mode 4, Flight Phase 2: Sustainer engine performance was subnormal due to reduced oxidizer flow through the gas generator. RSO terminated flight after a prolonged sustainer burn. Impact only 1100 miles downrange.
58. N-4, 25 July 62, Response Mode 4, Flight Phase 2: After about 60 seconds of Stage II burn, a fuel leak between the thrust chamber valve and the injector resulted in a

50% reduction of sustainer thrust for remainder of Stage II operation. Impact was 2888 miles short of target.

63. I (Yellow Jacket), 5 Dec 62, Response Mode 4T, Flight Phase 2: Missile was command destructed at 250 seconds. No other data available.
64. N-11, 6 Dec 62, Response Mode 4, Flight Phase 1: Stage I shut down 11.4 seconds early. As a result, no inertial velocity-dependent discrettes were issued and Stage II shut down prematurely, apparently due to an oxidizer bootstrap-line failure.
66. N-15, 10 Jan 63, Response Mode 4, Flight Phase 2: Stage II flight was terminated by backup SECO approximately 34 seconds after ignition because low thrust caused velocity to fall below performance criteria. Cause of low thrust was reduced oxidizer flow through the gas-generator injector. Impact only 556 miles downrange.
68. N-16, 6 Feb 63, Response Mode 4, Flight Phase 2: Oxidizer depletion prior to normal SECO resulted in impact 71 miles short of target.
69. N-7 (Awful Tired), 16 Feb 63, Response Mode 4T, Flight Phase 1: Missile self-destructed at 56 seconds at an altitude of 18,000 feet due to loss of roll control. Failure was caused by improper umbilical release at launch and subsequent loss of vehicle electrical control.
70. N-18, 21 Mar 63, Response Mode 4T, Flight Phase 2.5: Although vernier ignition was normal, vernier #2 received no commands, and gimballed erratically 2.8 seconds later. R/V attitude was incorrect at separation so that impact was 4 to 5 miles short of target.
74. N-21, 19 Apr 63, Response Mode 4, Flight Phase 2: Stage II engine shut down prematurely due to oxidizer bootstrap-line failure.
76. Titan I (Mares Tail), 1 May 63, Response Mode 2, Flight Phase 1: The missile was erratic from liftoff as one engine either failed at liftoff or shutdown immediately thereafter. The missile rose about 50 feet, then fell uprange from the launch pad about 7.5 seconds after liftoff.
77. N-14, 9 May 63, Response Mode 4, Flight Phase 2: Oxidizer depletion due to a leak resulted in premature Stage II shutdown and impact short of target.
80. N-20, 29 May 63, Response Mode 4, Flight Phase 1: A fuel leak in Stage I engine compartment at ignition caused a fire that spread through the engine compartment. Stage I destroyed itself at 52 seconds. Stage II was destroyed by RSO.

81. Titan II (Thread Needle), 20 June 63, Response Mode 5, Flight Phase 2: Flight appeared normal until BECO at about 146 seconds. The staging event seemed abnormally long, due to low second-stage thrust that remained considerably below normal thereafter because of reduced oxidizer flow through the gas-generator injector. The vehicle nevertheless followed closely to the intended ground track, albeit well behind schedule. At about 480 seconds (and some three minutes behind schedule), the missile began a slow turn to the left. A SECO indication was noted about 10 seconds later. Destruct was sent at 532 seconds after all track was lost.
82. Titan I (Silver Spur), 16 July 63, Response Mode 4, Flight Phase 2: The flight was normal through first-stage cutoff. Separation occurred but the second-stage failed to ignite.
85. Titan I (Polar Route), 30 Aug 63, Response Mode 4, Flight Phase 2.5: The flight appeared normal through the first and second-stage thrusting periods. At SECO the vernier engines also shut down, apparently due to shutdown of the gas generator.
89. II (Fire Truck), 9 Nov 63, Response Mode 4T, Flight Phase 1: Missile tumbled out of control at 130 seconds, then broke up.
104. IIIA (65-210), 1 Sep 64, Response Mode 4, Flight Phase 4: Nominal mission through first transtage burn. Transtage propellant-tank pressurization system failed with resultant reduction in thrust. Vehicle impacted about 2700 miles downrange.
107. Titan I (West Wind I), 8 Dec 64, Response Mode 5, Flight Phase 1: A first-stage power-level malfunction combined with guidance deviations caused the missile to drift far to the left, then over-correct far to the right, passing north of Midway Is. No other data available.
109. Titan I (West Wind III), 14 Jan 65, Response Mode 4, Flight Phase 2: First-stage flight was apparently normal, but second stage failed to ignite.
112. Titan I (West Wind II), 5 Mar 65, Response Mode 4, Flight Phase 2: Missile impacted on azimuth about 80 miles short of target due to propellant depletion.
116. Titan I (Card Deck), 30 Apr 65, Response Mode 4, Flight Phase 1: Flight appeared normal until around 100 seconds when the IP slowed and then stopped due to a turbopump failure. The missile self-destructed at about 115 seconds with the impact point about 115 miles offshore.
120. Titan II (Gold Fish), 14 Jun 65, Response Mode 4, Flight Phase 2.5: Vehicle apparently failed during the vernier solo phase due to loss of a vernier nozzle.

127. Titan II (Bold Guy), 21 Sep 65, Response Mode 4, Flight Phase 2: After a normal first-stage flight, the second stage was shut down immediately after start by an erroneous guidance command.
128. IIC (65-212), 15 Oct 65, Response Mode NA, Flight Phase 4 and 5: Normal mission through transtage second ignition and burn. One chamber of transtage engine failed to shutdown completely, resulting in a pitch-up deviation, loss of control, vehicle tumbling, and an unplanned orbit.
131. Titan II (Cross Fire), 30 Nov 65, Response Mode 5, Flight Phase 2: Trouble apparently began between 208 and 214 seconds when the rate and track beacons were lost. The radar tracked till about 360 - 380 seconds, indicating a ballistic-type trajectory veering to the right. Loss of control was due to a fuel leak at the crossover manifold.
134. IIC (66-001), 21 Dec 65, Vehicle 8, Response Mode NA, Flight Phase 5: Nominal mission through transtage second burn shutdown. Attitude control system engine failed to shutdown following vernier burn with resulting fuel depletion and loss of attitude control.
135. Titan II (Sea Rover), 22 Dec 65, Response Mode 4T, Flight Phase 2: Flight was apparently normal until some point well into second-stage burn. Track then indicated erratic movement left of nominal, then right of nominal, but with little downrange movement of the IP. Automatic fuel cutoff was sent at 396 seconds. Failure resulted from improper rigging of sustainer actuator that exceeded control-system capability.
142. Titan II (Silver Bullet), 24 May 66, Response Mode 4, Flight Phase 2.5: Flight was normal except that R/V did not separate, causing a 20-mile uprange miss.
148. IIC (66-005), 26 Aug 66, Vehicle 12, Response Mode 4T, Flight Phase 0: Payload fairing failed during Stage-0 powered flight. The failure at 79 seconds resulted in violent maneuvering and self destruct (ISDS).
159. Titan II (Glamour Girl), 12 Apr 67, Response Mode 4T, Flight Phase 2: First-stage flight was normal. About 15 seconds after second-stage ignition, failure of the yaw-rate gyro resulted in violent roll and pitch maneuvers. Missile impacted about 660 miles downrange.
160. IIIB/Agena D (Busy Tailor), 26 Apr 67, Response Mode 4, Flight Phase 2: Flight appeared normal through first-stage cutoff and separation. About 15 seconds into the second stage, a fuel-line blockage resulted in a drop in chamber pressure that reduced the thrust to about half its normal level. As a result, the velocity eventually stopped increasing. The IP moved slightly farther downrange and remained on azimuth until loss of signal at 300 seconds. Impact was about 600 miles downrange.

200. IIIC-19, 6 Nov 70, Vehicle 19, Response Mode NA, Flight Phase 3.5 and 5: All booster systems performed essentially as planned. Transtage experienced a guidance anomaly during coast prior to second burn resulting in an improper orbit.
212. IIIB/Agena D (AFSC), 16 Feb 72, Response Mode 4, Flight Phase 3: After an apparently normal Titan III B boost phase, the Agena failed to ignite. The payload impacted about 1500 miles downrange.
232. Titan IIIE, #E1, 11 Feb 74, Response Mode 4, Flight Phase 3: All Titan booster functions and Centaur separation were properly performed. Centaur stage failed to ignite.
244. TIIC-25, 20 May 75, Vehicle 25, Response Mode NA, Flight Phase 2.5: All systems performed satisfactorily through Stage II/III separation. About 230 milliseconds after staging discrete was issued, the IMU power supply failed. Transtage then tumbled and the first transtage burn failed to occur leaving transtage and attached payload in the parking orbit.
252. TIIC-29, 14 Dec 75, Vehicle 29, Response Mode NA, Flight Phase 5: All launch vehicle objectives were met. However, satellite propulsion system malfunctioned putting satellite in uncontrollable position with no possibility of restoring mission capability.
261. IIIB/Agena D (AFSC), 15 Sep 76, Response Mode 4, Flight Phase 2: The stage-2 engine failed to respond to shutdown commands and thus burned to propellant depletion. Cause was thought to be a hard contaminant that blocked the fuel valve.
268. 23E-6/Centaur D-1T, 5 Sep 77, Response Mode NA, Flight Phase 2: Flight was regarded as a success, although the second-stage velocity was low, probably due to a detached line diffuser lodged on top of the prevalue.
272. TIIC-17, 25 Mar 78, Vehicle 35, Response Mode 4T, Flight Phase 2: Vehicle performance was satisfactory until 16.4 seconds beyond Stage-2 start. At this time the Stage-2 hydraulic system began and continued over-pressurizing until the system burst after 125 seconds of Stage-2 operation. The pressure then dropped to zero, the vehicle tumbled out of control, and guidance shut down the second stage after detecting negative acceleration. The RSO sent arm at 629 seconds and destruct at 630 seconds.
306. 34D (AFSC), 28 Aug 85, Response Mode 4T, Flight Phase 1: The first-stage engine suffered three separate major anomalies: (1) during subassembly-2 (S/A-2) start transient (110 sec), a large oxidizer leak of 165 lb/sec occurred in the oxidizer suction line; (2) at 213 seconds, an internal fuel leak of 30 lb/sec occurred in S/A-1 downstream of the combustion chamber and created a vehicle side force; (3) the

S/A-1 shut down at 213 sec due to failure of its turbopump assembly. The vehicle continued flight till 221 seconds when erratic attitude rates were noted. At 229 seconds, the impact point stopped. At 257 seconds, the pressure dropped to zero in the stage-1 thrust-chamber assembly 2. At the same time, stages 1 and 2 separated as stage 2 ignited. After this time, stage-2 attitude rates were erratic. Destruct was sent by the RSO at 273 seconds.

307. 34D (AFSC), 18 Apr 86, Response Mode 4, Flight Phase 0: At about 8.8 seconds after liftoff, the insulation and case of SRM No. 2 debonded resulting in case rupture immediately thereafter. The core vehicle was destroyed by fragments from the ruptured motor. Auto-destruct was activated on SRM-1 at 9.0 seconds.
311. 34D-3/Transtage, 2 Sep 88, Response Mode NA, Flight Phase 5: Transtage pressurization system failed due to damage to the upper portion of the transtage fuel tank and pressurization lines. A leak of 1,340 pounds occurred during park orbit, and a large helium-tank gas leak occurred during transtage first burn. Not enough helium was left in system to allow start of second burn. The payload was left in a geostationary transfer orbit.
315. Titan IV-1/IUS, 14 June 89, Response Mode NA, Flight Phase 1: Late in Stage-1 burn, one of the engines failed and shut down. The other engine was able to gimbal sufficiently to maintain control until propellant depletion. Trajectory inaccuracies were compensated for during Stage-2 burn, and the mission was a success.
319. Commercial Titan, 14 Mar 90, Response Mode NA, Flight Phase 2.5 and 5: Boost phase was satisfactory. The payload separation system was designed for two satellites and had two discrete outputs from the missile guidance computer (MGC), but for this mission it carried only a single satellite. The wiring team miswired the harness, which connected the MGC payload-separation discretes to the payload separation device, so the satellite never received the separation signal. PKM and satellite did not separate from Stage II resulting in low-earth elliptical orbit. Ground controllers were able to separate satellite hours later but PKM remained attached to Stage II.
328. IV, 2 Aug 93, Response Mode 4, Flight Phase 0: A leak occurred in SRM#1 at 99.9 seconds that rapidly enveloped the vehicle in propellant gases. Approximately 1.6 seconds later the vehicle blew up and disintegrated, apparently due to activation of the inadvertent-separation destruct system. Destruct was transmitted at 104.5 seconds.
329. II/SLV (Landsat 6), 5 Oct 93, Response Mode 4, Flight Phase 2: Following a successful Titan-II second-stage burn and after payload separation, the apogee-kick motor failed to ignite and circularize the highly-elliptical orbit. The Landsat payload and Titan II followed a ballistic trajectory back into the atmosphere where burnup occurred.

## D.5 Thor Launch and Performance History (Not Including Delta)

The entire Thor history is depicted rather compactly in bar-graph form in Figure 40. The solid-black portion of each bar indicates the number of launches during the calendar year for which vehicle performance was entirely normal, in so far as could be determined. The clear white parts forming the tops of most bars show the number of launches that were either failures or flights where the launch vehicle experienced some sort of anomalous behavior. Every launch with an entry in the response mode column of Table 46 falls in this category. Such behavior did not necessarily prevent the attainment of some, or even all, mission objectives.

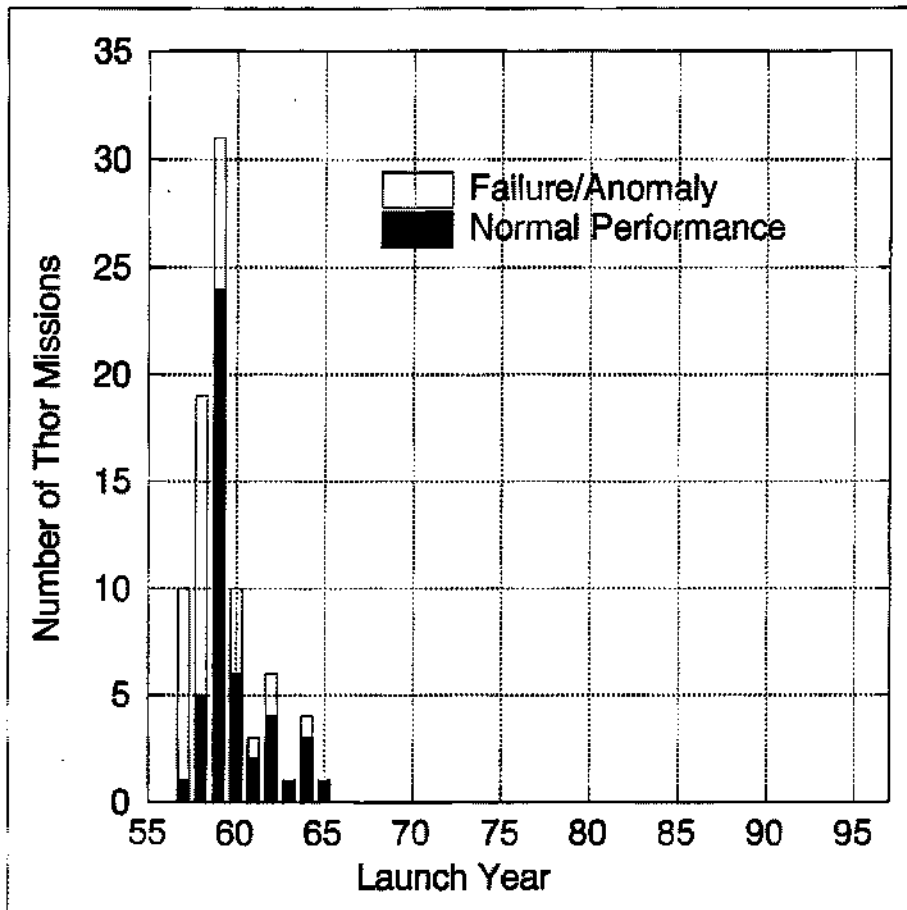


Figure 40. Thor Launch Summary

### D.5.1 Thor and Thor-Boosted Launch History

The data in Table 46 summarize all Thor and Thor-boosted space-vehicle launches since the program began. A launch sequence number is provided in the first column. A launch ID and date are provided in columns 2 and 3. The fourth column indicates the vehicle configuration. The fifth column indicates the launch range. The sixth column indicates the failure-response mode (1 through 5 and NA) that RTI has determined best describes the failures that occurred. For Mode 3 or 4 failures, a suffix of 'T' indicates the vehicle tumbled. Successful launches are indicated by a blank in the Response-

Mode column. The seventh column indicates the operational flight phase during which the failure occurred. The last column indicates whether the vehicle configuration is representative of those being launched today.

Table 46. Thor Launch History

No.	Mission/ID	Launch Date	Vehicle Configuration	Test Range	Response Mode	Flight Phase	Rep. Conf.
1	Weapons System (WS)	01/25/57	101	ER	1	1	0
2	WS	04/19/57	102	ER	4	1	0
3	WS	05/21/57	103	ER	1	1	0
4	WS	08/30/57	104	ER	4T	1	0
5	WS	09/20/57	105	ER	4	1	0
6	WS	10/03/57	107	ER	1	1	0
7	WS	10/11/57	108	ER	4	1	0
8	WS	10/24/57	109	ER			0
9	WS	12/07/57	112	ER	5	1	0
10	WS	12/19/57	113	ER	4	1.5	0
11	WS	01/28/58	114	ER	5	1	0
12	WS	02/28/58	120	ER	4	1	0
13	WS	04/19/58	121	ER	1	1	0
14	WS	04/23/58	ABLE I (116)	ER	4	1	0
15	WS	06/04/58	115	ER			0
16	WS	06/13/58	122	ER			0
17	WS	07/11/58	ABLE I (118)	ER			0
18	WS	07/12/58	123	ER	4	1	0
19	WS	07/23/58	ABLE I (119)	ER			0
20	WS	07/26/58	126	ER	4	1	0
21	WS	08/06/58	117	ER			0
22	PIONEER	08/17/58	ABLE I (127)	ER	4	1	0
23	PIONEER-I	10/11/58	ABLE I (130)	ER	NA	2 & 5	0
24	WS	11/05/58	138	ER	5	1	0
25	PIONEER-II	11/08/58	ABLE I (129)	ER	4	3	0
26	WS	11/26/58	140	ER	5	1	0
27	WS	12/05/58	145	ER	4	1	0
28	WS	12/16/58	146	ER	4	1	0
29	WS	12/30/58	149	ER	2	1	0
30	WS	01/23/59	ABLE II (128)	ER	4	1.5	0
31	WS	01/30/59	154	ER	4	1	0
32	WS	02/28/59	ABLE II (131)	ER	4	2	0
33	WS	03/21/59	ABLE II (132)	ER			0
34	WS	03/21/59	158	ER			0
35	WS	03/26/59	162	ER			0
36	WS	04/07/59	ABLE II (133)	ER			0
37	WS	04/22/59	176	ER			0
38	WS	04/24/59	164	ER			0
39	WS	05/12/59	187	ER			0
40	WS	05/21/59	ABLE II (135)	ER			0
41	WS	05/22/59	184	ER			0

No.	Mission/ID	Launch Date	Vehicle Configuration	Test Range	Response Mode	Flight Phase	Rep. Conf.
42	WS	06/11/59	ABLE II (137)	ER			0
43	WS	06/25/59	198	ER			0
44	WS	06/29/59	194	ER	NA	1.5	0
45	WS	07/21/59	203	ER	3	1	0
46	WS	07/24/59	202	ER			0
47	WS	08/05/59	208	ER			0
48	EXPLORER 6	08/07/59	ABLE III (134)	ER			0
49	WS	08/14/59	204	ER			0
50	WS	08/27/59	216	ER			0
51	WS	09/12/59	217	ER			0
52	TRANSIT 1A	09/17/59	ABLE (136)	ER	4	2.5	0
53	WS	09/22/59	222	ER			0
54	WS	10/06/59	235	ER			0
55	WS	10/13/59	221	ER			0
56	WS	10/28/59	230	ER			0
57	WS	11/03/59	238	ER			0
58	WS	11/19/59	244	ER			0
59	WS	12/01/59	254	ER	4T	1	0
60	WS	12/17/59	255	ER			0
61	WS	01/14/60	256	ER			0
62	WS	02/09/60	259	ER			0
63	WS	02/29/60	263	ER			0
64	PIONEER-5	03/11/60	ABLE (219)	ER			0
65	TIROS I	04/01/60	ABLE (148)	ER			0
66	TRANSIT-1B	04/13/60	ABLE-STAR (257)	ER	NA	1 & 5	0
67	TRANSIT-2A	06/22/60	ABLE-STAR (281)	ER	NA	2 & 5	0
68	COURIER-1A	08/18/60	ABLE-STAR (262)	ER	4T	1	0
69	COURIER-1B	10/04/60	ABLE-STAR (293)	ER			0
70	TRANSIT-3A	11/30/60	ABLE-STAR (283)	ER	4	1	0
71	TRANSIT-3B	02/21/61	ABLE-STAR (313)	ER	NA	4 & 5	0
72	TRANSIT-4A	06/28/61	ABLE-STAR (315)	ER			0
73	TRANSIT-4B	11/15/61	ABLE-STAR (305)	ER			0
74	BIG SHOT-1 (sub-orb.)	01/15/62	337	ER			0
75	COMPOSITE-1	01/24/62	ABLE-STAR (311)	ER	5	2	0
76	WS	05/02/62	177	ER			0
77	ANNA-1A	05/10/62	ABLE-STAR (314)	ER	4	2	0
78	BIG SHOT-II (sub-orb.)	07/18/62	338	ER			0
79	ANNA-1B	10/31/62	ABLE-STAR (319)	ER			0
80	ASSET ASV-1	09/18/63	232	ER			0
81	ASSET ASV-2	03/24/64	240	ER	4	2	0
82	ASSET ASV-3	07/22/64	250	ER			0
83	ASSET AEV-1	10/27/64	260	ER			0
84	ASSET AEV-2	12/08/64	SLV II (247)	ER			0
85	ASSET ASV-4	02/23/65	248	ER			0

## D.5.2 Thor and Thor-Boosted Failure Narratives

The following narratives provide information about flight failure of Thor weapons system and Thor-boosted space vehicle launches beginning with the first Thor launch in January 1957. The narratives are numbered to match the flight-sequence numbers in Section D.5.1.

1. 101, 25 Jan 57, Response Mode 1, Flight Phase 1: Failure of fuel-system valve resulted in loss of thrust. Missile fell back on pad after reaching an altitude of only 9 inches.
2. 102, 19 Apr 57, Response Mode 4, Flight Phase 1: Missile was apparently performing normally until destroyed by the RSO at 34.7 seconds. Erroneous DOVAP beat-beat plot showed missile heading uprange.
3. 103, 21 May 57, Response Mode 1, Flight Phase 1: Missile was destroyed on the pad at T - 5 minutes. A faulty fuel-tank regulator and relief valve resulted in over-pressurizing and bursting of fuel tank.
4. 104, 30 Aug 57, Response Mode 4T, Flight Phase 1: Spurious signals in the main-engine yaw feedback circuit resulted in missile breakup shortly after 92 seconds.
5. 105, 20 Sep 57, Response Mode 4, Flight Phase 1: Premature propellant depletion resulted in impact some 400 miles short of target.
6. 107, 3 Oct 57, Response Mode 1, Flight Phase 1: Main fuel valve closed 1.25 seconds after liftoff. Missile fell back on pad after reaching an altitude of about 17 feet.
7. 108, 11 Oct 57, Response Mode 4, Flight Phase 1: Due to a mechanical failure, an abnormal main-engine shutdown (one second early) resulted in loss of the vernier solo phase.
9. 112, 7 Dec 57, Response Mode 5, Flight Phase 1: An electrical-system failure at 107 seconds produced an abnormal loading on the missile converter. The missile began deviating at 110 seconds and finally broke up at about 224 seconds (well after MECO at 156 seconds). Missile impacted 200 miles downrange and 40 miles left of flight line.
10. 113, 19 Dec 57, Response Mode 4, Flight Phase 1.5: Flight was regarded as successful although there was no vernier solo operation and impact was 6 miles from target.
11. 114, 28 Jan 58, Response Mode 5, Flight Phase 1: Guidance system failure at 95 seconds resulted in erroneous steering commands causing the vehicle to yaw left and pitch down. Divergence began about 110 seconds and continued until the

vehicle was destroyed by the RSO at 152 seconds. Missile impacted about 60 miles downrange.

12. 120, 28 Feb 58, Response Mode 4, Flight Phase 1: Failure of fuel line caused premature main engine shutdown at 109.7 seconds.
13. 121, 19 Apr 58, Response Mode 1, Flight Phase 1: Failure of fuel system resulted in loss of thrust shortly after liftoff. Missile fell back on pad after reaching an altitude of about 4 feet.
14. 116 (Able I), 23 Apr 58, Response Mode 4, Flight Phase 1: A turbopump failure at 146.2 seconds resulted in main-engine shutdown and an explosion.
18. 123, 11 July 58, Response Mode 4, Flight Phase 1: Although the flight was regarded as a success, the main engine failed to respond to the guidance shutdown command due to a wiring failure. When the main engine was shut down 0.43 seconds later by a backup command, the vernier engines also shut down. A large overshoot resulted from the late shutdown.
20. 126, 26 July 58, Response Mode 4, Flight Phase 1: An inadvertent closing of the main-engine liquid-oxygen valve terminated thrust at 58.4 seconds. Missile components were recovered about 5 miles downrange.
22. 127 (Able I), 17 Aug 58, Response Mode 4, Flight Phase 1: A turbopump failure led to main engine shutdown at about 74 seconds. An explosion followed with impact about 10 miles downrange.
23. 130 (Pioneer I), 11 Oct 58, Response Mode NA, Flight Phase 2 & 5: Low upper-stage thrust reduced the planned orbital altitude from 250,000 nm to 90,000 nm.
24. 138, 5 Nov 58, Response Mode 5, Flight Phase 1: Shortly after liftoff the missile began drifting uprange and to the left, reaching a maximum uprange drift of 150 feet. It continued diverging to the left of the nominal flight path until a pitch-gyro failure caused an excessive pitch down. Shortly thereafter at 34.6 seconds, command destruct occurred.
25. 129 (Able I), 8 Nov 58, Response Mode 4, Flight Phase 3: After a normal boost phase, the third-stage (Allegheny Ballistic X-248-A3) solid-propellant motor failed to ignite.
26. 140, 26 Nov 58, Response Mode 5, Flight Phase 1: Erratic performance of the guidance-system inverter at 111.4 seconds resulted in erroneous accelerometer scale factors and a 37 mile overshoot of target. Flight was regarded as a success.
27. 145, 5 Dec 58, Response Mode 4, Flight Phase 1: Although the flight was considered successful, below-normal thrust throughout flight resulted in fuel

depletion before to reaching cutoff conditions. Impact was 28 miles short of target.

28. 146, 16 Dec 58, Response Mode 4, Flight Phase 1: Although flight was considered a success, the main-engine fuel valve remained partially open for 14 seconds after MECO command was given. This resulted in a 6-mile overshoot.
29. 149, 30 Dec 58, Response Mode 2, Flight Phase 1: A momentary ground in the electrical system at liftoff caused the guidance system to assume control at this time rather than the planned 108.5 seconds. Guidance immediately commanded a maximum pitch rate to place the missile in its proper orientation for 108.5 seconds. By 22 seconds the missile has pitched through 46°. As it attempted to maintain stability, a reverse pitch subsequently developed, but by 46.4 seconds the missile was tumbling to the right. Destruct was sent at 52.5 seconds.
30. 128 (Able II), 22 Jan 59, Response Mode 4, Flight Phase 1.5: An electrical failure prevented second-stage (Aerojet General AJ10-42) separation and ignition.
31. 154, 30 Jan 59, Response Mode 4, Flight Phase 1: Improper propellant mixture and low thrust resulted in fuel depletion before cutoff conditions were reached.
32. 131 (Able II), 28 Feb 59, Response Mode 4, Flight Phase 2: Flight appeared normal until 195 seconds when all track was lost. As a result, the RSO sent cutoff at 218 seconds and destruct at 222 seconds.
44. 194, 29 June 59, Response Mode NA, Flight Phase 1.5: Flight was normal except that reentry vehicle did not separate and retro rockets did not fire.
45. 203, 21 July 59, Response Mode 3, Flight Phase 1: The liftoff pin failed to extract so the pitch and roll programs were not initiated. Missile was destroyed at 45 seconds at an altitude of about 18,000 feet.
52. 136 (Transit 1A), 17 Sep 59, Response Mode 4, Flight Phase 2.5: First and second stages performed normally until stage 2/3 separation. Failure of the stage-2 retro system apparently led to a collision of the stages. As a result, the third stage failed to ignite.
59. 254, 1 Dec 59, Response Mode 4T, Flight Phase 1: A hydraulic-system failure resulted in premature closure of the main-engine liquid-oxygen valve. The hydraulic-system pressure decayed almost linearly from 8 seconds to 146 seconds when missile control was lost. Impact was 322 miles short of target.
66. 257 (Transit 1B), 13 Apr 60, Response Mode NA, Flight Phase 1 and 5: The flight was a partial success although satellite was placed in a lower-than-planned orbit. MECO velocity was 315 ft/sec below normal. Noisy data rejected by the guidance computer resulted in pitch-plane steering errors and the unplanned orbit.

67. 281 (Transit 2A), 22 June 60, Response Mode NA, Flight Phase 2 and 5: Although boost phase was normal, anomalous performance during second-stage burn produced an orbit with apogee of 570 miles and perigee of 341 miles instead of the planned 500-mile circular orbit.
68. 262 (Courier 1A), 18 Aug 60, Response Mode 4T, Flight Phase 1: Hydraulic pressure began a steady decay beginning about 18 seconds after liftoff. Severe transients were noted at 129.3 seconds. Uncontrolled yaw, pitch, and roll maneuvers began about 133 seconds. Between 138 and 143 seconds the missile turned through three full revolutions in pitch. The upper stages separated at 140.4 seconds and the first stage broke up about 142.8 seconds. The second stage remained intact and was beacon tracked until 400 seconds.
70. 283 (Transit 3A), 30 Nov 60, Response Mode 4, Flight Phase 1: The first stage shut down 11.2 seconds prematurely at 151.85 seconds when the MECO cutoff circuit was armed. Since velocity at that time was about 2500 ft/sec below the normal cutoff velocity, portions of the first stage impacted in Cuba. The second stage separated and performed normally until shut down by the RSO at MECO plus 159.9 seconds to prevent overflight of South America.
71. 313 (Transit 3B), 21 Feb 61, Response Mode NA, Flight Phase 4 and 5: Second burn of second stage failed to occur. This resulted in an orbit with perigee of 539 miles and apogee of 92 miles instead of the planned 500-mile circular orbit.
75. 311 (Composite I), 24 Jan 62, Response Mode 5, Flight Phase 2: Flight was within acceptable limits until second-stage ignition. Probably because of rupture of the lower oxidizer manifold, normal thrust levels never developed. About 50 milliseconds after ignition, severe thrust chamber motion developed and the second stage began to tumble. Telemetry indicated that the first tumble period was about 29 seconds. Propellant depletion occurred at MECO plus 212 seconds. The nominal first-burn duration was 378 seconds.
77. 314 (ANNA 1A), 10 May 62, Response Mode 4, Flight Phase 2: After a successful Thor flight, an electrical malfunction prevented separation and second-stage ignition.
81. 240 (Asset-2), 24 Mar 64, Response Mode 4, Flight Phase 2: The second stage either failed to ignite or burned for only one second.

## References

1. Montgomery, R. M., and Ward, J. A., "Computations of Hit Probabilities From Launch-Vehicle Debris", RTI/4666/02F, September 19, 1990.
2. Eastern Test Range Directorate of Safety Post-Test Report, Test D1000, 18 June 1991.
3. Ward, James A., "Baseline Launch-Area Risks for Atlas and Delta Launches", RTI/5180/60/40F, September 30, 1995.
4. "Spacelift Effective Capacity: Part 1 - Launch Vehicle Projected Success Rate Analysis", Draft, Booz•Allen & Hamilton, Inc., 19 February 1992, prepared for the Air Force Space Command Launch Services Office.
5. "Launch Options for the Future: Special Report", Office of Technology Assessment, July 1988.
6. Silke, Kevin, "Reliability Growth Model Overview", General Dynamics Reliability Bulletin 92-02.
7. "Eastern Range Launches, 1950 - 1954, Chronological Summary", 45th Space Wing History Office.
8. "Eastern Range Launches, Chronological Summary", 45th Space Wing History Office, Extension updating the launch summary through 30 December 1995.
9. "Vandenberg AFB Launch Summary", Headquarters 30th Space Wing, Office of History, Launch Chronology, 1958 - 1995.
10. Isakowitz, Steven J., (updated by Jeff Samella), *International Reference Guide to Space Launch Systems*, Second Edition, published and distributed by AIAA in 1995.
11. Smith, O. G., "Launch Systems for Manned Spacecraft", Draft, July 23, 1991.
12. "Comparison of Orbit Parameters - Table 1", prepared by McDonnell Douglas Space Systems Company, Delta launches through 4 Nov 95.
13. Missiles/Space Vehicle Files, 45th Space Wing, Wing Safety, Mission Flight Control and Analysis (SEO), 1957 through 1995.
14. Missile Launch Operations Logs, 30th Space Wing, copies provided via ACTA, Inc., (Mr. James Baeker), 1963 through 1995.

15. "Titan IV, America's Silent Hero", published by Lockheed Martin in *Florida Today*, 13 Nov 95.
16. "Atlas Program Flight History" (through April 1965), General Dynamics Report EM-1860, 26 April 1965.
17. Fenske, C. W., "Atlas Flight Program Summary", Lockheed Martin, April 1995.
18. Brater, Bob, "Launch History", Lockheed Martin FAX to RTI, March 13, 1996.
19. Several USAF Accident/Incident Reports for Atlas and Titan failures.
20. Quintero, Andrew H., "Launch Failures from the Eastern Range Since 1975", Aerospace memo, February 25, 1996, provided to RTI by Bill Zelinsky.
21. Set of "Titan Flight Anomaly/Failure Summary" since 1959, received from Lockheed Martin, April 4, 1996.
22. Chang, I-Shih, "Space Launch Vehicle Failures (1984 - 1995)", Aerospace Report No. TOR-96(8504)-2, January 1996.